Faculty of Science and Engineering

Degradation of Trace Organic Chemicals and Antibiotic Resistant Bacteria/Genes during Conventional and Advanced Oxidation Processes

Maolida Nihemaiti

This thesis is presented for the Degree of
Doctor of Philosophy
of
Curtin University

September 2018

Declaration

To the best of my knowledge and belief this thesis contains no material previously published by any other person except where due acknowledgment has been made.

This thesis contains no material which has been accepted for the award of any other degree or diploma in any university.

Signature: 

Maolida Nihemaiti

Date: 10/09/2018

Acknowledgments

Frist and foremost, I would like to express my deepest gratitude to my advisor, Professor Jean-Philippe Croué. I've had the great privilege of studying in JP's group starting from my master degree in 2012. He introduced me into scientific research. Without his valuable guidance, fantastic research ideas, and constant encouragements, this research work would not have been possible. I am thankful to him for being always supportive, friendly, and cheerful. I could not have imagined having a better mentor and advisor.

My sincere appreciation goes to Professor Jörg E. Drewes in Technical University of Munich, Germany and Professor Yunho Lee in Gwangju Institute of Science and Technology, South Korea for offering me the opportunities to visit their labs and conduct experimental work. I also want to thank Dr Uwe Hübner and David Miklos from Professor Drewes' group, and Younggun Yoon from Professor Lee's group, for their collaborative work and great support.

I am grateful to Professor David Reckhow, Professor Karl Linden, Dr Julien Le Roux, and Dr Christiane Hoppe-Jones, for their valuable advices and contributions to my paper.

It has been very challenging for me as a chemist to work on microbiological experiments, but I was so lucky to have a big support from a group of microbiologists at Curtin University. I would like to offer my special thanks to Dr Julie Glady-Croué, Dr Jeanne Le Masurier, Ratish Ramyad Permala, and Dr Sébastien Allard, for their patience, help, and valuable instructions.

I wish to thank my friends and staff at Curtin Water Quality Research Centre and Department of Chemistry for their support and companionship during my PhD study in no particular order: Xizhi Niu, Suona Zhang, Jianye Wei (Ida), Valentin Rougé, Rhys Carter, Zuotong How, Wei Hu, Ionut Caraene, Luis Restrepo Vieira, Jaime Cesar, Viktor Kesners, NanNan He, Yuru Wang, Bettina Schaefer, Shi Tang, Jaedon Shin, Siyu Hu, Yujie Yuan, Yijun Zhong, Ina Kristiana, Deborah Liew, Jace Tan, Peter Chapman, Grant Cope, Kathryn Linge , and Cynthia Joll.

I would like to extend my gratitude to Ms. Carolyn Bellamy from Water Research Australia and my WaterRA mentor Dr Annette Davison from Risk Edge Pty Ltd for their support and guidance over the years.

I also want to acknowledge the following organisations for their financial support: Curtin University (Curtin International Postgraduate Research Scholarship), Water Research Australia and Water Corporation of Western Australia (WaterRA Postgraduate Scholarship 4512-15).

Last but not least, I would like to express my deep gratitude to my parents, for their unconditional love and support. My heartfelt gratitude is extended to my lovely sisters, brother, sister-in-law, and my little niece (Ulpan Janim) for their continuous encouragements.

Abstract

Anthropogenic activities are increasingly impacting the quality of water resources. Trace Organic Chemicals (TOrCs), such as pharmaceuticals, personal care products, pesticides, and industrial compounds, are detected in sewage, surface water, ground water, and drinking water worldwide. TOrCs are generally present at trace concentrations (typically in ng L^{-1} to µg L^{-1}), however, many of them are extremely stable and biologically active with various adverse effects on human health and biota. Antibiotics are one of the most important TOrCs as they are related to the dissemination of antibiotic resistance, one of today's greatest public health challenges in the world. Despite the naturally occurring level of antibiotic resistance, overuse and discharge of antibiotics are accelerating the development of antibiotic resistant bacteria (ARB) and antibiotic resistance genes (ARG) in anthropogenic-impacted environment. The discharge of effluents from urban Wastewater Treatment Plant (WWTP) is an important source of chemical and microbial contaminants detected in surface water. Current treatment technologies practiced in WWTPs worldwide were not designed to remove TOrCs. Most TOrCs are characterized as poorly biodegradable and recalcitrant to conventional chemical processes. Biological treatments (e.g., activated sludge) can contribute to horizontal gene transfer and formation of multi-drug resistant bacteria. More and more water utilities and the scientific community express interests in additional treatment approaches with purpose of upgrading current treatment plants to reduce TOrCs and their associated biological risks in discharged and reused water. Switzerland has already adopted the use of ozone or activated carbon in WWTPs in order to meet the guideline on TOrCs load into the environment.

UV-based advanced oxidation processes (UV-AOPs) have received increasing attention as a promising technology for the elimination of contaminants in wastewater. The degradation of contaminants during UV-AOPs follows a dual mechanism, namely direct UV photolysis (depending on the photolytic characteristic of target compounds) and oxidation by highly reactive radical species. Hydroxyl radical (•OH)-based AOPs have been widely studied and UV/hydrogen peroxide (H_2O_2) are currently applied in some full-scale treatment plants for potable water reuse. UV/chlorine is another emerging AOP recently implemented in a full-scale water reclamation plant. Peroxydisulfate (PDS) and peroxymonosulfate (PMS)-based AOPs have been

explored for application in wastewater treatment and in *situ* chemical oxidation of contaminated soil and groundwater. Chelated iron and peroxide activated PDS were applied during full-scale field projects to treat contaminated soil and groundwater (e.g., chlorinated solvent contaminants). The combination of PDS and PMS with UV generates sulfate radical ($SO_4^{\bullet-}$), which is considered as a potential alternative for the removal of refractory contaminants.

Several knowledge gaps need to be investigated to support the application of UV-AOPs in wastewater treatment for TOrCs removal and disinfection, as well as to compare their efficiency with conventional chemical treatments.

First, as compared to $^{\bullet}OH$ known as a non-selective entity which reacts with almost all organic moieties at diffusion-controlled rates, thus easily affected by the water matrix components (e.g., dissolved organic matter, DOM), the reactivity of selective radicals (e.g., $SO_4^{\bullet-}$) with a variety of TOrCs in natural and waste waters are not well-documented. Most of the previous studies on UV/PDS were conducted at lab-scale with synthetic waters (e.g., phosphate buffer) with few or individual water matrix competitors. The foci of these studies were mostly on a single contaminant or a group of contaminants with common structures (e.g., sulfonamide antibiotics), which have comparable reactivity with $SO_4^{\bullet-}$, consequently not representing the mixture of TOrCs identified in the aquatic environment. It is not clear if selective radicals (e.g., $SO_4^{\bullet-}$) are more powerful oxidants than $^{\bullet}OH$ toward certain contaminants, especially in complex water matrix.

Second, it has been widely accepted that radicals play a major role for the degradation of TOrCs during AOPs. However, the reaction mechanisms of some AOPs are still not fully understood. The unique asymmetric structure of PMS makes it more reactive than H_2O_2 or PDS. Thus, the direct oxidation of organic contaminants by PMS during PMS-based AOPs cannot be ignored.

Third, the efficiency of UV-AOPs for the inactivation of ARB and the degradation of mobile genetic elements (e.g., cell-free DNA carrying ARG) did not receive a lot of attention to date. The intact remnant of DNA, which is released into the environment following the death of ARB cell, is still able to confer ARGs to non-resistant bacteria via horizontal gene transfer. Considering the capability of bacteria cells to repair DNA

lesions, it is important to study the efficiency of damaged DNA repair and uptake (gene transfer) by non-resistant recipient cells after various UV and radical exposure processes.

Fourth, even though conventional disinfection processes (e.g., chlorine and monochloramine) have been successfully applied for decades in water treatment to inactivate traditional pathogenic microorganisms, their efficiency to control the spread of antibiotic resistance still needs better understanding. As mentioned above, special attention should be paid to the elimination of ARG in parallel with the inactivation of ARB cells. While the classic cultivation-based methods (i.e., plate counts) is known to be time consuming with limited efficacy to detect the removal of ARG, there is a growing demand on the application of alternative approaches (e.g., flow cytometric analysis combing with nuclei acids staining) to comprehensively study the mitigation of antibiotic resistance dissemination during conventional disinfection processes.

Fifth, the efficiency of conventional chemical treatments and UV-AOPs should be evaluated in the presence of real water matrix components. Chlorination of ammonia and bromide containing water produces secondary oxidants, such as chloramines, bromine, and bromamines. Few studies have discussed the role of these reactive oxidant species as disinfectant to remove ARB/ARGs. The reactive species arising from the excitation of chromophoric DOM upon UV irradiation might also contribute to the elimination of target contaminant. However, DOM acts as radical sink during AOPs which reduces the efficiency of the treatment and leads to the formation of undesired products (e.g., disinfection by-products, DBPs). Although chloramination is known to reduce the formation of regulated DBPs (i.e., trihalomethanes and haloacetic acids) compared to chlorination, monochloramine (NH_2Cl) can be an additional source of nitrogen and produces highly toxic nitrogenous-DBPs, the majority fraction of which is still unknown.

This doctoral thesis was aimed to contribute to the above knowledge gaps.

Chapter 2 compared the elimination of TOrCs during UV/H_2O_2 and UV/PDS. Twelve TOrCs spaning a range of photolytic reactivity were selected based on their frequent detection in wastewater and their different physicochemical characteristics. The second-order rate constants of iopromide, phenytoin, caffeine, benzotriazole, and

primidone with $SO_4^{\bullet-}$ were reported for the first time. Lab-scale experiments were conducted in buffered pure water and wastewater effluent to study the influence of the water matrix. Results indicated that UV/PDS was more efficient than UV/H_2O_2 in buffered pure water due to the higher quantum yield of PDS at 254 nm and the lower scavenging capacity of phosphate buffer matrix on $SO_4^{\bullet-}$. However, UV/PDS showed more selectivity than UV/H_2O_2 in wastewater effluent and preferentially oxidized compounds with electron-rich moieties (e.g., diclofenac, venlafaxine, and metoprolol). The fluence-based rate constants of TOrCs (k_{obs}) during UV/H_2O_2 linearly increased with the increase of the H_2O_2 dose, indicating the constant scavenging effect of the water matrix on $^{\bullet}OH$. However, k_{obs} values determined for most TOrCs during UV/PDS showed a lag-phase at low PDS dose due to the competition between the water matrix (i.e., electron-rich site of effluent organic matter) and target contaminant. Pilot-scale experiments conducted at WWTP suggested that the performance of UV/PDS was strongly affected by DOC and nitrite.

While the wastewater matrix significantly reduced the efficiency of radical-based UV-AOPs, Chapter 3 reported a non-radical degradation pathway of TOrCs with PMS, which was less influenced by the presence of the water matrix components. Fluoroquinolones, one of most consumed antibiotics in the world, were found to be degraded by PMS without radical involvement. High resolution mass spectrometry analysis indicated that reaction was induced by direct electron transfer from the nitrogen moiety of fluoroquinolones (i.e., piperazine ring) to PMS, followed by the formation of amide and aldehyde molecules. Antibacterial activity tests suggested the good removal of antibacterial activity with the complete degradation of parent antibiotic, with the exception of the transformation products at the earlier stage of the reaction which might still exert antibacterial potency. Antibiotics and their antibacterial active transformation products can induce the development of antibiotic resistance in bacterial population.

Chapter 4 was dedicated to the inactivation of *Stenotrophomonas maltophilia* (*S. maltophilia*) during chemical oxidation and UV-AOPs. *S. maltophilia* is a multi-drug resistant bacteria which was isolated from the secondary effluent of a WWTP. A cultivation-independent method, flow cytometric analysis based on nucleic acids staining with the combination of SYBR Green I and propidium iodide was applied to

detect cells with damaged membranes. SYBR Green I stains all cells with nucleic acids regardless of membrane integrity while propidium iodide only enters cells with permibilized membrane. Membrane damage is a widely recognized indicator of cell death. Plate counting analysis based on the cultivability of cells was additionally applied for UV-AOP experiments. The efficiency of reactive oxidant species present in chlorinated water in the presence of ammonia and bromide, namely chlorine (HOCl), NH_2Cl, bromine (HOBr), and monobromamine (NH_2Br), were compared. Results showed that the membrane damage rates of *S. maltophilia* followed the order of: HOBr > HOCl > NH_2Br >> NH_2Cl. Based on plate counting analysis, UV direct irradiation, UV/H_2O_2, and UV/PDS efficiently led to cultivability loss of *S. maltophilia* (5.7-log at 22 mJ/cm^2). Flow cytometry results indicated that UV direct irradiation didn't cause significant membrane damage and comparable results were obtained from UV/H_2O_2 due to the substantial scavenging of $^{\bullet}OH$ by cell membrane components. Notably, UV/PDS dramatically diminished the green fluorescence intensity (SYBR Green I) on flow cytometry, most likely attributable to the nuclei acids damage induced by sulfate radical ($SO_4^{\bullet-}$). The formation of "injured" cells with partly compromised membrane were detected on flow cytometry when *S. maltophilia* was subjected to weak oxidants (i.e., NH_2Cl and NH_2Br) or strong oxidants (i.e., HOCl and HOBr) at low dose, which can be problematic during water disinfection processes, considering the potential of "injured" cells to transfer genes and recover. Overall results indicated that strong or non-selective oxidants (e.g., HOCl, HOBr, and $^{\bullet}OH$) were easily consumed by cell membrane components, whereas weaker or selective oxidants (e.g., NH_2Br and $SO_4^{\bullet-}$) can penetrate into ARB cell to reach the intracellular components, consequently demonstrating high potential of degrading ARGs.

Chapter 5 presents a more detailed work on the degradation of ARGs. The removal of cell-free DNA carrying ARG (i.e., ampicillin resistance gene, amp^R) by UV/H_2O_2 and UV/PDS were investigated at 254 and 300 nm. Quantitative polymerase chain reaction (qPCR) was applied to measure gene damage. Based on competition kinetics, the second-order rate constants of $^{\bullet}OH$ with amp^R segments were in the range of 10^{10}–10^{11} M^{-1} s^{-1}, which were 2−3 orders of magnitude higher than that of $SO_4^{\bullet-}$ (i.e., 10^7–10^9 M^{-1} s^{-1}). Thus, the trace amount of $^{\bullet}OH$ produced from $SO_4^{\bullet-}$ reaction with water mainly contributed to the degradation of ARG during UV/PDS. DNA electrophoresis gel images suggested that UV direct irradiation didn't induce conformational change

on plasmid DNA while radical exposure altered the base pair region and changed the supercoiled structure. Although qPCR results showed that radicals significantly promoted the degradation of ARG compared to UV direct irradiation, gene transformation assays suggested that DNA damage induced by radical exposure can be repaired within non-resistant recipient cells (*E.Coli* DH5α). Consequently, the reduction of gene transfer activity during UV/H_2O_2 (0.5 mM) and UV/PDS (0.5 mM) was only 1-log within the typical UV disinfection dose (40 mJ/cm^2 at 254 nm). UV/H_2O_2 and UV/PDS at 300 nm exhibited less efficiencies than that at 254 nm due to the lower UV absorbance of DNA and less formation of radicals at high wavelength. The presence of DOM (5.4 mg-C/L of effluent organic matter extract) accelerated the degradation of amp^R upon UV direct irradiation at 254 nm possibly because of the formation of reactive species induced by the excitation of chromophoric DOM (photosensitiser property); however DOM significantly reduced the gene degradation rates of UV/H_2O_2 and UV/PDS by scavenging radicals.

DOM in the water matrix also acts as DBPs precursors, especially during conventional chlorination and chloramination processes. As an example, chapter 6 reported that the inorganic nitrogen coming from monochloramine can incorporate into the phenolic moieties of DOM (e.g., resorcinol) to produce the known nitrogenous DBPs (e.g., dichloroacetonitrile, dichloroacetamide) as well as several nitrogenous heterocyclic compounds, which were structurally similar to MX (3-chloro-4-(dichloromethyl)-5-hydroxy-2(5H)-furanone), the strongest mutagen identified in chlorinated drinking water.

Table of Contents

List of Tables

Chapter 2−6:

Appendix 1−4:

List of Figures

Chapter 2−6:

List of Abbreviations

amp^R	Ampicillin Resistance Gene
AOP	Advanced Oxidation Process
ARB	Antibiotic Resistant Bacteria
ARG	Antibiotic Resistance Gene
C-DBPs	Carbonaceous Disinfection By-products
CIP	Ciprofloxacin
CPDs	Cyclobutane-Pyrimidine Dimers
DCAA	Dichloroacetic Acid
DCAcAl	Dichloroacetaldehyde
DCAcAm	Dichloroacetamide
DCAN	Dichloroacetonitrile
DOC	Dissolved Organic Carbon
E.coli	*Escherichia. coli*
EfOM	Effluent Organic Matter
ENR	Enrofloxacin
FEEM	Fluorescence Excitation-Emission Matrix
FLU	Flumequine
GC-QTOF	Gas Chromatography-Quadrupole Time-of-Flight Mass Spectrometry
HAAs	Haloacetic Acids
HAcAms	Haloacetamides
HANs	Haloacetonitriles
HPC	Heterotrophic Plate Counts
LC-HRMS	Liquid Chromatography-High Resolution Mass Spectrometry
LOQ	Limit of Quantification

LED	Light-Emitting Diode
MCAA	Monochloroacetic Acid
MET	Metoprolol
NB	Nitrobenzene
N-DBPs	Nitrogenous Disinfection By-products
NOM	Natural Organic Matter
NOR	Norfloxacin
*p*CBA	*para*-Chlorobenzoic Acid
PDS	Peroxydisulfate
PI	Propidium Iodide
PMS	Peroxymonosulfate
qPCR	Quantitative Polymerase Chain Reaction
SGI	SYBR Green I
S. maltophilia	*Stenotrophomonas Maltophilia*
t-BuOH	*tert*-Butanol
TCAA	Trichloroacetic Acid
TCAcAl	Trichloroacetaldehyde
TCAcAm	Trichloroacetamide
TCEP	Tris (2-Chloroethyl) Phosphate
THMs	Trihalomethanes
TOrCs	Trace Organic Chemicals
TOX	Total Organic Halogen
UVT	UV-Transmittance at 254 nm
VEN	Venlafaxine
WWTP	Wastewater Treatment Plant

List of Publications and Presentations Arising from this Thesis

Peer-reviewed journal articles

Nihemaiti, M., Miklos, D. B., Hübner, U., Linden, K. G., Drewes, J. E., and Croué, J.-P. (2018). Removal of Trace Organic Chemicals in Wastewater Effluent by UV/H_2O_2 and UV/PDS. *Water Research*, 145, 487-497

Nihemaiti, M., Le Roux, J., Hoppe-Jones, C., Reckhow, D. A., and Croué, J.-P. (2017). Formation of Haloacetonitriles, Haloacetamides, and Nitrogenous Heterocyclic By-products by Chloramination of Phenolic Compounds. *Environmental Science & Technology*, 51(1), 655-663

Nihemaiti, N., Permala, R., and Croué, J.-P. (2018). Degradation of Fluoroquinolones by Peroxymonosulfate: Transformation Products and Non-radical Reaction Mechanism with Nitrogenous Moieties (to be submitted to *Environmental Science and Technology*)

Nihemaiti, N., Glady- Croué, J., Edmands, J., Permala, R., Allard, S., and Croué, J.-P. (2018). Inactivation of Antibiotic Resistant Bacteria during Conventional and Advanced Oxidation Processes (to be submitted to *Environmental Science: Water Science and Technology*)

Nihemaiti, N., Yoon Y., Lee, Y., and Croué, J.-P. (2018). Degradation of Extracellular Antibiotic Resistance Genes and Elimination of Gene Transforming Activity during UV/H2O2 and UV/PDS (to be submitted to *Water Research*)

Oral presentations

M. Nihemaiti, D.B. Miklos, U. Hübner, K. G. Linden, J. E. Drewes, and J.P Croué. "Degradation of Micropollutants in Wastewater Effluent by UV/H_2O_2 and UV/PDS". IWA 15th Leading Edge Conference on Water and Wastewater Technologies, May 2018, Nanjing, China.

M. Nihemaiti, R. R. Permala and J.P. Croué. “Degradation of Ciprofloxacin in PMS/$CuFe_2O_4$ System: Effect of PMS and Natural Organic Matter”. IWA 10th Micropol and Ecohazard Conference, Sep 2017, Vienna, Austria.

M. Nihemaiti, J. Le Roux, C. Hoppe-Jones and J.P. Croué. “Formation of Haloacetonitriles, Haloacetamides and Nitrogenous Heterocyclic Compounds from Chloramination of Resorcinol”. 252nd ACS National Meeting and Exposition, Aug 2016, Philadelphia, USA.

Poster presentation

M. Nihemaiti, R. Permala, and J.P Croué. “Efficient Degradation of Fluoroquinolone Antibiotics by Peroxymonosulfate without Generation of Radicals”, Gordon Research Conference: Environmental Science _Water, June 2018, Boston, USA

Chapter 1. Thesis Overview

This dissertation contains 7 chapters. Chapter 1 introduces the thesis outline. Chapters 2−6 are presenting the results and the discussions of the different research topics developed during this PhD project, including two published peer-reviewed articles and 3 manuscripts nearly ready for submission. Chapter 7 gives the general conclusions and future perspectives. Supporting information for all journal articles and manuscripts being submitted are presented in Appendix 1−4. Publisher permissions for including published articles in thesis are attached as Appendix 5.

Chapter 2 presents the removal of trace organic chemicals (TOrCs) in wastewater effluent during UV/AOPs. This was a comparative investigation on UV/hydrogen peroxide (H_2O_2) and UV/peroxydisulfate (PDS) in terms of selected TOrCs elimination. Lab-scale experiments on UV/H_2O_2 and UV/ PDS were conducted with a collimated beam device with a low pressure UV lamp emitting light at 254 nm. Pilot-scale UV/PDS was carried out at a municipal wastewater treatment plant in Germany (collaboration with the Chair of Urban Water Systems Engineering, Technical University of Munich) under real feed water conditions. This work was published in Water Research: "Nihemaiti, M., Miklos, D. B., Hübner, U., Linden, K. G., Drewes, J. E., and Croué, J.-P. (2018). Removal of trace organic chemicals in wastewater effluent by UV/H_2O_2 and UV/PDS. Water Research, 145, 487-497".

The focus of Chapter 3 is non-radical mechanism of peroxymonosulfate (PMS) oxidation processes. Fluoroquinolone antibiotics, as well as other secondary (metoprolol) and tertiary (venlafaxine) nitrogenous compounds were treated by PMS. Quenching studies for the identification of reactive species and influence of common water matrix components were investigated. Transformation products of ciprofloxacin after PMS exposure were identified on high resolution mass spectrometer and reaction mechanisms were proposed. Agar diffusion tests were applied to investigate the residual antibacterial potency of ciprofloxacin and its transformation products. This work will be submitted to Environmental Science & Technology soon for peer-review.

Chapter 4 describes the inactivation of *Stenotrophomonas maltophilia* (*S. maltophilia*) during chemical oxidation and UV-based advanced oxidation processes. *S. maltophilia* was isolated from wastewater effluent and demonstrated to be a multi-drug resistant bacteria. Flow cytometric analysis combined with nucleic acid staining was applied to measure the membrane damage of *S. maltophilia* during various treatments. Plate

counting analysis was additionally applied for UV/AOPs to monitor the cultivability loss *S. maltophilia*. This work will be submitted to Environmental Science: Water Research & Technology for peer-review.

Chapter 5 focus on the degradation of extracellular antibiotic resistance genes (ARGs) during UV/ H_2O_2 and UV/PDS. Extracellular ARGs (i.e., ampicillin resistance gene, amp^R) were prepared by extracting plasmids from ampicillin resistant *E.Coli* DH5α. Two different UV wavelengths were applied for the photolysis of H_2O_2 and PDS (i.e., 254 and 300 nm) and the latter was designed to simulate the sunlight irradiation processes. Gene damage was measured by quantitative Polymerase Chain Reaction (qPCR). Gel electrophoresis analysis was conducted to investigate the conformational changes on plasmid DNA after treatments. Gene transformation assays were carried out to study the transfer of amp^R to non-resistant bacteria. These results were obtained with the collaboration of Gwangju Institute of Science and Technology in South Korea (Professor Yunho Lee's research group), and are going to be submitted to Water Research.

Chapter 6 presents the formation of nitrogenous disinfection by-products from chloramination of nitrogenous and non-nitrogenous aromatic compounds. Several previously unknown nitrogenous heterocyclic compounds were identified by high resolution Quadrupole Time-of-Flight GC–MS (GC–QTOF). This work was published in Environmental Science and Technology: "Nihemaiti, M., Le Roux, J., Hoppe-Jones, C., Reckhow, D. A., and Croué, J.-P. (2017). Formation of Haloacetonitriles, Haloacetamides, and Nitrogenous Heterocyclic By-products by Chloramination of Phenolic Compounds. Environmental Science & Technology, 51(1), 655-663".

Chapter 7 is a summary of results from Chapters 2−6, as well as recommendations for future research.

Chapter 2. Removal of Trace Organic Chemicals in Wastewater Effluent by UV/H_2O_2 and UV/PDS

Maolida Nihemaiti, David B. Miklos, Uwe Hübner, Karl G. Linden, Jörg E. Drewes, and Jean-Philippe Croué

Water Research, Volume 145, 15 November 2018, Pages 487-497

DOI: https://doi.org/10.1016/j.watres.2018.08.052

Statement of Contribution to Co-authored Published Paper

This Chapter includes the co-authored paper "Removal of Trace Organic Chemicals in Wastewater Effluent by UV/H_2O_2 and UV/PDS", published on Water Research. The bibliographic details of the co-authored paper, including all authors are:

Nihemaiti, M., Miklos, D. B., Hübner, U., Linden, K. G., Drewes, J. E., and Croué, J.-P. (2018). Removal of trace organic chemicals in wastewater effluent by UV/H_2O_2 and UV/PDS. Water Research, 145, 487-497.

I, Maolida Nihemaiti, as the primary author, conducted all the experimental work and data analysis, including creating figures and tables, and writing and editing the manuscript.

I, as a Co-Author, endorsed that this level of contribution by the candidate indicated above is appropriate.

David B. Miklos
Uwe Hübner
Karl G. Linden
Jörg E. Drewes
Jean-Philippe Croué

2.1 Abstract

In this study, we comparatively investigated the degradation of 12 trace organic chemicals (TOrCs) during UV/H_2O_2 and UV/peroxydisulfate (PDS) processes. Second-order rate constants for the reactions of iopromide, phenytoin, caffeine, benzotriazole and primidone with sulfate radical ($SO_4^{\bullet-}$) were determined for the first time. Experiments were conducted in buffered pure water and wastewater effluent with spiked TOrCs. UV/PDS degraded all TOrCs more efficiently than UV/H_2O_2 in buffered pure water due to the higher yield of $SO_4^{\bullet-}$ than that of hydroxyl radical ($^{\bullet}OH$) at the same initial molar dose of PDS and H_2O_2, respectively. UV/PDS showed higher selectivity toward TOrCs removal than UV/H_2O_2 in wastewater effluent. Compounds with electron-rich moieties, such as diclofenac, venlafaxine and metoprolol, were eliminated faster in UV/PDS whereas UV/H_2O_2 was more efficient in degrading compounds with lower reactivity to $SO_4^{\bullet-}$. The fluence-based rate constants (k_{obs-UV/H_2O_2}) of TOrCs in wastewater effluent linearly increased as a function of initial H_2O_2 dose during UV/H_2O_2, possibly due to the constant scavenging impact of the wastewater matrix on $^{\bullet}OH$. However, exponential increase of $k_{obs-UV/PDS}$ with increasing PDS dose was observed for most compounds during UV/PDS, suggesting the decreasing scavenging effect of the water matrix (electron-rich site of effluent organic matter (EfOM)) after initial depletion of $SO_4^{\bullet-}$ at low PDS dose. Fulvic and humic-like fluorophores appeared to be more persistent during UV/H_2O_2 compared to aromatic protein and soluble microbial product-like fluorophores. In contrast, UV/PDS efficiently degraded all identified fluorophores and showed less selectivity toward the fluorescent EfOM components. Removal pattern of TOrCs during pilot-scale UV/PDS was consistent with lab-scale experiments, however, overall removal rates were lower due to the presence of higher concentration of EfOM and nitrite.

2.2 Introduction

Trace organic chemicals (TOrCs) including pharmaceutical residues, personal care products and industrial chemicals are present in surface water, groundwater, wastewater effluents, reclaimed water and even in drinking water (Coday et al., 2014). Regardless of their relatively low occurrence (i.e., few ng/L to several µg/L), TOrCs in aquatic resources have been a growing concern due to their potential adverse effects on human health and ecosystem, such as endocrine disruption, spread of antibiotic resistance, and bioaccumulation (Dodd, 2012; Belhaj et al., 2015). Insufficiently treated effluent from municipal wastewater treatment plant (WWTP) is considered as one of the main sources of TOrCs to the aquatic environment. Many TOrCs are persistent during conventional biological and chemical treatment processes in WWTP. The removal efficiency of TOrCs always depends on their physicochemical and biological properties, as well as the removal principles of individual treatment processes (Grandclément et al., 2017).

Advanced oxidation processes (AOPs) involving the generation of powerful oxidant species, such as hydroxyl radicals ($^{\bullet}OH$), chlorine radicals ($Cl^{\bullet}$) and sulfate radicals ($SO_4^{\bullet-}$), have gained increasing interests as an alternative way to remove refractory and/or non-biodegradable pollutants (Huber et al., 2003; Wols et al., 2013; Lian et al., 2017).

Removal of TOrCs by hydroxyl radical-based AOPs has been extensively studied (Miklos, Remy, et al., 2018). Hydroxyl radical is a strong oxidant (1.8−2.7 V, depending on solution pH) with low selectivity (Neta et al., 1988). Previous studies confirmed the high potential of UV/H_2O_2 to remove TOrCs from WWTP effluents (Wols et al., 2015; Miklos, Hartl, et al., 2018). However, some TOrCs are resistant to $^{\bullet}OH$, such as tris-(2-chloroethyl)-phosphate (TCEP) and tris-(2-chloroisopropyl)-phosphate (Gerrity et al., 2011). Although UV/H_2O_2 process effectively limits the formation of toxic by-products (i.e., NDMA, bromate) as compared to ozonation or O_3/H_2O_2 and reduces the formation of disinfection by-products (e.g., haloacetamides) as a pre-oxidation (Chu et al., 2014), the process needs high energy input due to the low UV molar absorbance of H_2O_2 (e.g., 18.6 $M^{-1}cm^{-1}$) to generate sufficient $^{\bullet}OH$, especially in complex water matrix (Lee et al., 2016). High reactivity of $^{\bullet}OH$ with water matrix components (e.g., organic matter, carbonate, nitrite) results in a low

steady-state $^{\bullet}OH$ concentration that is available to degrade target contaminants (Rosario-Ortiz et al., 2010; Lee et al., 2013).

Sulfate radical (2.5−3.1 V) has a comparable or even higher redox potential than $^{\bullet}OH$ (Neta et al., 1988). Unlike $^{\bullet}OH$, $SO_4^{\bullet-}$ reacts mainly through electron transfer, less by addition or H-atom abstraction (Neta et al., 1988), which makes $SO_4^{\bullet-}$ more selective to compounds with electron-rich moieties (Li et al., 2017). Recent statistical analysis indicated that TOrCs with electron-donating groups (e.g., $-NH_2$, $-OH$) have higher second-order rate constants with $SO_4^{\bullet-}$ than compounds with electron-withdrawing groups (e.g., $-COOH$) (Ye et al., 2017). $SO_4^{\bullet-}$ can be generated from the activation of peroxydisulfate (PDS) or peroxymonosulfate by transition metal ions, heating, UV irradiation, and quinones (Ike et al., 2018).

Limited studies are available on the removal of TOrCs during sulfate radical-based AOPs. Previous work has reported the efficient degradation of cyanotoxin cylindrospermopsin (He et al., 2014), chlorotriazine pesticides (Holger V. Lutze et al., 2015), and sulfonamide antibiotics (R. Zhang et al., 2016) by $SO_4^{\bullet-}$. Contaminants that show low reactivity to $^{\bullet}OH$ can be degraded by $SO_4^{\bullet-}$, such as perfluorocarboxylic acids (Hori et al., 2005). Recent studies comparing UV/H_2O_2 and UV/PDS treatment of pharmaceuticals present in reverse osmosis brines (Yang et al., 2016) and wastewater effluent (Lian et al., 2017) confirmed that $SO_4^{\bullet-}$ reacted more selectively than $^{\bullet}OH$. UV/PDS was reported to effectively control the formation of nitrogenous disinfection by-products in organic nitrogen-rich waters (Chu et al., 2015). The removal of TOrCs during UV/AOPs was recently assessed at full-scale WWTP and radical-based processes (e.g., UV/H_2O_2 and UV/peroxymonosulfate) were proven to be more efficient than UV direct irradiation (Rodríguez-Chueca et al., 2018). Similar to $^{\bullet}OH$, $SO_4^{\bullet-}$ is also scavenged by organic matter and inorganic ions in the water matrix, which further reduces the degradation efficiency of TOrCs (T. Zhang et al., 2013; H. V. Lutze et al., 2015).

The aim of this study was to investigate the removal efficiency of TOrCs by UV/PDS in comparison to UV/H_2O_2. $SO_4^{\bullet-}$ and $^{\bullet}OH$ were generated by UV irradiation (low pressure UV lamp) of PDS and H_2O_2, respectively. Experiments were conducted in pure water (5 mM phosphate buffer) and municipal WWTP effluent with spiked TOrCs to study the influence of the water matrix on treatment efficiency. Additionally,

pilot-scale experiments were carried out at a municipal WWTP to explore the feasibility of UV/PDS treatment under real feed water conditions.

2.3 Materials and Methods

2.3.1 Chemical reagents

All TOrCs and isotope labeled analytical standards for TOrCs analysis were of analytical grade. Details on TOrCs were provided in Appendix 1 (Table A-1-1). All solvents used for Liquid Chromatography were in HPLC-grade. A mixture of all TOrCs was prepared in Milli-Q water with a concentration of 0.5 mg/L for each compound. Hydrogen peroxide 30% (Thermo Fisher Scientific) and sodium persulfate (≥98%, Sigma-Aldrich) were used to prepare the stock solutions of H_2O_2 and PDS, respectively.

2.3.2 Wastewater treatment plant effluent

The WWTP Gut Marienhof (Munich, Germany) treats wastewater from the city of Munich. The treatment plant consists of a mechanical treatment stage including screens, aerated sand/fat traps and preliminary sedimentation, followed by a two-stage activated sludge process for biological carbon and nutrient removal (solids retention time of 2−3 and 6−8 days, respectively). The water is then filtered using tertiary granular media filters with a resulting UV-transmittance at 254 nm (UVT) of 65−75% prior to UV disinfection. In this study, samples were collected directly after granular media filtration. Hach cuvette tests were applied to measure bulk water parameters. Dissolved organic carbon (DOC) was analyzed on a vario TOC cube (Elementar, Germany) after filtration through cellulose nitrate membrane filters (0.45 µm, Sartorius AG, Germany). The concentrations of relevant parameters in WWTP effluent are summarized in Table 2-1.

Table 2-1. Water quality parameters of WWTP effluent[a] and the scavenging capacity of each componentb for •OH and $SO_4^{\bullet-}$

	Lab-scale experiments			Pilot-scale experiments	
	Concentration	Scavenging capacity (s^{-1})		Concentration	Scavenging capacity (s^{-1})
		UV/H_2O_2	UV/PDS		UV/PDS
DOC (mg-C/L)	6.8	2.23×10^5	6.35×10^4	10.7	1.01×10^5
Bicarbonate (mg/L)	307	4.33×10^4	1.41×10^4	319	1.47×10^4
Nitrite (mg-N/L)	0.028	2×10^4	1.76×10^3	0.15	9.28×10^3
Nitrate (mg-N/L)	10.6	<75	22.7	13.5	29.0
Chloride[c] (mg/L)	110±13	NA	$9.30\pm1.10\times10^5$	110±13	$9.30\pm1.10\times10^5$
UV_{254} (m^{-1})	14.5			16.7	
pH	7.4			7.5	

[a] WWTP effluent samples used for lab and pilot-scale experiments were from different days (i.e., 17/10/16 and 03/11/16, respectively); [b] Calculated by multiplying the molar concentration of each component with its second-order reaction rate constants with radicals. Reaction rate constants and references are provided in Table A-1-2; [c] Annual average concentration; NA: not applicable

2.3.3 Trace organic chemicals analysis

All samples were filtered through 0.22 µm PVDF syringe filters (Berrytec, Germany) before TOrCs quantification. Samples were measured using a high-performance liquid chromatography (Knauer PLATINBLUE UHPLC) coupled with a tandem mass spectrometry (LC-MS/MS) (SCIEX QTRAP 6500) by direct injection. Isotope dilution was used to account for matrix suppression and instrument response. A detailed description of the analytical method was reported elsewhere (Müller et al., 2017). The concentrations of TOrCs in wastewater effluent during lab- and pilot-scale experiments are presented in Table 2-2.

Table 2-2. Fluence-based rate constants [a], second-order rate constants and initial concentrations of TOrCs

Compounds	Fluence-based rate constant (k_{obs-UV}) (10^{-4} cm² mJ^{-1})	Second-order rate constants (10^9 M^{-1} s^{-1})		Initial concentration (ng/L)	
		$k_{\bullet OH}$	$k_{SO_4^{\bullet-}}$	Lab-scale[b]	Pilot-scale[c]
Group I: k_{obs-UV} > 1×10^{-3} cm² mJ^{-1}					
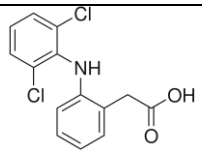 Diclofenac	68.3 (R^2=0.99)	8.38±1.24[d]	9.2±0.6[e]	3,601	2,979±60
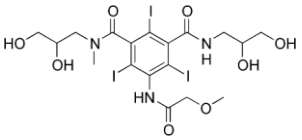 Iopromide	26.5 (R^2=0.99)	3.3±0.6[f]	0.36±0.07 (in this study)	2,867	6,268±469
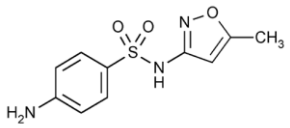 Sulfamethoxazole	19.7 (R^2=0.99)	5.82±1.99[d]	12.5±1.9[e]	1,564	348±30
Group II: 1×10^{-4} < k_{obs-UV}< 1×10^{-3} cm² mJ^{-1}					
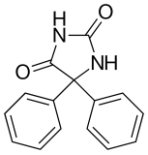 Phenytoin	7.74 (R^2=0.97)	6.28[g]	0.62±0.02 (in this study)	1,082	13±2
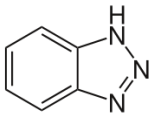 Benzotriazole	2.21 (R^2=0.86)	8.34±0.37[h]	0.87±0.03 (in this study)	9,552	9,490±391
Group III: k_{obs-UV}< 1×10^{-4} cm² mJ^{-1}					
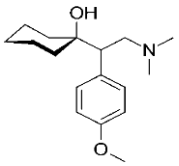 Venlafaxine	0.54 (R^2=0.65)	8.8±1.5[i]	3.53±0.05[j] 4.99±0.05 (in this study)	1,245	630±31
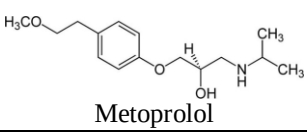 Metoprolol	0.30 (R^2=0.60)	7.84±0.77[d]	5.11±0.12[j] 3.89±0.01 (in this study)	1,453	551±7
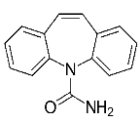 Carbamazepine	< 1	8.02±1.9[d]	1.92±0.01[k] 1.50±0.21 (in this study)	1,737	650±40

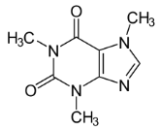 Caffeine	< 1	6.4±0.71[d]	2.39±0.18 (in this study)	965	71±32
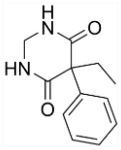 Primidone	< 1	6.7±0.2[l]	0.53±0.03 (in this study)	1,048	124±4
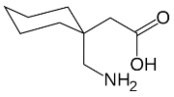 Gabapentin	< 1	9.1[m]	< 1[n]	3,013	4,404±93
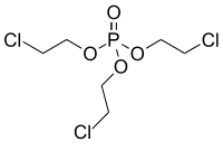 TCEP	< 1	0.56[o]	< 1[n]	1,312	125±6

[a] Obtained during direct UV photolysis of TOrCs in wastewater effluent (115−1,380 mJ/cm^2). The exact k_{obs-UV} was not calculated for group III (except venlafaxine and metoprolol) due to their low removal (see section 3.1); [b] Sum of background and spiked concentrations; [c] Average concentration from triplicated samplings within 6 hours; [d] Wols and Hofman-Caris (2012) ; [e] Mahdi Ahmed et al. (2012); [f] Huber et al. (2003); [g] Yuan et al. (2009); [h] Bahnmüller et al. (2015); [i] Wols et al. (2013); [j] Lian et al. (2017); [k] Matta et al. (2011); [l] Real et al. (2009); [m] Lee et al. (2014); [n] Estimated in this study (see Text S3); [o] Watts and Linden (2009).

2.3.4 Fluorescence excitation-emission matrix analysis

Fluorescence excitation-emission matrix (FEEM) were recorded using an Aqualog Fluorescence Spectrometer (Horiba Scientific, Germany). Four fluorescence peaks were selected from different regions on fluorescence spectra previously defined by Chen et al. (2003). The fluorescence intensities of selected peaks were used as representative indices of effluent organic matter (EfOM) in wastewater to study the effect of radical exposure on EfOM during UV/H_2O_2 and UV/PDS (Sgroi et al., 2017). More information on FEEM analysis is provided in Appendix 1 (Text A-1-1).

2.3.5 Lab-scale experiments

Bench-scale experiments were conducted using a LP-UV collimated beam device following the standard operation procedure suggested by Bolton and Linden (2003). The collimated beam device contained three 15 W low-pressure Hg UV-lamps (UV Technik Meyer, Germany). To precisely determine the petri factor, a xy-cross slide table with a magnetic stirrer was placed below the collimator, on top of which was the

mounting for the petri dishes. Average UV-C intensity across the petri dish was determined as 1–1.4 mW/cm^2 by a certified UV-C radiometer (UV-surface-D, sglux, Germany).

Fluences were applied to 30 mL of solution in a 100 mm glass petri dish. Experiments were conducted in solutions prepared with 5 mM of phosphate buffer (pH 7) (57.5−920 mJ/cm²) and wastewater effluent (115−1,380 mJ/cm²) spiked with 1 µg/L of each TOrC. Due to the natural buffering capacity of wastewater effluent (i.e., bicarbonate=307 mg/L, Table 2-1), its pH remained stable at pH 7.4 throughout UV-AOP experiments. H_2O_2 and PDS were added directly from stock solutions before UV-exposure. 0.15 mM of oxidant was applied for buffered pure water experiments. The oxidant doses used for wastewater effluent experiments were 0.15, 0.30, 0.45, and 0.60 mM. Dark experiments to investigate the effect of H_2O_2 and PDS on TOrCs attenuation were conducted in duplicates for 30 minutes and 24 hours with oxidant dose of 0.15, 0.30, 0.45, and 0.60 mM. Residual oxidants were quenched with excess sodium thiosulfate at the end of each experiment. All samples were stored in amber glass bottles at 4°C and analyzed for TOrCs within 24 hours.

The second-order rate constants for the reaction of TOrCs with $SO_4^{\bullet-}$ were determined by competition kinetics based on the methods published before (Holger V. Lutze et al., 2015; Lian et al., 2017). *para*-chlorobenzoic acid (*p*CBA) was used as a probe compound, k ($SO_4^{\bullet-}$ + *p*CBA) = 3.6×10^8 M^{-1} s^{-1} (Neta et al., 1977). Experiments were conducted in phosphate buffer (2.5 mM) at pH=7 with 20 µM of *p*CBA and target compound. $SO_4^{\bullet-}$ was generated by UV photolysis of PDS (1 mM). 10 mM of *tert*-Butanol was added as $^{\bullet}OH$ scavenger. Nitrobenzene (1 µM) was monitored to confirm that $^{\bullet}OH$ was scavenged efficiently by 10 mM of *tert*-Butanol. The concentrations of *p*CBA and TOrCs were analysed on a HPLC (Agilent 1100) equipped with an Agilent XDB-C18 column (5 µm, 4.6 × 150 mm). Details on competition kinetic experiments are provided in Text A-1-2.

2.3.6 Pilot-scale experiments

Pilot-scale UV/PDS investigations were conducted using a container-based AOP system designed by WEDECO (Xylem, Germany) consisting of two LP-UV reactors (WEDECO LBX 90e and LBX 10, Xylem, Germany) operated to deliver the required fluence range. The pilot system was fed with wastewater effluent delivered by an

external process water pump station at WWTP Gut Marienhof (Munich, Germany) directly after tertiary granular media filtration. Specific details about the pilot system are described elsewhere (Miklos, Hartl, et al., 2018).

For pilot-scale experiments, fluences were set by adjusting flow rates to current UV-intensities, and UVT in each reactor. Fluence of 200, 400 and 800 mJ/cm^2 were maintained in reactor LBX 10, while 1,200 mJ/cm² was maintained in reactor LBX 90e. Oxidant dosing was targeted at concentrations of 0.30 and 0.60 mM and was adjusted based on the flow rate. The concentration of PDS was determined iodometrically (Liang et al., 2008). Before sampling, the system was constantly operated with a minimum of ten reactor volumes to establish steady-state conditions. Samples from reactor influent and effluent were filled in amber glass bottles and stored at 4°C until analysis. UVT as well as nitrate, nitrite, acid capacity and oxidant concentration were analyzed on site. TOrCs and DOC analysis were conducted within 24 hours.

2.4 Results and Discussion

2.4.1 Characteristics of selected TOrCs: photolytic reactivity and rate constants with $^{\bullet}OH$ and $SO_4^{\bullet-}$

Twelve TOrCs spanning a range of photolytic reactivity were selected based on their frequent detection in wastewater effluent and diverse physicochemical characteristics (Gerrity et al., 2011; Luo et al., 2014). Degradation of selected TOrCs by direct photolysis was investigated in WWTP effluent (115–1,380 mJ/cm^2). The relative removal of TOrCs is illustrated in Figure A-1-1 and their fluence-based rate constants (k_{obs-UV}) are presented in Table 2-2. The percent removal of diclofenac, iopromide and sulfamethoxazole were >90% at 1,380 mJ/cm^2, followed by phenytoin (68%) and benzotriazole (30%). About 9% of venlafaxine and 5% of metoprolol were eliminated at 1,380 mJ/cm^2. The removal of other TOrCs was negligible within the applied fluence.

The selected TOrCs were classified into 3 groups in accordance with literature (Miklos, Hartl, et al., 2018). Group I includes photo-sensitive compounds (i.e., diclofenac, iopromide, and sulfamethoxazole) with k_{obs-UV} >1×10^{-3} cm^2/mJ. Group II are moderately photo-sensitive compounds (i.e., phenytoin and benzotriazole) (1×10^{-4} < k_{obs-UV} < 1×10^{-3} cm^2/mJ). All other selected TOrCs belong to group III and are considered as photo-resistant compounds (k_{obs-UV} <1×10^{-4} cm^2/mJ).

The second-order rate constants of selected TOrCs with $^{\bullet}OH$ and $SO_4^{\bullet-}$ are shown in Table 2-2. The $k_{\bullet OH}$ values of TOrCs were obtained from literature. Unlike the well-studied hydroxyl radical-based oxidation processes, $k_{SO_4^{\bullet-}}$ values of most TOrCs are not known. To the best of our knowledge, the $k_{SO_4^{\bullet-}}$ of iopromide, phenytoin, caffeine, benzotriazole and primidone were determined for the first time in this study. The $k_{SO_4^{\bullet-}}$ of venlafaxine, metoprolol and carbamazepine are in good agreement with literature values (Matta et al., 2011; Lian et al., 2017). The selected TOrCs have complex structures with multiple functional groups. Hydroxyl radicals react with almost all organic moieties with nearly diffusion-controlled rates (Buxton et al., 1988). As shown in Table 2-2, $^{\bullet}OH$ reacts relatively slowly with TCEP (i.e., 5.6×10^8 M^{-1} s^{-1}) (Watts and Linden, 2009) while all other TOrCs have $k_{\bullet OH}$ values greater than 1×10^9 M^{-1} s^{-1}. In contrast, $SO_4^{\bullet-}$ is a selective oxidant and preferentially reacts with electron-rich groups (Neta et al., 1988). Compounds with activated aromatic ring and amine

moieties, such as diclofenac (aromatic amine), sulfamethoxazole (aromatic amine), venlafaxine (methoxybenzene and tertiary amine), metoprolol (methoxybenzene and secondary amine) are highly reactive with $SO_4^{\bullet-}$ among the selected TOrCs (i.e., $k_{SO_4^{\bullet-}}$>3.89×10^9 M^{-1} s^{-1}). Carbamazepine (olefin) and caffeine (imidazole) exhibit slightly lower reactivity toward $SO_4^{\bullet-}$ (i.e., $k_{SO_4^{\bullet-}}$=1.5–2.39×10^9 M^{-1} s^{-1}). Iopromide contains benzene ring substituted by multiple halogens and electron-withdrawing amide group. Phenytoin and primidone are composed of weakly-activated benzene ring as well as electron-withdrawing amide group. Benzotriazole has a protonated triazole ring at pH 7 (pK_a=8.2). Consequently these compounds might have limited electron transfer to $SO_4^{\bullet-}$ and their $k_{SO_4^{\bullet-}}$ values are <1×10^9 M^{-1} s^{-1}. However, phenytoin, benzotriazole and primidone are still highly reactive towards $^{\bullet}$OH, with $k_{^{\bullet}OH}$ values of one order of magnitude higher than their $k_{SO_4^{\bullet-}}$ values, possibly due to the rapid benzene ring addition mechanism (Vel Leitner and Roshani, 2010; Lee et al., 2014). The $k_{SO_4^{\bullet-}}$ of gabapentin and TCEP were not determined by competition kinetics but estimated to be below 1×10^9 M^{-1} s^{-1} based on their removal in pure water during UV/PDS (Text A-1-3).

2.4.2 Degradation of TOrCs in pure water during UV/H_2O_2 and UV/PDS

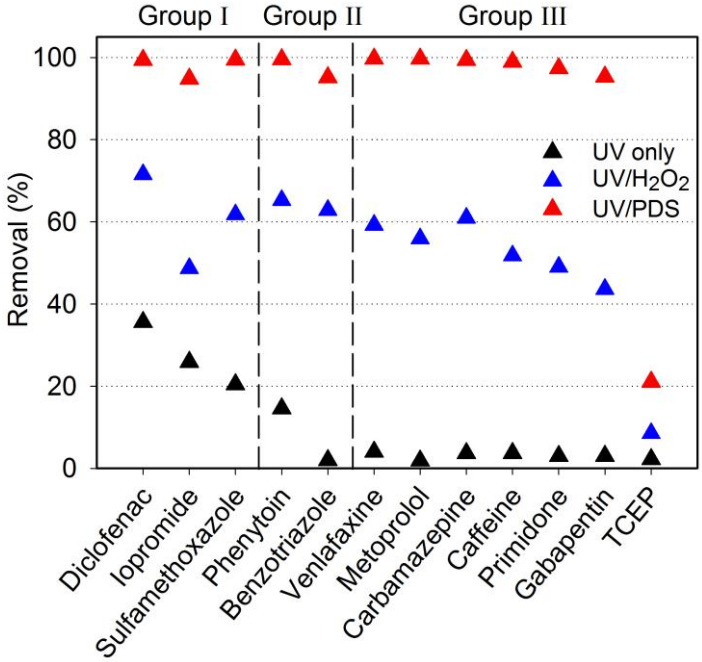

Figure 2-1. Percent removal of TOrCs in pure water (Fluence=57.5 mJ/cm2, Oxidants = 0.15 mM, 5 mM phosphate buffer, pH 7)

Preliminary experiments indicated that the oxidation of selected TOrCs by H_2O_2 and PDS in the dark was negligible (Figure A-1-2). Figure 2-1 presents the percent removal of TOrCs during UV/H_2O_2 and UV/PDS in buffered pure water (57.5 mJ/cm^2, 0.15 mM oxidants). Radical oxidation significantly improved the degradation efficiency of TOrCs compared to direct photolysis. About 40−70% removal of TOrCs (except TCEP) was found during UV/H_2O_2, while the concentration of all TOrCs (except TCEP) reached the limit of quantification (LOQ) during UV/PDS within the same applied fluence and molar oxidant dose. For this reason, expected differences in TOrCs removal based on second-order rate constants with $SO_4^{\bullet-}$ could not be illustrated in UV/PDS experiments. The photolysis rate of PDS is higher than that of H_2O_2 due to its higher quantum efficiency (i.e., 0.7 mol/E for PDS and 0.5 mol/E for H_2O_2) and higher molar extinction coefficient (i.e., 21.1 M^{-1} cm^{-1} for PDS and 18.6 M^{-1} cm^{-1} for H_2O_2) at 254 nm (Ike et al., 2018). Moreover, the main radical scavengers in buffered pure water included the phosphate buffer ions (i.e., mainly HPO_4^{2-} and $H_2PO_4^-$ at pH 7, pK_{a2}=7.2), primary oxidants (H_2O_2 or PDS) and TOrCs. The scavenging capacity of each component was calculated by multiplying its molar concentration with its second-order rate constants with radicals. As shown in Table A-1-3, the overall scavenging capacity of the buffered pure water matrix on $SO_4^{\bullet-}$ (3.4×10^3 s^{-1}) was lower compared to that on $^{\bullet}OH$ (4.8×10^3 s^{-1}). The product phosphate radicals (e.g., $HPO_4^{\bullet-}$) are known to be less reactive than $^{\bullet}OH$ and $SO_4^{\bullet-}$ (Neta et al., 1988), thus their contribution to TOrCs removal should be insignificant and can be ignored. Therefore, the more efficient removal of TOrCs during UV/PDS in buffered pure water was attributed to two factors: the higher photolysis rate of PDS at 254 nm and the lower scavenging effect of the water matrix on $SO_4^{\bullet-}$, which led to the higher steady-state concentration of $SO_4^{\bullet-}$ than $^{\bullet}OH$ (Y. Xiao et al., 2016; Pari et al., 2017).

TCEP was degraded much slower than other compounds due to its low second-order rate constants with radicals (Table 2-2). In buffered pure water experiments, only about 10% of TCEP was removed by UV/H_2O_2 at 57.5 mJ/cm^2 and the removal was increased to 43% at 920 mJ/cm^2 (Figure A-1-3). However, the degradation of TCEP was faster in UV/PDS and reached LOQ at 920 mJ/cm^2, which was attributed to the high $SO_4^{\bullet-}$ exposure in pure water during UV/PDS.

2.4.3 Degradation of TOrCs in wastewater effluent during UV/H_2O_2 and UV/PDS

Experiments with 0.15 mM of H_2O_2 or PDS in wastewater effluent spiked with 1 µg/L of each TOrC, resulted in significantly reduced percent removal compared to pure water experiments (e.g., <12% of degradation for group II and III compounds at 115 mJ/cm^2) (Figure A-1-4), indicating the strong scavenging effect of the water matrix (e.g., EfOM, inorganic species) on both radicals. The effect of the water matrix can be overcome by increasing the UV fluence and oxidant dose. Figure A-1-5 presents the percent removal of TOrCs in wastewater effluent at 1,380 mJ/cm^2 and 0.6 mM of oxidant. Direct photolysis was effective for the degradation of group I compounds (>90%). UV/H_2O_2 and UV/PDS substantially enhanced the removal of group II and III compounds (except TCEP). TCEP was persistent to both UV/H_2O_2 and UV/PDS in wastewater effluent, and less than 4% removal was obtained for the highest fluence (1,380 mJ/cm^2) and oxidant dose (0.6 mM) applied. Ozonation was also reported to be inefficient for the elimination of TCEP in municipal WWTP effluent (e.g., 25% of removal at 1.5 mg O_3/mg DOC), because of its low reaction rate constants with ozone and $^{\bullet}$OH (Lee et al., 2013).

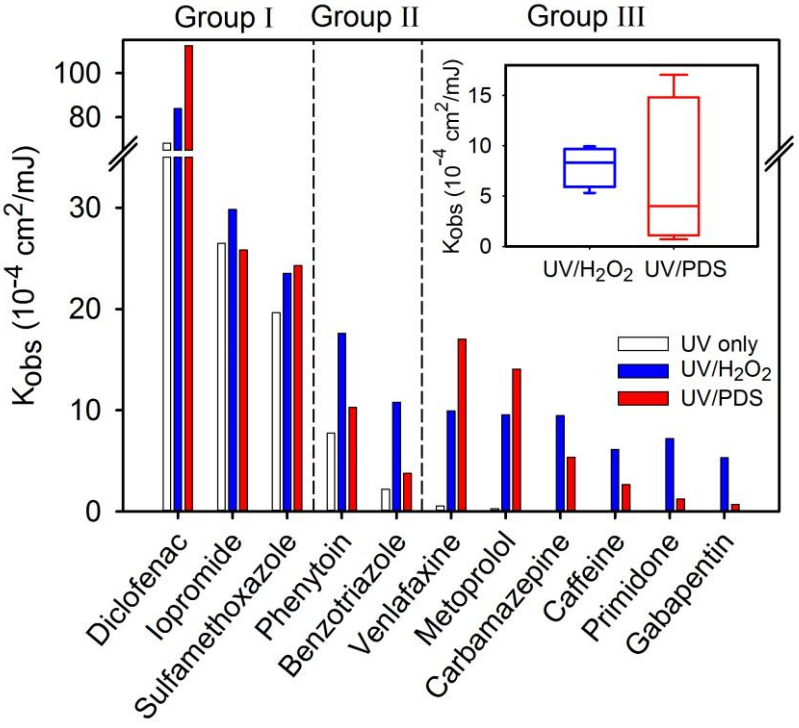

Figure 2-2. Fluence-based rate constants of TOrCs in wastewater effluent during UV only, UV/H_2O_2 and UV/PDS processes (Fluence= 115−1,380 mJ/cm^2;

Oxidants=0.3 mM). Inset boxplot shows the statistical evaluation of fluence-based rate constants of all group III compounds

Figure 2-2 presents the fluence-based rate constants (k_{obs}) of TOrCs calculated for UV only (k_{obs-UV}), UV/H_2O_2 (k_{obs-UV/H_2O_2}) and UV/PDS ($k_{obs-UV/PDS}$) experiments performed in wastewater effluent (0.3 mM of oxidant). k_{obs} was not calculated for TCEP due to its low removal. The $k_{obs-UV}/k_{obs-UV/AOP}$ was calculated to be greater than 0.8 for group I compounds (except diclofenac in UV/PDS), indicating that their degradation was mainly attributed to direct photolysis. During UV/PDS, the removal rate of diclofenac was enhanced to 1.12×10^{-2} cm^2/mJ, suggesting that both direct photolysis and radical oxidation contributed to its elimination (i.e., $k_{obs-UV}/k_{obs-UV/PDS}$= 0.6). The removal of group II compounds followed both direct photodegradation and radical oxidation, whereas the radical oxidation was the dominant process for group III compounds.

The inset boxplot in Figure 2-2 shows the fluence-based rate constants of group III compounds (except TCEP). The $k_{obs-UV/PDS}$ covered a wider range than k_{obs-UV/H_2O_2}, suggesting that UV/PDS showed higher selectivity towards TOrCs removal than UV/H_2O_2. Similar results were reported on UV/H_2O_2 and UV/PDS treatment of TOrCs in reverse osmosis brines (Yang et al., 2016) and wastewater effluent (Lian et al., 2017). Moreover, the removal pattern of group III compounds during both processes was consistent with their second-order rate constants with $^{\bullet}OH$ and $SO_4^{\bullet-}$ shown in Table 2-2. Group III compounds with high $k_{\bullet OH}$ ($>7\times10^9$ M^{-1} s^{-1}) such as venlafaxine, metoprolol and carbamazepine had similar k_{obs-UV/H_2O_2} ($\sim1\times10^{-3}$ cm^2/mJ). Slightly lower removal rate was observed from caffeine (6.13×10^{-4} cm^2/mJ) and primidone (7.20×10^{-4} cm^2/mJ), which was consistent with their lower $k_{\bullet OH}$ ($<7\times10^9$ M^{-1} s^{-1}). The k_{obs-UV/H_2O_2} of gabapentin was 5.31×10^{-4} cm^2/mJ, suggesting that its $k_{\bullet OH}$ might have been overestimated previously (i.e., 9.1×10^9 M^{-1} s^{-1}) (Lee et al., 2014). Similarly, compounds with higher $k_{SO_4^{\bullet-}}$ ($1.50-4.99\times10^9$ M^{-1} s^{-1}) such as venlafaxine, metoprolol, carbamazepine and caffeine showed higher removal rate than those with lower $k_{SO_4^{\bullet-}}$ ($<1\times10^9$ M^{-1} s^{-1}), such as primidone and gabapentin.

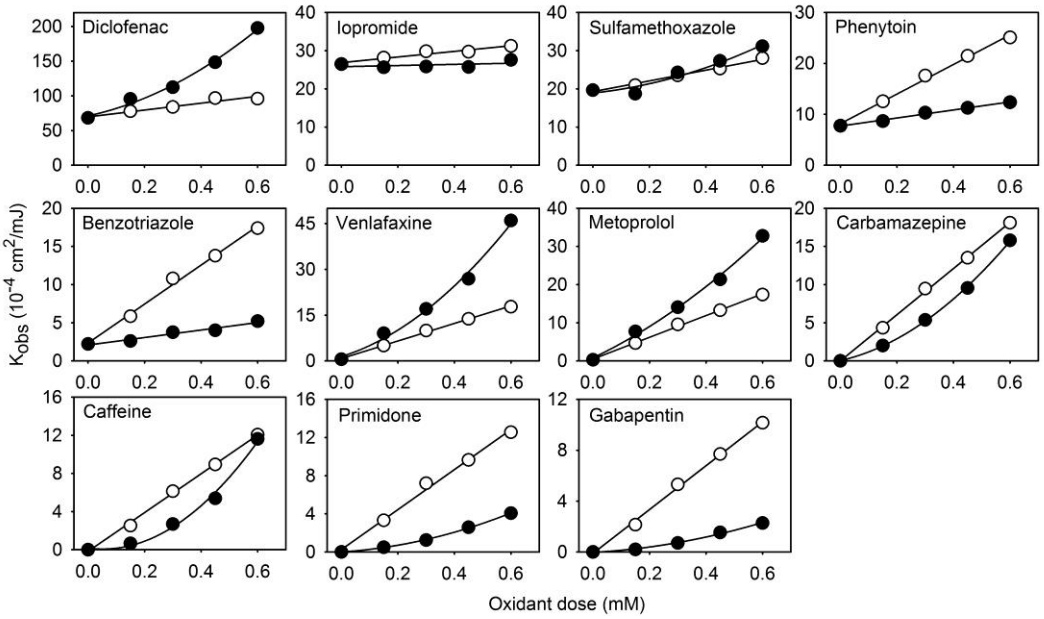

Figure 2-3. Fluence-based rate constants of TOrCs in wastewater effluent during UV/H_2O_2 (open circles) and UV/PDS (filled circles) (Fluence=115−1,380 mJ/cm^2; Oxidants = 0, 0.15, 0.30, 0.45 and 0.60 mM)

Figure 2-3 shows the evolution of fluence-based rate constants of TOrCs as a function of initial oxidant dose. The k_{obs-UV/H_2O_2} and $k_{obs-UV/PDS}$ values of each TOrC (except for iopromide) gradually increased, suggesting that the radical exposure was promoted with increasing H_2O_2 and PDS dose (Rosario-Ortiz et al., 2010).

During UV/H_2O_2, the k_{obs-UV/H_2O_2} values of TOrCs increased linearly as a function of initial H_2O_2 dose. Previous study showed that the log-transformation of TOrCs (i.e., $\log(C/C_o)$) in wastewater effluent was linearly proportional to the initial H_2O_2 dose during UV/H_2O_2, which indicated that the competition between TOrCs and the wastewater effluent matrix for $^{\bullet}OH$ consumption remained constant during the oxidation process (Lee and von Gunten, 2010). However, the $k_{obs-UV/PDS}$ values of TOrCs, especially those with high reactivity towards $SO_4^{\bullet-}$ (i.e., $k_{SO_4^{\bullet-}}$ >1×10^9 M^{-1} s^{-1}), such as diclofenac, sulfamethoxazole, venlafaxine, metoprolol, carbamazepine and caffeine, exhibited exponential increase with increasing of PDS dose.

Our results are comparable with previous studies on the treatment of TOrCs in wastewater effluent using selective oxidants (e.g., ozone, chlorine) (Lee and von Gunten, 2010), which are highly reactive with the electron-rich organic moieties. When selective oxidants are applied, the degradation of TOrCs tends to have a "lag-

phase" at low oxidant dose due to the high competition between the targeted TOrC and the wastewater effluent matrix (e.g., electron-rich site of EfOM). When the oxidant dose is increased to be above the initial water matrix demand, the degradation rates of TOrCs can be enhanced significantly (Lee and von Gunten, 2010). To support our hypothesis, the fluorescence intensities of FEEM regions (see section 2.4.5) were progressively reduced with increasing initial PDS concentration during UV/PDS. About 62−76% fluorophores were degraded at 1,380 mJ/cm^2 and 0.6 mM of PDS (Figure A-1-6), indicating the large depletion of electron-rich organic moieties in EfOM at high PDS dose. Alternatively, more $SO_4^{\bullet-}$ will be available in solution to oxidize TOrCs. Although about 43−77% of the fluorescence intensity were removed during UV/H_2O_2 under the same experimental conditions (Figure A-1-6), $^{\bullet}$OH is a non-selective oxidant and it might react with all fractions of EfOM and the transformation products of EfOM as fast as their initial compounds, resulting in the constant scavenging rates of water matrix for $^{\bullet}$OH during the entire oxidation processes (Lee and von Gunten, 2010).

Diclofenac, venlafaxine and metoprolol were more efficiently eliminated by UV/PDS compared to UV/H_2O_2 because they can more easily overcome the scavenging impact of EfOM due to their high reactivity with $SO_4^{\bullet-}$. The UV/PDS process was also reported to be more efficient than UV/H_2O_2 for venlafaxine and metoprolol in wastewater effluent (Lian et al., 2017). Sulfamethoxazole was degraded faster in UV/PDS when PDS dose was above 0.3 mM. For caffeine and carbamazepine, $k_{obs-UV/PDS}$ was comparable with k_{obs-UV/H_2O_2} at 0.6 mM oxidant dose, thus UV/PDS is expected to outcompete UV/H_2O_2 for removal of these two compounds if higher PDS dose is applied (>0.6 mM). For phenytoin, benzotriazole, primidone and gabapentin, UV/H_2O_2 was more efficient as they have low reactivity with $SO_4^{\bullet-}$ to overcome the scavenging effect of the water matrix during UV/PDS. The k_{obs-UV/H_2O_2} of iopromide was only increased by less than 20% compared to k_{obs-UV} and its $k_{obs-UV/PDS}$ value was almost stable in various initial H_2O_2 and PDS doses, respectively. This can be explained by the low reactivity of iopromide with $^{\bullet}$OH and $SO_4^{\bullet-}$ (Table 2-2). Hence, direct photodegradation is mainly responsible for the removal of iopromide in wastewater effluent and upgrading UV process to UV/H_2O_2 or UV/PDS will not contribute substantially to its removal efficiency.

2.4.4 Effect of wastewater matrix components

The water matrix components (e.g., DOC, bicarbonate, nitrite and halides) react with $^{\bullet}OH$ and $SO_4^{\bullet-}$, lowering the efficiency of UV/H_2O_2 and UV/PDS processes. Table 2-1 shows the water quality parameters of wastewater effluent used in this study. The exact concentration of chloride is not available, but the annual average concentration in this WWTP effluent is provided. The scavenging capacity of the known inorganic constituents were calculated by multiplying their concentrations with their second-order reaction rate constants with $^{\bullet}OH$ and $SO_4^{\bullet-}$ (rate constants and references are shown in Table A-1-2). DOC and chloride were the most efficient scavengers for UV/H_2O_2 and UV/PDS, respectively.

The product radicals (e.g., $CO_3^{\bullet-}$, $NO_2^{\bullet}$ and $Cl_2^{\bullet}$) generated from the reactions between inorganic components and $^{\bullet}OH$ or $SO_4^{\bullet-}$ (Table A-1-2) might also participate in the degradation of TOrCs (Wols and Hofman-Caris, 2012; Lian et al., 2017). The product radicals are moderate oxidants (i.e., 1.63 V, 1.03 V and 2.0 V for $CO_3^{\bullet-}$, $NO_2^{\bullet}$ and $Cl_2^{\bullet}$, respectively) and even more selective than $SO_4^{\bullet-}$ toward electron-rich moieties (i.e., activated aromatics like phenols and anilines, olefines) (Zuo et al., 1999; Guo et al., 2017; Ji et al., 2017). The impact of individual inorganic ions (i.e., bicarbonate, nitrite, nitrate and chloride) on the removal pattern of TOrCs during UV/H_2O_2 and UV/PDS was investigated in buffered pure water applying the concentration of each inorganic constituent in Table 2-1. The influence of chloride was simulated by applying 35 and 350 mg/L of chloride. The fluence-based rate constants of TOrCs are shown in Figure A-1-7. The effect of nitrate (10.6 mg-N/L) was negligible for both processes. The k_{obs-UV/H_2O_2} and $k_{obs-UV/PDS}$ of TOrCs (except for diclofenac and sulfamethoxazole) in the presence of bicarbonate (307 mg/L) were lower than that in the presence of nitrite (0.028 mg-N/L), indicating that bicarbonate scavenged radicals more efficiently than nitrite. This is consistent with the calculated scavenging capacity of bicarbonate and nitrite shown in Table 2-1. However, nitrite was present at low concentration (0.028 mg-N/L) in this specific wastewater sample. The second-order rate constant of nitrite with $^{\bullet}OH$ (1.0×10^{10} M^{-1} s^{-1}) (Coddington et al., 1999) and $SO_4^{\bullet-}$ (8.8×10^{8} M^{-1} s^{-1}) (Neta et al., 1988) is the highest among the known wastewater components in Table 2-1, suggesting that the scavenging capacity of nitrite can be significant at higher concentration. A previous study reported that the efficiency of TOrCs elimination during UV/H_2O_2 was strongly influenced by nitrite concentration fluctuations in

WWTP effluent (Miklos, Hartl, et al., 2018). Interestingly, sulfamethoxazole and diclofenac were degraded faster in bicarbonate containing solution than in the presence of nitrite during both processes, which suggests that $CO_3^{\bullet-}$ contributed to their removal. Recent studies also reported the degradation of sulfamethoxazole and diclofenac by $CO_3^{\bullet-}$ (Lu et al., 2017; Yang et al., 2017). No significant reduction of k_{obs-UV/H_2O_2} was found for UV/H_2O_2 in the presence of chloride. This finding was expected because the reaction between chloride and $^{\bullet}OH$ is reversible and the rate constant of forward reaction (4.3×10^9 M^{-1} s^{-1}) is even lower than that for the backward reaction (6.1×10^9 M^{-1} s^{-1}) (Jayson et al., 1973) (Table A-1-2). The concentration of TOrCs reached LOQ at 57.5 mJ/cm^2 during UV/PDS in the presence of 35 mg/L of chloride. When the chloride was increased to 350 mg/L, the removal rate of TOrCs decreased. Although the scavenging capacity of 350 mg/L of chloride (i.e., 3×10^6 s^{-1}) is about two and three orders of magnitude higher than that of bicarbonate and nitrite, respectively, the $k_{obs-UV/PDS}$ values in the presence of chloride were comparable or even higher than those in the presence of bicarbonate and nitrite for most compounds, indicating that reactive chlorine species (e.g., $Cl_2^{\bullet}$) might promote the degradation of TOrCs. Consequently, the presence of chloride in wastewater effluent reduces the steady-state concentration of $SO_4^{\bullet-}$ during UV/PDS, but might less affect the removal rate of TOrCs compared to bicarbonate and nitrite at similar scavenging capacity.

However, the importance of inorganic ions might be different in wastewater effluent compared to the buffered pure water with individual inorganic components. As shown in Table 2-1, DOC is a strong scavenger for $^{\bullet}OH$ and $SO_4^{\bullet-}$, resulting in lower steady-state concentrations of primary radicals in wastewater effluent compared to pure water. Moreover, the product radicals can also be scavenged by the wastewater components. For instance, bicarbonate is reactive with $Cl^{\bullet}$ and $Cl_2^{\bullet}$ to produce more $CO_3^{\bullet-}$ (Table A-1-2). DOC was reported to scavenge $Cl^{\bullet}$ efficiently (i.e., 1.3×10^4 $(mg\text{-}C/L)^{-1}$ s^{-1}) (Fang et al., 2014).

2.4.5 Oxidative inactivation of fluorescent effluent organic matter components during UV/H_2O_2 and UV/PDS

Figure A-1-8 illustrates the FEEM spectra of wastewater effluent during UV/H_2O_2 and UV/PDS processes. The FEEM spectra of wastewater effluent (before AOP treatment) exhibited 4 characteristic regions with maximum fluorescence intensity identified as follows (Table A-1-2): aromatic protein-like peak (P_II, Excitation/Emission=

242/358 nm), fulvic-like peak (P_III, 242/430 nm), soluble microbial product-like peak (P_IV, 287/353 nm) and humic-like peak (P_V, 329/412 nm) (Chen et al., 2003).

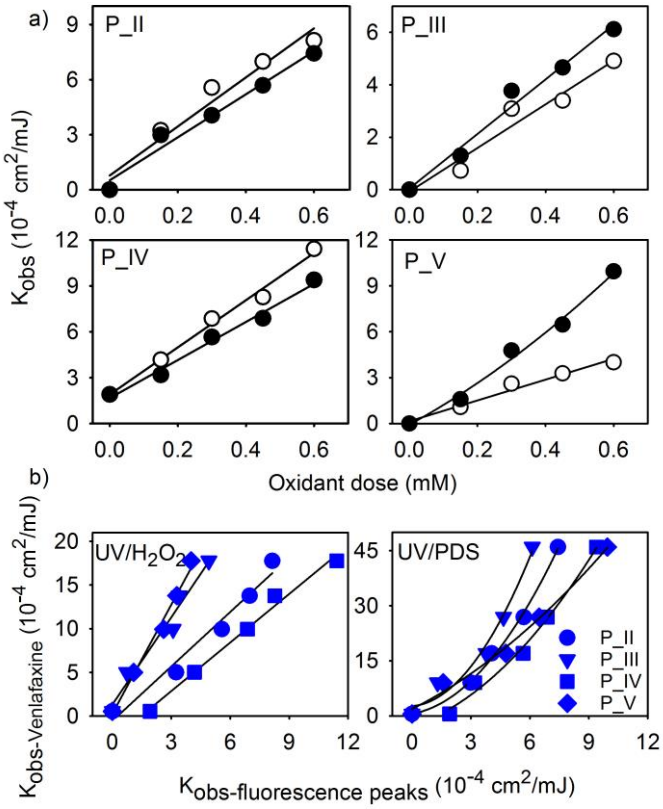

Figure 2-4. a) Fluence-based rate constants of selected fluorescence peaks in wastewater effluent during UV/H_2O_2 (open circles) and UV/PDS (filled circles). b) Correlations between the fluence-based rate constants of venlafaxine and selected fluorescence peaks

The fluorescence intensity of P_IV was reduced by 15% during direct photolysis at 920 mJ/cm^2, suggesting the presence of relatively photo-sensitive fluorophores in soluble microbial product-like region. The intensity of the other fluorescence peaks was stable during direct photolysis (115−1,380 mJ/cm^2). Once adding H_2O_2 and PDS, the fluorescence intensities of all the selected peaks decreased following first-order reaction kinetics, indicating the contribution of $^{\bullet}OH$ and $SO_4^{\bullet-}$, respectively. Their fluence-based reaction rate constants (k_{obs-UV/H_2O_2} and ($k_{obs-UV/PDS}$) linearly increased as a function of initial oxidant dose (Figure 2-4a), except the $k_{obs-UV/PDS}$ of P_V, which appeared to increase exponentially. The fluorescence extinction of fulvic and humic-like fluorophores were much slower than that of soluble microbial product-like and aromatic protein-like fluorophores during UV/H_2O_2. This is in accordance with previous observation that some fluorophores in humic-like region

might be more resistant to •OH attack than fluorophores from the protein-like region (Abdelmelek et al., 2011). Interestingly, unlike the removal of TOrCs, UV/PDS reduced the fluorescence intensities of all identified fluorophores and showed less selectivity toward fluorophores removal. This is consistent with the literature that $SO_4^{\bullet-}$ is a strong electrophile and preferentially oxidizes electron rich moieties (e.g., unsaturated and aromatic compounds) (R. Xiao et al., 2015), which is the primary characteristic of fluorescent compounds (Świetlik and Sikorska, 2004). The fluorescence loss of humic and fulvic-like fluorophores during UV/PDS were even faster than that during UV/H_2O_2. Addition and hydrogen abstraction are the main pathways for •OH, whereas the electron transfer is predominant for $SO_4^{\cdot-}$ (Neta et al., 1988). During UV/H_2O_2, humic substances might mainly undergo hydroxylation and breakdown of macromolecules into smaller ones, but the main structural characteristic remains intact (González et al., 2013). The direct electron transfer from aromatic rings to $SO_4^{\cdot-}$ followed by the hydroxylation in aqueous solution can generate similar hydroxylated aromatics as •OH (Olmez-Hanci and Arslan-Alaton, 2013). However, the electron transfer can also lead to the formation of unstable radical cation intermediates or the decarboxylation following the oxidation of aromatic ring, which might induce the rapid ring cleavage during UV/PDS (Neta et al., 1977). Therefore, the prevalence of radical reactions with EfOM can impact differently on fluorescence during UV/H_2O_2 and UV/PDS.

Several studies investigated fluorescence as a surrogate to predict the elimination of TOrCs during various water treatment processes (Gerrity et al., 2012; Park et al., 2017). The possible correlation of fluence-based rate constants between selected fluorescence peaks and individual group III compounds (except TCEP) was examined in this study. Figure 2-4b presents venlafaxine as an example. Other group III compounds are shown in Figure A-1-9 and Figure A-1-10. The k_{obs-UV/H_2O_2} value of individual group III compounds was linearly correlated with that of selected fluorescence peaks, suggesting that fluorescence may be a useful indicator for group III compounds removal during UV/H_2O_2. The $k_{obs-UV/PDS}$ values of group III compounds exponentially increased with respect to $k_{obs-UV/PDS}$ of selected fluorescence peaks. Due to the selective oxidizing property of $SO_4^{\bullet-}$, the elimination of compounds that are less reactive with $SO_4^{\bullet-}$ can be eliminated much slower than fluorophores. For example, only about 28% of gabapentin was removed when 62−76% fluorophores

were degraded during UV/PDS (Figure A-1-5 and Figure A-1-6). Therefore, the development of compound-specific surrogate model on fluorescence would be required during UV/PDS.

2.4.6 Degradation of TOrCs during pilot-scale UV/PDS

Pilot-scale UV/PDS treatment of TOrCs was conducted at WWTP. The concentrations of TOrCs in WWTP effluent before UV/PDS treatment are shown in Table 2-2. Phenytoin (13±2 ng/L) and caffeine (71±32 ng/L) were present at very low initial concentrations, which were close to LOQ and consequently showing large uncertainties. Therefore, the elimination of phenytoin and caffeine was not monitored during pilot-testing. Figure 2-5 shows the relative removal of TOrCs during UV only and UV/PDS processes. Group I compounds were efficiently removed. More than 98% of diclofenac was degraded at 1,200 mJ/cm^2 when only UV was applied, with the addition of 0.6 mM of PDS, the same removal of 98% was already achieved at 800 mJ/cm^2. Comparable to lab-scale experiments, the elimination of iopromide and sulfamethoxazole was mainly caused by direct photolysis, with 94% and 91% removal at 1,200 mJ/cm^2, respectively. No significant contribution of $SO_4^{\bullet-}$ was observed to iopromide within experimental uncertainties due to its low $k_{SO_4^{\bullet-}}$ (i.e., $<1\times10^9$ M^{-1} s^{-1}). Sulfamethoxazole is highly reactive with $SO_4^{\bullet-}$ (i.e., $k_{SO_4^{\bullet-}} = 12.5\times10^9$ M^{-1} s^{-1}) (Mahdi Ahmed et al., 2012). Furthermore, the potential inner filter effect of PDS was excluded as the UV fluence was adjusted after PDS spiking during pilot-testing. However, the removal of sulfamethoxazole was slower during UV/PDS than direct UV photolysis for unknown reason. Venlafaxine and metoprolol were removed most efficiently among the group II and III compounds, which was consistent with the lab-scale experiments. About 77% of venlafaxine, 49% of metoprolol and 27% of carbamazepine were eliminated at 1,200 mJ/cm^2 and 0.6 mM PDS. Compounds showing low reactivity toward $SO_4^{\bullet-}$ were less removed. For instance, about 58% of benzotriazole and 11% of primidone were degraded at 1,200 mJ/cm^2 with 0.6 mM PDS. Similar to iopromide, the direct photodegradation was mainly responsible for the elimination of benzotriazole due to its low $k_{SO_4^{\bullet-}}$ (i.e., $<1\times10^9$ M^{-1} s^{-1}) (Figure A-1-11). Gabapentin and TCEP appeared to be resistant to UV photolysis and UV/PDS in these experimental conditions.

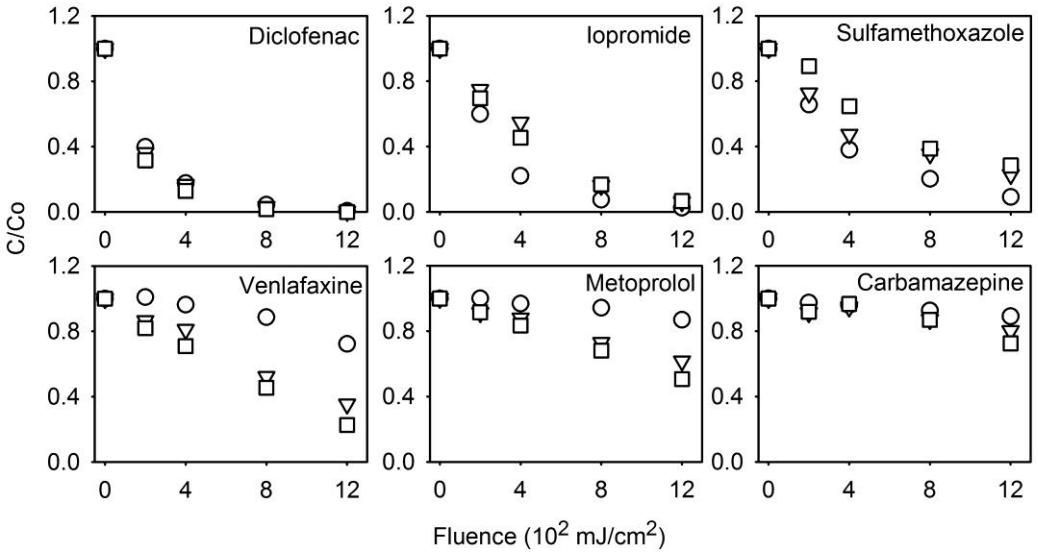

Figure 2-5. Relative removal of TOrCs in pilot-scale experiments by direct photolysis (circles) and UV/PDS (triangle: 0.3 mM of PDS; square: 0.6 mM of PDS) (Fluence= 0−1,200 mJ/cm^2)

The removal pattern of TOrCs during pilot-testing was comparable to lab-scale experiments, but their removal rates were lower. Higher concentrations of DOC and nitrite were observed during pilot-scale tests compared to lab-scale experiments, resulting in about 1.7 and 5.3 times higher scavenging capacity of the wastewater matrix on $SO_4^{\bullet-}$ (Table 2-1). Fluorescence intensity was reduced only by 35−54% at 1,200 mJ/cm^2 with 0.6 mM PDS (Figure A-1-12 and Figure A-1-13), confirming the overall lower oxidation efficiency due to the scavengers during pilot-testing.

2.5 Conclusions

1) When the same molar dose of PDS and H_2O_2 are applied, UV/PDS can eliminate all TOrCs more efficiently than UV/H_2O_2 in buffered pure water due to the higher yield of $SO_4^{\bullet-}$.

2) $SO_4^{\bullet-}$ preferentially oxidizes TOrCs with electron-rich moieties (e.g., activated aromatic ring, olefines, and amines) as well as the electron-rich site of EfOM (e.g., fluorophores), while $^{\bullet}OH$ reacts with almost all organic moieties with nearly diffusion-controlled rates.

3) High competition between the target TOrCs and the electron-rich site of EfOM (scavenger) was observed at low PDS dose. However, the initial oxidant demand was followed by an exponential increase in the fluence-based rate constants of most

compounds with increasing PDS dose. In contrast, the scavenging impact of the water matrix on $^{\bullet}OH$ was constant during UV/H_2O_2, leading to a linear increase of fluence-based rate constants with increasing H_2O_2 dose.

4) Selectivity of $SO_4^{\bullet-}$ results in more efficient removal of TOrCs with electron-rich moieties by UV/PDS in wastewater effluent while UV/H_2O_2 better oxidizes compounds with less reactivity toward $SO_4^{\bullet-}$.

5) The scavenging capacities of DOC and chloride were calculated to be the highest among the known water parameters during UV/H_2O_2 and UV/PDS, respectively. Experiments conducted in the presence of individual inorganic species indicated that $CO_3^{\bullet-}$ enhanced the degradation of diclofenac and sulfamethoxazole during both processes. Chlorine radicals might contribute to the degradation of most compounds during UV/PDS.

6) The efficiency of pilot-scale UV/PDS was affected by the variation of DOC and nitrite in wastewater effluent. Higher UV fluences and oxidant doses are needed to overcome the impact of the water matrix. However, the energy requirements and the effect of sulfate ion on the salinity of treated water should be evaluated prior to UV/PDS application in wastewater effluent.

2.6 Acknowledgments

Curtin University (Curtin International Postgraduate Research Scholarship) and Water Research Australia (WaterRA Postgraduate Scholarship) are gratefully acknowledged for providing financial support for M. Nihemaiti. This work was additionally supported by Municipal Sewage Company of the City of Munich (Münchner Stadtentwässerung, MSE). The authors would like to thank Johann Müller from Chair of Urban Water Systems Engineering at TUM for his support on LC-MS/MS analysis. We also really appreciate the valuable revision suggestions of anonymous reviewers.

2.7 Reference

Abdelmelek, S. B., Greaves, J., Ishida, K. P., Cooper, W. J., and Song, W. (2011). Removal of Pharmaceutical and Personal Care Products from Reverse Osmosis Retentate Using Advanced Oxidation Processes. *Environmental Science & Technology, 45*(8), 3665-3671.

Bahnmüller, S., Loi, C. H., Linge, K. L., von Gunten, U., and Canonica, S. (2015). Degradation rates of benzotriazoles and benzothiazoles under UV-C irradiation and the advanced oxidation process UV/H2O2. *Water Research, 74*(Supplement C), 143-154.

Belhaj, D., Baccar, R., Jaabiri, I., Bouzid, J., Kallel, M., Ayadi, H., and Zhou, J. L. (2015). Fate of selected estrogenic hormones in an urban sewage treatment plant in Tunisia (North Africa). *Science of the Total Environment, 505*, 154-160.

Bolton, J. R., and Linden, K. G. (2003). Standardization of methods for fluence (UV Dose) determination in bench-scale UV experiments. *Journal of Environmental Engineering, 129*(3), 209-215.

Buxton, G. V., Greenstock, C. L., Helman, W. P., and Ross, A. B. (1988). Critical Review of rate constants for reactions of hydrated electrons, hydrogen atoms and hydroxyl radicals (·OH/·O−) in Aqueous Solution. *Journal of Physical and Chemical Reference Data, 17*(2), 513-886.

Chen, W., Westerhoff, P., Leenheer, J. A., and Booksh, K. (2003). Fluorescence Excitation-Emission Matrix Regional Integration to Quantify Spectra for Dissolved Organic Matter. *Environmental Science and Technology, 37*(24), 5701-5710.

Chu, W., Gao, N., Yin, D., Krasner, S. W., and Mitch, W. A. (2014). Impact of UV/H2O2 Pre-Oxidation on the Formation of Haloacetamides and Other Nitrogenous Disinfection Byproducts during Chlorination. *Environmental Science & Technology, 48*(20), 12190-12198.

Chu, W., Li, D., Gao, N., Templeton, M. R., Tan, C., and Gao, Y. (2015). The control of emerging haloacetamide DBP precursors with UV/persulfate treatment. *Water Research, 72*, 340-348.

Coday, B. D., Yaffe, B. G. M., Xu, P., and Cath, T. Y. (2014). Rejection of trace organic compounds by forward osmosis membranes: A literature review. *Environmental Science and Technology, 48*(7), 3612-3624.

Coddington, J. W., Hurst, J. K., and Lymar, S. V. (1999). Hydroxyl Radical Formation during Peroxynitrous Acid Decomposition. *Journal of the American Chemical Society, 121*(11), 2438-2443.

Dodd, M. C. (2012). Potential impacts of disinfection processes on elimination and deactivation of antibiotic resistance genes during water and wastewater treatment. *Journal of Environmental Monitoring, 14*(7), 1754-1771.

Fang, J., Fu, Y., and Shang, C. (2014). The roles of reactive species in micropollutant degradation in the UV/free chlorine system. *Environmental Science and Technology, 48*(3), 1859-1868.

Gerrity, D., Gamage, S., Holady, J. C., Mawhinney, D. B., Quiñones, O., Trenholm, R. A., and Snyder, S. A. (2011). Pilot-scale evaluation of ozone and biological activated carbon for trace organic contaminant mitigation and disinfection. *Water Research, 45*(5), 2155-2165.

Gerrity, D., Gamage, S., Jones, D., Korshin, G. V., Lee, Y., Pisarenko, A., Trenholm, R. A., von Gunten, U., Wert, E. C., and Snyder, S. A. (2012). Development of surrogate correlation models to predict trace organic contaminant oxidation and microbial inactivation during ozonation. *Water Research, 46*(19), 6257-6272.

González, O., Justo, A., Bacardit, J., Ferrero, E., Malfeito, J. J., and Sans, C. (2013). Characterization and fate of effluent organic matter treated with UV/H2O2 and ozonation. *Chemical Engineering Journal, 226*, 402-408.

Grandclément, C., Seyssiecq, I., Piram, A., Wong-Wah-Chung, P., Vanot, G., Tiliacos, N., Roche, N., and Doumenq, P. (2017). From the conventional biological wastewater treatment to hybrid processes, the evaluation of organic micropollutant removal: A review. *Water Research, 111*, 297-317.

Guo, K., Wu, Z., Shang, C., Yao, B., Hou, S., Yang, X., Song, W., and Fang, J. (2017). Radical Chemistry and Structural Relationships of PPCP Degradation by UV/Chlorine Treatment in Simulated Drinking Water. *Environmental Science & Technology, 51*(18), 10431-10439.

He, X., de la Cruz, A. A., O'Shea, K. E., and Dionysiou, D. D. (2014). Kinetics and mechanisms of cylindrospermopsin destruction by sulfate radical-based advanced oxidation processes. *Water Research, 63*, 168-178.

Hori, H., Yamamoto, A., Hayakawa, E., Taniyasu, S., Yamashita, N., Kutsuna, S., Kiatagawa, H., and Arakawa, R. (2005). Efficient Decomposition of Environmentally Persistent Perfluorocarboxylic Acids by Use of Persulfate as a Photochemical Oxidant. *Environmental Science & Technology, 39*(7), 2383-2388.

Huber, M. M., Canonica, S., Park, G. Y., and von Gunten, U. (2003). Oxidation of pharmaceuticals during ozonation and advanced oxidation processes. *Environmental Science & Technology, 37*(5), 1016-1024.

Ike, I. A., Linden, K. G., Orbell, J. D., and Duke, M. (2018). Critical review of the science and sustainability of persulphate advanced oxidation processes. *Chemical Engineering Journal, 338*, 651-669.

Jayson, G. G., Parsons, B. J., and Swallow, A. J. (1973). Some simple, highly reactive, inorganic chlorine derivatives in aqueous solution. Their formation using pulses of radiation and their role in the mechanism of the Fricke dosimeter. *Journal of the Chemical Society, Faraday Transactions 1: Physical Chemistry in Condensed Phases, 69*, 1597-1607.

Ji, Y., Wang, L., Jiang, M., Lu, J., Ferronato, C., and Chovelon, J. M. (2017). The role of nitrite in sulfate radical-based degradation of phenolic compounds: An unexpected nitration process relevant to groundwater remediation by in-situ chemical oxidation (ISCO). *Water Research, 123*(Supplement C), 249-257.

Lee, Y., Gerrity, D., Lee, M., Bogeat, A. E., Salhi, E., Gamage, S., Trenholm, R. A., Wert, E. C., Snyder, S. A., and von Gunten, U. (2013). Prediction of Micropollutant Elimination during Ozonation of Municipal Wastewater Effluents: Use of Kinetic and Water Specific Information. *Environmental Science & Technology, 47*(11), 5872-5881.

Lee, Y., Gerrity, D., Lee, M., Gamage, S., Pisarenko, A., Trenholm, R. A., Canonica, S., Snyder, S. A., and von Gunten, U. (2016). Organic Contaminant Abatement in Reclaimed Water by UV/H2O2 and a Combined Process Consisting of O3/H2O2 Followed by UV/H2O2: Prediction of Abatement Efficiency, Energy Consumption, and Byproduct Formation. *Environmental Science & Technology, 50*(7), 3809-3819.

Lee, Y., Kovalova, L., McArdell, C. S., and von Gunten, U. (2014). Prediction of micropollutant elimination during ozonation of a hospital wastewater effluent. *Water Research, 64*, 134-148.

Lee, Y., and von Gunten, U. (2010). Oxidative transformation of micropollutants during municipal wastewater treatment: Comparison of kinetic aspects of selective (chlorine, chlorine dioxide, ferrateVI, and ozone) and non-selective oxidants (hydroxyl radical). *Water Research, 44*(2), 555-566.

Li, W., Jain, T., Ishida, K., and Liu, H. (2017). A mechanistic understanding of the degradation of trace organic contaminants by UV/hydrogen peroxide, UV/persulfate and UV/free chlorine for water reuse. *Environmental Science: Water Research and Technology, 3*(1), 128-138.

Lian, L., Yao, B., Hou, S., Fang, J., Yan, S., and Song, W. (2017). Kinetic Study of Hydroxyl and Sulfate Radical-Mediated Oxidation of Pharmaceuticals in Wastewater Effluents. *Environmental Science & Technology, 51*(5), 2954-2962.

Liang, C., Huang, C. F., Mohanty, N., and Kurakalva, R. M. (2008). A rapid spectrophotometric determination of persulfate anion in ISCO. *Chemosphere, 73*(9), 1540-1543.

Lu, X., Shao, Y., Gao, N., Chen, J., Zhang, Y., Xiang, H., and Guo, Y. (2017). Degradation of diclofenac by UV-activated persulfate process: Kinetic studies, degradation pathways and toxicity assessments. *Ecotoxicology and Environmental Safety, 141*, 139-147.

Luo, Y., Guo, W., Ngo, H. H., Nghiem, L. D., Hai, F. I., Zhang, J., Liang, S., and Wang, X. C. (2014). A review on the occurrence of micropollutants in the aquatic environment and their fate and removal during wastewater treatment. *Science of the Total Environment, 473-474*, 619-641.

Lutze, H. V., Bircher, S., Rapp, I., Kerlin, N., Bakkour, R., Geisler, M., von Sonntag, C., and Schmidt, T. C. (2015). Degradation of Chlorotriazine Pesticides by Sulfate Radicals and the Influence of Organic Matter. *Environmental Science & Technology, 49*(3), 1673-1680.

Lutze, H. V., Kerlin, N., and Schmidt, T. C. (2015). Sulfate radical-based water treatment in presence of chloride: Formation of chlorate, inter-conversion of sulfate radicals into hydroxyl radicals and influence of bicarbonate. *Water Research, 72*, 349-360.

Mahdi Ahmed, M., Barbati, S., Doumenq, P., and Chiron, S. (2012). Sulfate radical anion oxidation of diclofenac and sulfamethoxazole for water decontamination. *Chemical Engineering Journal, 197*, 440-447.

Matta, R., Tlili, S., Chiron, S., and Barbati, S. (2011). Removal of carbamazepine from urban wastewater by sulfate radical oxidation. *Environmental Chemistry Letters, 9*(3), 347-353.

Miklos, D. B., Hartl, R., Michel, P., Linden, K. G., Drewes, J. E., and Hübner, U. (2018). UV/H2O2 process stability and pilot-scale validation for trace organic chemical removal from wastewater treatment plant effluents. *Water Research, 136*, 169-179.

Miklos, D. B., Remy, C., Jekel, M., Linden, K. G., Drewes, J. E., and Hübner, U. (2018). Evaluation of advanced oxidation processes for water and wastewater treatment – A critical review. *Water Research, 139*, 118-131.

Müller, J., Drewes, J. E., and Hübner, U. (2017). Sequential biofiltration – A novel approach for enhanced biological removal of trace organic chemicals from wastewater treatment plant effluent. *Water Research, 127*, 127-138.

Neta, P., Huie, R. E., and Ross, A. B. (1988). Rate constants for reactions of inorganic radicals in aqueous solution. *Journal of Physical and Chemical Reference Data, 17*(3), 1027-1284.

Neta, P., Madhavan, V., Zemel, H., and Fessenden, R. W. (1977). Rate constants and mechanism of reaction of SO4·− with aromatic compounds. *Journal of the American Chemical Society, 99*(1), 163-164.

Olmez-Hanci, T., and Arslan-Alaton, I. (2013). Comparison of sulfate and hydroxyl radical based advanced oxidation of phenol. *Chemical Engineering Journal, 224*, 10-16.

Pari, S., Wang, I. A., Liu, H., and Wong, B. M. (2017). Sulfate radical oxidation of aromatic contaminants: a detailed assessment of density functional theory and high-level quantum chemical methods. *Environmental science. Processes & impacts, 19*(3), 395-404.

Park, M., Anumol, T., Daniels, K. D., Wu, S., Ziska, A. D., and Snyder, S. A. (2017). Predicting trace organic compound attenuation by ozone oxidation: Development of indicator and surrogate models. *Water Research, 119*, 21-32.

Real, F. J., Benitez, F. J., Acero, J. L., Sagasti, J. J. P., and Casas, F. (2009). Kinetics of the Chemical Oxidation of the Pharmaceuticals Primidone, Ketoprofen, and Diatrizoate in Ultrapure and Natural Waters. *Industrial & Engineering Chemistry Research, 48*(7), 3380-3388.

Rodríguez-Chueca, J., Laski, E., García-Cañibano, C., Martín de Vidales, M. J., Encinas, Á., Kuch, B., and Marugán, J. (2018). Micropollutants removal by full-scale UV-C/sulfate radical based Advanced Oxidation Processes. *Science of the Total Environment, 630*, 1216-1225.

Rosario-Ortiz, F. L., Wert, E. C., and Snyder, S. A. (2010). Evaluation of UV/H2O2 treatment for the oxidation of pharmaceuticals in wastewater. *Water Research, 44*(5), 1440-1448.

Sgroi, M., Roccaro, P., Korshin, G. V., Greco, V., Sciuto, S., Anumol, T., Snyder, S. A., and Vagliasindi, F. G. A. (2017). Use of fluorescence EEM to monitor the removal of emerging contaminants in full scale wastewater treatment plants. *Journal of Hazardous Materials, 323*(Part A), 367-376.

Świetlik, J., and Sikorska, E. (2004). Application of fluorescence spectroscopy in the studies of natural organic matter fractions reactivity with chlorine dioxide and ozone. *Water Research, 38*(17), 3791-3799.

Vel Leitner, N. K., and Roshani, B. (2010). Kinetic of benzotriazole oxidation by ozone and hydroxyl radical. *Water Research, 44*(6), 2058-2066.

Watts, M. J., and Linden, K. G. (2009). Advanced oxidation kinetics of aqueous tri alkyl phosphate flame retardants and plasticizers. *Environmental Science & Technology, 43*(8), 2937-2942.

Wols, B. A., Harmsen, D. J. H., Wanders-Dijk, J., Beerendonk, E. F., and Hofman-Caris, C. H. M. (2015). Degradation of pharmaceuticals in UV (LP)/H2O2 reactors simulated by means of kinetic modeling and computational fluid dynamics (CFD). *Water Research, 75*, 11-24.

Wols, B. A., and Hofman-Caris, C. H. M. (2012). Review of photochemical reaction constants of organic micropollutants required for UV advanced oxidation processes in water. *Water Research, 46*(9), 2815-2827.

Wols, B. A., Hofman-Caris, C. H. M., Harmsen, D. J. H., and Beerendonk, E. F. (2013). Degradation of 40 selected pharmaceuticals by UV/H2O2. *Water Research, 47*(15), 5876-5888.

Xiao, R., Ye, T., Wei, Z., Luo, S., Yang, Z., and Spinney, R. (2015). Quantitative Structure–Activity Relationship (QSAR) for the Oxidation of Trace Organic Contaminants by Sulfate Radical. *Environmental Science & Technology, 49*(22), 13394-13402.

Xiao, Y., Zhang, L., Zhang, W., Lim, K.-Y., Webster, R. D., and Lim, T. T. (2016). Comparative evaluation of iodoacids removal by UV/persulfate and UV/H2O2 processes. *Water Research, 102*, 629-639.

Yang, Y., Lu, X., Jiang, J., Ma, J., Liu, G., Cao, Y., Liu, W., Li, J., Pang, S., Kong, X., and Luo, C. (2017). Degradation of sulfamethoxazole by UV, UV/H2O2 and UV/persulfate (PDS): Formation of oxidation products and effect of bicarbonate. *Water Research, 118*(Supplement C), 196-207.

Yang, Y., Pignatello, J. J., Ma, J., and Mitch, W. A. (2016). Effect of matrix components on UV/H2O2 and UV/S2O82− advanced oxidation processes for trace organic degradation in reverse osmosis brines from municipal wastewater reuse facilities. *Water Research, 89*, 192-200.

Ye, T., Wei, Z., Spinney, R., Tang, C. J., Luo, S., Xiao, R., and Dionysiou, D. D. (2017). Chemical structure-based predictive model for the oxidation of trace organic contaminants by sulfate radical. *Water Research, 116*, 106-115.

Yuan, F., Hu, C., Hu, X., Qu, J., and Yang, M. (2009). Degradation of selected pharmaceuticals in aqueous solution with UV and UV/H2O2. *Water Research, 43*(6), 1766-1774.

Zhang, R., Yang, Y., Huang, C. H., Zhao, L., and Sun, P. (2016). Kinetics and modeling of sulfonamide antibiotic degradation in wastewater and human urine by UV/H2O2 and UV/PDS. *Water Research, 103*, 283-292.

Zhang, T., Zhu, H., and Croué, J. P. (2013). Production of sulfate radical from peroxymonosulfate induced by a magnetically separable CuFe2O4 spinel in water: Efficiency, stability, and mechanism. *Environmental Science and Technology, 47*(6), 2784-2791.

Zuo, Z., Cai, Z., Katsumura, Y., Chitose, N., and Muroya, Y. (1999). Reinvestigation of the acid–base equilibrium of the (bi)carbonate radical and pH dependence of its reactivity with inorganic reactants. *Radiation Physics and Chemistry, 55*(1), 15-23.

Chapter 3. Degradation of Fluoroquinolones by Peroxymonosulfate: Transformation Products and Non-radical Reaction Mechanism with Nitrogenous Moieties

The contents of Chapter 3 & Appendix 2 are unable to be reproduced here as they are under embargo due to current consideration for publication in the journal *Environmental Science & Technology*.

3.1 Abstract

Recent work has demonstrated that peroxymonosulfate (PMS), a peroxide commonly applied as a radical precursor during advanced oxidation processes (AOPs), can degrade organic contaminants without radical involvement. However, little is known about this non-radical reaction mechanism. In this study, we reported that fluoroquinolone antibiotics (except flumequine) can be rapidly degraded by the direct PMS oxidation. Unlike the radical-based AOPs, the degradation of fluoroquinolones by PMS was less influenced by the scavenging effect of the water matrix. The degradation rate followed second-order kinetic and was highly pH and structure-dependent. High resolution mass spectrometry analysis demonstrated that the piperazine ring of fluoroquinolones was the main reaction site. While the oxygen transformation from PMS to contaminants (e.g., sulfur-containing compounds) were previously explained as a main reaction pathway for PMS non-radical process, our study showed that the direct electron-transfer from nitrogenous moieties (piperazine ring) to PMS can produce amide and aldehyde compounds. An amide-containing compound (P320) was found to be the major product, which was also reported from ozonation of ciprofloxacin. Agar disk-diffusion tests indicated that PMS treatment well removed the antibacterial activity of ciprofloxacin with the complete degradation of parent antibiotic, except the transformation products in earlier stage which might still exert antibacterial potency. Study on PMS reactivity was extended to other nitrogenous compounds and results indicated that compounds with tertiary alkyl amine appeared to be more reactive with PMS than those with secondary alkyl amine.

3.2 Introduction

Advanced oxidation processes (AOPs) have gained increasing interests in recent years for the removal of refractory contaminants during water treatment and soil remediation. Hydrogen peroxide (H_2O_2), peroxydisulfate ($S_2O_8^{2-}$, PDS), and peroxymonosulfate (HSO_5^-, PMS) are the commonly used peroxides for AOPs. The activation of these peroxides by energy (e.g., UV irradiation) and electron transfer (e.g., transition metal-based catalysis) generates strong oxidizing species such as hydroxyl radical ($^{\bullet}OH$, 1.9−2.7 V) and sulfate radical ($SO_4^{\bullet-}$, 2.5−3.1 V) (Neta et al., 1988). Many studies have demonstrated that $^{\bullet}OH$ and $SO_4^{\bullet-}$ have high potential to eliminate pharmaceuticals, pesticides and industrial contaminants (Lutze et al., 2015; Wols et al., 2015). However, certain water matrix components (e.g., organic matter, bicarbonate, and halides) are known to reduce the efficiency of AOPs by significantly scavenging the radicals (T. Zhang et al., 2013; Y. Yang et al., 2016). Moreover, the leaching of heavy metal (e.g., cobalt) can be an important issue during transition metal-based AOPs (Ike et al., 2018).

PMS is commercially available and known as Oxone ($2KHSO_5.KHSO_4.K_2SO_4$). It is relatively stable, thus convenient for storage and transportation. The price of PMS (1.36 USD/mol) is higher than that of H_2O_2 (0.05 USD/mol) and PDS (0.18 USD/mol) (Wacławek et al., 2017). PMS has been applied as a non-chlorine disinfectant in swimming pools and for delignification in paper and pulp industry. The electron-transfer from transition metal-based catalysts (e.g., cobalt, copper, iron) and the cleavage of peroxide bond in PMS by UV irradiation and ultrasound can generate $SO_4^{\bullet-}$ and $^{\bullet}OH$ (Ghanbari and Moradi, 2017).

It was recently reported that organic contaminants (e.g., carbamazepine, sulfamethoxazole, chlorophenol) can be decomposed by direct PMS oxidation (i.e., no radical initiator). Quenching studies and electron paramagnetic resonance spectrometry analysis had confirmed that contaminant transformation was attributed to the direct oxidation by PMS without the contribution of radicals (Yang et al., 2018). However, little is known about the reaction mechanism of this non-radical process. Previous studies have found that the reaction might involve the transfer of the distal oxygen in peroxide bond of PMS to contaminants. PMS can efficiently oxidize arsenite As (III) to As (V) through oxygen transfer mechanism (Z. Wang et al., 2014). The

thioether sulfur of β-lactam antibiotics can be substituted by the oxygen from PMS to produce sulfoxide products (Chen et al., 2018). The aniline moieties of sulfonamide antibiotics can be converted to nitroso or nitrobenzene moieties through PMS oxygen substitution (Yin et al., 2018). However, the oxygen substitution pathway can be affected by the steric hindrance, especially for contaminants with complex structures (Chen et al., 2018).

PMS is a strong electron-acceptor with redox potential (E^0 (HSO_5^-/HSO_4^{2-}) =1.82 V_{NHE}) (Steele and Appelman, 1982). Because of its strong electrophilic character, PMS can oxidise/degrade contaminants by electrons withdrawing with carbon nanotube as electron-transfer mediator (Yun et al., 2017). It was reported that PMS can rapidly inactivate the disease-associated prion protein. In this process, the amino acid residues of prion protein was oxidised by PMS through the formation of methionine sulfone and hydroxylated tryptophan residues (Chesney et al., 2016). The transformation of methionine sulfoxide to methionine sulfone might be explained by the oxygen transfer mechanism mentioned above. However, the formation of hydroxylated tryptophan residues suggested that there might be other reaction pathways for PMS non-radical process, especially for nitrogenous compounds.

In this study, we focused on fluoroquinolone antibiotics (ciprofloxacin, norfloxacin, enrofloxacin, and flumequine) and their structurally related compound 1-(2-fluorophenyl) piperazine (Table 3-1). Fluoroquinolones are among the most consumed antibiotic classes in the world. Due to their resistance to biodegradation and high adsorption affinity, fluoroquinolones show long half-life times in the environment (e.g., 10.6 days in surface water and 580 days in soil). Fluoroquinolones were detected from wastewater, surface water, ground water and sediment/soil with concentrations ranging from ng/L to mg/L (Van Doorslaer et al., 2014). As shown in Table 3-1, fluoroquinolones are characterized with a core quinolone ring structure containing a nitrogen atom. Ciprofloxacin, norfloxacin, and enrofloxacin also have a piperazine ring with 2 more amine nitrogen atoms. The aim of this study was to investigate the reactivity of PMS toward fluoroquinolones. The degradation kinetics as well as the effect of pH and common water matrix components were carefully studied. The transformation products of ciprofloxacin after PMS exposure were tentatively identified by high resolution mass spectrometry. MS^2 and MS^3 fragmentation were

applied for most compounds for structural identification. Based on the characteristics of the transformation products, possible reaction mechanisms of PMS reaction with nitrogenous compounds were proposed. Agar diffusion tests were applied to investigate the residual antibacterial activity of ciprofloxacin after PMS oxidation. Finally, the study on PMS reactivity was extended to other nitrogenous compounds (i.e., metoprolol and venlafaxine) to investigate the efficiency of PMS toward secondary and tertiary amine moieties.

Table 3-1. Properties of compounds investigated in this study

Compounds	MW	p*K*a[a]	Structures
Ciprofloxacin (CIP)	331.3	pK_{a1}=6.2 pK_{a2}=8.8	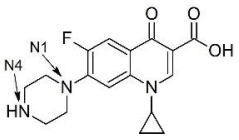
Norfloxacin (NOR)	319.3	pK_{a1}=6.22 pK_{a2}=8.51	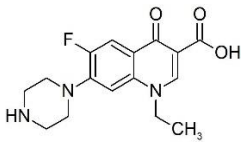
Enrofloxacin (ENR)	359.3	pK_{a1}=6.1 pK_{a2}=7.7	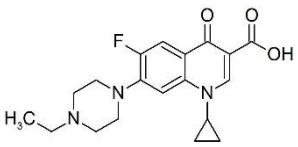
Flumequine (FLU)	261.2	6.5	
1-(2-fluorophenyl) piperazine	180.2	pK_{a1}=4.49 pK_{a2}=8.63	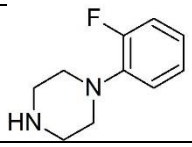
Metoprolol	267.3	9.7	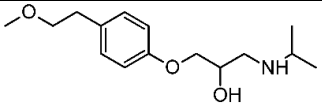
Venlafaxine	277.4	9.4	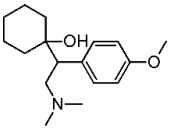

[a] p*K*a values were obtained from Jiang et al. (2016).

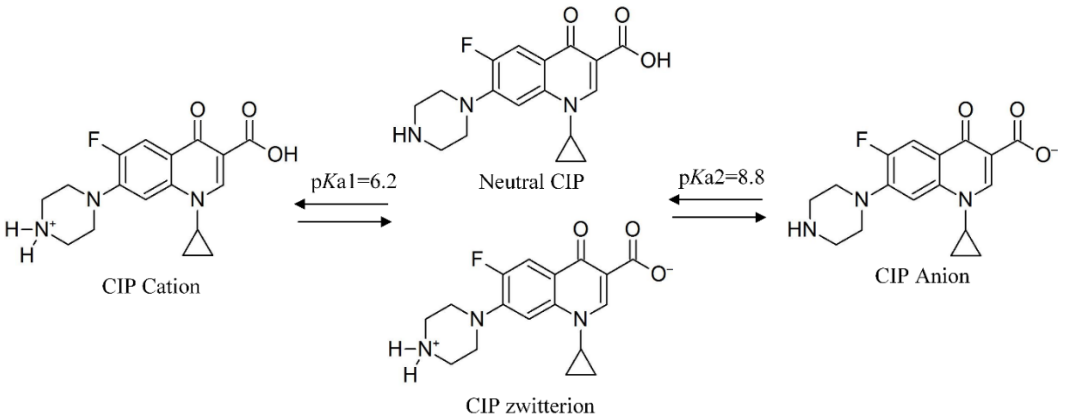

Figure 3-1. The acid-base species of ciprofloxacin (CIP)

3.3 Materials and Methods

3.3.1 Chemical reagents

All chemicals were in analytical grade or higher and used as received without further purification. Potassium peroxymonosulfate (available as Oxone®), ciprofloxacin (≥98%), norfloxacin (≥98%), enrofloxacin (≥98%), flumequine (≥97%), 1-(2-fluorophenyl) piperazine (97%), metoprolol ((≥98.5%), venlafaxine (≥98%), *tert*-butanol (≥99%), and ethanol (pure) were purchased from Sigma-Aldrich. Suwannee River hydrophobic fraction was applied as natural organic matter isolate, which was extracted according to previously published method (Leenheer et al., 2000). All solutions were prepared in Milli-Q water (18 MΩ cm, Millipore).

3.3.2 Experimental procedures

Experiments were conducted in amber glass bottles at room temperature (22 ± 1℃). Predetermined volumes of target compounds and PMS stock solutions were injected into 25 mL of 10 mM phosphate (pH = 6.2−8) or borate (pH = 8.2−11) buffer to get the desired initial concentrations. Samples were periodically withdrawn and quenched with excess sodium thiosulfate. For most experiments, the initial concentrations applied for target compound and PMS were 5 and 100 μM, respectively. Reaction time was ranged from 2 to 120 min. In order to better identify the transformation products, high concentration of ciprofloxacin (50 μM) was treated with 50 μM and 1 mM of PMS. For antibacterial activity tests, 5 μM of ciprofloxacin was degraded by 100 and 250 μM of PMS. Most experiments were conducted at least in duplicate.

3.3.3 Analytical methods

Quantitative analysis of target compounds were carried out with a High Performance Liquid Chromatography (HPLC, Agilent 1100) coupled with a Diode Array Detector (DAD, Agilent 1100) and a XDB-C18 column (5 μm, 4.6 × 150 mm, Agilent). Mobile phase composition followed various isocratic mixtures of methanol or acetonitrile with 0.1% phosphoric acid. All compounds were analysed on their maximum UV absorption. A detailed information on HPLC methods are provided in supporting information (Table A-2-1).

The transformation products of ciprofloxacin were identified using an Accela 600 liquid chromatography system coupled to a high resolution mass spectrometry (LC-

HRMS, LTQ Orbitrap XL, Thermo Fisher), fitted with an electrospray ion source (ESI). Compounds were separated on a kinetex C18 column (2.6 µm, 100× 2.1 mm, phenomenex). Full scan and MS^2 fragmentation scan were conducted in positive ionisation mode (+eV). MS^3 fragmentation was additionally applied for compounds with major peak areas on LC-HRMS. Details on LC-HRMS parameters are provided in Table A-2-2.

3.3.4 Antibacterial activity test

Agar disk-diffusion tests were conducted to investigate the antibacterial activity of ciprofloxacin (5 µM) after PMS exposure (100 and 250 µM) using *Escherichia. coli* B (*E. coli* B) as the test microorganism according to the Clinical and Laboratory Standards Institute (CLSI, 2012). Briefly, lysogeny (LB) agar plates were inoculated with 100 µL of an overnight culture of *E. coli* B equivalent to 0.5 McFarland. Then, blank antibiotic cartridges (about 6 mm in diameter), containing the test solutions, were placed on the agar surface. The diameters of inhibition zones around discs were measured after the plate was incubated overnight at 37 ℃. A wider zone of no growth indicates a stronger antibacterial activity of the test solution. By comparing the diameters of the inhibition zones from PMS treated samples of ciprofloxacin and the ciprofloxacin standards with known concentrations (0.2, 0.5, 1, 2, 3, 4 and 5 µM), the removal of ciprofloxacin antibacterial activity after PMS exposure can be determined. Each sample was tested in triplicates.

3.4 Results and Discussion

3.4.1 Degradation kinetics of fluoroquinolones and their structurally related compound by PMS

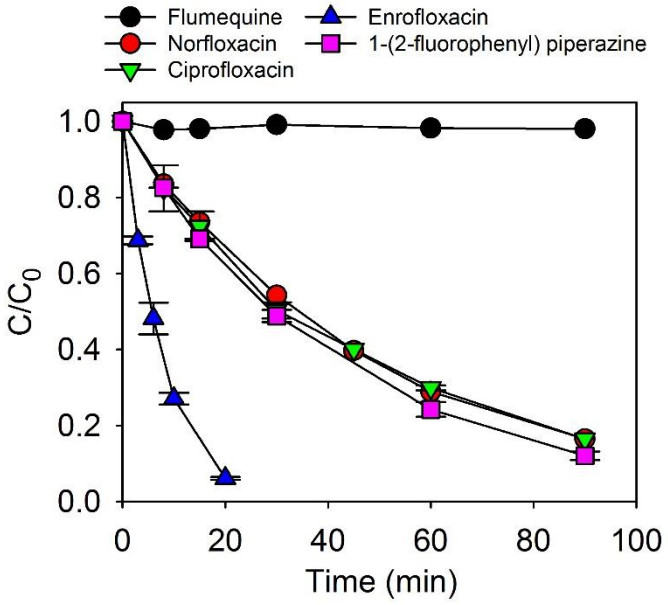

Figure 3-2. Relative removal of selected fluoroquinolones and 1-(2-fluorophenyl) piperazine by PMS (Target compounds=5 µM; PMS=100 µM; 10 mM phosphate buffer at pH 8. Error bars represent the standard deviations of duplicated experiments)

The degradation of selected fluoroquinolones i.e., ciprofloxacin (CIP), norfloxacin (NOR), enrofloxacin (ENR), and flumequine (FLU) as well as 1-(2-fluorophenyl) piperazine by PMS was investigated in the absence of chemical catalysts or UV irradiation (Figure 3-2). The degradation efficiencies of the investigated compounds by PMS varied significantly depending on their structural characteristics. FLU, a fluoroquinolone without piperazine ring (Table 3-1), was found to be stable in the presence of PMS in these experimental conditions, suggesting that PMS does not react with quinolone ring. The cyclopropane ring of CIP is substituted by an ethyl group in NOR. 1-(2-fluorophenyl) piperazine has a fluorobenzene ring instead of the quinolone ring. However, CIP, NOR and 1-(2-fluorophenyl) piperazine all have the same piperazine ring structure and exhibited comparable degradation rates toward PMS. These results indicated that piperazine ring was the main reaction site for PMS. This was further supported by LC-HRMS analyses (Section 3.4.4) from which only piperazine ring cleavage products were identified after PMS exposure. The N4 (see CIP in Table 3-1 for atom numbering) in piperazine ring of ENR is substituted by an

ethyl group (tertiary amine), which differs from CIP (secondary amine). ENR was degraded by PMS much faster than CIP. The structure dependence of PMS reaction with fluoroquinolones will be discussed in Section 3.4.6.

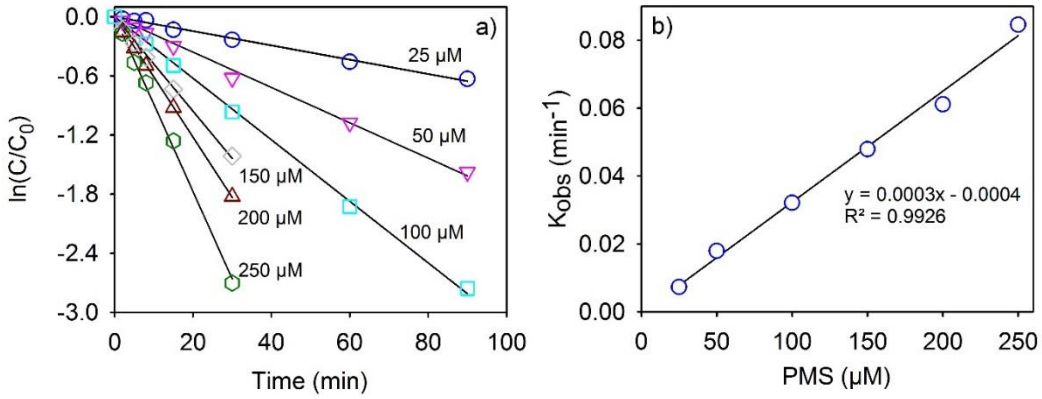

Figure 3-3. a) Effect of the initial concentration of PMS on ciprofloxacin degradation; b) k_{obs} versus initial concentration of PMS (Ciprofloxacin=5 μM; 10 mM borate buffer at pH 8.2)

The degradation of CIP was promoted with increasing of initial PMS dose, following the pseudo-first order kinetics (R^2>0.99) (Figure 3-3a). The measured rate constants, k_{obs}, were derived from the slope of ln(C/C$_0$) versus time. As shown in Figure 3-3b, k_{obs} exhibited a linear relationship toward initial PMS dose, suggesting that the overall reaction rate can be described by the second-order kinetic at the given pH of 8.2. According to the equation 1 and 2, the apparent second-order rate constant, k_{app}, of CIP with PMS was calculated to be 5.28 ± 0.08 (M^{-1} s^{-1}) at pH 8.2.

$$\frac{d[CIP]}{dt} = -k_{obs}[CIP] \qquad (1)$$

$$\frac{d[CIP]}{dt} = -k_{app}[CIP][PMS] \qquad (2)$$

3.4.2 Effect of pH

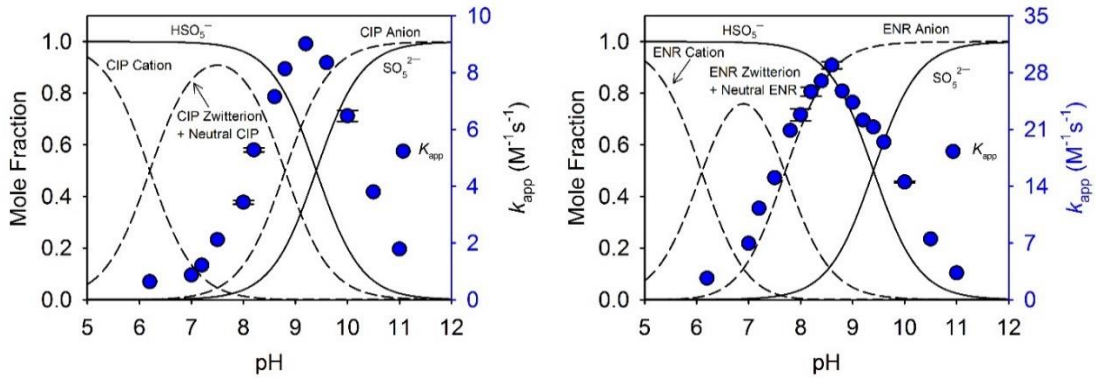

Figure 3-4. Effect of pH on the distribution of acid-base species of fluoroquinolones and their apparent second-order constants with PMS. (Ciprofloxacin (a. CIP)= Enrofloxacin (b. ENR)= 5 μM; PMS=100 μM; 10 mM phosphate or borate buffer at pH 6.2−11; The acid-base species of CIP were shown in Scheme 1 as an example; Error bars represent the standard deviations of duplicated experiments)

As illustrated in Figure 3-4, the degradation efficiency (k_{app}) of CIP and ENR by PMS were highly pH-dependent. The pH-dependent reactivity of fluoroquinolones was also observed with free chlorine (Dodd et al., 2005), manganese oxide (H. Zhang and Huang, 2005), ozone (Dodd et al., 2006), and chlorine dioxide (P. Wang et al., 2010). The pH-dependence of fluoroquinolones degradation can be explained by the change in distribution of fluoroquinolones and PMS acid-base species with pH. The pK_a values of CIP and ENR relevant to these experimental conditions were given in Table 3-1. As shown in Figure 3-1, pK_{a1} and pK_{a2} are related to the deprotonation of the carboxylic group and the protonation of N4 in the piperazine ring, respectively (Takács-Novák et al., 1990). PMS is dissociated into SO_5^{2-} at alkaline pH ($HSO_5^- + H_2O \rightleftarrows SO_5^{2-} + H_3O^+$, p$K_{a2}$=9.4) (Ball and Edwards, 1956). The k_{app} values of CIP and ENR increased with the increasing molar fraction of the anionic species (Figure 3-4), suggesting that the anion forms of CIP and ENR were most susceptible to PMS oxidation. In general, N4 in piperazine ring is deprotonated when CIP and ENR are present in anionic form, consequently showing stronger nucleophilic character. The highest k_{app} values of CIP and ENR were found around pH 9 and pH 8.6, respectively, then sharply decreased with the increasing of SO_5^{2-} mole fraction, suggesting that SO_5^{2-} is a weaker oxidant compared to PMS. SO_5^{2-} was also reported to be less reactive than PMS with β-lactam antibiotics, due to its weaker electrophilic property (Chen et al., 2018).

3.4.3 Identification of reactive species and effect of the water matrix

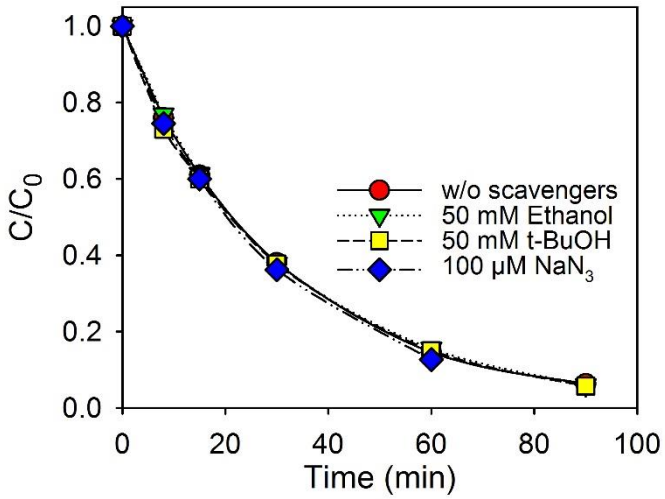

Figure 3-5. Effect of alcohols and NaN_3 on the degradation of ciprofloxacin by PMS (Ciprofloxacin=5 μM; PMS= 100 μM; Alcohols= 50 mM; NaN_3= 100 μM; 10 mM borate buffer at pH 8.2)

Generally, $SO_4^{\bullet-}$ and $^{\bullet}OH$ are considered as the main reactive species during PMS activation by UV irradiation, heat and transition metal-based catalysts. Quenching studies with alcohols are widely employed during AOPs to investigate the contribution of radicals. *tert*-Butyl alcohol (*t*-BuOH) reacts with $^{\bullet}OH$ ($k_{\bullet OH}$=6 × 10^8 M^{-1} s^{-1}) with rate constant 3 orders of magnitude higher than that with $SO_4^{\bullet-}$ ($k_{SO_4^{\bullet-}}$=7.6 ×10^5 M^{-1} s^{-1}) (Yang et al., 2015), while ethanol effectively scavenges both radicals ($k_{\bullet OH}$=1.2−2.8 × 10^9 M^{-1} s^{-1} and $k_{SO_4^{\bullet-}}$=1.6−7.8 ×10^7 M^{-1} s^{-1}) (T. Zhang et al., 2013). As shown in Figure 3-5, the presence of excess ethanol and *t*-BuOH didn't affect the degradation kinetic of CIP, indicating there was no $SO_4^{\bullet-}$ and $^{\bullet}OH$ involvement. It is well known that the self-decomposition of PMS generates $^1O_2$ ($HSO_5^- + SO_5^{2-} \rightarrow HSO_4^- + SO_4^{2-} + {}^1O_2$) (Ball and Edwards, 1956; Evans and Upton, 1985). The rate of self-decomposition strongly depends on the ionic strength and pH of the aqueous solution, reaching the maximum around pH 9−9.4 (Yang et al., 2018). It was recently reported to be 0.013 ± 0.0003 M^{-1} s^{-1} at pH 9.4 with 0.5 M of ionic strength (controlled by $NaClO_4$) (Yang et al., 2018), which was about 700 times lower than the k_{app} of CIP determined in this study (9.02 M^{-1} s^{-1} at pH 9.2). Ketones and quinones can accelerate the self-decomposition of PMS for $^1O_2$ production due to the nucleophilic interaction of PMS with carbonyl group (C=O) (Lange and Brauer, 1996; Zhou et al., 2015). As shown in Table 3-1, the fluoroquinolones investigated in this study had a carbonyl

group in their quinolone ring, which might be associated with the formation of $^1O_2$ as an active oxidizing species. However, 100 µM of NaN_3, a commonly used quencher for $^1O_2$ (1×10^9 M^{-1} s^{-1}) (Cheng et al., 2017), didn't inhibit CIP kinetic, indicating $^1O_2$ was not responsible for the degradation of fluoroquinolones by PMS (Figure 3-5). Previous studies also demonstrated that the contribution of $^1O_2$ (if formed) to the oxidation of organic compounds by PMS non-radical mechanism was minor, possibly because of its insufficient formation and quenching by water (Yang et al., 2018; Yun et al., 2018).

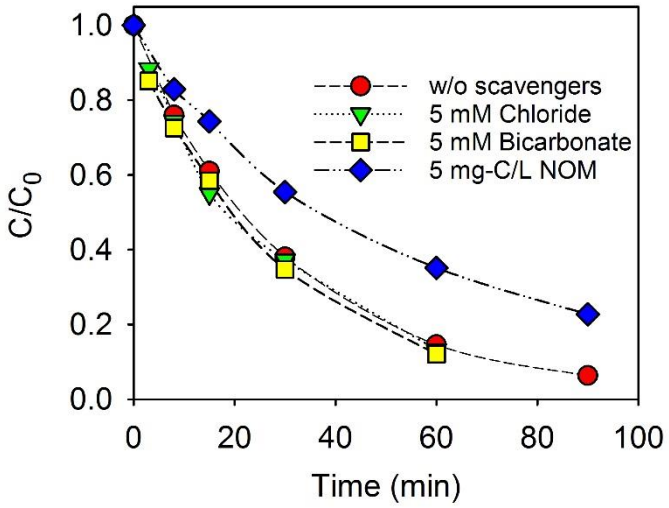

Figure 3-6. Effect of the water matrix on the degradation of ciprofloxacin by PMS (Ciprofloxacin= 5 µM; PMS= 100 µM; Chloride= Bicarbonate= 5 mM; NOM= 5 mg-C/L; 10 mM borate buffer at pH 8.2)

The water matrix components can compete with the target contaminants to consume radicals during AOPs, consequently lowering the efficiency of treatment. The effect of the common water matrix components (i.e., NOM, chloride and bicarbonate) on the CIP degradation by PMS were investigated. Unlike the radical-based AOPs, the degradation of CIP by PMS was not impacted by the presence of 5 mM of chloride and bicarbonate (Figure 3-6). PMS was previously reported to oxidize chloride ion into chlorine, which can contribute to contaminant degradation (Fortnum et al., 1960). However, the acceleration of CIP degradation rate was not observed in this study upon the addition of 5 mM of chloride. This can be explained by the insufficient formation of chlorine due to the low reaction rate constant of chloride with PMS (1.4×10^{-3} M^{-1} s^{-1}) (Fortnum et al., 1960), which was about 3 orders of magnetic lower than k_{app} of

CIP with PMS in this study (5.28 ± 0.08 M^{-1} s^{-1} at pH 8.2). The addition of 5 mg-C/L NOM slightly inhibited the removal of CIP, suggesting that PMS can be scavenged by NOM.

3.4.4 Transformation products and possible reaction mechanism

Table 3-2. Transformation products of ciprofloxacin (CIP) detected by LC-HRMS

Compound	RT[a]	Molecular Formula	Molecular Mass[b]	MS^{2c} *m/z*	Proposed Structures
CIP	12.6	$C_{17}H_{19}O_3N_3F$	332.1404 (-0.169)	314, 288	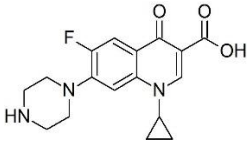
P263	16.7	$C_{13}H_{12}O_3N_2F$	263.0826 (-0.369)	245, 263	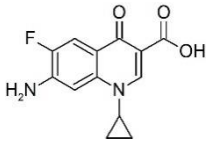
P291	17.4	$C_{14}H_{12}O_4N_2F$	291.0775 (-0.177)	273, 291	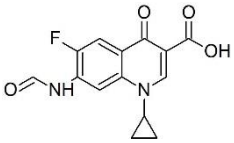
P306	12.3	$C_{15}H_{17}O_3N_3F$	306.1248 (-0.183)	306, 288	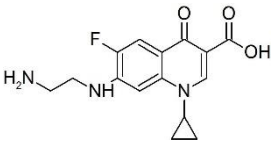
P320	18.0	$C_{15}H_{15}O_4N_3F$	320.1034 (-0.252)	302, 320 MS^3: 258, 265, 285, 302, 224, 245, 217	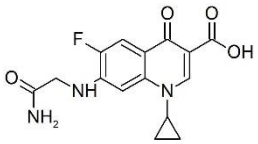
P334a	11.1	$C_{16}H_{17}O_4N_3F$	334.1198 (-0.750)	316, 317, 314, 306, 296 MS^3: 296, 245, 230, 271, 288	
P334b	17.3	$C_{16}H_{17}O_4N_3F$	334.1199 (-0.301)	316 MS^3: 271, 289, 298	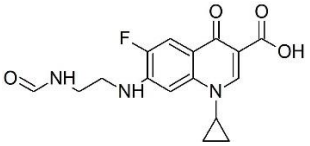

P348a	8.2	$C_{17}H_{19}O_4N_3F$	348.1348 (-1.841)	331, 287, 304 MS^3: 287, 273	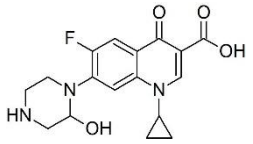
P348b	17.3	$C_{17}H_{19}O_4N_3F$	348.1354 (-0.002)	330, 287, 316 MS^3:285, 272, 310, 282	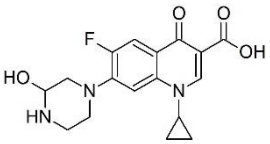
P362	13.2	$C_{17}H_{17}O_5N_3F$	362.1143 (-0.985)	344, 362	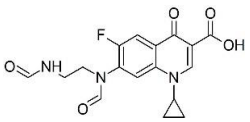
P364a	12.4	$C_{17}H_{19}O_5N_3F$	364.1302 (-0.372)	346, 364 MS^3: 326, 288, 271	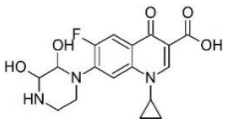
P364b	16.5	$C_{17}H_{19}O_5N_3F$	364.1239 (-0.372)	346, 364, 328 MS^3: 346, 328, 275, 257	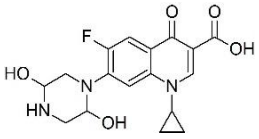

[a] Retention time (min); [b] Experimental mass for $[M+H]^+$; numbers in brackets reperesent the error (ppm); [b] MS^3 fragmentation was additionally applied for P320, P334a,b, P348a,b and P364a,b.

Eleven transformation products of CIP after PMS oxidation were detected by LC-HRMS (Table 3-2). Their structures were tentatively proposed based on the accurate mass derived from HRMS and MS^2 fragmentation pattern. MS^3 fragmentation was also applied for compounds with major peak areas. The proposed structures of transformation products indicated that the reaction occurred by the hydroxylation and dealkylation of piperazine ring, with subsequent formation of aldehyde and amide moieties. The core quinolone ring of CIP remained intact and no defluorination or decarboxylation products were detected, suggesting that PMS generated less transformation products from CIP compared to the Fenton oxidation (Giri and Golder, 2014), $SO_4^{\bullet-}$ (Jiang et al., 2016) and photolytic reactions (Paul et al., 2010). These results were consistent with the fact that FLU, which does not incorporate a piperazine ring, did not react with PMS (Figure 3-2). Most of transformation products (e.g., P263, P291, P306, P334, P348, P362, and P364) were analogues to those found during the oxidative transformation of CIP by manganese oxide (H. Zhang and Huang, 2005),

chlorine dioxide (P. Wang et al., 2010), permanganate (Hu et al., 2011) and Ferrate (VI) (B. Yang et al., 2016), revealing that PMS may share a similar reaction mechanism with these oxidants. Interestingly, and to the best of our knowledge, transformation product P320 was only reported from the ozonation of CIP (Liu et al., 2012). The MS^3 spectrum of P320 exhibited a dominant ion cluster *m/z* 258 corresponding to the loss of an amide group ($-CH_2ON$) from the major ion cluster *m/z* 302 in its MS^2 spectrum. Thus the postulated structure of P320 is an amide moiety formed at the secondary aliphatic amine (N4) of the piperazine ring.

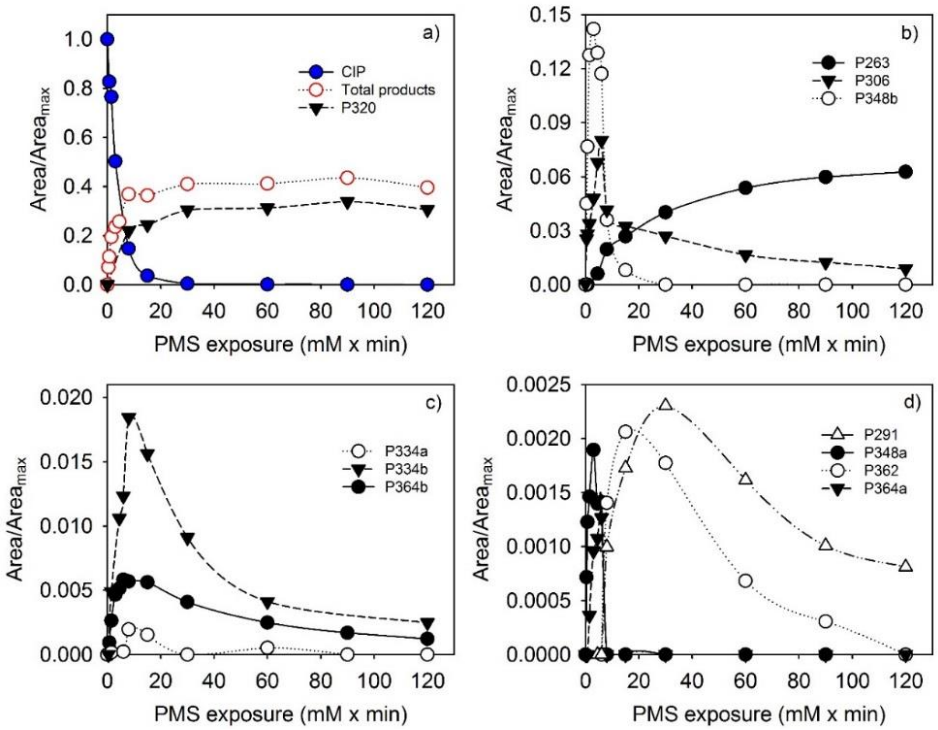

Figure 3-7. The evolution of the normalized peak areas of ciprofloxacin (CIP) and its transformation products with PMS exposure. Area$_{max}$ represents the peak area of ciprofloxacin at t=0 (Ciprofloxacin= 50 µM; PMS= 0.05 and 1 mM; 10 mM borate buffer at pH 8.2)

Figure 3-7 presents the evolution of the normalized peak areas of CIP and its transformation products with PMS exposure. P320 exerted the largest peak area among all identified transformation products; its peak area was close to the sum of the peaks areas of all transformation products. P320 was formed rapidly with the degradation of CIP and reached a plateau after an exposure of 30 mM × min. P263, which refers to the complete loss of the piperazine ring, gradually increased with exposure time. Thus P320 and P263 were the final products in these experimental conditions while all other

compounds were intermediates showing maximum production at different oxidant exposure. For example, P334b and P362 reached their highest peak areas while P320 almost reached a plateau, indicating that P334b and P362 were unlikely the intermediates of P320.

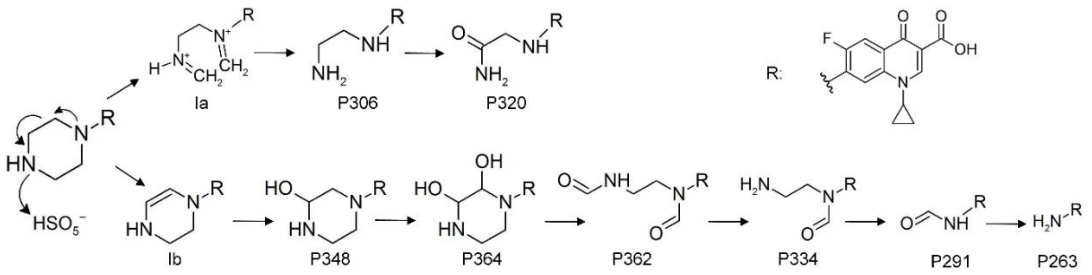

Figure 3-8. Proposed degradation mechanism of ciprofloxacin by PMS (Ia, b are the proposed intermediates)

In accordance with the postulated structures of the transformation products and the evolution of their peak areas on LC-HRMS chromatograms, two reaction pathways were proposed for the oxidative transformation of CIP by PMS (Figure 3-8). The reaction was initiated by the direct electron transfer from piperazine ring to PMS. In this process, PMS acted as an electron acceptor, rather than a radical precursor, to directly oxidize CIP without involving radicals. Notably, unlike PMS, PDS and H_2O_2 did not react with CIP under the same experimental conditions (Figure A-2-1), suggesting that PMS is a more efficient electron acceptor than PDS and H_2O_2, possibly due to its asymmetric structure (Lei et al., 2016). This is consistent with previous findings that PMS was superior to PDS for the removal of organic contaminants during the mediated electron transfer through carbon nanotubes (Yun et al., 2017; Yun et al., 2018).

The N4 atom of piperazine ring was the critical site for the electrophilic attack of PMS. The N1 atom is known to be less reactive to electrophiles than N4 due to its direct connection to fluoroquinolone ring substituted by strong electron-withdrawing fluorine and –COOH (Dodd et al., 2005; Giri and Golder, 2014). Nevertheless, previous studies have demonstrated that piperazine ring should be considered as a whole reaction centre with the contribution of both nitrogen atoms to electron-transfer (P. Wang et al., 2010). The initial electron transfer from piperazine ring to PMS produces an imine intermediate (Ia, Figure 3-8) as proposed by Dodd et al. (2005) and P. Wang et al. (2010) for the oxidation of CIP by free chlorine and chlorine dioxide,

respectively. Hydrolysis of the imine intermediate rapidly induced the dealkylation of the piperazine ring to generate P306. The subsequent electron transfer from the amine group of P306 to PMS was followed by hydrolysis producing P320. The presence of highly electron-withdrawing carbonyl group (C=O) in P320 possibly limited the electron transfer from amide-N to PMS, thus P320 was stable in the presence of excess PMS (Figure 3-7a). The formation of hydroxylated products P348 and P364 suggested the presence of a similar enamine intermediate (Ib, Figure 3-8), which has been proposed for the reactions of permanganate (Hu et al., 2011) and Ferrate (IV) (B. Yang et al., 2016) with CIP. The double bond of enamine can be oxidized to aldehyde moieties (P362, P334 and P291), leading to the complete degradation of piperazine ring.

3.4.5 Antibacterial activity assays

An important step when investigating the efficiency of a treatment to degrade an antibiotic is to evaluate the elimination of its antibacterial activity. The transformation products of parent antibiotics might still possess antibacterial activity, thus maintaining the risk of dissemination of antibiotic resistance in the environment. Fluoroquinolones inhibit the bacterial DNA replication by hydrogen binding and charge interactions with the relaxed DNA. The core quinolone structure is believed to be responsible for DNA-binding (Dodd et al., 2006), while the fluorine substitute plays an important role in inhibiting the DNA gyrase and enhancing cell permeation (Serna-Galvis et al., 2017).

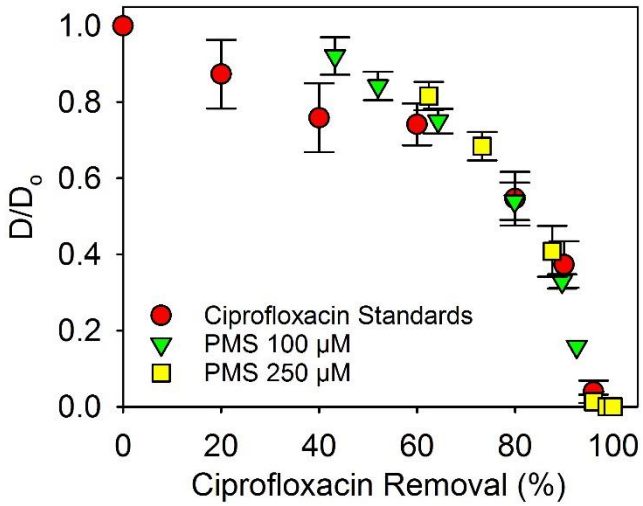

Figure 3-9. Antibacterial activity removal of ciprofloxacin (CIP) during PMS treatment. D_0 represents the diameter of the inhibition zone in agar plate formed by 5 µM of CIP standard solution (CIP standards: 0.2, 0.5, 1, 2, 3, 4 and 5 µM; for PMS treatment, initial concentration of CIP=5 µM, PMS= 100 and 250 µM, 10 mM borate buffer at pH 8.2; Error bars represent the standard deviations of triplicated experiments)

Based on LC-HRMS results, the transformation products of CIP after PMS treatment still retained the core quinolone structure, raising concerns about the residual antibacterial activity. Thus agar diffusion assays were conducted with *E.coli B* as an indicator. As shown in Figure 3-9, the antibacterial activity of the solution gradually reduced with the removal of CIP during PMS treatment. However, after 40 to 50% removal of CIP with 100 µM of PMS, the sample resulted in a larger inhibition zone in agar plate than CIP standard solutions. This result indicated that the transformation products at earlier stage (e.g., hydroxylated product P348b, Figure 3-7b) might still exert antibacterial potency. The residual antibacterial activity was removed efficiently with the complete degradation of CIP, suggesting that the major final products P320 and P263 showed negligible antibacterial activity compared to CIP. The structural modifications on piperazine ring alters the acid-base speciation and significantly affects fluoroquinolones cell permeation (Paul et al., 2010). Although the amide and aldehyde moieties produced after PMS exposure kept the core quinolone structure in this study, they possibly changed the physicochemical characteristics of CIP, consequently reduced its uptake by bacteria cell and binding to DNA. Our results were in agreement with previous findings that the photolytic transformation products of CIP

retaining the quinolone ring significantly diminished the antibacterial potency of parent antibiotic (Paul et al., 2010).

3.4.6 Reactivity of PMS with other nitrogenous compounds

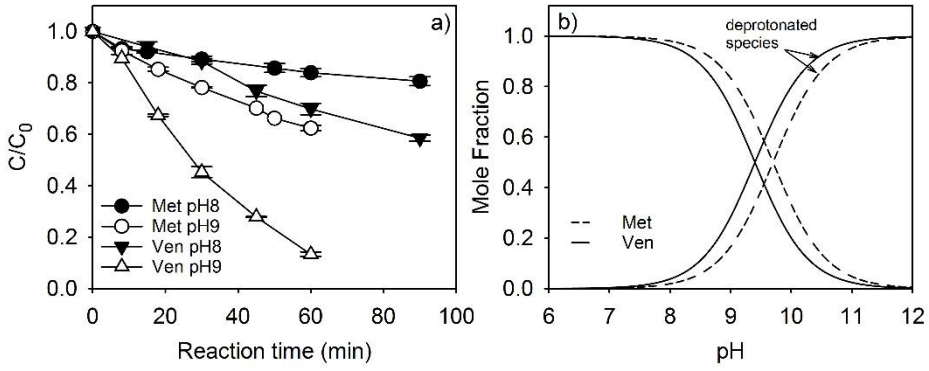

Figure 3-10. a) Degradation of metoprolol (Met) and venlafaxine (Ven) by PMS (Met=Ven=5 µM, PMS= 100 µM); b) Distribution of the acid-base species of Met and Ven (Error bars represent the standard deviations of duplicated experiments).

As shown in Figure 3-2 and 3-4, ENR was degraded much faster by PMS compared to CIP probably because the N4 atom of ENR is a tertiary amine substituted by an electron-donating ethyl group. Interestingly, chlorine dioxide was also found to be more reactive with ENR than CIP (P. Wang et al., 2010), while free chlorine was more reactive with CIP than ENR (Dodd et al., 2005). While the reactivity of free chlorine with tertiary amine to produce N-chlorinated moieties can be limited due to the steric hindrance phenomenon, PMS might be more reactive toward tertiary alkyl amine than secondary alkyl amine via electron transfer, a similar reactivity trend found from chlorine dioxide (Lee and von Gunten, 2010; P. Wang et al., 2010). To support these findings, the oxidative transformation of metoprolol and venlafaxine by PMS were investigated at pH 8 and 9. As shown in Table 3-1, metoprolol contains a secondary amine (p*K*a=9.7) whereas venlafaxine (p*K*a=9.4) has a tertiary amine. The degradation of both compounds by PMS were impacted by pH (Figure 3-10a), suggesting that the amine group was likely the main reaction site. The degradation rates were faster at pH 9 than pH 8 for both compounds due to the presence of more deprotonated fractions at higher pH (p*K*a>9) (Figure 3-10b). PMS was more reactive with venlafaxine than metoprolol in both conditions. The fraction of deprotonated venlafaxine was 0.28 at pH 9, which was 1.7 times higher than metoprolol ($\alpha_{\text{deprotonated metoprolol}}$=0.17). However, k_{obs} of venlafaxine (0.031 min^{-1}) was about 4 times higher than that of metoprolol

($0.008\ min^{-1}$). These results were consistent with the structure-dependent reactivity of fluoroquinolones mentioned above that PMS was more reactive with tertiary alkyl amine than secondary alkyl amine.

3.5 Conclusions

1) PMS can efficiently degrade the selected fluoroquinolones (except FLU) without activation. Quenching studies have confirmed that there was no involvement of $SO_4^{\bullet-}$, $^{\bullet}OH$ and $^1O_2$.

2) The degradation of CIP by PMS followed the second-order reaction kinetic and was highly pH-dependent. The distribution of acid-base species of both fluoroquinolones and PMS affected the reaction rate. The deprotonated fraction of CIP and ENR were more reactive compared to the protonated fractions. PMS was found to be a stronger oxidant than SO_5^{2-}.

3) Eleven transformation products of CIP were tentatively identified by LC-HRMS. According to the characteristics of transformation products as well as the structure-dependent reactivity of fluoroquinolones with PMS, the piperazine ring was identified as the main reaction site. The electron transfer from piperazine ring to PMS induced the dealkylation and hydroxylation of piperazine ring, eventually led to the formation of amide and aldehyde moieties. P320 with an amide group was the main transformation product based on its peak area on LC-HRMS. Compounds with tertiary alkyl amine group (i.e., ENR and venlafaxine) were more susceptible to PMS attack than the compounds containing secondary alkyl amine (i.e., CIP and metoprolol).

4) PMS efficiently removed the antibacterial activity of CIP. However, the transformation products in earlier stage of the reaction might still exert antibacterial potency. A complete elimination of parent compound as well as its transformation products is required during fluoroquinolones treatment by PMS.

5) CIP degradation by PMS was less impacted by the common water matrix components (e.g., bicarbonate, chloride), suggesting that the fluoroquinolones treatment by PMS might be applied in real water matrix. However, NOM slightly inhibited the removal of CIP. Therefore, future studies are needed to investigate the

reactivity of PMS with NOM fractions of different character with the objective to optimize the PMS dose for its best treatment efficiency.

3.6 Reference

Ball, D. L., and Edwards, J. O. (1956). The Kinetics and Mechanism of the Decomposition of Caro's Acid. I. *Journal of the American Chemical Society, 78*(6), 1125-1129.

Chen, J., Fang, C., Xia, W., Huang, T., and Huang, C.-H. (2018). Selective Transformation of β-Lactam Antibiotics by Peroxymonosulfate: Reaction Kinetics and Nonradical Mechanism. *Environmental Science & Technology, 52*(3), 1461-1470.

Cheng, X., Guo, H., Zhang, Y., Wu, X., and Liu, Y. (2017). Non-photochemical production of singlet oxygen via activation of persulfate by carbon nanotubes. *Water Research, 113*, 80-88.

Chesney, A. R., Booth, C. J., Lietz, C. B., Li, L., and Pedersen, J. A. (2016). Peroxymonosulfate Rapidly Inactivates the Disease-Associated Prion Protein. *Environmental Science & Technology, 50*(13), 7095-7105.

CLSI. (2012). Performance Standards for Antimicrobial Disk Susceptibility Tests. Approved Standard, 7th ed *CLSI documnet M02-A11*. Wayne, Pennsylvania, USA: Clinical and Laboratory Standards Institute.

Dodd, M. C., Buffle, M.-O., and von Gunten, U. (2006). Oxidation of Antibacterial Molecules by Aqueous Ozone: Moiety-Specific Reaction Kinetics and Application to Ozone-Based Wastewater Treatment. *Environmental Science & Technology, 40*(6), 1969-1977.

Dodd, M. C., Shah, A. D., von Gunten, U., and Huang, C.-H. (2005). Interactions of Fluoroquinolone Antibacterial Agents with Aqueous Chlorine: Reaction Kinetics, Mechanisms, and Transformation Pathways. *Environmental Science & Technology, 39*(18), 7065-7076.

Evans, D. F., and Upton, M. W. (1985). Studies on singlet oxygen in aqueous solution. Part 3. The decomposition of peroxy-acids. *Journal of the Chemical Society, Dalton Transactions*(6), 1151-1153.

Fortnum, D. H., Battaglia, C. J., Cohen, S. R., and Edwards, J. O. (1960). The Kinetics of the Oxidation of Halide Ions by Monosubstituted Peroxides. *Journal of the American Chemical Society, 82*(4), 778-782.

Ghanbari, F., and Moradi, M. (2017). Application of peroxymonosulfate and its activation methods for degradation of environmental organic pollutants: Review. *Chemical Engineering Journal, 310*, 41-62.

Giri, A. S., and Golder, A. K. (2014). Ciprofloxacin degradation from aqueous solution by Fenton oxidation: reaction kinetics and degradation mechanisms. *RSC Advances, 4*(13), 6738-6745.

Hu, L., Stemig, A. M., Wammer, K. H., and Strathmann, T. J. (2011). Oxidation of Antibiotics during Water Treatment with Potassium Permanganate: Reaction Pathways and Deactivation. *Environmental Science & Technology, 45*(8), 3635-3642.

Ike, I. A., Linden, K. G., Orbell, J. D., and Duke, M. (2018). Critical review of the science and sustainability of persulphate advanced oxidation processes. *Chemical Engineering Journal, 338*, 651-669.

Jiang, C., Ji, Y., Shi, Y., Chen, J., and Cai, T. (2016). Sulfate radical-based oxidation of fluoroquinolone antibiotics: Kinetics, mechanisms and effects of natural water matrices. *Water Research, 106*, 507-517.

Lange, A., and Brauer, H.-D. (1996). On the formation of dioxiranes and of singlet oxygen by the ketone-catalysed decomposition of Caro's acid. *Journal of the Chemical Society, Perkin Transactions 2*(5), 805-811.

Lee, Y., and von Gunten, U. (2010). Oxidative transformation of micropollutants during municipal wastewater treatment: Comparison of kinetic aspects of selective (chlorine, chlorine dioxide, ferrateVI, and ozone) and non-selective oxidants (hydroxyl radical). *Water Research, 44*(2), 555-566.

Leenheer, J. A., Croué, J.-P., Benjamin, M., Korshin, G. V., Hwang, C. J., Bruchet, A., and Aiken, G. R. (2000). Comprehensive Isolation of Natural Organic Matter from Water for Spectral Characterizations and Reactivity Testing *Natural Organic Matter and Disinfection By-Products* (Vol. 761, pp. 68-83): American Chemical Society.

Lei, Y., Chen, C.-S., Ai, J., Lin, H., Huang, Y.-H., and Zhang, H. (2016). Selective decolorization of cationic dyes by peroxymonosulfate: non-radical mechanism and effect of chloride. *RSC Advances, 6*(2), 866-871.

Liu, C., Nanaboina, V., Korshin, G. V., and Jiang, W. (2012). Spectroscopic study of degradation products of ciprofloxacin, norfloxacin and lomefloxacin formed in ozonated wastewater. *Water Research, 46*(16), 5235-5246.

Lutze, H. V., Bircher, S., Rapp, I., Kerlin, N., Bakkour, R., Geisler, M., von Sonntag, C., and Schmidt, T. C. (2015). Degradation of Chlorotriazine Pesticides by Sulfate Radicals and the Influence of Organic Matter. *Environmental Science & Technology, 49*(3), 1673-1680.

Neta, P., Huie, R. E., and Ross, A. B. (1988). Rate Constants for Reactions of Inorganic Radicals in Aqueous Solution. *Journal of Physical and Chemical Reference Data, 17*(3), 1027-1284.

Paul, T., Dodd, M. C., and Strathmann, T. J. (2010). Photolytic and photocatalytic decomposition of aqueous ciprofloxacin: Transformation products and residual antibacterial activity. *Water Research, 44*(10), 3121-3132.

Serna-Galvis, E. A., Ferraro, F., Silva-Agredo, J., and Torres-Palma, R. A. (2017). Degradation of highly consumed fluoroquinolones, penicillins and cephalosporins in distilled water and simulated hospital wastewater by UV254 and UV254/persulfate processes. *Water Research, 122*, 128-138.

Steele, W. V., and Appelman, E. H. (1982). The standard enthalpy of formation of peroxymonosulfate (HSO_5^-) and the standard electrode potential of the peroxymonosulfate-bisulfate couple. *The Journal of Chemical Thermodynamics, 14*(4), 337-344.

Takács-Novák, K., Noszál, B., Hermecz, I., Keresztúri, G., Podányi, B., and Szasz, G. (1990). Protonation Equilibria of Quinolone Antibacterials. *Journal of Pharmaceutical Sciences, 79*(11), 1023-1028.

Van Doorslaer, X., Dewulf, J., Van Langenhove, H., and Demeestere, K. (2014). Fluoroquinolone antibiotics: An emerging class of environmental micropollutants. *Science of the Total Environment, 500-501*, 250-269.

Wacławek, S., Lutze, H. V., Grübel, K., Padil, V. V. T., Černík, M., and Dionysiou, D. D. (2017). Chemistry of persulfates in water and wastewater treatment: A review. *Chemical Engineering Journal, 330*, 44-62.

Wang, P., He, Y.-L., and Huang, C.-H. (2010). Oxidation of fluoroquinolone antibiotics and structurally related amines by chlorine dioxide: Reaction kinetics, product and pathway evaluation. *Water Research, 44*(20), 5989-5998.

Wang, Z., Bush, R. T., Sullivan, L. A., Chen, C., and Liu, J. (2014). Selective Oxidation of Arsenite by Peroxymonosulfate with High Utilization Efficiency of Oxidant. *Environmental Science & Technology, 48*(7), 3978-3985.

Wols, B. A., Harmsen, D. J. H., Wanders-Dijk, J., Beerendonk, E. F., and Hofman-Caris, C. H. M. (2015). Degradation of pharmaceuticals in UV (LP)/H2O2 reactors simulated by means of kinetic modeling and computational fluid dynamics (CFD). *Water Research, 75*, 11-24.

Yang, B., Kookana, R. S., Williams, M., Ying, G.-G., Du, J., Doan, H., and Kumar, A. (2016). Oxidation of ciprofloxacin and enrofloxacin by ferrate(VI): Products identification, and toxicity evaluation. *Journal of Hazardous Materials, 320*, 296-303.

Yang, Y., Banerjee, G., Brudvig, G. W., Kim, J.-H., and Pignatello, J. J. (2018). Oxidation of Organic Compounds in Water by Unactivated Peroxymonosulfate. *Environmental Science & Technology, 52*(10), 5911-5919.

Yang, Y., Jiang, J., Lu, X., Ma, J., and Liu, Y. (2015). Production of Sulfate Radical and Hydroxyl Radical by Reaction of Ozone with Peroxymonosulfate: A Novel Advanced Oxidation Process. *Environmental Science & Technology, 49*(12), 7330-7339.

Yang, Y., Pignatello, J. J., Ma, J., and Mitch, W. A. (2016). Effect of matrix components on UV/H2O2 and UV/S2O82− advanced oxidation processes for trace organic degradation in reverse osmosis brines from municipal wastewater reuse facilities. *Water Research, 89*, 192-200.

Yin, R., Guo, W., Wang, H., Du, J., Zhou, X., Wu, Q., Zheng, H., Chang, J., and Ren, N. (2018). Selective degradation of sulfonamide antibiotics by peroxymonosulfate alone: Direct oxidation and nonradical mechanisms. *Chemical Engineering Journal, 334*, 2539-2546.

Yun, E.-T., Lee, J. H., Kim, J., Park, H.-D., and Lee, J. (2018). Identifying the Nonradical Mechanism in the Peroxymonosulfate Activation Process: Singlet Oxygenation Versus Mediated Electron Transfer. *Environmental Science & Technology, 52*(12), 7032-7042.

Yun, E.-T., Yoo, H.-Y., Bae, H., Kim, H.-I., and Lee, J. (2017). Exploring the Role of Persulfate in the Activation Process: Radical Precursor Versus Electron Acceptor. *Environmental Science & Technology, 51*(17), 10090-10099.

Zhang, H., and Huang, C.-H. (2005). Oxidative Transformation of Fluoroquinolone Antibacterial Agents and Structurally Related Amines by Manganese Oxide. *Environmental Science & Technology, 39*(12), 4474-4483.

Zhang, T., Zhu, H., and Croué, J. P. (2013). Production of sulfate radical from peroxymonosulfate induced by a magnetically separable CuFe2O4 spinel in water: Efficiency, stability, and mechanism. *Environmental Science and Technology, 47*(6), 2784-2791.

Zhou, Y., Jiang, J., Gao, Y., Ma, J., Pang, S.-Y., Li, J., Lu, X.-T., and Yuan, L.-P. (2015). Activation of Peroxymonosulfate by Benzoquinone: A Novel Nonradical Oxidation Process. *Environmental Science & Technology, 49*(21), 12941-12950.

Chapter 4. Inactivation of Antibiotic Resistant Bacteria during Conventional and Advanced Oxidation Processes

The content of Chapter 4 is unable to be reproduced here as they are under embargo due to current consideration for publication in the journal *Environmental Science: Water Research & Technology*.

4.1 Abstract

This study investigated the inactivation of antibiotic resistant bacteria (ARB) during various chemical oxidation and UV (254 nm)-based advanced oxidation processes (UV-AOPs). *Stenotrophomonas maltophilia* (*S. maltophilia*) was the target ARB strain, which is a multi-drug resistant bacteria isolated from the secondary effluent of a wastewater treatment plant. Bacterial viability was determined based on membrane damage (flow cytometric analysis combining with nucleic acids staining with SYBR Green I and propidium iodide). Membrane damage has been widely acknowledged as an indicator of cell death. Cultivability analysis (plate counting) was additionally applied for UV-AOPs. The disinfection efficacy of reactive oxidant species commonly produced during chlorination processes, namely monochloramine (NH_2Cl), bromine (HOBr), and monobromamine (NH_2Br) were compared. The membrane integrity loss followed in the order of : HOBr > HOCl > NH_2Br >> NH_2Cl. 3-log reduction of intact cells was achieved when *S. maltophilia* was subjected to 1.8, 0.4, and 138 mg as Cl_2×min/L of HOCl, HOBr, and NH_2Br, respectively. Chloramination at 600 mg as Cl_2×min/L led to 0.3-log of reduction. UV direct irradiation, UV/H_2O_2, and UV/PDS effectively induced cultivability loss of *S. maltophilia* (5.7-log at 22 mJ/cm^2). UV direct irradiation didn't cause significant membrane damage. The efficacy of UV/hydrogen peroxide (H_2O_2) was comparable with UV alone due to the scavenging of hydroxyl radical ($^{\bullet}OH$) by cell membrane. UV/peroxydisulfate (PDS) dramatically diminished the green fluorescence intensity on flow cytometric analysis most likely attributable to the nuclei acid damage induced by sulfate radical ($SO_4^{\bullet-}$). Overall results indicated that weak or selective oxidants (e.g., NH_2Br and $SO_4^{\bullet-}$) were less consumed by cell membrane and able to penetrate into cells, consequently demonstrating high potential of degrading intracellular DNA carrying antibiotic resistance genes. The formation of "injured" ARB cells by weak oxidants or strong oxidants at low dose can be a concern during disinfection processes, considering the potential risk of gene transfer by "injured" cells and their capability of recover.

4.2 Introduction

Disinfection (e.g., free and combined chlorine, UV) is generally applied for waterborne pathogens control for the production of drinking water and also used in many countries as a final step of wastewater treatment. In recent years, antibiotic resistance has become a serious public health concern globally. Antibiotic resistant bacteria (ARB) and antibiotic resistance genes (ARGs) are linked with the dissemination of antibiotic resistance (i.e., horizontal gene transfer) to human pathogens and the formation of multi-drug resistant bacteria, thus considered as emerging contaminants in water (Pruden, 2014). As a result, the disinfection of wastewater and contaminated natural waters should not only focus on the inactivation of pathogens but also aim to remove ARB and ARGs (Dodd, 2012).

Chlorine ($HOCl/ClO^-$) is widely applied as disinfectant during water treatment processes due to its low cost and strong ability to inactivate a wide range of pathogenic microorganisms. Due to the presence of halides and ammonia in the water matrix, various reactive species can be generated during chlorination. Monochloramine (NH_2Cl) can be formed during chlorination of ammonia containing water (Jafvert and Valentine, 1992):

$$HOCl + NH_3 \rightarrow NH_2Cl + H_2O \qquad k = 4.2 \times 10^6\ M^{-1}s^{-1} \qquad (1)$$

NH_2Cl is often used as secondary disinfectant in drinking water distribution system because of its higher stability and lower reactivity with organic matter to produce regulated disinfection by-products (e.g., trihalomethanes, haloacetic acids) (Karanfil et al., 2008).

Bromide presents in all fresh water sources with concentration ranging from a few µg/L to mg/L. Natural water in coastal area is often influenced by salt water intrusion and contains high level of bromide (Agus et al., 2009). In Western Australia, bromide in source water is about 0.4−8.4 mg/L due to the impact of saline soil (Tan et al., 2016). During chlorination, HOCl rapidly reacts with bromide to generate bromine (HOBr) (Kumar and Margerum, 1987):

$$HOCl + Br^- \rightarrow HOBr + Cl^- \qquad k = 1.55 \times 10^3\ M^{-1}s^{-1} \qquad (2)$$

HOBr is highly reactive with ammonia and generates bromamines (as monobromamine, NH_2Br, an example) (Heeb et al., 2014):

$$HOBr + NH_3 \rightarrow NH_2Br + H_2O \qquad k = (4 - 7.5) \times 10^7\ M^{-1}s^{-1}\ (3)$$

Numerus studies have reported the formation of oxidative species during chlorination (e.g., HOBr, chloramines, and bromamines) as well as their reactivity with organic contaminants and potential capability to produce disinfection by-products (see Heeb et al. (2014) and Heeb et al. (2017) and references therein). However, few studies have discussed the role of these reactive species as disinfectants to inactivate ARB and remove ARGs.

UV disinfection (generally at 254 nm) induces DNA deactivation by pyrimidine dimerization, consequently inhibits cell growth (Hijnen et al., 2006). Unlike conventional chemical oxidation (e.g., chlorination), UV disinfection is free from chemical addition and doesn't produce disinfection by-products (Song et al., 2016). UV-based advanced oxidation processes (UV-AOPs) can be seen as a promising technology especially for wastewater reclamation purposes. UV combined with hydrogen peroxide (H_2O_2) or peroxydisulfate (PDS) (i.e., UV/H_2O_2 and UV/PDS, respectively) generates powerful radical species such as hydroxyl radical ($^{\bullet}OH$) and sulfate radical ($SO_4^{\bullet-}$) (Wols and Hofman-Caris, 2012; Lutze et al., 2015).

Heterotrophic plate counts (HPC) is a cultivation-based method, which has been applied routinely for microbiological monitoring during water treatment. In the last 2 decades, application of cultivation-independent methods, such as flow cytometry analysis, demonstrated that more complex and abundant microbial community exist in aquatic environment compared to that cultivable and detectable by traditional HPC method (Van Nevel et al., 2017). Flow cytometric analysis is generally used with combination of microbial cells staining with different dyes for various bacterial viability assessments (e.g., membrane integrity, pump activity, and metabolic activity) (Léonard et al., 2016). Bacteria cell with severe membrane damage is unable to maintain a unique intracellular environment, hence can be considered as "dead" (Hammes et al., 2011). Propidium iodide (PI) is the most commonly used dye for membrane integrity analysis. PI is large, double charged and red-fluorescent dye. It only enters cells with permibilised membrane and intercalates with double-stranded DNA (Berney et al., 2007; Hammes et al., 2011). PI is employed along with a green-fluorescent dye such as SYBR Green I (SGI). SGI can penetrate and stain all cells with nucleic acids, regardless of membrane integrity. Therefore, the combination of SGI and PI allows to investigate ARB inactivation during disinfection by measuring the

membrane intact and damaged cell counts (Van Nevel et al., 2017). Moreover, non-specific intracellular DNA damage can be indirectly obtained from total cell counts on flow cytometry, which was based on the intensity of green fluorescence (nucleic acids staining with SGI) (Phe et al., 2005).

In this study, we investigated the inactivation of ARB during chemical oxidation processes (i.e., HOCl, NH_2Cl, HOBr, and NH_2Br) and UV-AOPs (i.e., UV, UV/H_2O_2, and UV/PDS at 254 nm). A multi-drug resistant bacteria, *Stenotrophomonas maltophilia* (*S. maltophilia*) was chosen as target strain. *S. maltophilia* was isolated from the secondary effluent of a wastewater treatment plant located in Western Australia. It is a gram-negative bacteria and proven to be resistant to several antibiotics (i.e., tetracycline, amoxicillin, ciprofloxacin, sulfamethoxazole, and rifampicin) as well as resistant to artificial solar irradiation (Glady-Croue et al., 2018). Flow cytometric analysis combining with SGI and PI staining was applied to study the membrane integrity loss of *S. maltophilia* after various treatments. Plate counts analysis was additionally applied for UV-based experiments to study the cultivability of *S. maltophilia*.

4.3 Materials and Methods

4.3.1 Chemical reagents

All chemicals were in analytical grade or higher and used as received without further purification. Sodium hypochlorite solution (10−15%), sodium bromide (≥99%), and sodium persulfate (≥98%) were purchased from Sigma-Aldrich. Sodium chloride (≥99%), disodium hydrogen phosphate (≥99%), and potassium dihydrogen phosphate (≥99%) were supplied from Ajax Finechem. Hydrogen peroxide 30% was from Thermo Fisher Scientific. All solutions were prepared in Milli-Q water (18 MΩ cm, Millipore).

4.3.2 Preparation of *S. maltophilia*

S. maltophilia AB550 strain was grown overnight in sterile lysogeny broth (LB medium diluted by half using filter sterilised Milli-Q) at 37 ℃ with shaking at 170 rpm. Aliquots of 10 mL overnight culture were harvested by centrifugation (3275 g, 7 min, Allegra X-12R centrifuge, Beckman Coulter). The supernatant was discarded and bacterial pellets were resuspended in sterile phosphate buffer followed by centrifugation again. This process was repeated 5 times with the objective to avoid the presence of residual LB medium. Finally, cell suspensions were diluted using filter sterilised phosphate buffer using a 0.5 McFarland standard as the reference. The initial concertation of cells was in the range of $(1.5–2)\times10^7$ cells/mL for chemical oxidation and about 5.6×10^7 cells/mL for UV-AOP experiments as measured by flow cytometer. The initial total organic carbon concentration was about 3 mg-C/L, which was consistent with the biomass brought by bacterial cells (based on the assumption that each cell contains about 10^{10} carbon atoms).

4.3.3 Preparation of oxidants

Sodium hypochlorite commercial solution was standardized by monitoring the absorbance of hypochlorite anion at 292 nm (ε = 362 $M^{-1}cm^{-1}$) (Lei et al., 2004) using a UV spectrometer (Cary 60, Agilent Technologies). Chlorine solution (1 g/L as Cl_2) was prepared daily by diluting sodium hypochlorite commercial solution with Milli-Q water.

Preformed monochloramine solution was prepared daily by dropwise addition of sodium hypochlorite into rapidly stirred ammonium sulfate solution (pH= 8.5, N:Cl

molar ratio of 1.2:1). Initial monochloramine and dichloramine concentrations were spectrophotometrically measured at 245 and 295 nm (Nihemaiti et al., 2017).

Bromine solution was prepared by reacting sodium hypochlorite with bromide (pH 11, Br:Cl molar ratio of 1.05:1). Reaction was allowed to proceed for 3 days. The final concentration of bromine was determined on UV spectrometer at 329 nm (ε = 332 $M^{-1}cm^{-1}$) (Liu et al., 2012). Formation yield of bromine was 99%. Bromine solution was kept at 4 ℃ and used for maximum 3 weeks.

Monobromamine was prepared freshly prior to each experiment by mixing equal volumes of HOBr and ammonium sulfate. Both HOBr and ammonium sulfate solutions were prepared in borate buffer (20 mM) at pH 9. Ammonium was added in large excess to prevent the formation of dibromamine (N:Br molar ratio of 1000:1). Initial concentrations of monobromamine and dibromamine were measured at 278 nm and 232 nm (Lei et al., 2004).

4.3.4 Experimental procedures

All glassware used in this study were chlorine demand free and autoclaved. Chemical oxidations were initiated by spiking predetermined volume of oxidant into 20 mL of bacterial suspension (phosphate buffer at pH 7.5). Solution was gently mixed using magnetic stir bar. The concentration of oxidant was continuously monitored to make sure that residual oxidant was present in solution during the sampling period. DPD colorimetric method was applied to measure HOCl and HOBr. The same method was used for the determination of residual NH_2Cl and NH_2Br with addition of KI (Allard et al., 2018). Oxidant exposure (CT values) were calculated based on the area below the oxidant decay curve and expressed in mg as Cl_2×min/L.

UV-experiments were conducted with a UV collimated beam setup as described previously (Nihemaiti et al., 2018). This collimated beam device contained three low-pressure UV lamps emitting light at 254 nm (UV Technik Meyer, Germany). Experiments were carried out with 30 mL of bacterial suspension (phosphate buffer at pH 7.5) in a petri dish (dimeter: 8.4 cm, path length: 0.5 cm). Magnetic stir bar was used to gently mix the solution. UV intensity in solution surface was measured using a radiometer (UV-surface-D, sglux, Germany). Average UV intensity (0.79 mW/cm^2) was corrected according to published method (Bolton and Linden, 2003). Refraction, divergence, and petri factors were > 0.9. Bacterial solution absorbance at 254 nm was 0.575 cm^{-1}. Thus, the water factor was calculated to be 0.731. UV fluence applied

varied from 3.7 to 73 mJ/ cm^2. The doses of H_2O_2 and PDS used for UV/H_2O_2 and UV/PDS experiments, respectively, were 0.5 mM. Control experiments have confirmed that H_2O_2 and PDS had no influence on the membrane integrity of *S.maltophilia* in these experimental conditions (data not shown).

Aliquots from chemical oxidation and UV-based experiments were taken in predetermined time intervals and immediately quenched with excess sodium thiosulfate. Samples were analysed on flow cytometry within 1 h. Details on experimental conditions were summarized in Table 4-1.

Table 4-1. Conditions for chemical oxidation and UV-AOP experiments in this study

Chemical Oxidation				UV-AOPs	
Oxidants	Initial concentration (mg as Cl_2/L)	Residual concentration [a] (mg as Cl_2/L)	Sampling period (min)	Treatments	Fluence (mJ/cm^2)
HOCl	1	0.2	0.17−10	UV	3.7−73
	5	0.3	10	UV/H_2O_2 (0.5 mM)	3.7−73
NH_2Cl	5	4.7	5−120		
HOBr	1	0.1	0.17−10	UV/PDS (0.5 mM)	3.7−73
NH_2Br	4.6	3.1	2−120		
[a] residual concentration of oxidants at the last sampling point					

4.3.5 Fluorescence staining and flow cytometry analysis

SYBR® Green I (SGI, Invitrogen, Thermo Fisher Scientific) was diluted by 5 times with filter sterilised (0.45 µM) Milli-Q. One µL of diluted SGI and 1 µL of propidium iodide (PI, Miltenyi Biotec) were mixed with 1 mL of sample. The mixture was incubated at room temperature in the dark for 12 min prior to analysis. The stained samples were analysed on a flow cytometer (BD FACS Canto II, BD Biosciences) equipped with 20 mW solid state blue laser emitting light at a fixed wavelength of 488 nm. Each sample was acquired for 30 s at 10 µL/min. Green fluorescence (SGI) was collected in FL1 channel (530 nm) and red fluorescence (PI) was collected in FL3 channel (670 nm). The data collection (threshold) trigger was set on the green fluorescence channel (FL1) and threshold level was 500 based on green fluorescence intensity. Electronic gates were constructed manually using BDFACS Diva 8.0.2 software to separate bacteria cells from background noise. Data was analysed using FlowJo® software (Tree Star) and presented in density plots using green versus red

fluorescence intensity (area), where each dot represented the signals for each particle that was detected.

4.3.6 Plate counts

Plate counting method was applied in addition to flow cytometric analysis for UV-based experiments to investigate the cultivability of *S. maltophilia* after UV irradiation and radical exposure. 100 µL of sample was plated on LB agar plate and incubated overnight at 37 ℃. About $(5.4\pm0.6)\times10^7$ colony forming units (CFU)/mL of *S. maltophilia* was grown in agar plate before treatment.

4.4 Results and Discussion

4.4.1 Flow cytometric analysis of *S.maltophilia* during various oxidants exposure

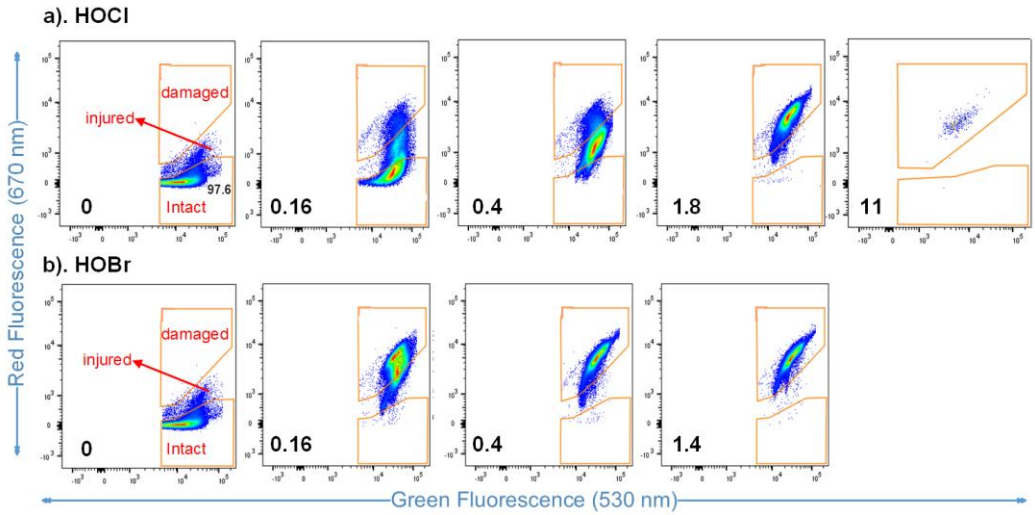

Figure 4-1. Flow-cytometric density plots (530 nm vs. 670 nm) of *S.maltophilia* treated with a) HOCl (0−11 mg as Cl_2×min/L) and b) HOBr (0−1.4 mg as Cl_2×min/L) as a function of oxidant exposure (oxidant exposure value was indicated in lower left of each plot; samples were stained with SGI+PI; pH 7.5 phosphate buffer)

Figure 4-1 illustrates flow-cytometric density plots of *S.maltophilia* after various HOCl and HOBr exposure. Samples were stained with SGI and PI. Before treatment (density plot at oxidant exposure=0), cells exhibited intense green fluorescence and weak red fluorescence. This region was called "intact" as cells were with intact membrane and only SGI can penetrate into the cell. With increasing of oxidant exposure, cells started to take up PI due to the permibilization of their membrane. Thus, red fluorescence signal gradually increased and bacterial cluster migrated into a region called "damaged". An intermediate state was observed during cell movement from "intact" to "damaged" region (e.g., 0.4 mg as Cl_2×min/L, Figure 4-1a), which was called "injured". The intensity of red fluorescence in intermediate state was lower than that in "damaged" region, indicating that cell membrane was partly damaged in "injured" cells, hence less PI entered into cell compared to "damaged" region with completely permeabilized membrane. Intermediate states were also observed from flow cytometric pattern of *legionella* strains subjected to heat shock (Allegra et al., 2008), as well as *E.coli* cells exposed to UVA irradiation (Berney et al., 2007) and chlorine (Nocker et al., 2017). The green fluorescence intensity of "injured" and "damaged" cells were slightly higher than "intact" cells, which was probably attributed

to the increased uptake of SGI with membrane damage (Berney et al., 2006). Further increase of HOCl exposure to 11 mg as Cl_2×min/L resulted in dramatic decrease in the size of bacterial cluster, revealing that intracellular nucleic acids were severely damaged by excess HOCl and cannot be stained by SGI (Phe et al., 2005).

Migration of cells on flow cytometry density plot was much faster during bromination (Figure 4-1b) under the similar oxidant exposure conditions, suggesting the higher reactivity of HOBr with *S.maltophilia* membrane (see further discussions below).

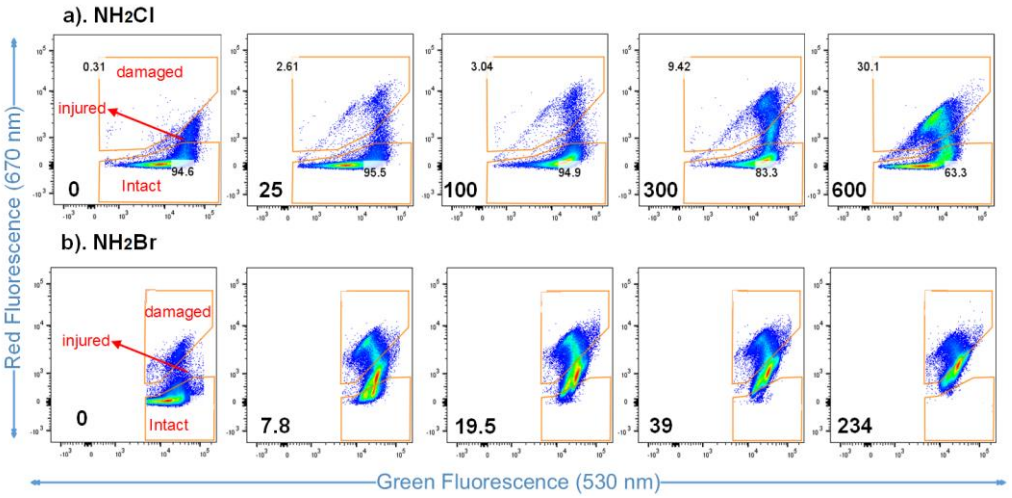

Figure 4-2. Flow-cytometric density plots (530 nm vs. 670 nm) of S.maltophilia treated with a) NH_2Cl (0−600 mg as Cl_2×min/L) and b) NH_2Br (0−234 as mg as Cl_2×min/L) as a function of oxidant exposure (oxidant exposure value was indicated in lower left of each plot; samples were stained with SGI+PI, pH 7.5 phosphate buffer)

Similar flow cytometric patterns were obtained from chloramination and bromamination processes (Figure 4-2). However much higher oxidant exposure was required for the shift of bacterial cluster into the "damaged" region. The majority of cells were located in "intact" and "injured" regions after NH_2Cl and NH_2Br oxidation, respectively, at the maximum oxidant exposure applied in this study.

Combined staining of nucleic acids with SGI and PI followed by flow cytometric analysis provides information on membrane integrity, discriminating between cells with intact and damaged membrane. Previous studies have reported that the physiological indices of *E.Coli* exposed to chlorine were affected in the order of: viable plate counts > substrate responsiveness > membrane potential > respiratory activity > membrane integrity (Lisle et al., 1999). Culturaility was influenced earlier than membrane damage during chlorination (Nocker et al., 2017). Thus, membrane

integrity assessment was considered as a conservative tool for cell death identification during water disinfection (Hammes et al., 2011; Ramseier et al., 2011).

However, concerns might rise from "injured" cells in intermediate state with partly compromised membrane. The fate of bacteria in intermediate state depends on strain types and the intensity of treatments (e.g., heat, UV, oxidants, antimicrobial agents). Nevertheless, it was reported that the "injured" cells might be in a status of "viable but non-cultivable", where cells still keep their metabolic activity as well as other potential activities such as horizontal gene transfer (Wang et al., 2010; Léonard et al., 2016). This might be critical during water disinfection processes as the "injured" ARB cells are not easy to be detected by traditional plate counting method, but still be able to contribute to the transfer of ARG among bacterial population. There were evidences that the sub-inhibitory concentrations of disinfectants (e.g., HOCl and NH_2Cl) promoted the horizontal transfer of ARGs by increasing the permeability of cell membrane and altering the expression of conjugation-related genes (Guo et al., 2015; Zhang et al., 2017). Furthermore, there is a risk of bacteria recover and regrowth as the "injured" cells with reversible membrane permibilization can repair the damage (Amor et al., 2002). Huang et al. (2011) has reported the reactivation of ARB after exposure to a low dose of chlorine (< 2 mg as Cl_2 for 10 min) in secondary effluent.

4.4.2 Comparison of different oxidants

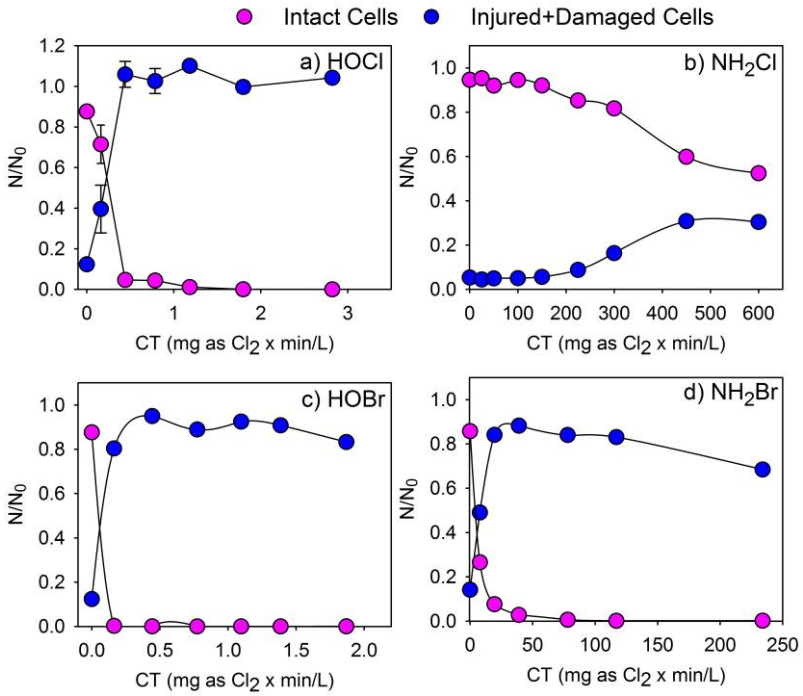

Figure 4-3. Relative numbers of "Intact" and "Injured+ Damaged" cells subjected to a) HOCl, b) NH_2Cl, c) HOBr, and d) NH_2Br. Cell numbers were normalized to initial total cell number.

Figure 4-3 presents the evolution of membrane intact and membrane compromised cells (sum of injured and damaged cells) under various oxidant exposures. The membrane integrity loss followed the order of: HOBr > HOCl > NH_2Br >> NH_2Cl (see discussion below for specific rate constants). Approximately 3-log reduction of intact cells was achieved during chlorination, bromination, and bromamination at oxidant exposure of 1.8, 0.4, and 138 mg as Cl_2×min/L, respectively. Only half of cells lost their membrane integrity (0.3 log) at 600 mg as Cl_2×min/L of NH_2Cl exposure. These results were consistent with previous studies that HOBr is highly reactive with electron-rich moieties (e.g., activated aromatic ring, amines, olefins) with second-order rate constants up to 3 orders of magnitude higher than HOCl (Heeb et al., 2014). NH_2Cl exhibits significantly lower oxidation and disinfection capability compared to HOCl. Bromamines are more reactive than their chloramine analogues (Heeb et al., 2017).

Although the intact cell numbers substantially decreased during chlorination and bromination, the majority of the cells were still detectable by flow cytometry as damaged cells within 1−3 mg as Cl_2×min/L of exposure. The number of injured and damaged cells reached a plateau during chlorination (Figure 4-3a) or were slightly

reduced after initial increase during bromination (Figure 4-3c). These results indicates that HOCl and HOBr were largely consumed by cell membrane before penetrating into the cell to react with nucleic acids, which was consistent with the residual HOCl and HOBr concentrations measured after 10 min of reaction (i.e., 0.2 and 0.1 mg as Cl_2, respectively; initial concentration=1 mg as Cl_2/L, Table 1). Alternatively, HOCl and HOBr can efficiently inactivate ARB cells, but intracellular components (e.g., DNA carrying ARG) are hardly degraded under the same oxidant exposure. It was reported previously that chlorine-induced ARG damage was much slower than the corresponding loss of cell cultivability and membrane integrity (Yoon et al., 2017)

The fraction of injured + damaged cells was gradually decreased after initial increase during bromamination (i.e., 0.68 at 234 mg as Cl_2×min/L, Figure 4-3d). Interestingly, as shown in Figure 4-2b, the majority of cells at high NH_2Br exposure was still in intermediate state (injured). These results suggested that NH_2Br can penetrate into the cell to react with nucleic acids before cell membrane was completely permeable for PI. It was reported that a weaker oxidant can more efficiently diffuse into cell to attack inner cell components (e.g., DNA) without causing significant damage of the cell surface compared to a oxidant, which is highly reactive with cell wall components (Cho et al., 2010; Dodd, 2012).

4.4.3 Kinetics of membrane damage

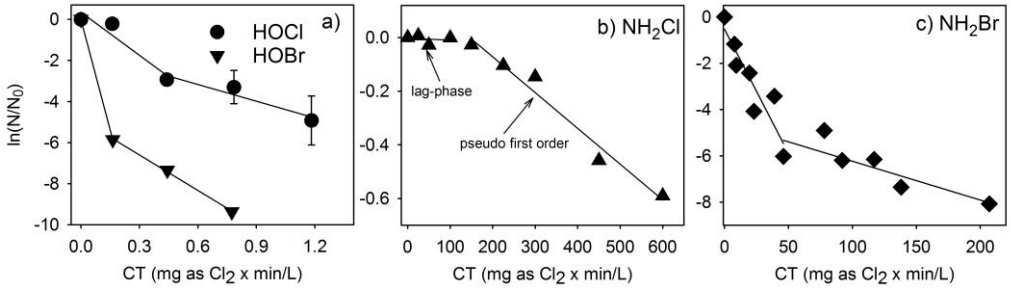

Figure 4-4. Plots of ln(N/No) versus oxidant exposure. a) HOCl and HOBr, b) NH_2Cl, c) NH_2Br (Error bars represent the standard deviations of duplicated experiments).

Kinetic rates of membrane damage during oxidative inactivation of *S.maltophilia* by HOCl, HOBr, and NH_2Br were described by Chick and Watson disinfection model as suggested previously (Ramseier et al., 2011):

$$\ln \frac{[N]}{[No]} = -k \int [c] dt \qquad (4)$$

Where [N] is the intact cell number, $\int[c]dt$ is the oxidant exposure and *k* is the second-order rate constant. Two stages of membrane damage kinetics were observed from *S.maltophilia* subjected to HOCl, HOBr (Figure 4-4a), and NH_2Br (Figure 4-4c): an initial fast damage followed by a slower phase of pseudo-first order kinetic. This was probably due to the decay of oxidants with exposure time. Chick and Watson model is based on the assumption that the residual disinfectant $[c]$ is constant in short disinfection time (Crittenden et al., 2012). However, oxidants were rapidly consumed along with membrane damage, which resulted in slower rate constants at longer exposure. Two phases of membrane damage and inactivation were also found during chlorination of drinking water bacteria cells (Ramseier et al., 2011) and *Mycobacterium* (Luh and Mariñas, 2007), respectively. Rate constants of HOCl, HOBr, and NH_2Br were derived from slopes of linear curves in Figure 4-4 and presented in Table 4-2. The reaction of HOBr in first stage was too fast. Thus, the minimum rate constant was estimated based on the first data point.

Notably, the membrane damage appeared to have a shoulder (lag-phase) at the early stage of chloramination followed by pseudo-first order kinetic. Its kinetic was characterized by the delayed Chick and Watson disinfection model as mentioned by Rennecker et al. (1999):

$$\ln\frac{[N]}{[No]} = 0 \qquad \int[c]dt \le b \qquad \text{(5a)}$$

$$\ln\frac{[N]}{[No]} = -k(\int[c]dt - b) \qquad \int[c]dt > b \qquad \text{(5b)}$$

Where b is the lag coefficient (mg as Cl_2×min/L) and estimated to be 100 (mg as Cl_2×min/L) in this study. Alternatively, about 100 (mg as Cl_2×min/L) of chloramine exposure was required before membrane was permeable for PI. The rate constant of NH_2Cl for pseudo-first order kinetic was derived from the linear curve in Figure 4-4b and listed in Table 4-2. A similar lag phase and subsequent pseudo-first order kinetic was also observed from chloramination of *Nitrosomonas europaea* (Wahman et al., 2009). The potential effect of cell aggregation for the presence lag-phase in this study was excluded as the green fluorescence signal

of single events (individual cells) was identical throughout chloramination and no apparent cell aggregation was observed by flow cytometry. These results suggested that cell membrane of *S.maltophilia* was resistant to chloramination under 100 (mg as Cl_2×min/L) possibly attributable to the composition and thickness of cell wall.

Table 4-2. Rate constants, *k* in L/(mg as Cl_2×min), of various oxidants for the membrane damage of *S.maltophilia* in this study and other microorganisms in previous studies when available

	This study	Previous studies	Ref.
HOCl	k_1=6.99±2.19 (0−0.4 mg as Cl_2×min/L) k_2=2.71±0.86 (0.4−1.2 mg as Cl_2×min/L)	k_1=1.1; k_2=9.1×10^{-2} (SGI+PI, native drinking water bacterial cells)	(Ramseier et al., 2011)
		38 (SGI+PI, *E.Coli* pure culture)	(Yoon et al., 2017)
NH_2Cl	*b* (lag coefficient)=100 (mg as Cl_2×min/L) *k*=$(1.3\pm0.1)\times10^{-3}$ (150−600 mg as Cl_2×min/L)	$(3.6-4.6)\times10^{-5}$ (SGI+PI, native drinking water bacterial cells)	(Ramseier et al., 2011)
		4.0×10^{-3} (SYTo9+PI, *Nitrosomonas europaea* pure culture)	(Wahman et al., 2009)
HOBr	k_1>35.8 [a] (0−0.16 mg as Cl_2×min/L) k_2=5.8 ±0.23 (0.16−0.77 mg as Cl_2×min/L)	n/a	n/a
NH_2Br	k_1=$(1.07\pm0.21)\times10^{-1}$ (0−46 mg as Cl_2×min/L) k_2=$(1.68\pm0.53)\times10^{-2}$ (46−207 mg as Cl_2×min/L)	n/a	n/a

[a] estimated based on the first data point

As shown in Table 4-2, rate constants of HOBr with *S.maltophilia* for membrane damage were higher than that of HOCl by a factor of 2 to 5. NH_2Br was at least 50 times less reactive than HOCl. Rate constant of NH_2Cl was 2-order of magnitude lower than NH_2Br. Previously reported rate constants of HOCl and NH_2Cl for inactivation of bacteria cells were also included in Table 4-2. Cultivation-based methods generally give higher inactivation rates than flow cytometric analysis as discussed above (Ramseier et al., 2011). Thus, only membrane damage rate constants measured by flow cytometry were shown for comparison. The rate constant of HOCl with *S.maltophilia* in this study (extracted from secondary wastewater effluent and prepared in laboratory conditions), was higher than the value obtained for the native drinking water bacteria cells, but smaller than the one determined for pure culture of *E.Coli*. It was reported that environmental bacteria growing in lower nutrient conditions might be more tolerant to oxidants than laboratory pure cultured bacteria (Ramseier et al., 2011). Our results suggested that disinfection studies on ARB should more focus on indigenous bacterial community or isolates of environmental bacteria, which can be more

representative for the real water disinfection conditions, rather than model bacterial cells prepared within laboratory.

4.4.4 Inactivation *S.maltophilia* during UV, UV/H_2O_2, and UV/PDS

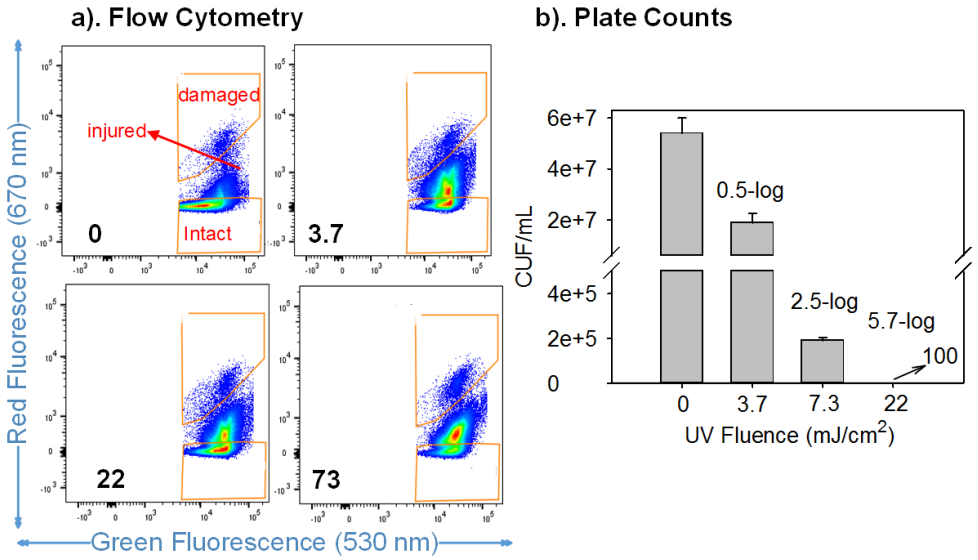

Figure 4-5. a) Flow Cytometric density plots (0−73 mJ/cm^2) and b) Plate counts results (0−22 mJ/cm^2) of S.maltophilia during UV direct irradiation. UV fluence was indicated in lower left of each flow cytometry density plot in (a); Numbers written on the top of each bar in (b) indicates the average log removal from duplicate analysis. Error bars represent the standard deviations of duplicated experiments.

The inactivation of *S.maltophilia* during UV direct irradiation, UV/H_2O_2, and UV/PDS were comparatively investigated. Figure 4-5a presents the flow cytometry density plots of *S.maltophilia* after various UV exposure (0, 3.7, 22, and 73 mJ/cm^2). The majority of the cells were located in the "intact" region before treatment and gradually shifted to "injured" region. Unlike chemical oxidation processes mentioned above (i.e., HOCl and HOBr), UV irradiation didn't cause significant membrane damage of *S.maltophilia* (0.3-log at 73 mJ/cm^2). However, (5.7±0.03)-log of cultivability loss was already achieved at 22 mJ/cm^2 based on plate counting method (Figure 4-5b). McKinney and Pruden (2012) also reported that about 10−20 mJ/cm^2 was required for 4-5 log reduction of ARB (e.g., *Pseudomonas aeruginosa*, *E. coli* SMS-3-5). It is well known that UV disinfection inactivates cells by inducing DNA lesions (e.g., pyrimidine dimers), which inhibits the normal replication of genome, without immediate damage of membrane (Hijnen et al., 2006).

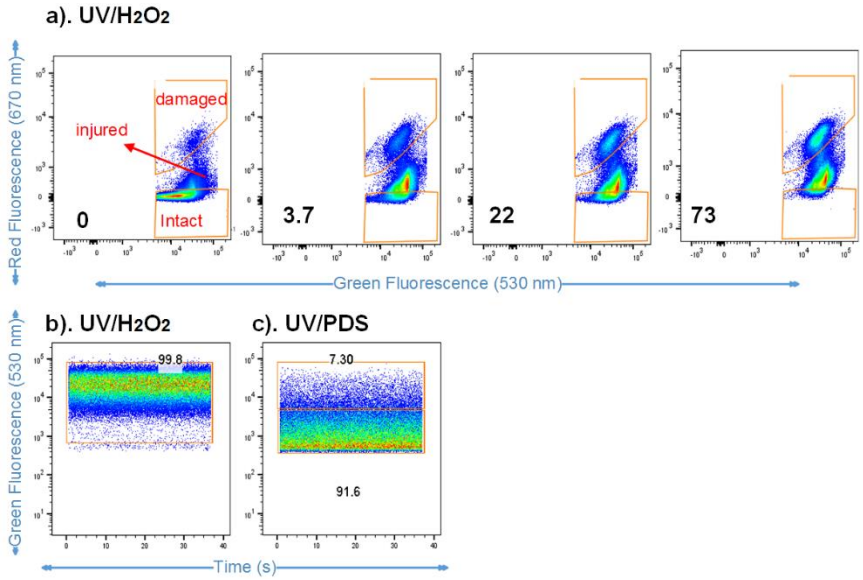

Figure 4-6. a) Flow Cytometric density plots of S.maltophilia during UV/H_2O_2 (UV fluence was indicated in lower left of each density plot). Intensity of green fluorescence versus scan time during UV/H_2O_2 (b) and UV/PDS (c) at 3.7 mJ/cm^2.

Flow cytometric pattern of *S.maltophilia* during UV/H_2O_2 is given in Figure 4-6a. Under UV/H_2O_2 exposure a slightly higher portion of cells (16%) was shifted to the "damaged" region at 73 mJ/cm^2 as compared to UV direct irradiation (Figure 4-5a). However, the majority of cells still appeared as "injured", which indicated that $^{\bullet}OH$ was inefficient to damage the membrane. Interestingly, UV/PDS treatment dramatically changed the flow cytometric pattern of *S.maltophilia*. Figure 4-6 (b) and (c) present the green fluorescence intensity of cells within 30 seconds of flow cytometric scan following UV/H_2O_2 and UV/PDS treatments, respectively. The intensity of green fluorescence after UV/PDS was about 2 orders of magnitude lower than that after UV/H_2O_2 exposure. No density plot was shown for UV/PDS as the green fluorescence signal was too low to locate single events within electronic gates (data collection trigger was set in green fluorescence channel, Material and Methods section). These results revealed that unlike $^{\bullet}OH$, $SO_4^{\bullet-}$ entered into cells and caused damage of intracellular DNA, which inhibited SGI binding to DNA. Distinct trends of $^{\bullet}OH$ and $SO_4^{\bullet-}$ in cell membrane damage were also reported previously (Wordofa et al., 2017).

$^{\bullet}OH$ is a highly reactive and non-selective oxidant, while $SO_4^{\bullet-}$ selectively reacts with electron-rich moieties. In Chapter 5 of this dissertation, we reported the rate constants of $^{\bullet}OH$ with extracellular DNA was in the range of 10^{10}–10^{11} M^{-1} s^{-1}, which were 2–3 orders of magnitude higher than that of $SO_4^{\bullet-}$. However, in the case of bacteria cells, $^{\bullet}OH$ was strongly scavenged by cell membrane components before reaching

intercellular DNA whereas $SO_4^{\bullet-}$ was less affected and able to diffuse into cell. Previous studies based on qPCR analysis also demonstrated that UV/H_2O_2 had negligible contribution to the degradation of intercellular ARG compared to UV direct irradiation due to significant scavenging of $^{\bullet}OH$ by cellular components (Yoon et al., 2017). Results from this study suggested that UV/PDS treatment has high potential of degrading intercellular ARG via the generation of selective $SO_4^{\bullet-}$. Although UV/PDS dramatically impacted the flow cytometric pattern of *S.maltophilia*, the cultivability loss during UV/PDS was comparable with UV direct irradiation and UV/H_2O_2 (data not shown), revealing the possibility that the DNA damage induced by UV/PDS might be repaired during plate counting analysis of *S.maltophilia*. This will be confirmed in future studies.

4.5 Conclusions

1) The loss of membrane integrity of *S.maltophilia* during chemical disinfection followed the order of: HOBr > HOCl > NH_2Br >> NH_2Cl. The rate constants of HOBr for membrane damage was higher than HOCl by a factor of 3 to 6. NH_2Br was at least 50 times less reactive than HOCl. Rate constant of NH_2Cl was 2-order of magnitude lower than NH_2Br.

2) "Chick and Watson" and "delayed Chick and Watson" disinfection models were applied to describe the kinetics of membrane integrity. Two phase of kinetics were observed from HOCl, HOBr, and NH_2Br: an initial fast reaction followed by a slower pseudo-first order kinetic. Chloramination reaction was characterized by a lag-phase with subsequent pseudo-first order kinetic.

3) About 1.8, 0.4, and 138 mg as Cl_2×min/L of oxidant exposure were required to achieve 3-log reduction of intact cells during chlorination, bromination, and bromamination, respectively. Only 0.3-log reduction was found during chloramination at 600 mg as Cl_2×min/L.

4) HOCl and HOBr were largely consumed by cell membrane before reaching inner cell components. NH_2Br was a weaker oxidant, but can penetrate into the cell to react with intracellular DNA, without causing complete membrane damage.

5) The formation of “injured” cells might be problematic during water disinfection processes, which was more pronounced in the case of weak oxidants exposure or strong oxidants at low dose.

6) UV direct irradiation effectively led to cultivability loss of *S.maltophilia* ((5.7±0.03)-log at 22 mJ/cm^2), but didn’t cause significant membrane damage compared to chemical oxidation processes.

7) UV/H_2O_2 was inefficient in membrane damage due to the scavenging of $^{\bullet}OH$ by membrane components. $SO_4^{\bullet-}$ was less impacted by cell membrane and can penetrate into cell. The green fluorescence intensity of *S.maltophilia* exposed to UV/PDS largely diminished due to nucleic acids damage induced by $SO_4^{\bullet-}$.

4.6 Reference

Agus, E., Voutchkov, N., and Sedlak, D. L. (2009). Disinfection by-products and their potential impact on the quality of water produced by desalination systems: A literature review. *Desalination, 237*(1-3), 214-237.

Allard, S., Hu, W., Le Menn, J.-B., Cadee, K., Gallard, H., and Croué, J.-P. (2018). Method Development for Quantification of Bromochloramine Using Membrane Introduction Mass Spectrometry. *Environmental Science & Technology, 52*(14), 7805-7812.

Allegra, S., Berger, F., Berthelot, P., Grattard, F., Pozzetto, B., and Riffard, S. (2008). Use of Flow Cytometry To Monitor Legionella Viability. *Applied and Environmental Microbiology, 74*(24), 7813-7816.

Amor, K. B., Breeuwer, P., Verbaarschot, P., Rombouts, F. M., Akkermans, A. D. L., De Vos, W. M., and Abee, T. (2002). Multiparametric Flow Cytometry and Cell Sorting for the Assessment of Viable, Injured, and Dead Bifidobacterium Cells during Bile Salt Stress. *Applied and Environmental Microbiology, 68*(11), 5209-5216.

Berney, M., Hammes, F., Bosshard, F., Weilenmann, H.-U., and Egli, T. (2007). Assessment and Interpretation of Bacterial Viability by Using the LIVE/DEAD BacLight Kit in Combination with Flow Cytometry. *Applied and Environmental Microbiology, 73*(10), 3283-3290.

Berney, M., Weilenmann, H.-U., and Egli, T. (2006). Flow-cytometric study of vital cellular functions in Escherichia coli during solar disinfection (SODIS). *Microbiology, 152*(6), 1719-1729.

Bolton, J. R., and Linden, K. G. (2003). Standardization of methods for fluence (UV Dose) determination in bench-scale UV experiments. *Journal of Environmental Engineering, 129*(3), 209-215.

Cho, M., Kim, J., Kim, J. Y., Yoon, J., and Kim, J.-H. (2010). Mechanisms of Escherichia coli inactivation by several disinfectants. *Water Research, 44*(11), 3410-3418.

Crittenden, J. C., Trussell, R. R., Hand, D. W., Howe, K. J., and Tchobanoglous, G. (2012). MWH's Water Treatment - Principles and Design (3rd Edition): John Wiley & Sons.

Dodd, M. C. (2012). Potential impacts of disinfection processes on elimination and deactivation of antibiotic resistance genes during water and wastewater treatment. *Journal of Environmental Monitoring, 14*(7), 1754-1771.

Glady-Croue, J., Niu, X.-Z., Ramsay, J. P., Watkin, E., Murphy, R. J. T., and Croue, J.-P. (2018). Survival of antibiotic resistant bacteria following artificial solar radiation of secondary wastewater effluent. *Science of the Total Environment, 626*, 1005-1011.

Guo, M.-T., Yuan, Q.-B., and Yang, J. (2015). Distinguishing Effects of Ultraviolet Exposure and Chlorination on the Horizontal Transfer of Antibiotic Resistance Genes in Municipal Wastewater. *Environmental Science & Technology, 49*(9), 5771-5778.

Hammes, F., Berney, M., and Egli, T. (2011). Cultivation-independent Assessment of Bacterial Viability. In S. Müller & T. Bley (Eds.), *High Resolution Microbial Single Cell Analytics* (pp. 123-150). Berlin, Heidelberg: Springer Berlin Heidelberg.

Heeb, M. B., Criquet, J., Zimmermann-Steffens, S. G., and von Gunten, U. (2014). Oxidative treatment of bromide-containing waters: Formation of bromine and its reactions with inorganic and organic compounds — A critical review. *Water Research, 48*, 15-42.

Heeb, M. B., Kristiana, I., Trogolo, D., Arey, J. S., and von Gunten, U. (2017). Formation and reactivity of inorganic and organic chloramines and bromamines during oxidative water treatment. *Water Research, 110*, 91-101.

Hijnen, W. A. M., Beerendonk, E. F., and Medema, G. J. (2006). Inactivation credit of UV radiation for viruses, bacteria and protozoan (oo)cysts in water: A review. *Water Research, 40*(1), 3-22.

Huang, J.-J., Hu, H.-Y., Tang, F., Li, Y., Lu, S.-Q., and Lu, Y. (2011). Inactivation and reactivation of antibiotic-resistant bacteria by chlorination in secondary effluents of a municipal wastewater treatment plant. *Water Research, 45*(9), 2775-2781.

Jafvert, C. T., and Valentine, R. L. (1992). Reaction scheme for the chlorination of ammoniacal water. *Environmental Science & Technology, 26*(3), 577-586.

Karanfil, T., Hong, Y., and Song, H. (2008). HAA Formation and Speciation during Chloramination *Disinfection By-Products in Drinking Water* (Vol. 995, pp. 124-140): American Chemical Society.

Kumar, K., and Margerum, D. W. (1987). Kinetics and Mechanism of General-Acid-Assisted Oxidation of Bromide by Hypochlorite and Hypochlorous Acid. *Inorganic Chemistry, 26*(16), 2706-2711.

Lei, H., Mariñas, B. J., and Minear, R. A. (2004). Bromamine Decomposition Kinetics in Aqueous Solutions. *Environmental Science & Technology, 38*(7), 2111-2119.

Léonard, L., Bouarab Chibane, L., Ouled Bouhedda, B., Degraeve, P., and Oulahal, N. (2016). Recent Advances on Multi-Parameter Flow Cytometry to Characterize Antimicrobial Treatments. *Frontiers in Microbiology, 7*, 1225.

Lisle, J. T., Pyle, B. H., and McFeters, G. A. (1999). The use of multiple indices of physiological activity to access viability in chlorine disinfected Escherichia coli O157:H7. *Letters in Applied Microbiology, 29*(1), 42-47.

Liu, C., von Gunten, U., and Croué, J.-P. (2012). Enhanced Bromate Formation during Chlorination of Bromide-Containing Waters in the Presence of CuO: Catalytic Disproportionation of Hypobromous Acid. *Environmental Science & Technology, 46*(20), 11054-11061.

Luh, J., and Mariñas, B. J. (2007). Inactivation of Mycobacterium avium with Free Chlorine. *Environmental Science & Technology, 41*(14), 5096-5102.

Lutze, H. V., Kerlin, N., and Schmidt, T. C. (2015). Sulfate radical-based water treatment in presence of chloride: Formation of chlorate, inter-conversion of sulfate radicals into hydroxyl radicals and influence of bicarbonate. *Water Research, 72*, 349-360.

McKinney, C. W., and Pruden, A. (2012). Ultraviolet disinfection of antibiotic resistant bacteria and their antibiotic resistance genes in water and wastewater. *Environmental Science and Technology, 46*(24), 13393-13400.

Nihemaiti, M., Le Roux, J., Hoppe-Jones, C., Reckhow, D. A., and Croué, J.-P. (2017). Formation of Haloacetonitriles, Haloacetamides, and Nitrogenous Heterocyclic Byproducts by Chloramination of Phenolic Compounds. *Environmental Science & Technology, 51*(1), 655-663.

Nihemaiti, M., Miklos, D. B., Hübner, U., Linden, K. G., Drewes, J. E., and Croué, J.-P. (2018). Removal of trace organic chemicals in wastewater effluent by UV/H2O2 and UV/PDS. *Water Research, 145*, 487-497.

Nocker, A., Cheswick, R., Dutheil de la Rochere, P.-M., Denis, M., Léziart, T., and Jarvis, P. (2017). When are bacteria dead? A step towards interpreting flow cytometry profiles after chlorine disinfection and membrane integrity staining. *Environmental Technology, 38*(7), 891-900.

Phe, M.-H., Dossot, M., Guilloteau, H., and Block, J.-C. (2005). Nucleic acid fluorochromes and flow cytometry prove useful in assessing the effect of chlorination on drinking water bacteria. *Water Research, 39*(15), 3618-3628.

Pruden, A. (2014). Balancing Water Sustainability and Public Health Goals in the Face of Growing Concerns about Antibiotic Resistance. *Environmental Science & Technology, 48*(1), 5-14.

Ramseier, M. K., von Gunten, U., Freihofer, P., and Hammes, F. (2011). Kinetics of membrane damage to high (HNA) and low (LNA) nucleic acid bacterial clusters in drinking water by ozone, chlorine, chlorine dioxide, monochloramine, ferrate(VI), and permanganate. *Water Research, 45*(3), 1490-1500.

Rennecker, J. L., Mariñas, B. J., Owens, J. H., and Rice, E. W. (1999). Inactivation of Cryptosporidium parvum oocysts with ozone. *Water Research, 33*(11), 2481-2488.

Song, K., Mohseni, M., and Taghipour, F. (2016). Application of ultraviolet light-emitting diodes (UV-LEDs) for water disinfection: A review. *Water Research, 94*, 341-349.

Tan, J., Allard, S., Gruchlik, Y., McDonald, S., Joll, C. A., and Heitz, A. (2016). Impact of bromide on halogen incorporation into organic moieties in chlorinated drinking water treatment and distribution systems. *Science of the Total Environment, 541*, 1572-1580.

Van Nevel, S., Koetzsch, S., Proctor, C. R., Besmer, M. D., Prest, E. I., Vrouwenvelder, J. S., Knezev, A., Boon, N., and Hammes, F. (2017). Flow cytometric bacterial cell counts challenge conventional heterotrophic plate counts for routine microbiological drinking water monitoring. *Water Research, 113*, 191-206.

Wahman, D. G., Wulfeck-Kleier, K. A., and Pressman, J. G. (2009). Monochloramine Disinfection Kinetics of Nitrosomonas europaea by Propidium Monoazide Quantitative PCR and Live/Dead BacLight Methods. *Applied and Environmental Microbiology, 75*(17), 5555-5562.

Wang, Y., Claeys, L., van der Ha, D., Verstraete, W., and Boon, N. (2010). Effects of chemically and electrochemically dosed chlorine on Escherichia coli and Legionella beliardensis assessed by flow cytometry. *Applied Microbiology and Biotechnology, 87*(1), 331-341.

Wols, B. A., and Hofman-Caris, C. H. M. (2012). Review of photochemical reaction constants of organic micropollutants required for UV advanced oxidation processes in water. *Water Research, 46*(9), 2815-2827.

Wordofa, D. N., Walker, S. L., and Liu, H. (2017). Sulfate Radical-Induced Disinfection of Pathogenic Escherichia coli O157:H7 via Iron-Activated Persulfate. *Environmental Science & Technology Letters, 4*(4), 154-160.

Yoon, Y., Chung, H. J., Wen Di, D. Y., Dodd, M. C., Hur, H.-G., and Lee, Y. (2017). Inactivation efficiency of plasmid-encoded antibiotic resistance genes during water treatment with chlorine, UV, and UV/H2O2. *Water Research, 123*, 783-793.

Zhang, Y., Gu, A. Z., He, M., Li, D., and Chen, J. (2017). Subinhibitory Concentrations of Disinfectants Promote the Horizontal Transfer of Multidrug Resistance Genes within and across Genera. *Environmental Science & Technology, 51*(1), 570-580.

Chapter 5. Degradation of Extracellular Antibiotic Resistance Genes and Elimination of Gene Transforming Activity during UV/H_2O_2 and UV/PDS

The contents of Chapter 5 and Appendix 3 are unable to be reproduced here as they are under embargo due to current consideration for publication in the journal *Water Research.*

5.1 Abstract

Antibiotic resistance gene (ARG) is considered as an emerging contaminant in water. While conventional disinfection processes showed limited capability of removing ARGs, few studies have focused on UV-based advanced oxidation processes (UV-AOPs). In this study, we investigated the degradation kinetics of plasmid-encoded ampicillin resistance gene (*amp*^{R}) during UV/H_2O_2 and UV/PDS at 254 and 300 nm. Radicals enhanced the decay rate of *amp*^{R} compared to the UV direct irradiation. Hydroxyl radical ($^{\bullet}OH$) showed higher reactivity towards plasmid DNA than sulfate radical ($SO_4^{\bullet-}$). According to the competition kinetics with radical probe compounds, the second-order rate constants of $^{\bullet}OH$ with *amp*^{R} segments were in the range of 10^{10}–10^{11} M^{-1} s^{-1}, which were 2–3 orders of magnitude higher than that of $SO_4^{\bullet-}$ (i.e., 10^7–10^9 M^{-1} s^{-1}). Therefore, the gene degradation during UV/PDS was mainly attributed to the trace amount of $^{\bullet}OH$ produced by the reaction of $SO_4^{\bullet-}$ with water. DNA electrophoresis gel images suggested that UV direct irradiation at 300 nm didn't induce conformational change on plasmid DNA while radical exposure altered the base pair region and changed the supercoiled structure. However, gene transformation assays indicated that the transforming activity loss of *amp*^{R} during UV/H_2O_2 and UV/PDS were mainly attributed to UV direct irradiation and the gene damage induced by $^{\bullet}OH$ and $SO_4^{\bullet-}$ can be repaired by recipient cells. Wastewater effluent organic matter was found to accelerate the degradation of *amp*^{R} upon UV irradiation at 254 nm, possibly due to the formation of reactive species by the excitation of chromophoric dissolved organic matter. Overall, UV-AOPs at 300 nm exhibited less efficiencies than that at 254 nm because of the lower UV absorbance of DNA and less formation of radicals at high wavelength.

5.2 Introduction

Antibiotic resistance is one of today's greatest public health concerns. Although antibiotic resistance is a natural phenomenon, anthropogenic activities (e.g., overuse and disposal of antibiotics) are providing constant selection and pressure on antibiotic resistant bacteria (ARB) (Vikesland et al., 2017). Antibiotic resistance can be developed and disseminated within the bacterial population by genetic mutation, cell division, as well as by the transfer of antibiotic resistance genes (ARGs) (Davies and Davies, 2010). ARG is considered as an emerging contaminant in natural and engineered aquatic systems, as ARG transfer can be linked with the spread of antibiotic resistance to human pathogens (Dodd, 2012; Pruden, 2014). Mobile genetic elements carrying ARGs (e.g., plasmids, integrons, and transposons) are disseminated to recipient cells through horizontal gene transfer, including conjugation (cell to cell contact), transduction (bacteriophage mediated), and transformation (uptake of naked DNA) (Lorenz and Wackernagel, 1994). Cell-free (naked) DNA generates during the secretion of live cells and lysis of dead cells. It can be persistent in the environment by adsorption onto soil and sediments, as well as by dissolving in water (Lorenz and Wackernagel, 1994).

Although conventional disinfection (e.g., chlorine and UV) efficiently inactivates ARB, intracellular ARGs are difficult to degrade due to the protection of the cell envelope (McKinney and Pruden, 2012; Yoon et al., 2017) and can be released into water following the death of ARB cells (Dodd, 2012; J. Zheng et al., 2017). The sub-inhibitory concentrations of disinfectants (e.g., chlorine and monochloramine) were found to promote the horizontal transfer of ARGs by increasing the permeability of cell membrane and altering the expression of conjugation-related genes (Guo et al., 2015; Ye Zhang et al., 2017). The proportion of cell-free DNA carrying ARGs was reported to increase after various biological and chemical treatment processes in wastewater treatment plant, revealing the potential risk of antibiotic resistance dissemination in discharged effluent and receiving environment (Liu et al., 2018; Yan Zhang et al., 2018).

UV-based advanced oxidation processes (UV-AOPs) are considered as a promising technology for the removal of refractory contaminants during water treatment. Powerful radical species are generated during UV-AOPs. UV irradiation of hydrogen

peroxide (H_2O_2) and peroxydisulfate (PDS) produce hydroxyl radical ($^{\bullet}OH$) and sulfate radical ($SO_4^{\bullet-}$), respectively, which can effectively degrade contaminants in nearly diffusion-controlled rates (Buxton et al., 1988; Neta et al., 1988). UV/H_2O_2 and UV/PDS were reported to efficiently inactivate ARB cells (Michael-Kordatou et al., 2015; Ferro et al., 2016; Giannakis et al., 2018). However, the contribution of $^{\bullet}OH$ to the degradation of inner cell components (e.g., intracellular ARGs) was limited due to the consumption of $^{\bullet}OH$ by the cell membrane constituents and the water matrix components (Ferro et al., 2017; Yoon et al., 2017). To the best of our knowledge, there is no study on the degradation of ARGs by $SO_4^{\bullet-}$. Furthermore, previous studies on UV-AOPs applied various doses of UV and oxidants (i.e., H_2O_2) in different water matrix conditions and no information was available on radical concentrations. Thus, it is difficult to compare their efficiencies in terms of ARB and ARGs removal. Gene transformation should be evaluated in complement to the monitoring of gene degradation, as previous studies have demonstrated that the damaged DNA can be repaired by recipient cells (Chang et al., 2017; Yoon et al., 2018).

The aim of this study was to investigate the degradation kinetics of plasmid-encoded ARGs (i.e., ampicillin resistant gene, amp^R) by $^{\bullet}OH$ and $SO_4^{\bullet-}$. Extracellular ARG was preferred to intracellular ARG to avoid the effect of cell membrane. Quantitative polymerase chain reaction (qPCR) was applied to measure the gene damage. Transfer genes after radical exposure to non-resistant bacteria (*E.Coli* DH5α) was investigated. Gel electrophoresis analysis was conducted to monitor the conformational characteristics of plasmid DNA before and after treatments. $^{\bullet}OH$ and $SO_4^{\bullet-}$ were generated by the UV irradiation of H_2O_2 and PDS, respectively. Two different UV wavelengths (i.e., 254 and 300 nm) were applied and the latter was designed to simulate the sunlight irradiation processes. Low pressure mercury UV lamp emitting light at 254 nm was used for UV254 nm (hereafter UV_{254})-based experiments. UV light-emitting diode (LED) emitting light at 300 nm was applied for UV300 nm (hereafter UV_{300})-based experiments. The steady-state concentrations of $^{\bullet}OH$ and $SO_4^{\bullet-}$ under various experimental conditions were measured by radical probe compounds and used to determine the second-order rate constants of ARG with radicals. Effect of wastewater effluent organic matter (EfOM) on gene degradation during UV-AOPs was studied in the presence of dissolved organic matter (DOC) isolated from treated wastewater effluent.

5.3 Materials and Methods

5.3.1 Chemical reagents

All chemicals were in analytical grade or higher and used as received without further purification. Ampicillin sodium salt (#A0166), agar powder (#A1296), sodium chloride (≥99.5%), *para*-chlorobenzoic acid (99%), and nitrobenzene (≥99%) were purchased from Sigma-Aldrich. Tryptone (#1612) and yeast extract (#1702) were supplied from Laboratorios CONDA. Hydrogen peroxide 30% (Thermo Fisher Scientific) and sodium peroxydisulfate (≥98%, Sigma-Aldrich) were used to prepare the stock solutions of H_2O_2 and PDS, respectively. All solutions were prepared in Milli-Q water (18 MΩ cm, Millipore). EfOM was previously extracted from a wastewater treatment plant in Jeddah, Saudi-Arabia, with XAD resins (X. Zheng et al., 2014).

5.3.2 Plasmid extraction

Plasmid pUC19 was extracted from *E.Coli* DH5α. Plasmid pUC19 (2686 bp) is a commercially available *E.Coli* vector carrying an ampicillin resistance gene (amp^R, 861 bp). One hundred µL of *E.Coli* DH5α mid-exponential growth phase culture in LB broth medium containing 50 mg/L of ampicillin was transferred into 150 mL of LB broth medium with 50 mg/L of ampicillin and incubated overnight (200 rpm, 37 ℃). Plasmids were extracted from this overnight stock solution using AccuPrep Plasmid Mini Extraction kit (Bioneer, 2016). The extracted solutions contained 60−100 ng/µL of plasmid DNA measured by a NanoDrop ND-2000 Spectrophotometer (NanoDrop Products, Wilmington, USA).

5.3.3 Experimental procedure

All glassware used in this study were autoclaved prior to each experiment. Experimental solutions were prepared in autoclaved 2 mM phosphate buffer at pH 7. Predetermined volumes of plasmid stock solution were spiked into phosphate buffer. Solutions of EfOM were prepared by dissolving the hydrophobic and transphilic fractions (2:1 by mass) of EfOM in phosphate buffer.

UV_{254}-based experiments were carried out with a UV collimated beam device equipped with a low pressure mercury lamp emitting UV light primarily at 254 nm

(Sankyo Denki Ltd., Tokyo, Japan). The UV light was collimated onto a petri dish containing the experimental solution and placed on a magnetic stirrer. The average UV intensity (0.301 mW/cm^2) was determined with atrazine chemical actinometry (Lee et al., 2016). Initial concentration of plasmid DNA was 0.31 ng/µL. The fluence applied were 0−180 mJ/cm^2. The initial doses of H_2O_2 and PDS were 0.5 mM for UV/H_2O_2 and UV/PDS, respectively.

UV_{300}-based experiments were performed using a PearlBeam collimated beam device with UV-LED emitting light at 300 nm (AquiSense Technologies, Erlanger, USA). UV intensity (0.6 mW/cm^2) was determined by a UVX digital radiometer (Ultra-Violet Products Ltd., Upland, USA). UV fluence were 0−2,160 mJ/cm^2. The plasmid DNA concentration was 2 ng/µL. The molar extinction coefficients of H_2O_2 and PDS are lower at 300 nm than that in 254 nm. Thus, much higher oxidant doses (i.e., 10 mM) were applied for UV_{300}/H_2O_2 and UV_{300}/PDS, respectively, in order to increase the formation yield of radicals.

Samples were withdrawn in predetermined time intervals. Residual H_2O_2 and PDS were quenched with excess bovine catalase and sodium thiosulfate, respectively. Samples for biological analysis (500 µL) were stored at -20 ℃ and analysed within 24h.

5.3.4 Radical probe compounds

para-chlorobenzoic acid (*p*CBA) was used as $^{\bullet}OH$ probe during UV_{254}/H_2O_2 and UV_{300}/H_2O_2. Both *p*CBA and nitrobenzene were applied during UV_{254}/PDS and UV_{300}/PDS. Nitrobenzene was a probe for $^{\bullet}OH$, which was produced from $SO_4^{\bullet-}$ reaction with water (see Results and Discussion). *p*CBA and nitrobenzene were analysed on a High Performance Liquid Chromatography (HPLC, Dionex Ultimate 3000, Thermo Scientific) equipped with a XDB-C18 column (5 µm, 4.6 × 150 mm, Agilent). The mobile phase contained acetonitrile and 10 mM phosphoric acid (40:60, v/v). Compounds were analysed on their maximum absorbance (i.e., 240 and 270 nm for *p*CBA and nitrobenzene, respectively).

5.3.5 qPCR Analysis

Gene degradation was measured by qPCR using CFX96 Real-Time PCR detection system (Bio-Rad, Hercules, CA, USA). Four different amplicons (i.e., 192, 400, 603,

and 851 bp) were monitored, which covered a fraction of *amp*^{R} as shown in Figure 5-1. The longest size of *amp*^{R} segment targeted on qPCR was 851 bp instead of the whole *amp*^{R} gene (861 bp), due to the low amplification efficiency of 861 bp amplicon in these experimental conditions. The reaction mixture (20 µL) was consisted of 1 µL of each primer, 1 µL of sample, 10 µL of EvaGreen® supermix, and 7 µL of autoclaved DNAse free water. qPCR protocol included one cycle at 95 ℃ for 2 min, 30 cycles at 95 ℃ for 5 s, an annealing step at 55 ℃ for 60 s, and an elongation at 72 ℃ for 20 s, followed by a melt curve analysis from 65 ℃ to 95 ℃. Each sample was analysed in triplicates. More information on qPCR analysis and DNA sequence of *amp*^{R} and qPCR target amplicons were described elsewhere (Yoon et al., 2018).

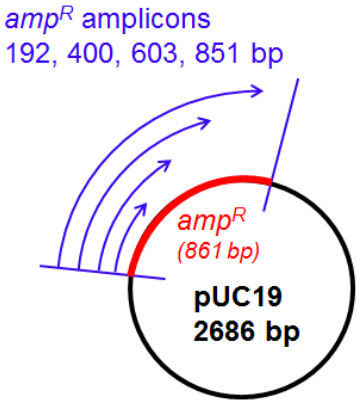

Figure 5-1.The position of *amp*^{R} (861 bp) and target qPCR amplicons (i.e., 192, 400, 603, and 851 bp) on pUC19 plasmid (2686 bp)

5.3.6 Gel electrophoresis analysis

Samples following UV_{300}-based treatments were analysed by DNA gel electrophoresis. Linearized plasmids were incubated with type II restriction enzyme EcoRI (NEB, USA) at 37 ℃ for 1 h, followed by enzyme inactivation at 65 ℃ for 20 min. Plasmid samples from UV_{300}-based and enzyme treatments, as well as a 1 kb DNA ladder (Enzynomics, Korea) were loaded on 0.8% agarose gels at 4 V cm^{-1} for 35 min. The bands were visualized by ethidium bromide staining. Gel images were captured on a UV transilluminator (Universal mutation detection system, UVP, LLC, USA).

5.3.7 Gene transformation assays

Non-resistant *E.Coli* DH5α (without *amp*^{R}) was used as a recipient cell for gene transformation assays. Details on transformation assays were described by Yoon et al. (2018). In brief, competent cells were prepared by chemical treatment of non-resistant

E.Coli DH5α using calcium chloride and glycerol (Shanehbandi et al., 2013) and preserved at -80 ℃ until use. Fifty µL of treated plasmid sample was mixed with 100 µL of thawed competent cells. After incubating in ice for 30 min, the mixture was quickly transferred onto a digital test tube heater (45 ℃) for 45 s and then placed back in ice for 2 min. After the heat shock, the samples were mixed with 900 µL of LB broth and cultured for 45 min (200 rpm, 37 ℃). Finally, the incubated samples were serially diluted with LB broth and plated onto LB agar plates containing 50 mg/L of ampicillin. After 24 h of incubation at 37 ℃, the number of ARB colonies (transformant) detected in selective plates (with ampicillin) were compared with the total recipient cells growing in nonselective agar plates (without ampicillin). The gene transforming activity was calculated as follows:

$$\text{Transforming activity} = \frac{Transformant_{selective\ plate}\ (CFU/mL)}{Total\ E.Coli\ \text{DH5}\alpha_{nonselective\ plate}\ (CFU/mL)}$$

A calibration curve prepared with known concentration of plasmid DNA indicated that the transforming activity linearly increased with the increasing of plasmid DNA concentration (i.e., 10^{-5}–10^{-1} µg/mL). The limit of quantification for transforming activity was ~10^{-8}.

5.3.8 Statistical analysis

Statistical analysis were conducted using SigmaPlot 13.0 and GraphPad Prism 7.04. The fluence-based rate constants for gene degradation and transforming activity loss under various experimental conditions were compared by multiple linear regression analysis. The null hypothesis was that the first-order rate constants were identical as p=0.05 the threshold significance level.

5.4 Results and Discussion

5.4.1 Degradation of *amp*^{R} during UV$_{254}$-AOPs

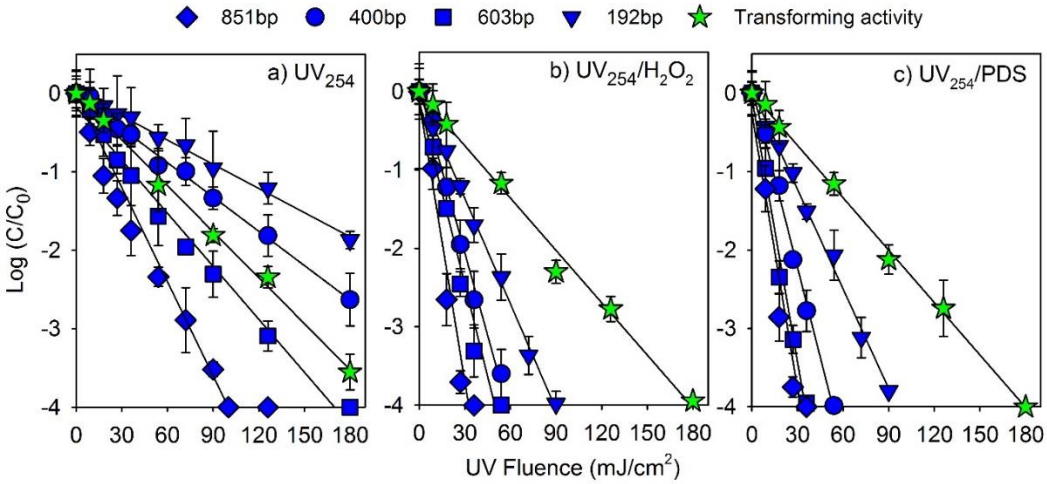

Figure 5-2. Degradation of *amp*^{R} segments (192, 400, 603, and 851 bp) and elimination of gene transforming activity as a function of UV fluence (254 nm) during UV$_{254}$, UV$_{254}$/H$_2$O$_2$ and UV$_{254}$/PDS (Plasmid DNA= 0.31 ng/µL, Fluence= 0−180 mJ/cm^2, H$_2$O$_2$= PDS= 0.5 mM, 2 mM phosphate buffer at pH 7, Error bars represent the standard deviations of triplicated experiments).

Control experiments indicated that H_2O_2, PDS, and quenching reagents didn't affect the qPCR and gene transforming activity analysis within these experimental conditions (data not shown). The $\log_{10}$ degradation of *amp*^{R} amplicons as a function of UV fluence followed first-order kinetics (R^2 > 99%) during UV$_{254}$, UV$_{254}$/H$_2$O$_2$, and UV$_{254}$/PDS (Figure 5-2). Their fluence-based rate constants derived from the slopes of linear curves, k_{obs} =2.303× slope, were shown in Table 5-1. For all treatments, the degradation rates of *amp*^{R} segments increased with amplicon size, which was consistent with the increasing of reaction sites on plasmid. 192 bp *amp*^{R} segment was degraded by 1-log at 90 mJ/cm^2 during UV direct irradiation, whereas 4-log reduction was achieved from 851 bp segment, which was close to the overall size of *amp*^{R} (861 bp). Nevertheless, the UV fluence required to degrade the plasmid-encoded *amp*^{R} segments in this study (> 90 mJ/cm^2) were much higher than the reported values for ARB inactivation (< 20 mJ/cm^2 for 4−5 log reduction) (McKinney and Pruden, 2012). Figure A-3-1 presents the UV absorbance spectra of pUC19 plasmid solution, which exhibited a peak with a maximum intensity at around 260 nm, corresponding to the maximum UV absorbance of pyrimidine and purine nucleobases (Hijnen et al., 2006).

The gene damage during UV irradiation is mainly caused by the formation of toxic and mutagenic DNA lesions, such as cyclobutane-pyrimidine dimers (CPDs) and 6−4 photoproducts (pyrimidine adducts) (Sinha and Häder, 2002). k_{obs} of amp^R segments during UV_{254}/H_2O_2 and UV_{254}/PDS were about 4−5 times higher than that during UV_{254} direct irradiation, indicating the contribution of radicals to gene damage. $^{\bullet}OH$ and $SO_4^{\bullet-}$ induce DNA damage by reacting with DNA bases and sugar moieties, which can result in strand breaks and abasic sites (Cadet et al., 1999; Sonntag, 2006).

Table 5-1.Fluence-based rate constants, k_{obs} ($\times 10^{-2}$ cm^2/mJ), of amp^R segments and gene transforming activity loss

Treatment	amp^R segments				Transforming activity loss
	192 bp	400 bp	603 bp	851 bp	
UV_{254}	2.37±0.07	3.36±0.09	5.25±0.18	8.15±0.35	4.49±0.12
UV_{254}/H_2O_2	10.34±0.21	14.81±0.78	19.34±0.97	29.99±2.10	5.11±0.18
UV_{254}/PDS	10.50±0.48	17.09±0.46	22.87±1.57	31.85±1.57	5.16±0.09
UV_{254}+DOC	3.04±0.11	3.87±0.12	6.22±0.10	9.51±0.37	n/a
UV_{254}/H_2O_2 +DOC	3.09±0.07	4.12±0.16	7.23±0.32	10.06±0.44	n/a
UV_{254}/PDS +DOC	3.27±0.12	3.80±0.16	6.10±0.32	10.45±0.32	n/a
UV_{300}	0.14±0.003	0.23±0.01	0.30±0.01	0.39±0.02	0.16±0.01

2 mM phosphate buffer at pH 7; For UV_{254}-based experiments: Fluence= 0−180 mJ/cm^2, H_2O_2= PDS= 0.5 mM, DOC=5.4 mg-C/L; For UV_{300}-based experiments: Fluence= 0−2,160 mJ/cm^2, H_2O_2= PDS= 10 mM.

5.4.2 Rate constants of *amp*^{R} with $^{\bullet}OH$ and $SO_4^{\bullet-}$

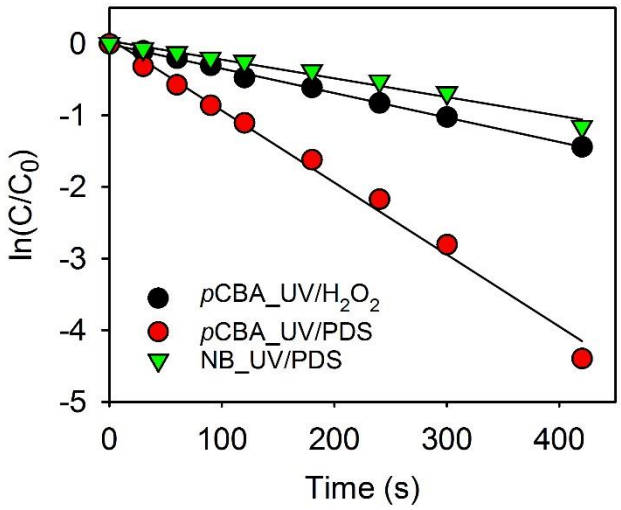

Figure 5-3. Degradation of pCBA (1 µM) and nitrobenzene (NB, 1 µM) during UV_{254}/H_2O_2 and UV_{254}/PDS (Fluence= 0−180 mJ/cm^2, H2O2= PDS= 0.5 mM, 2 mM phosphate buffer at pH 7)

Quantification $^{\bullet}OH$ during UV_{254}/H_2O_2 *p*CBA was applied as $^{\bullet}OH$ probe compound during UV_{254}/H_2O_2. There was no loss of *p*CBA by UV direct irradiation (Figure A-3-2). Thus, its degradation was mainly due to $^{\bullet}OH$ and can be expressed as follows:

$$-\frac{d[pCBA]}{dt} = k_{p\mathrm{CBA}+^{\cdot}OH}[^{\cdot}OH]_{\mathrm{ss}}[pCBA] \quad (1)$$

Integration of equation (1) gives:

$$-ln\frac{[pCBA]}{[pCBA]_0} = k_{p\mathrm{CBA}+^{\cdot}OH}[^{\cdot}OH]_{\mathrm{ss}}t = k_{obs,pCBA,UV/H2O2}t \quad (2)$$

Where $k_{p\mathrm{CBA}+^{\cdot}OH}$ is the second-order rate constant of *p*CBA with $^{\bullet}OH$ (5×10^9 M^{-1} s^{-1}) (Buxton et al., 1988) and $[^{\bullet}OH]_{ss}$ is the steady-state concentration of $^{\bullet}OH$. The pseudo-first order rate constant of *p*CBA was obtained from the slope of the linear curve shown in Figure 5-3 ($k_{obs,pCBA,UV/H2O2}$ =0.0034 s^{-1}). Therefore, $[^{\bullet}OH]_{ss}$ was quantified as 6.8×10^{-13} M, which was in good agreement with the general concentration of $^{\bullet}OH$ (10^{-12}–10^{-13} M) produced from UV (254 nm) irradiation of H_2O_2 in collimated beam devices (Mamane et al., 2007).

Quantification of $SO_4^{\bullet-}$ and $^{\bullet}OH$ in UV_{254}/PDS $SO_4^{\bullet-}$ is the primary radical generated from the UV photolysis of PDS. However, $SO_4^{\bullet-}$ further reacts with H_2O and OH^- in

aqueous solution to produce •OH (Table 5-2), which can contribute to the degradation of target compounds. Nitrobenzene and *p*CBA were applied as radical probes for UV_{254}/PDS experiments. Nitrobenzene was •OH probe compound ($k_{\bullet OH}$=3.9 × 10^9 M^{-1} s^{-1}) (Buxton et al., 1988) due to its low reactivity with $SO_4^{\bullet-}$ ($k_{SO_4^{\bullet-}}$<10^6 M^{-1} s^{-1}) (Neta et al., 1977), while *p*CBA reacted with both radicals (i.e., $k_{SO_4^{\bullet-}}$=3.6 × 10^8 M^{-1} s^{-1} and $k_{\bullet OH}$=5 × 10^9 M^{-1} s^{-1}) (Neta et al., 1977; Buxton et al., 1988). UV direct irradiation had no influence on nitrobenzene and *p*CBA (Figure A-3-2). Thus, their degradation rates during UV_{254}/PDS can be expressed as follows:

$$-\frac{d[NB]}{dt} = k_{NB+^{\cdot}OH}[^{\cdot}OH]_{ss}[NB] \quad (3)$$

$$-\frac{d[pCBA]}{dt} = k_{p\text{CBA}+^{\cdot}OH}[^{\cdot}OH]_{ss}[pCBA] + k_{p\text{CBA}+SO_4^{\bullet-}}[SO_4^{\bullet-}]_{ss}[pCBA] \quad (4)$$

Integration of equation 3 and 4 yield 5 and 6, respectively:

$$-ln\frac{[NB]}{[NB]_0} = k_{NB+^{\cdot}OH}[^{\cdot}OH]_{ss}t = k_{obs,NB}t \quad (5)$$

$$-ln\frac{[pCBA]}{[pCBA]_0} = k_{p\text{CBA}+^{\cdot}OH}[^{\cdot}OH]_{ss}t + k_{p\text{CBA}+SO_4^{\bullet-}}[SO_4^{\bullet-}]_{ss}t = k_{obs,pCBA,UV/PDS}t \quad (6)$$

Where $k_{obs,NB}$ (i.e., 0.0025 s^{-1}) and $k_{obs,pCBA,UV/PDS}$ (i.e., 0.0098 s^{-1}) were obtained from the slopes of the linear curves shown in Figure 5-3. According to equation 5 and 6, the steady-state concentrations of $[^{\bullet}OH]_{ss}$ and $[SO_4^{\bullet-}]_{ss}$ during UV/PDS were quantified as 6.4×10^{-13} M and 1.8×10^{-11} M, respectively.

$[^{\bullet}OH]_{ss}$ during UV/PDS can be estimated theoretically by taking into account all the main reactions related to •OH (Table 5-2) (Wordofa et al., 2017), including the scavenging effect of PDS, phosphate buffer ions, *p*CBA, and nitrobenzene. Based on steady-state assumption (i.e., formation rate=consumption rate, $\frac{d[^{\cdot}OH]}{dt} = 0$), rearrangement of equation Table_5-2 (8) gives equation Table_5-2 (9). Under the experimental conditions of the present work (i.e., $[S_2O_8^{2-}]$ = 0.5 mM, *p*CBA and nitrobenzene = 1 µM, 2 mM phosphate buffer at pH 7), $[^{\cdot}OH]_{ss} = 0.041\ [SO_4^{\cdot-}]_{ss}$. Thus, the concentration of •OH was approximately 2 orders of magnitude lower than that of $SO_4^{\bullet-}$, which was comparable with the experimental values mentioned above.

During UV_{254}/PDS, if the target compound has similar or higher rate constant with $SO_4^{\bullet-}$ than $^{\bullet}OH$, the contribution of $^{\bullet}OH$ produced from $SO_4^{\bullet-}$ reactions with water can be negligible due to its very low formation compared to $SO_4^{\bullet-}$ (R. Zhang et al., 2015). However, in this study, ARG was more reactive with $^{\bullet}OH$ (see discussion below), thus its contribution to gene degradation during UV_{254}/PDS cannot be ignored.

Table 5-2.Main reactions related to $^{\bullet}OH$ during UV_{254}/PDS

	Reactions	[a] Rate constants
1)	$SO_4^{\bullet-} + H_2O \rightarrow SO_4^{2-} + {}^{\bullet}OH + H^+$	k_1=660 s^{-1}
2)	$SO_4^{\bullet-} + OH^- \rightarrow SO_4^{2-} + {}^{\bullet}OH$	k_2=7×10^7 M^{-1} s^{-1}
3)	$^{\bullet}OH + S_2O_8^{2-} \rightarrow S_2O_8^{\bullet-} + OH^-$	k_3=1.4 ×10^7 M^{-1} s^{-1}
4)	$^{\bullet}OH + HPO_4^{2-} \rightarrow HPO_4^{\bullet-} + OH^-$	k_4=1.5 ×10^5 M^{-1} s^{-1}
5)	$^{\bullet}OH + H_2PO_4^- \rightarrow HPO_4^{\bullet-} + H_2O$	k_5=2.0 × 10^4 M^{-1} s^{-1}
6)	$^{\bullet}OH$ + *p*CBA → products	k_6=5 × 10^9 M^{-1} s^{-1}
7)	$^{\bullet}OH$ + NB → products	k_7=3.9 × 10^9 M^{-1} s^{-1}
8)	$-\frac{d[^{\bullet}OH]}{dt} = k_1[SO_4^{\bullet-}] + k_2[SO_4^{\bullet-}][OH^-] - k_3[^{\bullet}OH][S_2O_8^{2-}] - k_4[^{\bullet}OH][HPO_4^{2-}] - k_5[^{\bullet}OH][H_2PO_4^-] - k_6[^{\bullet}OH][pCBA] - k_7[^{\bullet}OH][NB]$	
9)	$[^{\bullet}OH]_{ss} = \frac{k_1 + k_2[OH^-]}{k_3[S_2O_8^{2-}] + k_4[HPO_4^{2-}] + k_5[H_2PO_4^-] + k_6[^{\bullet}OH][pCBA] + k_7[^{\bullet}OH][NB]}[SO_4^{\bullet-}]_{ss}$	

[a] k_1–k_5 were obtained from Yang et al. (2016); k_6 was from Buxton et al. (1988); k_7 was from Neta et al. (1977)

Radical rate constants of amp^R It is known that $^{\bullet}OH$ and $SO_4^{\bullet-}$ react with free nucleobases in nearly diffusion-controlled rates (~10^9 M^{-1} s^{-1}) (Buxton et al., 1988; Cadet et al., 2014). Few studies have reported the rate constants of $^{\bullet}OH$ and $SO_4^{\bullet-}$ with DNA molecule. The degradation of *amp^R* during UV_{254}/H_2O_2 was attributed to the UV direct irradiation and $^{\bullet}OH$ oxidation as follows:

$$-\frac{d[ARG]}{dt} = k'_{UV\ only,ARG}[ARG] + k_{ARG+^{\bullet}OH}[^{\bullet}OH]_{ss}[ARG] \quad (7)$$

$$-ln\frac{[ARG]}{[ARG]_0} = k'_{UV\ only,ARG}t + k_{ARG+^{\bullet}OH}[^{\bullet}OH]_{ss}t = k'_{obs,ARG\_UV/H2O2}t \quad (8)$$

$$\text{Thus, } k_{ARG+^{\bullet}OH} = \frac{k'_{obs,ARG\_UV/H2O2} - k'_{UV\ only,ARG}}{[^{\bullet}OH]_{ss}} \quad (9)$$

For UV_{254}/PDS, UV direct irradiation, $SO_4^{\bullet-}$, and $^{\bullet}OH$ contributed to the degradation of *amp^R*:

$$-\frac{d[ARG]}{dt} = k'_{UV\ only,ARG}[ARG] + k_{ARG+SO_4^{\bullet-}}[SO_4^{\bullet-}]_{ss}[ARG] + k_{ARG+^{\bullet}OH}[^{\bullet}OH]_{ss}[ARG] \quad (10)$$

$$-ln\frac{[ARG]}{[ARG]_0} = k'_{UV\ only,ARG}t + k_{ARG+SO_4^{\bullet-}}[SO_4^{\bullet-}]_{ss}t + k_{ARG+^{\cdot}OH}[^{\cdot}OH]_{ss}t = k'_{obs,ARG\_UV/PDS}t \quad (12)$$

Thus, $k_{ARG+SO_4^{\bullet-}} = \frac{k'_{obs,ARG\_UV/PDS} - k'_{UV\ only\ ,ARG} - k_{ARG+^{\cdot}OH}[^{\cdot}OH]_{ss}}{[SO_4^{\bullet-}]_{ss}}$ (13)

$k'_{UV\ only,ARG}$, $k'_{obs,ARG\_UV/H2O2}$, and $k'_{obs,ARG\_UV/PDS}$ were the pseudo-first order rate constants (s^{-1}) of amp^R during UV_{254} direct irritation, UV_{254}/H_2O_2, and UV_{254}/PDS, respectively. The second-order rate constants of each amp^R segment with $^{\bullet}OH$ and $SO_4^{\bullet-}$ were calculated according to equations 9 and 13 and presented in Table 5-3.

Table 5-3. Second-order rate constants (M^{-1} s^{-1}) of *amp*^{R} segments with $^{\bullet}OH$ and $SO_4^{\bullet-}$

	amp^R segments			
	192 bp	400 bp	603 bp	851 bp
$k_{ARG+^{\cdot}OH}$	3.56×10^{10}	5.16×10^{10}	6.01×10^{10}	9.10×10^{10}
$k_{ARG+SO_4^{\bullet-}}$	2.16×10^{7}	4.23×10^{8}	9.14×10^{8}	5.64×10^{8}

As shown in Table 5-3, the second-order rate constants of $SO_4^{\bullet-}$ with *amp*^{R} segments were in the range of 10^7–10^9 (M^{-1} s^{-1}), which were 2–3 orders of magnitude lower than that of $^{\bullet}OH$ (10^{10}–10^{11} M^{-1} s^{-1}). $^{\bullet}OH$ reacts with DNA by addition to nucleobases producing adduct radicals and by abstracting a hydrogen from 2-deoxyribose (Sonntag, 2006; Dizdaroglu and Jaruga, 2012). Unlike $^{\bullet}OH$, $SO_4^{\bullet-}$ preferentially reacts with electron-rich moieties mainly through electron-transfer, less by addition and hydrogen abstraction (Neta et al., 1988). Moreover, $SO_4^{\bullet-}$ is larger than $^{\bullet}OH$ and negatively charged. Thus, electrostatic repulsion might reduce its reaction rate with negatively charged DNA molecules. $SO_4^{\bullet-}$ was also reported to be less efficient than $^{\bullet}OH$ for the inactivation of microbial strains (e.g., *E.Coli*, bacteriophage MS2) (Sun et al., 2016). Comparable amounts of $^{\bullet}OH$ were generated during UV_{254}/H_2O_2 and UV_{254}/PDS in the present work. Although $[SO_4^{\bullet-}]_{ss}$ in UV_{254}/PDS was 2 orders of magnitude higher than $[^{\bullet}OH]_{ss}$ in UV_{254}/H_2O_2, the fluence-based rate constants of *amp*^{R} amplicons (Table 5-1) during UV_{254}/PDS were not significantly different from that in UV_{254}/H_2O_2 (i.e., p=0.1367, 0.0334, 0.0151, and 0.9236 for 192, 400, 603, and 851 bp, respectively) due to the lower reactivity of $SO_4^{\bullet-}$. Gene degradation during UV_{254}/PDS was mainly attributed to the trace amount of $^{\bullet}OH$ present in solution (same amount as the one produced during UV_{254}/H_2O_2), which contributed to about 70–98% of the gene damage in our experimental conditions.

Notably, the rate constant of $^{\bullet}OH$ with *amp*^{R} segments were in the range of 10^{10}–10^{11} M^{-1} s^{-1}, which were higher than the commonly reported diffusion-controlled rate constants (i.e., 10^8–10^9 M^{-1} s^{-1}) (Buxton et al., 1988). $^{\bullet}OH$ was found to react with *E.coli* cells at the rate constant of ~10^{12} M^{-1} s^{-1} which was explained by the large difference in the size of two reactants (Berg and von Hippel, 1985; Sun et al., 2016). $k_{ARG+^{\cdot}OH}$ increased with the number of base pair while $k_{ARG+SO_4^{\bullet-}}$ appeared to have a maximum value at 603 bp. The reactivity of free radicals with DNA depends on the conformation of DNA macromolecule, which affects the accessibility of radicals to reactive sites. The type and number of nucleobases within DNA segment also

influence the reaction rate. For example, guanine moieties have significantly higher reactivity with •OH ($8–9\times10^9$ M^{-1} s^{-1}) compared to other nucleobases (Masuda et al., 1980; Michalik et al., 1995). Future work will focus on developing a model for •OH and $SO_4^{\bullet-}$ rate constants with ARGs based on the experimental values listed in Table 5-3, in order to estimate the degradation efficiency of various ARGs during radical-based treatment processes.

5.4.3 Effect of wastewater effluent organic matter

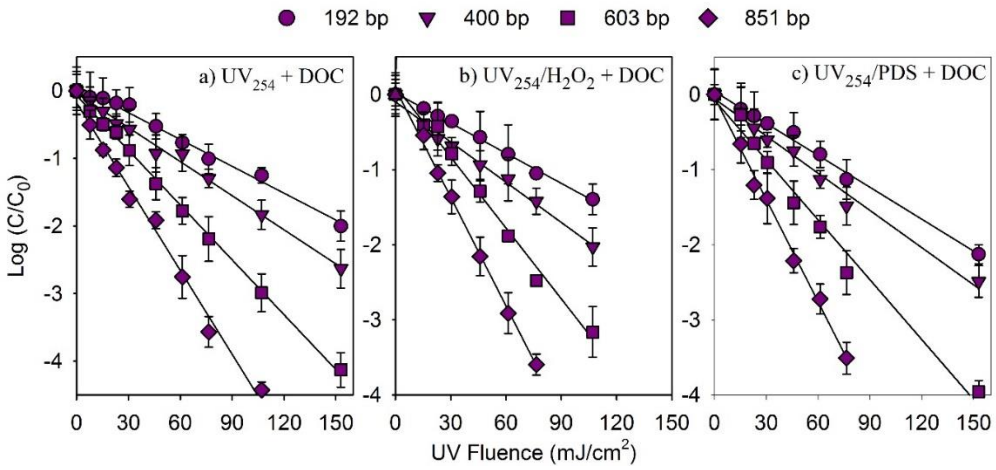

Figure 5-4. Degradation of *amp*^{R} segments (192, 400, 603, and 851 bp) in the presence of wastewater effluent organic matter during UV_{254}, UV_{254}/H_2O_2, and UV_{254}/PD (DOC=5.4 mg-C/L, Plasmid DNA= 0.31 ng/µL, Fluence= 0−180 mJ/cm^2, H2O2= PDS= 0.5 mM, 2 mM phosphate buffer at pH 7, Error bars represent the standard deviations of triplicated experiments)

The efficiencies of *amp*^{R} degradation during UV_{254}, UV_{254}/H_2O_2, and UV_{254}/PDS in the presence of 5.4 mg-C/L of EfOM were investigated. Control experiments have confirmed that EfOM by itself had no effect on *amp*^{R} and qPCR analysis in these experimental conditions (data not shown). The UV 254 nm absorbance of EfOM solution was 0.103 cm^{-1}. The path length in petri dish was 1.6 cm. Thus, the water factor, $WF=(1-10^{-aL})/(aLln10)$ (Bolton and Linden, 2003), was calculated to be 0.835. Average UV intensity in petri dish was corrected as 0.255 mW/cm^2 based on the calculated water factor (Lee et al., 2016). As shown in Figure 5-4, *amp*^{R} segments were linearly degraded with UV fluence. The fluence-based rate constants were shown in Table 5-1. Interestingly, k_{obs} of each segment during UV direct irradiation in the presence of EfOM was approximately 1.2 times higher than the corresponding values from UV irradiation without EfOM (p<0.0001). Chromophoric dissolved organic matter (DOM) is known to generate reactive species upon UV irradiation, such as

triplet-excited state of DOM (^{3}DOM*), singlet oxygen, and $^{\bullet}$OH, which have been proven to contribute to the oxidation of organic pollutants (Chin et al., 2004; Batista et al., 2016). Bacteriophage MS2 was found to be inactivated by ^{3}DOM* and singlet oxygen generated from sunlight irradiation of wastewater and river water DOM isolates (Rosado-Lausell et al., 2013). Reactive oxygen species generated by the photooxidation of oxygen during UVA irradiation was proposed to inactivate bacteria by damaging DNA, proteins, and cell membranes (Song et al., 2016). Our findings are suggesting that through its photosensitiser property, DOM is indirectly contributing to the photo-degradation of cell-free (naked) DNA. This degradation pathway can play an important role especially during solar disinfection process, due to the low UV absorbance characteristic of DNA at high wavelength.

EfOM mainly acted as radical scavenger during UV_{254}/H_2O_2 and UV_{254}/PDS. k_{obs} of amp^R segments were approximately reduced by 3 times compared to the conditions without EfOM (Table 5-1). The secondary rate constants of EfOM with $^{\bullet}$OH and $SO_4^{\bullet-}$ were reported to be 3.3 $\times10^4$ and 9.4 $\times10^3$ (mg-C/L)$^{-1}$ s^{-1}, respectively (Yang et al., 2016). Thus, the scavenging capacities of EfOM on $^{\bullet}$OH and $SO_4^{\bullet-}$ were estimated to be 1.78×10^5 and 5.08×10^4 s^{-1}, respectively. Kinetics of *p*CBA and NB degradation (Figure A-3-3) also confirmed less formation of $^{\bullet}$OH and $SO_4^{\bullet-}$ in the presence of EfOM (i.e., $[^{\bullet}OH]_{ss}=1.6\times10^{-13}$ M and 5.1×10^{-14} M for UV/H_2O_2 and UV/PDS, respectively; $[SO_4^{\bullet-}]_{ss}=9.5\times10^{-13}$ M).

5.4.4 Degradation of amp^R during UV_{300}-AOPs

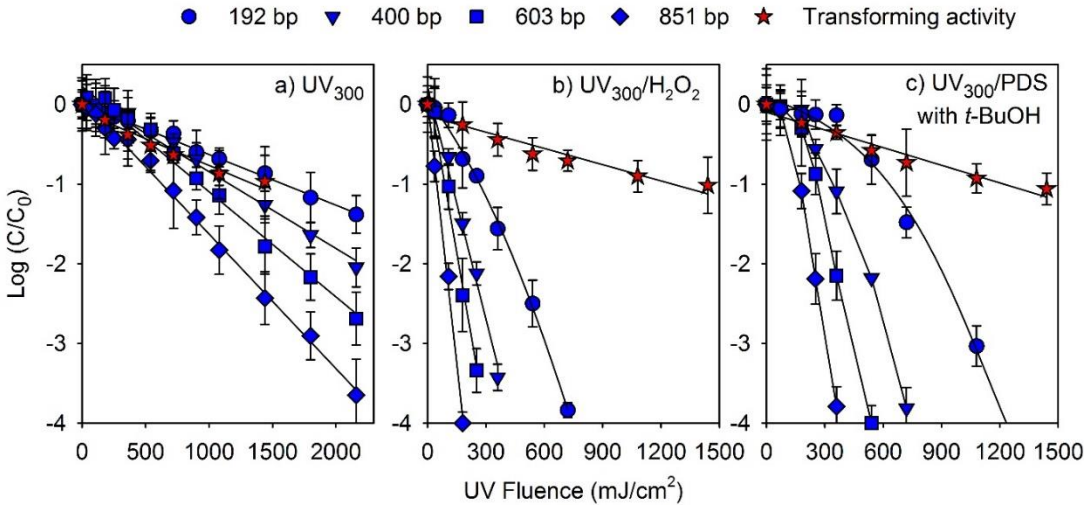

Figure 5-5. Degradation of amp^R segments (192, 400, 603, and 851 bp) and elimination of gene transforming activity as a function of UV fluence (300 nm)

during UV_{300}, UV_{300}/H2O2, and UV_{300}/PDS (Plasmid DNA= 2 ng/µL, Fluence= 0−2,160 mJ/cm^2, H2O2= PDS= 10 mM, 2 mM phosphate buffer at pH 7. For UV_{300}/PDS, 1 mM of *t*-BuOH was added, Error bars represent the standard deviations of triplicated experiments)

Although UVB range (280-315 nm) of solar spectrum accounts for less than 1% of the total solar energy, it plays significant role in the inactivation of microorganisms. Similar to UV_{254}, UV_{300} irradiation was reported to induce DNA damage by producing CPDs, 6−4 photoproducts, and their Dewar isomers (Rastogi et al., 2010). As shown in Figure 5-5a, the $\log_{10}$ removal of amp^R segments linearly increased with increasing UV fluence. However, the degradation rates were much slower compared to the values determined with UV_{254} (Figure 5-2a). The fluence-based rate constants of amp^R segments during UV_{300} irradiation (Table 5-1), were about 15−20 times lower than the corresponding rate constants obtained during UV_{254} irradiation. This can be explained by the low UV absorption of plasmid DNA at 300 nm. About 720 mJ/cm^2 of UV dose was required for 1-log reduction of amp^R segment with 851 bp, which was much higher than the required dose for the inactivation of *E.Coli* at 310 nm (i.e., 95 mJ/cm^2 for per log inactivation) (Song et al., 2016).

UV_{300}/H_2O_2 and UV_{300}/PDS accelerated the decay of amp^R segments (Figure 5-5 b and c). 4−log reduction of 851 bp were achieved within 180 and 360 mJ/cm^2 during UV_{300}/H_2O_2 and UV_{300}/PDS, respectively, whereas more than 2,000 mJ/cm^2 was needed in UV_{300} direct irradiation. However, the contribution of radicals for gene degradation were not as efficient as previously observed from UV_{254} –AOPs (Figure 5-2b and c). Although high dose of H_2O_2 (10 mM) was applied, the concentration of $^{\bullet}OH$ (i.e., 6×10^{-14} M) during UV_{300}/H_2O_2 was 1-order of magnitude lower than UV_{254}/H_2O_2 (0.5 mM), due to the lower molar extinction coefficient of H_2O_2 at 300 nm. It is important to indicate that $^{\bullet}OH$ can be quenched by H_2O_2 itself (2.7×10^7 M^{-1} s^{-1}) (Buxton et al., 1988). The concentration of $SO_4^{\bullet-}$ during UV_{300}/PDS (i.e., 1×10^{-11} M) was slightly higher than the one determined during UV_{254}/PDS exposure. As mentioned above, the gene degradation during UV_{254}/PDS was mainly attributed to $^{\bullet}OH$ (70−98% contribution). However, 1 mM of *tert*-butanol was applied during UV_{300}/PDS to scavenge $^{\bullet}OH$. Therefore, about 20 times less $^{\bullet}OH$ (i.e., 3.6×10^{-14} M) was generated compared to UV_{254}/PDS and the contribution of $^{\bullet}OH$ to the overall gene degradation was reduced to 15−23%. Thus, amp^R segments were degraded slower during UV_{300}/PDS than UV_{300}/H_2O_2.

The fluence-based rate constants of amp^R segments during UV_{300}/H_2O_2 and UV_{300}/PDS were not calculated because their $\log_{10}$ degradation curve appeared to have a lag-phase at low UV fluence (Figure 5-5b and c). Radical probe compounds within the same solution (i.e., *p*CBA and NB) exhibited linear correlations between $\ln(C/C_0)$ and UV fluence ($R^2 > 0.98\%$) (Figure A-3-4). Hence, the concentrations of radicals were assumed to be at steady-state throughout the experiments. The reason for the lag-phase in gene degradation during UV_{300}/H_2O_2 and UV_{300}/PDS remained unclear. One possible explanation could be the lack of sensitivity of the qPCR analysis to detect the DNA damage in earlier stage of radical exposure.

5.4.5 Plasmid damage measured by gel electrophoresis

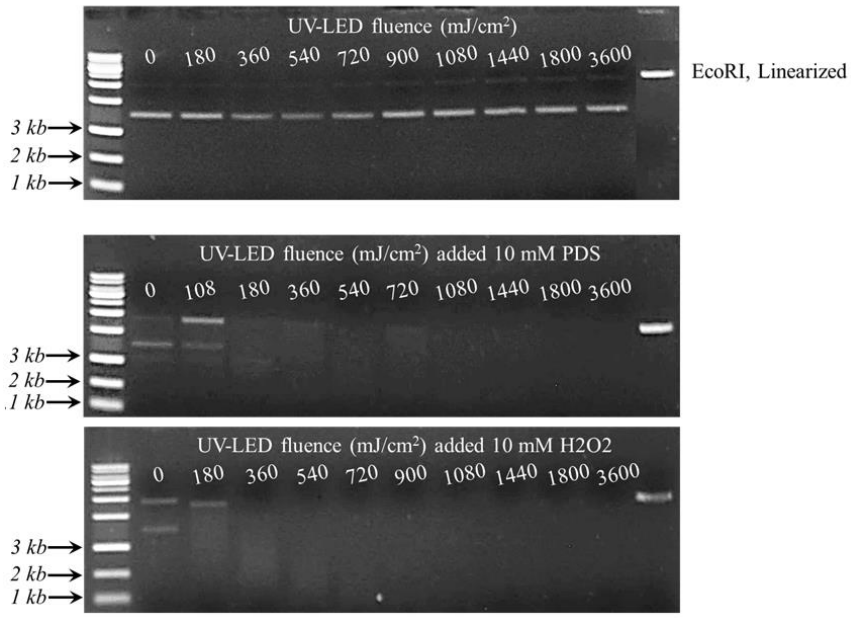

Figure 5-6. DNA electrophoresis gel of pUC19 plasmids treated by UV_{300}, UV_{300}/H_2O_2, and UV_{300}/PDS (Fluence= 0−3,600 mJ/cm^2, H_2O_2= PDS= 10 mM). First column shows the standard DNA ladders. Last column shows linearized pUC19 plasmid after treating with EcoRI restriction enzyme.

Figure 5-6 presents the electrophoresis gel of pUC19 plasmids during UV_{300}, UV_{300}/H_2O_2, and UV_{300}/PDS. pUC19 plasmid before treatment (fluence=0) showed a band located lower than the linearized pUC19 (EcoRI, linearized), because plasmid DNA generally exists in a supercoiled form, which is smaller than its linear form and migrates faster in electrophoresis gel. UV_{300} direct irradiation didn't change the position of the band under various UV doses, which suggested that plasmid kept its supercoiled form. Alternatively, no significant conformational change occurred on

plasmid upon UV_{300} irradiation and the DNA base damage (e.g., nucleobase dimers) was not detected by gel electrophoresis. However, bands moved upwards at 108 and 180 mJ/cm^2 during UV_{300}/H_2O_2 and UV_{300}/PDS, respectively, revealing that plasmid was changed into its nicked circle forms or linearized after radical exposure. With further increase of UV fluence, plasmid bands gradually disappeared from gel electrophoresis images. In this analysis, ethidium bromide staining method was applied for the visualization of plasmid in electrophoresis gel. Ethidium bromide forms a strong fluorescent complex by intercalating between DNA base pairs (Prütz, 1984). Our results indicated that radical oxidation led to alterations in base pair region of plasmid DNA, which weakened the DNA-ethidium bromide fluorescence. Overall, UV_{300} direct irradiation had no influence on the structure of plasmid DNA. In contrast, $^{\bullet}OH$ and $SO_4^{\bullet-}$ exposure modified the base pair region and changed the supercoiled conformation of plasmid DNA, which might be the result of strand breaks.

5.4.6 Gene damage repair in recipient cells and the elimination of transforming activity during UV-AOPs

Control experiment has confirmed that recipient cells (i.e., non-resistant *E.Coli* DH5α) cannot grow in agar plate containing 50 mg/L of ampicillin due to lack of amp^R. The total recipient cells in nonselective agar plate (without ampicillin) was approximately 2×10^8 CFU/mL. About 7×10^5 CFU/mL of transformants were observed in selective plate (with ampicillin) after incubating the recipient cells with 15 ng/mL of pUC19 plasmid carrying amp^R, indicating that recipient cells became resistant to ampicillin after taking up amp^R. The gene transforming activity was calculated to be 3.6×10^{-3}, which was comparable with previous studies (Chang et al., 2017; Yoon et al., 2018). As shown in Figure 5-2, the transforming activity of amp^R gradually decreased with increasing UV fluence due to the damage on amp^R. The curve for transforming activity loss during UV direct irradiation (Figure 5-2a) was located between 400 and 603 bp, revealing that not all damage occurred sites on ARG segments were critical for the loss of transforming activity or the gene damage induced by UV irradiation was repaired within host cells (Yoon et al., 2018). Interestingly, only 2-log of transforming activity loss was observed while all amp^R segments were degraded by 4-log during UV_{254}/H_2O_2 and UV_{254}/PDS (Figure 5-2b and c). Although the radical exposure significantly accelerated the gene damage rates, the transforming activity loss during UV_{254}/H_2O_2 and UV_{254}/PDS were only about 1.1 times faster than that during UV_{254} direct

irradiation (p=0.0180 and 0.0018 for UV_{254}/H_2O_2 and UV_{254}/PDS, respectively) (Table 5-1). These results indicated that the transforming activity loss during UV_{254}/H_2O_2 and UV_{254}/PDS were mainly due to the gene damage by UV_{254} direct irradiation and radicals induced damage can be repaired by recipient cells. Consequently, the gene degradation rate obtained from qPCR analysis have overestimated the elimination of transforming activity in radical processes. Comparable results were found from UV_{300}-based experiments (Figure 5-5). k_{obs} of transforming activity loss during UV_{300}, UV_{300}/H_2O_2, and UV_{300}/PDS were ~1.61×10^{-3} cm^2/mJ and no significant difference was observed between different treatments (p=0.7763). These results further supported above findings that UV induced DNA damage was mainly responsible for the loss of amp^R transforming activity and DNA damages induced by $^{\bullet}OH$ and $SO_4^{\bullet-}$ were repaired within recipient cells.

Bacteria cells have developed the ability to repair DNA lesions induced by UV irradiation and oxidant stress (e.g., radicals) by a number of enzyme activities. DNA dimers produced after UV exposure can be repaired through nucleotide excision repair mechanism with the help of polymerases (Sinha and Häder, 2002). Apart from the supercoiled conformation change and base pair region modification discussed above, the exact oxidation products of pUC19 plasmid DNA after $^{\bullet}OH$ and $SO_4^{\bullet-}$ exposure were not clear in this study. However, it was reported that the damaged nucleobases (e.g., hydroxylated and ring opening products) and strand breaks can be removed by DNA exo- and endonucleases and by DNA glycosylases (i.e., excision-repair) (Teebor et al., 1988). Previous studies have hypothesised that although the degradation of DNA by direct irradiation is less efficient during solar disinfection processes (especially in UVA range) compared to UVC irradiation, the indirect damage caused by reactive oxygen species might be irreparable, thus might be more important than the repairable damage induced by UV irradiation (Song et al., 2016). Our study indicated that the radicals induced gene damage is also susceptible to DNA repair mechanism. The repair capability of DNA damage depends on the type of recipient cells and the characteristics of genes (Chang et al., 2017; Yoon et al., 2018). Therefore, more studies are needed on other types of recipient cells and genes to compare the gene degradation rate with gene transforming activity loss. The transformation of gene was only reduced by1-log within the typical UV disinfection dose for water treatment

(40 mJ/cm^2) in our experimental conditions regardless of treatment types, raising concerns about the dissemination of antibiotic resistance in treated water.

5.5 Conclusions

1) *amp*^{R} was degraded following first-order kinetics as a function of UV fluence during UV_{254} and UV_{300}-based treatments. The degradation rates increased with size of segments.

2) The UV fluence required for the removal of *amp*^{R} during UV_{254} and UV_{300} were much higher than the reported UV doses for the inactivation of bacteria at similar wavelengths, suggesting that the degradation of extracellular ARGs by UV can be challenging.

3) $^{\bullet}OH$ and $SO_4^{\bullet-}$ exposure enhanced the degradation rates of *amp*^{R} compared to UV direct irradiation. The second-order rate constants of $^{\bullet}OH$ and $SO_4^{\bullet-}$ with *amp*^{R} segments were in the range of 10^{10}–10^{11} and 10^7–10^9 M^{-1} s^{-1}, respectively. The gene degradation during UV_{254}/PDS was mainly attributed to the trace amount of $^{\bullet}OH$ produced by the reaction of $SO_4^{\bullet-}$ with water, due to the higher reactivity of $^{\bullet}OH$ with plasmid DNA than $SO_4^{\bullet-}$.

4) Gel electrophoresis analysis indicated that UV direct irradiation didn't cause significant conformation change on plasmid DNA, while radical exposure modified the base pair region and changed the supercoiled structure of plasmid DNA.

5) Although radical oxidation accelerated the degradation of *amp*^{R} measured by qPCR, transforming activity loss were comparable within various treatment processes, indicating that the gene damage caused by radical exposure was repaired by recipient cells and UV induced damage was mainly responsible for the loss of transforming activity. Therefore, gene degradation rate measured by qPCR might overestimate the elimination of gene transforming activity.

6) DNA repair capability of bacteria depends on the type of recipient cells and characteristic of ARGs. Future studies should focus on the identification of DNA damage induced by $^{\bullet}OH$ and $SO_4^{\bullet-}$, and the efficiency of DNA damage repair by different recipient cells.

5.6 Reference

Batista, A. P. S., Teixeira, A. C. S. C., Cooper, W. J., and Cottrell, B. A. (2016). Correlating the chemical and spectroscopic characteristics of natural organic matter with the photodegradation of sulfamerazine. *Water Research, 93*, 20-29.

Berg, O. G., and von Hippel, P. H. (1985). Diffusion-Controlled Macromolecular Interactions. *Annual Review of Biophysics and Biophysical Chemistry, 14*(1), 131-158.

Bioneer. (2016). AccuPrep® Nano-Plus Plasmid Mini/Midi/Maxi Extraction Kit. *User's Guide, Available at http://us.bioneer.com/Protocol/AccuPrep%20Nano Plus%20Plasmid%20Extraction%20Kit.pdf*

Bolton, J. R., and Linden, K. G. (2003). Standardization of methods for fluence (UV Dose) determination in bench-scale UV experiments. *Journal of Environmental Engineering, 129*(3), 209-215.

Buxton, G. V., Greenstock, C. L., Helman, W. P., and Ross, A. B. (1988). Critical Review of rate constants for reactions of hydrated electrons, hydrogen atoms and hydroxyl radicals (·OH/·O−) in Aqueous Solution. *Journal of Physical and Chemical Reference Data, 17*(2), 513-886.

Cadet, J., Delatour, T., Douki, T., Gasparutto, D., Pouget, J.-P., Ravanat, J.-L., and Sauvaigo, S. (1999). Hydroxyl radicals and DNA base damage. *Mutation Research/Fundamental and Molecular Mechanisms of Mutagenesis, 424*(1), 9-21.

Cadet, J., Wagner, J. R., Shafirovich, V., and Geacintov, N. E. (2014). One-electron oxidation reactions of purine and pyrimidine bases in cellular DNA. *International Journal of Radiation Biology, 90*(6), 423-432.

Chang, P. H., Juhrend, B., Olson, T. M., Marrs, C. F., and Wigginton, K. R. (2017). Degradation of Extracellular Antibiotic Resistance Genes with UV254 Treatment. *Environmental Science & Technology, 51*(11), 6185-6192.

Chin, Y.-P., Miller, P. L., Zeng, L., Cawley, K., and Weavers, L. K. (2004). Photosensitized Degradation of Bisphenol A by Dissolved Organic Matter. *Environmental Science & Technology, 38*(22), 5888-5894.

Davies, J., and Davies, D. (2010). Origins and Evolution of Antibiotic Resistance. *Microbiology and Molecular Biology Reviews : MMBR, 74*(3), 417-433.

Dizdaroglu, M., and Jaruga, P. (2012). Mechanisms of free radical-induced damage to DNA. *Free Radical Research, 46*(4), 382-419.

Dodd, M. C. (2012). Potential impacts of disinfection processes on elimination and deactivation of antibiotic resistance genes during water and wastewater treatment. *Journal of Environmental Monitoring, 14*(7), 1754-1771.

Ferro, G., Guarino, F., Castiglione, S., and Rizzo, L. (2016). Antibiotic resistance spread potential in urban wastewater effluents disinfected by UV/H2O2 process. *Science of the Total Environment, 560-561*, 29-35.

Ferro, G., Guarino, F., Cicatelli, A., and Rizzo, L. (2017). β-lactams resistance gene quantification in an antibiotic resistant Escherichia coli water suspension treated by advanced oxidation with UV/H2O2. *Journal of Hazardous Materials, 323*, 426-433.

Giannakis, S., Le, T.-T. M., Entenza, J. M., and Pulgarin, C. (2018). Solar photo-Fenton disinfection of 11 antibiotic-resistant bacteria (ARB) and elimination

of representative AR genes. Evidence that antibiotic resistance does not imply resistance to oxidative treatment. *Water Research, 143*, 334-345.

Guo, M.-T., Yuan, Q.-B., and Yang, J. (2015). Distinguishing Effects of Ultraviolet Exposure and Chlorination on the Horizontal Transfer of Antibiotic Resistance Genes in Municipal Wastewater. *Environmental Science & Technology, 49*(9), 5771-5778.

Hijnen, W. A. M., Beerendonk, E. F., and Medema, G. J. (2006). Inactivation credit of UV radiation for viruses, bacteria and protozoan (oo)cysts in water: A review. *Water Research, 40*(1), 3-22.

Lee, Y., Gerrity, D., Lee, M., Gamage, S., Pisarenko, A., Trenholm, R. A., Canonica, S., Snyder, S. A., and von Gunten, U. (2016). Organic Contaminant Abatement in Reclaimed Water by UV/H2O2 and a Combined Process Consisting of O3/H2O2 Followed by UV/H2O2: Prediction of Abatement Efficiency, Energy Consumption, and Byproduct Formation. *Environmental Science & Technology, 50*(7), 3809-3819.

Liu, S.-S., Qu, H.-M., Yang, D., Hu, H., Liu, W.-L., Qiu, Z.-G., Hou, A.-M., Guo, J., Li, J.-W., Shen, Z.-Q., and Jin, M. (2018). Chlorine disinfection increases both intracellular and extracellular antibiotic resistance genes in a full-scale wastewater treatment plant. *Water Research, 136*, 131-136.

Lorenz, M. G., and Wackernagel, W. (1994). Bacterial gene transfer by natural genetic transformation in the environment. *Microbiological Reviews, 58*(3), 563-602.

Mamane, H., Shemer, H., and Linden, K. G. (2007). Inactivation of E. coli, B. subtilis spores, and MS2, T4, and T7 phage using UV/H2O2 advanced oxidation. *Journal of Hazardous Materials, 146*(3), 479-486.

Masuda, T., Shinohara, H., Eda, M., and Kondo, M. (1980). Reactivity of Nucleotides and Polynucleotides Toward Hydroxyl Radical in Aqueous Solution. *Journal of Radiation Research, 21*(2), 173-179.

McKinney, C. W., and Pruden, A. (2012). Ultraviolet disinfection of antibiotic resistant bacteria and their antibiotic resistance genes in water and wastewater. *Environmental Science and Technology, 46*(24), 13393-13400.

Michael-Kordatou, I., Iacovou, M., Frontistis, Z., Hapeshi, E., Dionysiou, D. D., and Fatta-Kassinos, D. (2015). Erythromycin oxidation and ERY-resistant Escherichia coli inactivation in urban wastewater by sulfate radical-based oxidation process under UV-C irradiation. *Water Research, 85*, 346-358.

Michalik, V., Maurizot, M. S., and Charlier, M. (1995). Calculation of Hydroxyl Radical Attack on Different Forms of DNA. *Journal of Biomolecular Structure and Dynamics, 13*(3), 565-575.

Neta, P., Huie, R. E., and Ross, A. B. (1988). Rate Constants for Reactions of Inorganic Radicals in Aqueous Solution. *Journal of Physical and Chemical Reference Data, 17*(3), 1027-1284.

Neta, P., Madhavan, V., Zemel, H., and Fessenden, R. W. (1977). Rate constants and mechanism of reaction of SO4·- with aromatic compounds. *Journal of the American Chemical Society, 99*(1), 163-164.

Pruden, A. (2014). Balancing Water Sustainability and Public Health Goals in the Face of Growing Concerns about Antibiotic Resistance. *Environmental Science & Technology, 48*(1), 5-14.

Prütz, W. A. (1984). Inhibition of DNA-ethidium bromide intercalation due to free radical attack upon DNA. *Radiation and Environmental Biophysics, 23*(1), 1-6.

Rastogi, R. P., Richa, Kumar, A., Tyagi, M. B., and Sinha, R. P. (2010). Molecular Mechanisms of Ultraviolet Radiation-Induced DNA Damage and Repair. *Journal of Nucleic Acids, 2010*

Rosado-Lausell, S. L., Wang, H., Gutiérrez, L., Romero-Maraccini, O. C., Niu, X.-Z., Gin, K. Y. H., Croué, J.-P., and Nguyen, T. H. (2013). Roles of singlet oxygen and triplet excited state of dissolved organic matter formed by different organic matters in bacteriophage MS2 inactivation. *Water Research, 47*(14), 4869-4879.

Shanehbandi, D., Saei, A. A., Zarredar, H., and Barzegari, A. (2013). Vibration and glycerol-mediated plasmid DNA transformation for Escherichia coli. *FEMS Microbiology Letters, 348*(1), 74-78.

Sinha, R. P., and Häder, D.-P. (2002). UV-induced DNA damage and repair: a review. *Photochemical & Photobiological Sciences, 1*(4), 225-236.

Song, K., Mohseni, M., and Taghipour, F. (2016). Application of ultraviolet light-emitting diodes (UV-LEDs) for water disinfection: A review. *Water Research, 94*, 341-349.

Sonntag, C. V. (2006). *Free-radical-induced DNA damage and its repair: A chemical perspective*: Springer Science & Business Media.

Sun, P., Tyree, C., and Huang, C.-H. (2016). Inactivation of Escherichia coli, Bacteriophage MS2, and Bacillus Spores under UV/H2O2 and UV/Peroxydisulfate Advanced Disinfection Conditions. *Environmental Science & Technology, 50*(8), 4448-4458.

Teebor, G. W., Boorstein, R. J., and Cadet, J. (1988). The Repairability of Oxidative Free Radical Mediated Damage to DNA: A Review. *International Journal of Radiation Biology, 54*(2), 131-150.

Vikesland, P. J., Pruden, A., Alvarez, P. J. J., Aga, D., Bürgmann, H., Li, X.-d., Manaia, C. M., Nambi, I., Wigginton, K., Zhang, T., and Zhu, Y.-G. (2017). Toward a Comprehensive Strategy to Mitigate Dissemination of Environmental Sources of Antibiotic Resistance. *Environmental Science & Technology, 51*(22), 13061-13069.

Wordofa, D. N., Walker, S. L., and Liu, H. (2017). Sulfate Radical-Induced Disinfection of Pathogenic Escherichia coli O157:H7 via Iron-Activated Persulfate. *Environmental Science & Technology Letters, 4*(4), 154-160.

Yang, Y., Pignatello, J. J., Ma, J., and Mitch, W. A. (2016). Effect of matrix components on UV/H2O2 and UV/S2O82− advanced oxidation processes for trace organic degradation in reverse osmosis brines from municipal wastewater reuse facilities. *Water Research, 89*, 192-200.

Yoon, Y., Chung, H. J., Wen Di, D. Y., Dodd, M. C., Hur, H.-G., and Lee, Y. (2017). Inactivation efficiency of plasmid-encoded antibiotic resistance genes during water treatment with chlorine, UV, and UV/H2O2. *Water Research, 123*, 783-793.

Yoon, Y., Dodd, M. C., and Lee, Y. (2018). Elimination of transforming activity and gene degradation during UV and UV/H2O2 treatment of plasmid-encoded antibiotic resistance genes. *Environmental Science: Water Research & Technology*

Zhang, R., Sun, P., Boyer, T. H., Zhao, L., and Huang, C.-H. (2015). Degradation of Pharmaceuticals and Metabolite in Synthetic Human Urine by UV, UV/H2O2, and UV/PDS. *Environmental Science & Technology, 49*(5), 3056-3066.

Zhang, Y., Gu, A. Z., He, M., Li, D., and Chen, J. (2017). Subinhibitory Concentrations of Disinfectants Promote the Horizontal Transfer of Multidrug

Resistance Genes within and across Genera. *Environmental Science & Technology, 51*(1), 570-580.

Zhang, Y., Li, A., Dai, T., Li, F., Xie, H., Chen, L., and Wen, D. (2018). Cell-free DNA: A Neglected Source for Antibiotic Resistance Genes Spreading from WWTPs. *Environmental Science & Technology, 52*(1), 248-257.

Zheng, J., Su, C., Zhou, J., Xu, L., Qian, Y., and Chen, H. (2017). Effects and mechanisms of ultraviolet, chlorination, and ozone disinfection on antibiotic resistance genes in secondary effluents of municipal wastewater treatment plants. *Chemical Engineering Journal, 317*, 309-316.

Zheng, X., Khan, M. T., and Croué, J.-P. (2014). Contribution of effluent organic matter (EfOM) to ultrafiltration (UF) membrane fouling: Isolation, characterization, and fouling effect of EfOM fractions. *Water Research, 65*, 414-424.

Chapter 6. Formation of Haloacetonitriles, Haloacetamides and Nitrogenous Heterocyclic By-products by Chloramination of Phenolic Compounds

Maolida Nihemaiti, Julien Le Roux, Christiane Hoppe-Jones, David A. Reckhow, Jean-Philippe Croué

Environmental Science and Technology, Volume 51(1), 12 December 2016, Pages 655-663

DOI: https://doi.org/10.1021/acs.est.6b04819

Statement of Contribution to Co-authored Published Paper

This Chapter includes the co-authored paper "Formation of haloacetonitriles, haloacetamides and nitrogenous heterocyclic by-products by chloramination of phenolic compounds", published on Environmental Science and Technology. The bibliographic details of the co-authored paper, including all authors are:

Nihemaiti, M., Le Roux, J., Hoppe-Jones, C., Reckhow, D. A., and Croué, J.-P. (2017). Formation of Haloacetonitriles, Haloacetamides, and Nitrogenous Heterocyclic Byproducts by Chloramination of Phenolic Compounds. Environmental Science & Technology, 51(1), 655-663.

I, Maolida Nihemaiti, as the primary author, conducted all the experimental work and data analysis, including creating figures and tables, and writing and editing the manuscript.

I, as a Co-Author, endorsed that this level of contribution by the candidate indicated above is appropriate.

Julien Le Roux

Christiane Hoppe-Jones

David A. Reckhow

Jean-Philippe Croué

6.1 Abstract

The potential formation of nitrogenous disinfection by-products (N-DBPs) was investigated from the chloramination of nitrogenous and non-nitrogenous aromatic compounds. All molecules led to the formation of known N-DBPs (e.g., dichloroacetonitrile, dichloroacetamide) with various production yields. Resorcinol, a major precursor of chloroform, also formed di-/tri-chloroacetonitrile, di-/tri-chloroacetamide, and haloacetic acids, indicating that it is a precursor of both N-DBPs and carbonaceous DBPs (C-DBPs) upon chloramination. More detailed experiments were conducted on resorcinol to understand N-DBPs formation mechanisms and to identify reaction intermediates. Based on the accurate mass from high resolution Quadrupole Time-of-Flight GC-MS (GC-QTOF) and fragmentation patterns from electronic impact and positive chemical ionization modes, several products were tentatively identified as nitrogenous heterocyclic compounds (e.g., 3-chloro-5-hydroxy-1H-pyrrole-2-one with dichloromethyl group, 3-chloro-2,5-pyrroledione). These products were structurally similar to the heterocyclic compounds formed during chlorination, such as the highly mutagenic MX (3-chloro-4-(dichloromethyl)-5-hydroxy-2(5H)-furanone) or halogenated pyrroles. To our knowledge, this is the first time that the formation of halogenated nitrogenous heterocyclic compounds is reported from chloramination process. The formation of these nitrogenous by-products during chloramination might be of concern considering their potential toxicity.

6.2 Introduction

As an alternative to chlorine, monochloramine (NH_2Cl) is often used as a secondary disinfectant to obtain a more stable residual in distribution systems (Seidel et al., 2005). Chloramines generally form less trihalomethanes (THMs), haloacetic acids (HAAs), and total organic halogen (TOX) than free chlorine. However, the percentage of unknown TOX produced from chloramines is higher than that from free chlorine (Hua and Reckhow, 2007).

During chloramination, NH_2Cl can be an additional source of nitrogen and produce halogenated nitrogenous disinfection by-products (N-DBPs). N-DBPs, including haloacetonitriles (HANs) and haloacetamides (HAcAms), generally form in lower amounts than regulated DBPs (i.e., THMs and HAAs). It has been proposed that the mass of HANs represents around 10% of the THMs (Oliver, 1983; Krasner et al., 1989), whereas HAcAms formation was reported to be approximately 10 times lower than HAAs (Krasner et al., 2006). Regardless of their relatively low occurrence, HANs and HAcAms have been a growing health risk concern over the past decades because of their high toxicity (Plewa et al., 2004; Muellner et al., 2007).

Nitrogen-containing organic compounds (e.g., amino acids, pyrroles, and pyrimidines) are ubiquitous in surface water (Westerhoff and Mash, 2002) and have been associated with the formation of N-DBPs (Bond et al., 2011). Wastewater effluents and algal organic matter, which are enriched in organic nitrogen, enhance N-DBPs formation during drinking water treatment process (Dotson et al., 2009). It was recently reported that antibiotic chloramphenicols may contribute to the formation of HAcAms in heavily wastewater-impacted waters (W. Chu, Krasner, et al., 2016).

Most of the previous studies exploring the sources of nitrogen in N-DBPs focused on chloramination of nitrogenous model compounds (e.g., amino acids) or matrices enriched in nitrogenous moieties (e.g., algal organic matter) by the application of isotopically labeled monochloramine (i.e., $^{15}NH_2Cl$). Inorganic nitrogen incorporation into dichloroacetonitrile (DCAN) and dichloroacetamide (DCAcAm) has been reported during chloramination of wastewater effluents, algal extracellular organic matter, humic substances, and free amino acids (i.e., aspartic acid and asparagine) (Huang et al., 2012). ^{15}N-DCAN percentages in total DCAN were found to be 78%

and 92% by chloramination of tryptophan and Suwannee River NOM, respectively (X. Yang et al., 2010). More than 70% of DCAN originated from monochloramine during chloramination of NOM isolates (Huang et al., 2012), indicating that high amounts of inorganic nitrogen (i.e., monochloramine) can be incorporated into organic structure.

Only few studies are available on N-DBPs formation from non-nitrogenous precursors. Formaldehyde reacts with NH_2Cl to form cyanogen chloride (Pedersen et al., 1999). Chloroacetonitrile and N,2-dichloroacetamide formation was found from chloramination of chloroacetaldehyde (Kimura et al., 2013). Recent studies on chloramination of lignin phenols and low-molecular weight organic acids have reported the formation of DCAN, DCAcAm and trichloroacetamide (TCAcAm) through chloramine-nitrogen incorporation (Hua et al., 2014; Chuang et al., 2015; W. Chu, Li, et al., 2016).

Previous studies indicated that non-nitrogenous precursors can produce N-DBPs via inorganic nitrogen incorporation. However limited information is available on the nature of these N-DBPs precursors as well as the chloramine-nitrogen incorporation mechanism. Recent results showed that organic matter isolates enriched in aromatic moieties (i.e., high SUVA value) produced more N-DBPs by chloramine-nitrogen incorporation as compared to low-aromatic-content organic matter (Le Roux et al., 2016). In addition, chloramination of aromatic model compounds (i.e., phenol and resorcinol) formed more DCAN and DCAcAm than amino acids (e.g., tyrosine, aspartic acid), which were previously considered as important precursors of N-DBPs.

Meta-dihydroxybenzene structures were proposed as main reactive sites of NOM for the formation of THMs upon chlorination (Rook, 1977; Norwood et al., 1980). 1,3-hydroxybenzene (resorcinol) has been extensively studied as a model compound and is a major precursor of chloroform (TCM) during chlorination (Norwood et al., 1980; Rook, 1980; Boyce and Hornig, 1983). The reaction of resorcinol with monochloramine follows a similar mechanism to chlorination, involving aromatic ring-substitution, oxidation, hydrolysis, and decarboxylation reactions (Heasley et al., 1999). However, the reactions involving the formation of N-DBPs from resorcinol by incorporation of nitrogen from monochloramine have not been investigated yet.

The objective of this study was to investigate the formation of HANs and HAcAms from chloramination of resorcinol in comparison with TCM and HAAs formation and to elucidate their formation mechanisms through the identification of intermediate products. Effects of monochloramine dose, reaction time, and pH on by-products formation were examined. GC-MS/MS and high resolution GC-QTOF full scan analysis were conducted for the identification of unknown products.

6.3 Materials and Methods

6.3.1 Chemical reagents

All chemicals were of analytical grade or higher and were used as received without further purification. Milli-Q water (18.2 MΩ.cm, Millipore) was used for all experiments. Resorcinol (≥ 99.0%) and other model compounds were purchased from Sigma-Aldrich (Table A-4-1). Sodium hypochlorite (5.65-6%, Fisher Scientific) and ammonium chloride (99.6%, Acros Organics) were used for monochloramine preparation. ^{15}N-labeled ammonium chloride was obtained from Sigma-Aldrich (98%). Sodium thiosulfate (Fisher Scientific) was applied to quench residual oxidant. A trihalomethanes (THM) calibration mix, a mixed standard (EPA 551B Halogenated Volatiles Mix) containing haloacetonitriles (HANs), and a mixed standard (EPA 552.2 Methyl Ester Calibration Mix) containing 9 haloacetic acids (HAAs) were supplied from Supelco (Sigma-Aldrich). Chloro-, dichloro- and trichloroacetamide were obtained from Sigma-Aldrich. Decafluorobiphenyl (99%, Sigma-Aldrich, Supelco) was used as a surrogate standard. 2-bromopropionic acid (Fluka Analytical) was used as a surrogate for HAAs extraction and analysis. Fisher Scientific Methyl tert-butyl ether (MTBE) and ethyl acetate (> 99%) were used for DBP extractions.

6.3.2 Experimental procedures

Experiments were conducted at room temperature (22 ± 1 ^{o}C) in headspace-free amber glass bottles (individual bottle per contact time). Preformed monochloramine and ^{15}N-labeled monochloramine stock solutions were daily prepared by dissolving ammonium chloride or ^{15}N-labeled ammonium chloride, respectively, in Milli-Q water adjusted to pH 8.5 with sodium hydroxide. Sodium hypochlorite was then slowly added to the rapidly stirred solution (N:Cl molar ratio of 1.2:1). Initial NH_2Cl and $NHCl_2$ concentrations were spectrophotometrically measured at 245 and 295 nm (Schreiber and Mitch, 2005). Predetermined volumes of monochloramine and each model

compound stock solution were injected into 65 mL of 10 mM acetate (pH = 4.0-5.5), phosphate (pH = 7.0-8.0) or carbonate (pH = 10) buffer to get the desired initial concentrations (monochloramine:model compound molar ratio of 5.6 or 11.2). The concentration of residual oxidant was iodometrically determined (APHA., 1995). Residual monochloramine was quenched with a slight excess of sodium thiosulfate. Samples were extracted immediately after quenching to avoid any loss of by-products.

6.3.3 GC-MS and GC-QTOF-MS/MS analysis

TCM and two HANs (dichloroacetonitrile, trichloroacetonitrile) were analysed after liquid-liquid extraction following EPA Method 551. Three HAcAms (chloroacetamide, dichloroacetamide, trichloroacetamide) were analysed following the same protocol that was applied for HANs; however, the extraction solvent MTBE was replaced by ethyl acetate since it was shown to improve the recovery of HAcAms (W. H. Chu and Gao, 2009). HAAs were extracted and analysed following the EPA Method 552.2, which is based on a liquid-liquid extraction with MTBE in acidic condition followed by derivatization to methyl esters using acidic methanol. All DBPs were quantified using a gas chromatograph (Agilent 7890A) coupled with a mass spectrometer (Agilent 5975C, GC-MSD). Since ^{15}N-labeled DBPs are not commercially available, their concentrations were determined using ^{14}N-DBPs standards, based on the assumption that ^{15}N-DBPs and ^{14}N-DBPs have a similar MS response (Huang et al., 2012). DBPs were separated on a DB-1701 (30m × 250 µm × 0.25 µm) capillary column.

In order to identify unknown by-products, full scan analysis in electronic impact (EI) and positive chemical ionization (PCI, using methane as reagent gas) modes were performed on MTBE extracts at various reaction times. Two different GC-MS systems were used for full scan analysis: an Agilent 5975C GC-MSD, and an Agilent 7200 Accurate-Mass Quadrupole Time-of-Flight (GC-QTOF). MS/MS analysis at three different collision energies (i.e., 20 eV, 40 eV and 60 eV) were performed on GC-QTOF for all main peaks detected. Agilent MassHunter Qualitative analysis B.07.00 was used for deconvolution of data from GC-QTOF. The mass spectral similarity search was performed by using NIST MS Search 2.0 (NIST/EPA/NIH Mass Spectral Library, NIST 08, National Institute of Standards and Technology, 2008, Gaithersburg, MD, USA). The column used for GC-MSD was a DB-1701 (30 m × 250 µm × 0.25

µm) or a ZB-5MS (30 m × 250 µm × 1 µm). GC separation on GC-QTOF was performed with a DB-5MS UI column (30 m × 0.25 mm × 0.25 µm).

Details on quantification of DBPs and full scan analysis of unknown by-products are provided in Text A-4-1.

6.4 Results and Discussion

6.4.1 N-DBPs formation from model aromatic compounds

Preliminary experiments were conducted at pH 7 (10 mM phosphate buffer) for 72 h to investigate the formation potential of DCAN and DCAcAm from several aromatic compounds (250 µM) during chloramination (1.4 mM). $^{15}NH_2Cl$ was applied to nitrogenous model compounds and $^{14}NH_2Cl$ to others. N-DBPs formation was observed from both nitrogenous and non-nitrogenous compounds (Table 6-1). In the case of nitrogenous compounds (aniline and amino acids), more than 50% of DCAN and DCAcAm incorporated ^{15}N originating from $^{15}NH_2Cl$. Model compounds (i.e., resorcinol, phenol, aniline, and 3-hydroxybenzoic acid), including an aromatic ring activated by electron donating groups (i.e., –OH and $–NH_2$) in their structure, were the most important precursors of DCAN and DCAcAm. Despite their similar structures, tyrosine formed more DCAN and DCAcAm (i.e., 0.50% and 0.10% molar yield, respectively) than phenylalanine (i.e., 0.12% and 0.05%, respectively). The activation of the aromatic ring by the hydroxyl group in the case of tyrosine favours chlorine electrophilic substitution leading to N-DBPs formation via ring-cleavage reaction (Hureiki et al., 1994). Phenol produced the highest proportion of DCAN (4.44%) and resorcinol produced the highest proportion of DCAcAm (0.83%). Resorcinol is more reactive than phenol because of its additional hydroxyl group in meta position, resulting in chlorine substitutions in ortho and para positions of hydroxyl groups. Interestingly, TCM was the highest DBP produced from resorcinol, while DCAN was the dominant species from phenol (molar yield of TCM: 4.8% for resorcinol; 0.4% for phenol), suggesting different DBPs formation pathways from these two precursors. In this study, resorcinol was selected to explore N-DBPs formation mechanisms, since it produced DCAN and DCAcAm in relatively high concentrations.

Table 6-1.N-DBP yields from model aromatic compounds during chloramination[a]

	Molar yield (%) (SD)[b]		^{15}N-DBP proportion (%)	
	DCAN	DCAcAm	^{15}N-DCAN	^{15}N-DCAcAm
	Non-nitrogenous compounds			
Resorcinol	1.14(0.08)[c]	0.83(0.04)[c]	NA	NA
Phenol	4.44(0.29)[c]	0.22(0.01)[c]	NA	NA
3-Hydroxybenzoic acid	1.00(0.07)	0.22(0.01)	NA	NA
Benzoic acid	0.17(0.01)	0.09(0.01)	NA	NA
3-Phenylpropionic acid	0.10(0.01)	0.04(0.01)	NA	NA
	Nitrogenous compounds			
Aniline	1.73(0.11)	0.12(0.01)	85	74
Tyrosine	0.50(0.03)[c]	0.10(0.01)[c]	83	70
Phenylalanine	0.12(0.01)	0.05(0.01)	83	56

[a]Chloramination conditions: [model compound] = 250 µM; [NH_2Cl] = 1.4 mM; pH = 7.0 in 10 mM phosphate buffer; contact time 72 h. NA: not applicable. [b]SD = Standard Deviation on 3 replicates. [c]Previously published data (Le Roux et al., 2016).

6.4.2 Effect of monochloramine dose

Experiments were performed with resorcinol (500 µM) for 72 h using different NH_2Cl: resorcinol ratios (i.e., 1:1, 5:1 and 11.2:1) at pH 7 (10 mM phosphate buffer). TCM was the dominant DBP identified for all ratios (i.e., 0.3%, 11% and 20% yield), followed by DCAA (i.e., 0.1%, 3% and 7%) (Figure A-4-1). As hypothesized, the concentration of DBPs increased with increasing monochloramine dose, since the application of higher oxidant doses facilitates the production of smaller and more halogenated by-products (Boyce and Hornig, 1983). The increase in DCAN and DCAcAm concentrations were proportionally higher than those in TCM and DCAA. The highest dose (i.e., 11.2:1 ratio) was selected in the following experiments since it maximized DBP formation.

Previous studies on chloramination of resorcinol and its chlorinated derivatives have been conducted in ether solution (~0.3 M) with NH_2Cl:model compound ratio of 3:1 (Heasley et al., 1999). In these conditions, chloroketones were the major by-products identified (compound II and III in Scheme 1), and the formation of nitrogenous compounds was not reported, which could be due to the lower chloramine dose employed as compared to this study.

6.4.3 Effect of reaction time

Kinetic experiments were performed with 500 µM resorcinol at pH 7 (10 mM phosphate buffer). Initial NH_2Cl was 5.6 mM (NH_2Cl: resorcinol ratio of 11.2:1) and the total oxidant concentration remained in excess during all the reaction time (Figure A-4-2). Figure 6-1 illustrates the kinetic profiles of DBPs formation. TCM was the major DBP found (20% yield after 72 h), followed by DCAA (7.2%). MCAA and DCAA were rapidly formed during the first 9 h, suggesting that they might form directly from ring-cleavage. DCAN followed the same profile as TCM and reached 6.1% yield after 72 h. DCAcAm and TCAcAm formation was slow within the first 4 h and then gradually increased, reaching 3.3% and 1.4% yield after 72 h, respectively. Unlike DCAA and MCAA, TCAA slowly increased with time and its profile was very similar to that of TCAcAm. Low amounts of trichloroacetaldehyde (TCAcAl) (0.14% at 72 h), dichloroacetaldehyde (DCAcAl) (0.08%) and TCAN (0.02%) were detected.

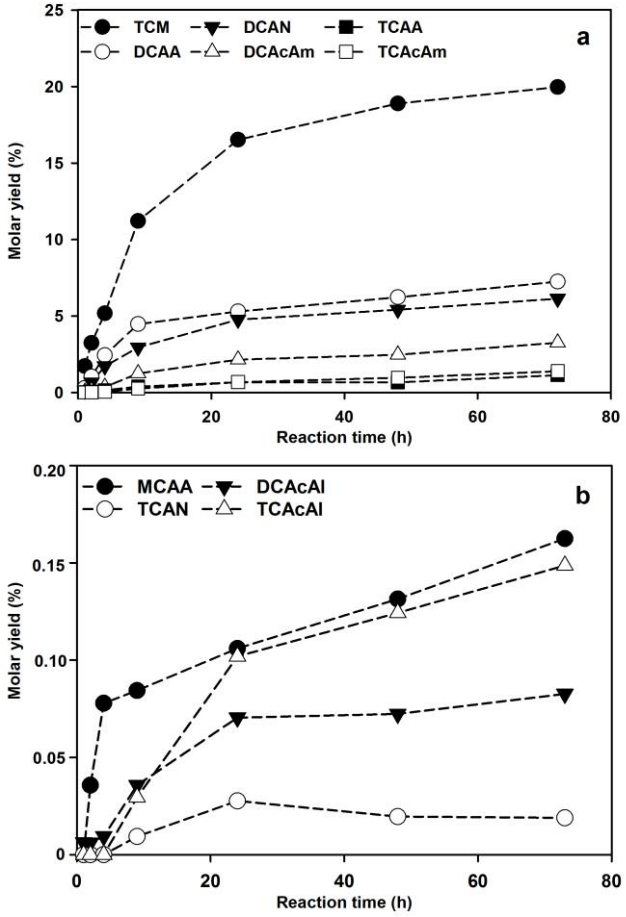

Figure 6-1.Kinetics of DBPs formation from chloramination of resorcinol. Resorcinol= 500 µM; NH_2Cl = 5.6 mM; pH=7.0 (10 mM phosphate buffer)

6.4.4 Effect of pH

Formation potential of DBPs from resorcinol upon 72 h of chloramination was evaluated at different pH values (Figure 6-2). Dichlorinated DBPs (i.e., DCAA, DCAN and DCAcAm) exhibited a maximum formation at pH 8, while the highest formation of trichlorinated DBPs (i.e., TCAA and TCAcAm) was found at pH 7. Taking into account the analytical error recorded at pH 5.5 (standard deviation: 3.5% of molar yield), the TCM yields obtained at pH 5.5 and pH 7 should be considered as relatively similar. Generally, the concentration of TCM increases with increasing pH during chlorination of natural water due to base-catalyzed reaction (Hua and Reckhow, 2008). In contrast to this, the TCM yields from chloramination of resorcinol gradually decreased as pH increased from pH 7. Our result is consistent with previous observations, where the formation of TCM from chloramination of resorcinol also decreased with increasing pH (pH 6.5-12) under similar experimental conditions (Cimetiere et al., 2010). It was proposed that the free chlorine released from NH_2Cl

hydrolysis plays a significant role on TCM formation during chloramination of resorcinol (Cimetiere et al., 2010). In the organic-free solution of monochloramine, the concentration of free chlorine is the lowest around pH 8.4 and increases with increasing of pH (Cimetiere et al., 2010). However, the free chlorine species shift from HOCl to OCl^- as pH increases. TCM was also demonstrated to form in significantly lower amounts during chlorination of resorcinol in alkaline conditions (pH > 10) (Boyce and Hornig, 1983), most likely due to the less reactivity of OCl^- with intermediate precursors of chloroform. Therefore, the pH-dependency of TCM yield might be related to the free chlorine from the hydrolysis of monochloramine, as well as the distribution of free chlorine species with pH. Most DBPs exhibited a substantially lower formation at pH 10, suggesting that an alternative degradation pathway of resorcinol may exist. Reduction of N-DBPs from pH 8 to pH 10 was possibly related to their base catalysed hydrolysis as well (Reckhow et al., 2001; Yu and Reckhow, 2015). No resorcinol or chlorinated analogues were detected in samples at pH 7, 8 and 10, indicating that they completely decomposed to intermediates or final by-products after 72 h, but large peaks of mono-, di- and tri-chlororesorcinol were still detected from GC-MS full scan after 72 h at pH 4 (Figure A-4-3). This might explain the low non-aromatic DBP formation at pH 4, as the reaction did not lead to significant ring-opening of resorcinol.

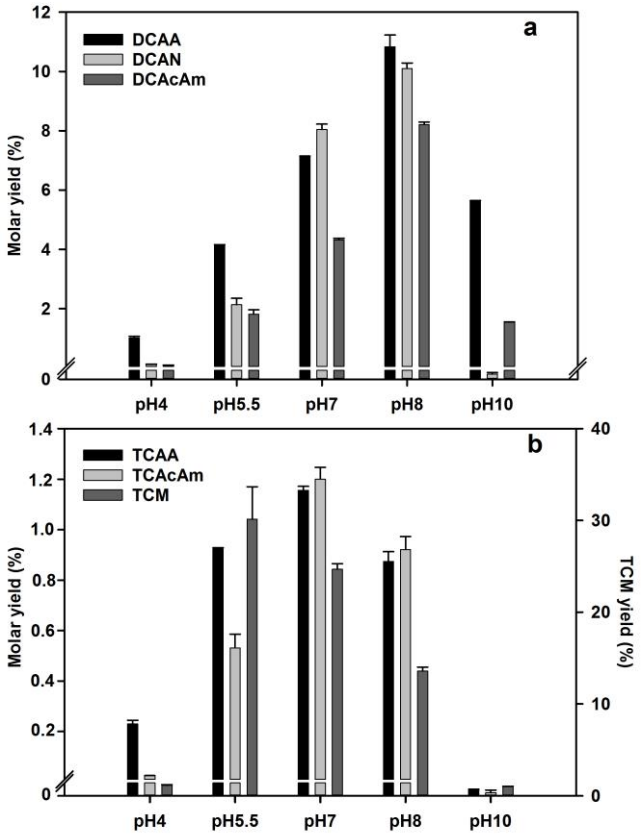

Figure 6-2. Effect of pH on DBPs formation from chloramination of resorcinol. Resorcinol= 500 µM; NH_2Cl = 5.6 mM; 72 h; Error bars represent standard deviation (n=2)

6.4.5 Identification of nitrogenous heterocyclic compounds

Resorcinol (500 µM) was chloraminated (5.6 mM NH_2Cl) at pH 7 to investigate its decomposition mechanism and to identify the intermediate products that could lead to the formation of N-DBPs (e.g., DCAcAm). Several peaks were observed in the PCI chromatogram recorded on the GC-QTOF such as DCAN (retention time (RT) =3.7 min), DCAcAm (RT = 7.5 min), TCAcAm (RT = 8.6 min), and other unknown compounds (P131 at RT = 8.5 min, P197 at RT= 10.6 min, P215 at RT = 11.0 min and P249 at RT = 11.5 min) (Figure A-4-4). P215 and P249 were two major compounds exhibiting larger peak areas than known DBPs (i.e., DCAN, DCAcAm and TCAcAm). Molecular formulas and structures of these compounds were proposed based on their accurate mass obtained from GC-QTOF and fragmentation patterns observed in EI and PCI modes (Table 6-2).

Table 6-2. Chloramination by-products of resorcinol detected by GC-QTOF

Compound	Exact Mass	Accurate Mass	Error (ppm)	Molecular Formula	Proposed Structures
P215	215.9380 $[M+H]^+$	215.9379 $[M+H]^+$	0.64	$C_5H_4NO_2Cl_3$	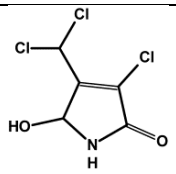 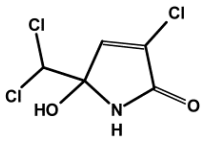
P249	249.8990 $[M+H]^+$	249.8988 $[M+H]^+$	1.06	$C_5H_3NO_2Cl_4$	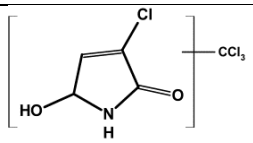 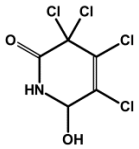
P131	131.9845 $[M+H]^+$	131.9847 $[M+H]^+$	-0.13	$C_4H_2NO_2Cl$	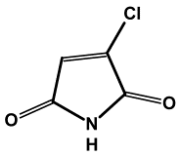
P197[a]	197.9270 $[M+H]^+$	197.9262 $[M+H]^+$	6.43	$C_5H_2NOCl_3$	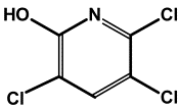
P179[b]	178.9540	N.D	N.D	$C_5H_3NO_2Cl_2$	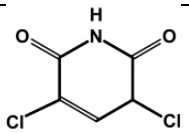 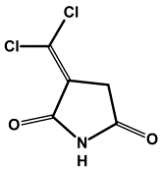

P198[c]	197.9042	197.9252	-106.05	$C_5HO_2Cl_3$	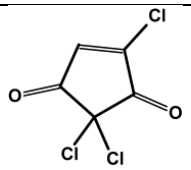

[a]Confirmed by NIST database (94% similarity).
[b]Detected by GC-MSD; also reported in a previous study (Haddon et al., 1996); N.D: not detected by GC-QTOF.
[c]Confirmed by NIST database (95% similarity); also reported in previous studies (Norwood et al., 1980; Boyce and Hornig, 1983).

The EI mass spectrum of P215 exhibited two dominant ion clusters (m/z 132/134 and 114/116) comprising one chlorine atom, with a difference of 18 Da corresponding to the loss of one water molecule (i.e., dehydroxylation) (Figure A-4-5a). The corresponding PCI mass spectrum contained a major ion cluster m/z 216/218/220/222 (i.e., $[M+H]^+$) with relative abundance, suggesting that this compound had three chlorine atoms (Figure A-4-5b). The odd-numbered nominal mass (i.e., 215 Da) indicated an odd-number of nitrogen atoms. Loss of 83 along with two chlorine was observed from m/z 215 to m/z 132, indicating the loss of a ($–CHCl_2$) group. The PCI mass spectrum obtained from GC-QTOF showed an accurate mass of 215.9379 for $[M+H]^+$. Accordingly, $C_5H_4NO_2Cl_3$ was confirmed to be the molecular formula of this compound (0.64 ppm). Based on the fragmentation pattern and accurate mass of fragments obtained from EI and PCI modes (Table A-4-2), the proposed molecular structure of this compound is 3-chloro-5-hydroxy-1H-pyrrole-2-one with dichloromethyl group. It is structurally very similar to MX (3-chloro-4-(dichloromethyl)-5-hydroxy-2(5H)-furanone), the strong mutagen found from chlorinated drinking water and humic water.(Hemming et al., 1986; Kronberg and Vartiaine, 1988) Additionally, the corresponding methyl ester form of P215 was also detected after derivatization of the MTBE extract using acidic methanol, with a molecular formula of $C_6H_6NO_2Cl_3$ (9.52ppm). The corresponding EI and PCI mass spectra presented a loss of 31 Da ($–OCH_3$ group) from m/z 229 to m/z 198 (Text A-4-2).

A similar method was used for the identification of other compounds. P249 exhibited a similar EI mass spectrum to P215, with dominant ion clusters m/z 132/134 and 114/116. However, its PCI mass spectrum showed a main molecular ion (i.e., $[M+H]^+$)

at m/z 250 including four chlorine atoms. Therefore, we proposed P249 as an analogue of P215 with an additional chlorine atom or as 6-hydroxy-2-pyridone with four chlorine atoms (Text A-4-3).

The EI mass spectrum of P131 contained ion clusters m/z 131/133, 103/105 and 88/90, which was similar to the mass spectrum of 3-chloro-2,5-furandione present in the NIST database. However the molecular ion m/z 132 (i.e., a nominal mass of 131 Da) obtained from PCI mass spectrum suggested the presence of a nitrogen atom. The accurate mass of ion m/z 131.9847 (i.e., $[M+H]^+$ adduct) supported a molecular formula of $C_4H_2NO_2Cl$ (-0.13 ppm). Accordingly, P131 was tentatively identified as 3-chloro-2,5-pyrroledione (chloromaleimide) (Text A-4-4).

Product P197 was confirmed as 2-hydroxy-3,5,6-trichloropyridine because a library match of its spectrum was obtained from NIST database (94% similarity) and the corresponding formula ($C_5H_2NOCl_3$) was derived from its accurate mass (Figure A-4-6).

Product P179 was proposed as another pyridine-based compound (i.e., dichloro-pyridine-dione) or its isomer, chloro-pyrrole-dione with dichloromethylene group. The formation of the latter was reported during chlorination of poultry chiller water.(Haddon et al., 1996) P179 was only detected from GC-MSD (DB-1701 column) (Figure A-4-7), but was not found by high resolution analysis on GC-QTOF. 2,2,4-trichloro-1,3-cyclopentenedione (P198) and its isomer were detected (95% similarity with NIST database) from the MTBE extract after derivatization using acidic methanol (RT= 9.7 min) (Figure A-4-8). The formation of 2,2,4-trichloro-1,3-cyclopentenedione has been reported as a chlorination by-product of resorcinol.(Norwood et al., 1980; Boyce and Hornig, 1983)

Because of the lack of analytical standards, the proposed structures of P215, P249, P131 and P179 could not be confirmed. However, the formation of halogenated heterocyclic compounds (e.g., halogenated furanones and pyrroles), which are structurally similar to the compounds found from this study, has been reported in several chlorination studies (Table A-4-3). The most known halogenated furanone formed by chlorination of drinking water is the highly mutagenic MX and its analogues (Hemming et al., 1986; Meier et al., 1986; Kronberg and Vartiaine, 1988). In a

previous study on chlorination of phenolic compounds, resorcinol was found to produce MX, but in low concentration at acidic pH (i.e., 0.01 mmol/mol, pH 2) (Långvik et al., 1991). Several compounds similar to MX were identified from chlorination of orcinol (Tretyakova et al., 1994). Moreover, it was found that MX can be produced during chloramination of humic water (Backlund et al., 1988) and fulvic acid solution (Kanniganti et al., 1992). Dichloromaleic anhydride (3,4-dichloro-2,5-furandione) and monochloromaleic anhydride (3-chloro-2,5-furandione), which are structurally similar to the chlorinated pyrroledione found from this study (i.e., P131), are major chlorination by-products of resorcinol (Rook, 1980) or swimming pool waters (Richardson et al., 2010). Similarly, 3-bromo-2,5-furandione was reported from bromination of resorcinol (Boyce and Hornig, 1983). Dichlorinated analogue of P131, 3,4-dichloro-2,5-pyrroledione, was detected with three other chlorinated cyclic imides in chlorinated poultry chiller water (Haddon et al., 1996). These five-carbon chlorinated cyclic imides were structurally similar to P215 and found to be direct acting Ames mutagens (Haddon et al., 1996; Freeman et al., 2001). Moreover, the presence of brominated pyrroles was reported from chlorinated saline wastewater effluents (M. Yang and Zhang, 2014). Tribromopyrrole is a major chlorination by-product of bromide-containing waters and has been demonstrated to be strongly cytotoxic and genotoxic to mammalian cells (Richardson et al., 2003).

Based on the potential toxicity of halogenated furanone, cyclic imide and pyrrole compounds (Hemming et al., 1986; Kronberg and Vartiaine, 1988; Haddon et al., 1996; Freeman et al., 2001; Richardson et al., 2003), the halogenated nitrogenous heterocyclic compounds identified from this study could be also strong mutagenic products and would require toxicity assays.

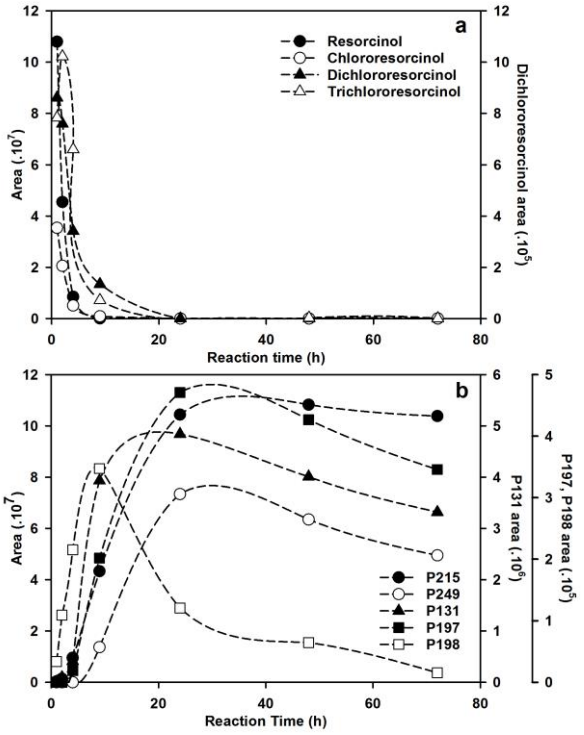

Figure 6-3. (a) Degradation of resorcinol and its chlorinated derivatives and (b) formation of by-products during chloramination (5.6 mM) of resorcinol (500 µM) at pH=7.0 (10 mM phosphate buffer)

6.4.6 Effect of reaction time and pH on heterocyclic compounds formation

Figure 6-3 shows the evolution of peak areas of chlorinated derivatives of resorcinol and identified by-products with reaction time. Mono-, di-and tri-chlorinated derivatives of resorcinol were detected after 1 h of reaction time, indicating a fast electrophilic substitution of the aromatic ring by chlorine. The majority of resorcinol and its chlorinated derivatives (> 90%) decomposed within the first 9 h of reaction (Figure 6-3a). It has been proposed that chlorination and chloramination of aqueous solutions of resorcinol lead to the formation of a pentachlororesorcinol intermediate (compound I in Scheme 1), which then undergoes hydrolysis and decarboxylation to produce chloroform and other chlorinated compounds (Rook, 1980; Boyce and Hornig, 1983; De Leer and Erkelens, 1985; Heasley et al., 1999). The nitrogenous heterocyclic compounds found in this study exhibited the largest peak areas on GC-MS chromatograms, suggesting that inorganic nitrogen incorporation is a major reaction pathway during chloramination of resorcinol. A chloramination mechanism of resorcinol is proposed on Figure 6-4, where the carbonyl group of the pentachlororesorcinol intermediate is attacked by electron pairs of nitrogen atom from NH_2Cl or oxygen atom from H_2O. The ring-cleavage by-product from nitrogen attack

then undergoes intramolecular nucleophilic substitution to form a nitrogenous heterocyclic compound and finally P249 (Figure 6-4a). A similar ring contraction mechanism is proposed for the formation of 2,2,4-trichloro-1,3-cyclopentenedione (i.e., P198), based on its formation pathway previously proposed during chlorination of resorcinol (Rook, 1980; Tretyakova et al., 1994) (Scheme 1b). P198 was formed rapidly from 1 h to 9 h and gradually degraded (Figure 6-3b). We propose that in excess of NH_2Cl, P198 will be an intermediate product of nitrogenous heterocyclic compounds (i.e., P131, P215 and P249) through nitrogen attack and intramolecular nucleophilic substitution. As shown in Figure 6-3b, P131 and P249 started to degrade after 24 h of reaction time. These compounds comprise a Cl-C-CO-NH- moiety, which could be responsible for HAcAms and haloacetaldehydes (HAcAls) formation with an excess of oxidant (Figure 6-4).

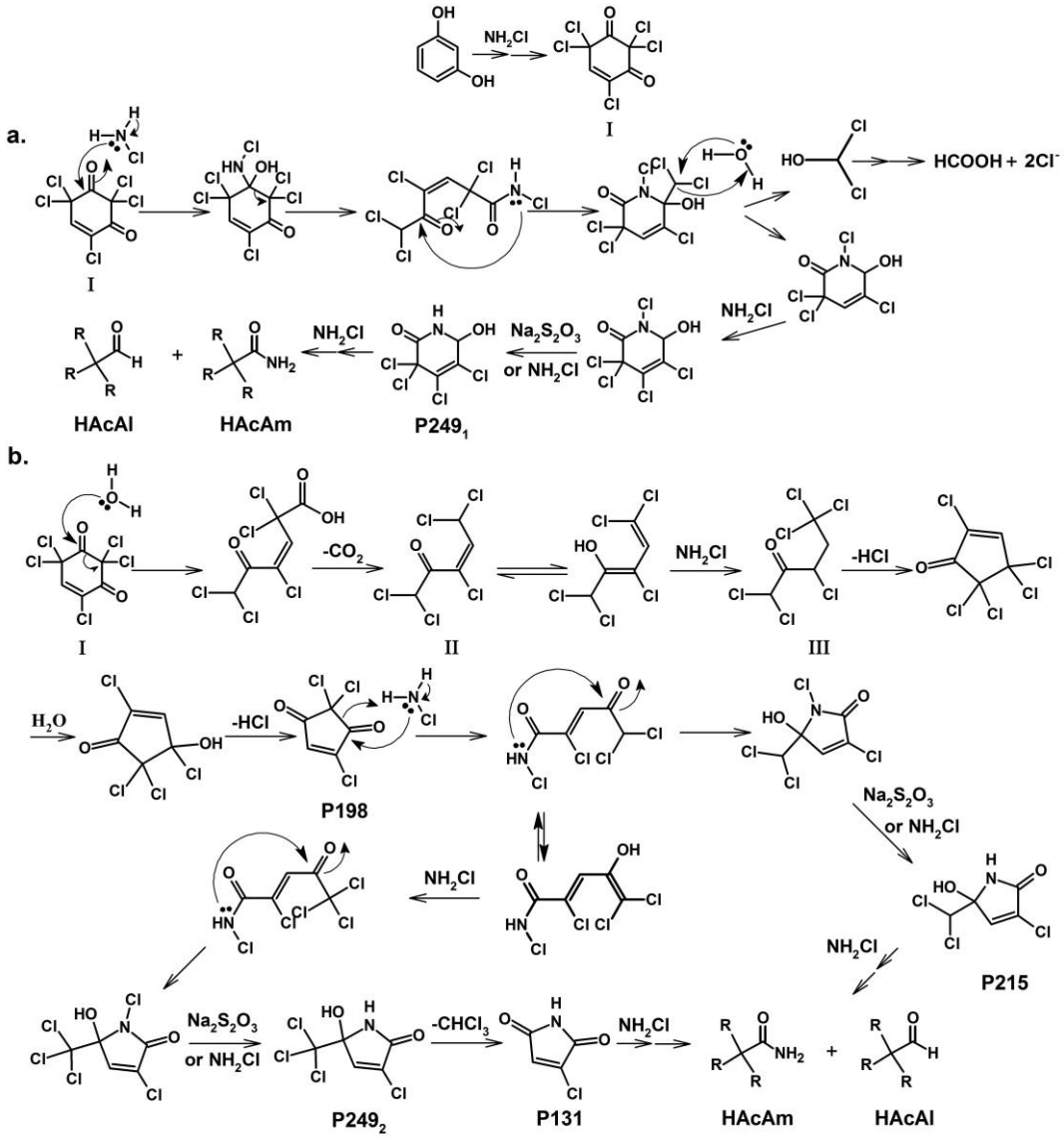

Figure 6-4. Proposed formation pathway of by-products from chloramination of resorcinol (I: pentachlororesorcinol; II, III: compounds identified in a previous study (Heasley et al., 1999). b: adapted from previous studies (Rook, 1980; Tretyakova et al., 1994. P215, P249$_{1,2}$: possible structures for P215, P249. R: Cl or H).

Figure A-4-9 presents the peak area of P131, P197, P198 and P215 after 72 h of reaction time at different pHs. The highest formation was found in neutral (pH 7 for P197 and P215) or weak acidic (pH 5.5 for P131 and P198) condition. Low formation of these compounds at pH 4 is in accordance with the higher formation of chlorinated derivatives of resorcinol (Figure A-4-3), supporting the hypothesis that the reaction at pH 4 did not lead to significant ring-opening of resorcinol. Little or no nitrogenous heterocyclic compounds were detected in alkaline conditions (pH 8.5 and 10), suggesting that they might decompose at higher pH to form other by-products. To

support our hypothesis, MX mainly undergoes hydrolytic degradation at pH higher than 8 (Kronberg and Christman, 1989).

6.5 Environmental significance

High concentrations of model compounds and high monochloramine doses were used in this study to maximize the formation of by-products and thus facilitate their detection and identification by GC-MS in full scan mode. The possible reasons why the products identified in this study (i.e., chlorinated nitrogenous heterocyclic compounds) have not yet been observed during the chloramination of real water samples, include: (1) many studies about the identification of unknown DBPs were mainly focused on chlorination process, and less on chloramination; (2) the amounts of by-products formed in real case disinfection scenarios (i.e., low precursors concentration and low monochloramine doses) were not sufficient to be detected during analytical screenings. From another study we detected a compound likely to be dibromo-pyrrole-dione (molecular ion m/z 253), similar base structure to P131, during chloramination (14.9 mg/L Cl_2) of a treated wastewater effluent (5 mg/L DOC) containing 2.5 mg/L of bromide ion. It exhibited a similar mass spectrum to dibromo-furan-dione (m/z 254). The accurate mass obtained from GC-QTOF (m/z 252.8408) supports the molecular formula of $C_4HNO_2Br_2$ (11 ppm) (Figure A-4-10). The occurrence of brominated pyrroledione indicated that this class of compounds can be formed during real chloramination scenarios. Similar screening of chlorinated or brominated pyrroledione compounds should be performed during chloramination of natural waters or NOM in order to confirm their formation from other organic matrices.

Aromatic compounds that do not contain nitrogen can react with monochloramine to produce N-DBPs through inorganic nitrogen incorporation. The potential formation of nitrogenous heterocyclic compounds is of importance for water treatment facilities using chloramine as disinfectant since they could be substantially toxic due to their similarity to known mutagenic compounds (e.g., MX). The removal of aromatic NOM must be optimized to avoid the production of these potentially toxic N-DBPs.

6.6 Acknowledgments

We acknowledge the financial support from Water Research Australia and Water Corporation of Western Australia (WaterRA Postgraduate Scholarship).

6.7 Reference

APHA. (1995). *Standard Methods for the Examination of Water and Wastewater* (19 ed.). Washington, DC: APHA.

Backlund, P., Kronberg, L., and Tikkanen, L. (1988). Formation of AMES mutagenicity and of the strong bacterial mutagen 3-chloro-4-(dichloromethyl)-5-hydroxy-2(5H)-furanone and other halogenated compounds during disinfection of humic water. *Chemosphere*, *17*(7), 1329-1336.

Bond, T., Huang, J., Templeton, M. R., and Graham, N. (2011). Occurrence and control of nitrogenous disinfection by-products in drinking water - A review. *Water Research, 45*(15), 4341-4354.

Boyce, S. D., and Hornig, J. F. (1983). Reaction pathways of trihalomethane formation from the halogenation of dihydroxyaromatic model compounds for humic acid. *Environmental Science & Technology, 17*(4), 202-211.

Chu, W., Krasner, S. W., Gao, N., Templeton, M. R., and Yin, D. (2016). Contribution of the Antibiotic Chloramphenicol and Its Analogues as Precursors of Dichloroacetamide and Other Disinfection Byproducts in Drinking Water. *Environmental Science and Technology, 50*(1), 388-396.

Chu, W., Li, X., Bond, T., Gao, N., and Yin, D. (2016). The formation of haloacetamides and other disinfection by-products from non-nitrogenous low-molecular weight organic acids during chloramination. *Chemical Engineering Journal, 285*, 164-171.

Chu, W. H., and Gao, N. Y. (2009). Determination of nitrogenous disinfection byproducts chloroacetamides in drinking water by gas chromatography-mass spectrometry. *Fenxi Huaxue/ Chinese Journal of Analytical Chemistry, 37*(1), 103-106.

Chuang, Y. H., McCurry, D. L., Tung, H. H., and Mitch, W. A. (2015). Formation Pathways and Trade-Offs between Haloacetamides and Haloacetaldehydes during Combined Chlorination and Chloramination of Lignin Phenols and Natural Waters. *Environmental Science and Technology, 49*(24), 14432-14440.

Cimetiere, N., Dossier-Berne, F., and De Laat, J. (2010). Effect of some parameters on the formation of chloroform during chloramination of aqueous solutions of resorcinol. *Water Research, 44*(15), 4497-4504.

De Leer, E., and Erkelens, C. (1985). Chloroform production from model compounds of aquatic humic material. The role of pentachlororesorcinol as an intermediate. *Science of the Total Environment, 47*(C), 211-216.

Dotson, A., Westerhoff, P., and Krasner, S. W. (2009). Nitrogen enriched dissolved organic matter (DOM) isolates and their affinity to form emerging disinfection by-products. *Water Science and Technology, 60*(1), 135-143.

Freeman, B. A., Wilson, R. E., Binder, R. G., and Haddon, W. F. (2001). Halogenated 2,5-pyrrolidinediones: Synthesis, bacterial mutagenicity in Ames tester strain TA-100 and semi-empirical molecular orbital calculations. *Mutation Research, 490*(2), 89-98.

Haddon, W. F., Binder, R. G., Wong, R. Y., Harden, L. A., Wilson, R. E., Benson, M., and Stevens, K. L. (1996). Potent Bacterial Mutagens Produced by Chlorination of Simulated Poultry Chiller Water. *Journal of Agricultural and Food Chemistry, 44*(1), 256-263.

Heasley, V. L., Alexander, M. B., Deboard, R. H., Hanley Jr, J. C., McKee, T. C., Wadley, B. D., and Shellhamer, D. F. (1999). Reactions of resorcinol and its chlorinated derivatives with monochloramine: Identification of intermediates and products. *Environmental Toxicology and Chemistry, 18*(11), 2406-2409.

Hemming, J., Holmbom, B., Reunanen, M., and Kronberg, L. (1986). Determination of the strong mutagen 3-chloro-4-(dichloromethyl)-5-hydroxy-2(5H)-furanone in chlorinated drinking and humic waters. *Chemosphere, 15*(5), 549-556.

Hua, G., Kim, J., and Reckhow, D. A. (2014). Disinfection byproduct formation from lignin precursors. *Water Research, 63*, 285-295.

Hua, G., and Reckhow, D. A. (2007). Comparison of disinfection byproduct formation from chlorine and alternative disinfectants. *Water Research, 41*(8), 1667-1678.

Hua, G., and Reckhow, D. A. (2008). DBP formation during chlorination and chloramination: Effect of reaction time. pH, dosage, and temperature. *Journal / American Water Works Association, 100*(8), 82-95+12.

Huang, H., Wu, Q. Y., Hu, H. Y., and Mitch, W. A. (2012). Dichloroacetonitrile and dichloroacetamide can form independently during chlorination and chloramination of drinking waters, model organic matters, and wastewater effluents. *Environmental Science and Technology, 46*(19), 10624-10631.

Hureiki, L., Croué, J. P., and Legube, B. (1994). Chlorination studies of free and combined amino acids. *Water Research, 28*(12), 2521-2531.

Kanniganti, R., Johnson, J. D., Ball, L. M., and Charles, M. J. (1992). Identification of compounds in mutagenic extracts of aqueous monochloraminated fulvic acid. *Environmental Science and Technology, 26*(10), 1998-2004.

Kimura, S. Y., Komaki, Y., Plewa, M. J., and Mariñas, B. J. (2013). Chloroacetonitrile and N,2-dichloroacetamide formation from the reaction of chloroacetaldehyde and monochloramine in water. *Environmental Science and Technology, 47*(21), 12382-12390.

Krasner, S. W., McGuire, M. J., Jacangelo, J. G., Patania, N. L., Reagan, K. M., and Aieta, E. M. (1989). The occurrence of disinfection by-products in US drinking water. *Journal / American Water Works Association, 81*(8), 41-53.

Krasner, S. W., Weinberg, H. S., Richardson, S. D., Pastor, S. J., Chinn, R., Sclimenti, M. J., Onstad, G. D., and Thruston, A. D. (2006). Occurrence of a new generation of disinfection byproducts. *Environmental Science and Technology, 40*(23), 7175-7185.

Kronberg, L., and Christman, R. F. (1989). Chemistry of mutagenic by-products of water chlorination. *Science of the Total Environment, 81-82*(C), 219-230.

Kronberg, L., and Vartiaine, T. (1988). Ames mutagenicity and concentration of the strong mutagen 3-chloro-4-(dichloromethyl)-5-hydroxy-2(5H)-furanone and of its geometric isomer E-2-chloro-3-(dichloromethyl)-4-oxo-butenoic acid in chlorine-treated tap waters. *Mutation Research/Genetic Toxicology, 206*(2), 177-182.

Långvik, V.-A., Hormi, O., Tikkanen, L., and Holmbom, B. (1991). Formation of the mutagen 3-chloro-4-(dichloromethyl)-5-hydroxy-2(5H)-furanone and related compounds by chlorination of phenolic compounds. *Chemosphere, 22*(5), 547-555.

Le Roux, J., Nihemaiti, M., and Croué, J.-P. (2016). The role of aromatic precursors in the formation of haloacetamides by chloramination of dissolved organic matter. *Water Research, 88*, 371-379.

Meier, J. R., Ringhand, H. P., and Coleman, W. E. (1986). Mutagenic by-products from chlorination of humic acid. *Environmental Health Perspectives, Vol. 69*, 101-107.

Muellner, M. G., Wagner, E. D., McCalla, K., Richardson, S. D., Woo, Y. T., and Plewa, M. J. (2007). Haloacetonitriles vs. regulated haloacetic acids: Are nitrogen-containing DBPs more toxic? *Environmental Science and Technology, 41*(2), 645-651.

Norwood, D. L., Johnson, J. D., Christman, R. F., Mass, J. R., and Bobenrieth, M. J. (1980). Reactions of chlorine with selected aromatic models of aquatic humic material. *Environmental Science and Technology, 14*(2), 187-190.

Oliver, B. G. (1983). Dihaloacetonitriles in drinking water: Algae and fulvic acid as precursors. *Environmental Science and Technology, 17*(2), 80-83.

Pedersen, I. E. J., Urbansky, E. T., Mariñas, B. J., and Margerum, D. W. (1999). Formation of cyanogen chloride from the reaction of monochloramine with formaldehyde. *Environmental Science and Technology, 33*(23), 4239-4249.

Plewa, M. J., Wagner, E. D., Jazwierska, P., Richardson, S. D., Chen, P. H., and McKague, A. B. (2004). Halonitromethane Drinking Water Disinfection Byproducts: Chemical Characterization and Mammalian Cell Cytotoxicity and Genotoxicity. *Environmental Science and Technology, 38*(1), 62-68.

Reckhow, D. A., Platt, T. L., MacNeill, A. L., and McClellan, J. N. (2001). Formation and degradation of dichloroacetonitrile in drinking waters. *Journal of Water Supply: Research and Technology - AQUA, 50*(1), 1-13.

Richardson, S. D., DeMarini, D. M., Kogevinas, M., Fernandez, P., Marco, E., Lourencetti, C., Ballesté, C., Heederik, D., Meliefste, K., McKague, A. B., Marcos, R., Font-Ribera, L., Grimalt, J. O., and Villanueva, C. M. (2010). What's in the pool? a comprehensive identification of disinfection by-products and assessment of mutagenicity of chlorinated and brominated swimming pool water. *Environmental Health Perspectives, 118*(11), 1523-1530.

Richardson, S. D., Thruston, A. D., Rav-Acha, C., Groisman, L., Popilevsky, I., Juraev, O., Glezer, V., McKague, A. B., Plewa, M. J., and Wagner, E. D. (2003). Tribromopyrrole, brominated acids, and other disinfection byproducts produced by disinfection of drinking water rich in bromide. *Environmental Science and Technology, 37*(17), 3782-3793.

Rook, J. J. (1977). Chlorination reactions of fulvic acids in natural waters. *Environmental Science and Technology, 11*(5), 478-482.

Rook, J. J. (1980). Possible pathways for the formation of chlorinated degradation products during chlorination of humic acids and resorcinol. In R. L. Jolley, Brungs, W. A., Cumming, R. B. (Ed.), *Water Chlorination: Environmental Impact and Health Effects* (pp. 85-98). Michigan: Ann Arbor Science.

Schreiber, I. M., and Mitch, W. A. (2005). Influence of the order of reagent addition on NDMA formation during chloramination. *Environmental Science and Technology, 39*(10), 3811-3818.

Seidel, C. J., McGuire, M. J., Summers, R. S., and Via, S. (2005). Have utilities switched to chloramines? *Journal / American Water Works Association, 97*(10), 87-97.

Tretyakova, N. Y., Lebedev, A. T., and Petrosyan, V. S. (1994). Degradative pathways for aqueous chlorination of orcinol. *Environmental Science and Technology, 28*(4), 606-613.

Westerhoff, P., and Mash, H. (2002). Dissolved organic nitrogen in drinking water supplies: a review. *Journal of Water Supply: Research and Technology - AQUA, 51*(8), 415-448.

Yang, M., and Zhang, X. (2014). Halopyrroles: A new group of highly toxic disinfection byproducts formed in chlorinated saline wastewater. *Environmental Science and Technology*, *48*(20), 11846-11852.

Yang, X., Fan, C., Shang, C., and Zhao, Q. (2010). Nitrogenous disinfection byproducts formation and nitrogen origin exploration during chloramination of nitrogenous organic compounds. *Water Research*, *44*(9), 2691-2702.

Yu, Y., and Reckhow, D. A. (2015). Kinetic Analysis of Haloacetonitrile Stability in Drinking Waters. *Environmental Science and Technology*, *49*(18), 11028-11036.

Chapter 7. Conclusions and Recommendations

This thesis provides several new insights in the application of UV-AOPs to wastewater for the removal of TOrCs and to control the dissemination of antibiotic resistance in comparison to conventional disinfection processes.

Two factors impact the performance of UV-AOPs: the physicochemical properties of target contaminant and the availability of radicals in aqueous solution (i.e., steady-state concentration). Physicochemical properties of contaminant include the photolytic characteristics (i.e., UV-resistant or susceptible) and the reactivity with radicals (i.e., second-order rate constants with radicals). UV-susceptible compounds (e.g., diclofenac, sulfamethoxazole) can be degraded by direct UV photolysis (90% removal at ~1,000 mJ/cm^2). Strong UV reactive property of some compounds can counteract their resistance to radicals (e.g., iopromide). Radical exposure plays a major role for the degradation of UV-resistant compounds. The second-order rate constants of TOrCs with radicals determined in this study or reported previously will help the water utilities to better estimate the percent removal of contaminants during UV-AOPs. UV/PDS is more suitable to target TOrCs with electron-rich moieties (e.g., metoprolol, venlafaxine) in wastewater. UV-AOPs cannot be proposed to eliminate TCEP, a contaminant inert to both UV and radical species. The steady-state concentrations of radicals during UV-AOPs were influenced by the quantum efficiency of radical precursors (e.g., H_2O_2 and PDS), as well as the scavenging capacity of the water matrix. UV/PDS generally demonstrates higher formation yield of radicals than UV/H_2O_2 due to the higher quantum efficacy of PDS at 254 nm, which makes UV/PDS more efficient than UV/H_2O_2 in the presence of less scavengers. The scavenging effect of wastewater on UV/H_2O_2 was found constant under our experimental conditions, while the electron-rich site of DOC generates oxidant demand for UV/PDS. UV/PDS potentially demonstrated better results than UV/H_2O_2 after the initial oxidant demand was satisfied. Overall results indicated that UV-AOP is sensitive to the quality of wastewater (e.g., DOC, nitrite), consequently requiring highly efficient pre-treatments for a successful application. Water utilities should carefully evaluate the energy input, as well as the effect of residual oxidants and concentration of sulfate ions (in the case of UV/PDS) on treated water before the application of UV-AOPs in wastewater treatment. Further efforts should focus on the chemical and biological assessment of UV-AOPs, including the identification of transformation products and toxicologically characterization of treated water.

The findings on the non-radical degradation of TOrCs via PMS direct oxidation suggested that PMS-based treatment can be selectively applied for nitrogenous compounds removal. Unlike the radical-based processes, this treatment can maintain its efficiency even in the presence of natural organic matter and inorganic ions. Because environmental components are susceptible to react with PMS, one should note that non-radical pathway might hinder the formation of radicals during PMS-activated AOPs and limit the elimination of hazardous compounds.

UV-AOPs can efficiently inactivate ARB (i.e., > 5-log of cultivability loss) within the typical UV dose applied in water treatment (40 mJ/cm^2 at 254 nm). UV/PDS might be more suitable to selectively degrade the inner cell components (e.g., intracellular ARG) because UV/H_2O_2 is easily affected by the scavenging effect of cell membrane components. The capability of bacteria cells to repair DNA lesions (e.g., UV and radicals induced damage) is the major challenge during UV-AOPs. Gene transformation assays might be more suitable to verify the functionality of extracellular DNA than qPCR analysis as qPCR overestimates the performance of treatment, especially the contributions of radicals. Future work should focus on the characterization of DNA damage caused by radicals and its repair efficiency within different recipient cells. This will help operators to optimize UV-AOPs in order to better benefit from radical exposure while looking at controlling the dissemination of antibiotic resistance.

Flow cytometric analysis combining with nucleic acids staining are useful tools to monitor the inactivation of ARB during conventional chlorination and chloramination processes. Weak oxidants (e.g., NH_2Cl and NH_2Br) and strong oxidants (e.g., HOCl and HOBr) at low dose induced the formation of "injured" ARB cells, which are detectable by flow cytometry but hardly identified by traditional plate counting method (non-cultivable). More research work is required to investigate the gene transfer potential of "injured" cells and their capability for repair and regrowth, especially in real water conditions.

The formation of undesired DBPs is one of major issues during conventional chlorination and chloramination processes. The potential formation of nitrogenous heterocyclic compounds from chloramination of phenolic compounds in this study is of importance for water treatment facilities using chloramine as disinfectant as these

compounds could be substantially toxic due to their similarity to known mutagen in chlorinated water (e.g., MX). Similar screening of halogenated pyridine and pyrimidine derivatives should be performed during chloramination of natural water or NOM. The detection of highly polar DBPs with large molecular weight would require the application of advanced analytical tools, such as hydrophilic interaction liquid chromatography coupled with HRMS.

Appendix 1

Table A- 1-1. TOrCs investigated in this study

TOrCs	CAS Number	Purity	Source	Product Number
Benzotriazole	95-14-7	99.8%	Cimachem	BTA-99
Caffeine	58-08-2	> 99%	Sigma Aldrich	C7050
Carbamazepine	298-46-4	>98%	Sigma Aldrich	C4024
Diclofenac	15307-86-5	>99%	Caymanchem	70680
Gabapentin	60142-96-3	European Pharmacopoeia (EP) Reference Standard	Sigma Aldrich	Y0001280
Iopromide	73334-07-3	98.7%	Sigma Aldrich	Y0001020
Metoprolol	56392-17-7	>98%	Sigma Aldrich	M5391
Phenytoin	57-41-0	HPLC grade	Sigma Aldrich	PHR1139
Primidone	125-33-7	HPLC grade	Sigma Aldrich	P7295
Sulfamethoxazole	723-46-6	HPLC grade	Sigma Aldrich	S7507
TCEP	51805-45-9	97%	Sigma Aldrich	119660
Venlafaxine	99300-78-4	>98% (HPLC)	Sigma Aldrich	V7264

Table A- 1-2. Reactions of the wastewater matrix with $^{\cdot}OH$ and $SO_4^{\cdot-}$

	Reactions	Rate constant	Reference
1	$^{\cdot}OH$ + EfOM→products	3.3 ×10^4 (mg-C/L)$^{-1}$ s^{-1}	(Yang et al., 2016)
2	$SO_4^{\cdot-}$ + EfOM→products	9.4 ×10^3 (mg-C/L)$^{-1}$ s^{-1}	(Yang et al., 2016)
3	$^{\cdot}OH + HCO_3^- \rightarrow CO_3^{\cdot-} + H_2O$	8.6 × 10^6 M^{-1} s^{-1}	(Buxton et al., 1988)
4	$SO_4^{\cdot-} + HCO_3^- \rightarrow CO_3^{\cdot-} + HSO_4^-$	2.8 × 10^6 M^{-1} s^{-1}	(Huie and Clifton, 1990)
5	$^{\cdot}OH + NO_2^- \rightarrow {}^{\cdot}NO_2 + OH^-$	1.0 × 10^{10} M^{-1} s^{-1}	(Coddington et al., 1999)
6	$SO_4^{\cdot-} + NO_2^- \rightarrow {}^{\cdot}NO_2 + SO_4^{2-}$	8.8 × 10^8 M^{-1} s^{-1}	(Neta et al., 1988)
7	$^{\cdot}OH + NO_3^- \rightarrow$products	<1 × 10^5 M^{-1} s^{-1}	(Keen et al., 2012)
8	$SO_4^{\cdot-} + NO_3^- \rightarrow NO_3^{\cdot} + SO_4^{2-}$	3.0 × 10^4 M^{-1} s^{-1}	(Buxton et al., 1988)
9	$^{\cdot}OH + Cl^- \rightarrow ClOH^{\cdot-}$	4.3 × 10^9 M^{-1} s^{-1}	(Jayson et al., 1973)
10	$ClOH^{\cdot-} \rightarrow {}^{\cdot}OH + Cl^-$	6.1 × 10^9 M^{-1} s^{-1}	(Jayson et al., 1973)
11	$SO_4^{\cdot-} + Cl^- \rightarrow Cl^{\cdot} + SO_4^{2-}$	3.0 × 10^9 M^{-1} s^{-1}	(Das, 2001)
12	$Cl^{\cdot} + Cl^- \rightarrow Cl_2^{\cdot-}$	8.5 × 10^9 M^{-1} s^{-1}	(Yu and Barker, 2003)
13	$Cl^{\cdot} + HCO_3^- \rightarrow CO_3^{\cdot-} + Cl^- + H^+$	2.2 × 10^8 M^{-1} s^{-1}	(Matthew and Anastasio, 2006)
14	$Cl_2^{\cdot-} + HCO_3^- \rightarrow CO_3^{\cdot-} + 2Cl^- + H^+$	8.0 × 10^7 M^{-1} s^{-1}	(Matthew and Anastasio, 2006)

Table A- 1-3. The scavenging capacity of the main water matrix components during buffered pure water experiments

Component	Concentration M	Second-order rate constants (M^{-1} s^{-1})		Scavenging capacity (s^{-1})[a]	
		$k_{\cdot OH}$	$k_{SO_4^{\cdot-}}$	UV/H_2O_2	UV/PDS
HPO_4^{2-}	2.5 × 10^{-3}	1.5 × 10^{5}[b]	1.2 × 10^{6}[c]	3.8 × 10^2	3.0 × 10^3

$H_2PO_4^-$	2.5×10^{-3}	2.0×10^{4}[b]	5×10^{4}[c]	50.0	1.3×10^{3}
H_2O_2	1.5×10^{-4}	2.7×10^{7}[c]	n.a.	4.1×10^{3}	n.a.
PDS	1.5×10^{-4}	n.a.	6.5×10^{5}[c]	n.a.	97.5
TOrCs[d]	1 μg/L each	see Table 2-2[e]		3.6×10^{2}	1.5×10^{2}
SUM				4.8×10^{3}	3.4×10^{3}

[a] Calculated by multiplying the molar concentration of each component with its second-order reaction rate constants with radicals; [b] Crittenden et al. (1999); [c] Yang et al. (2016); [d] Sum of the scavenging capacity of each TOrC; [e] The rate constants of TCEP and gabapentin with $SO_4^{\bullet-}$ were estimated to be 1.0×10^9 M^{-1} s^{-1}.

Table A- 1-4. Fluorescence EEM regions and the Excitation/Emission wavelengths of the selected peaks

Region[a]	Dissolved organic matter components	Selected peaks		
		Name	Excitation wavelength (nm)	Emission wavelength (nm)
II	aromatic proteins, tryptophan-like	P_II	242	358
III	Fulvic acid-like	P_III	242	430
IV	soluble microbial by-product-like	P_IV	287	353
V	Humic acid-like	P_V	329	412

[a] From Chen et al. (2003).

Table A- 1-5. HPLC-UV parameters [a] for the detection of *p*CBA and TOrCs

Compounds	Mobile phase	Flow rate (mL/min)	Wavelength (nm)
*p*CBA	60% Methanol+40% MQ (0.1% phosphoric acid)	1	238
phenytoin	50% Methanol+50% MQ (0.1% phosphoric acid)	1	230
caffeine	25% Methanol+75% MQ (0.1% phosphoric acid)	1	273
benzotriazole	25% Methanol+75% MQ (0.1% phosphoric acid)	1	273
primidone	25% Methanol+75% MQ (0.1% phosphoric acid)	1	218
metoprolol	30% Methanol+70% MQ (0.1% phosphoric acid)	1	225
venlafaxine	25% Acetonitrile+75% MQ (0.1% phosphoric acid)	1	225
carbamazepine	50% Methanol+50% MQ (0.1% phosphoric acid)	1	285
Iopromide	4% Acetonitrile+96% MQ (0.3% phosphoric acid)	1	238[b]

[a] Compounds were separated on a XDB-C18 column (5 µm, 4.6 × 150 mm, Agilent).

[b] The sum of the peak areas of 2 isomers were followed for quantification.

Text A- 1-1. Fluorescence excitation-emission matrix analysis

Fluorescence excitation-emission matrices (EEM) were measured using an Aqualog Fluorescence Spectrometer (Horiba Scientific, Germany). Samples were filtered through 0.45 µm cellulose nitrate membrane filters (Sartorius, Germany) and measured using a 10 mm quartz cuvette. The fluorescence response of a blank solution (Milli-Q water) was subtracted from the EEM of each sample. The wastewater specific fluorescence signal was tested for linearity in a preliminary experiment using 5 dilutions with ultrapure water ranging from 2:1 to 10:1. Data processing included corrections using inner filter effects, Raman normalization, Rayleigh masking and diagram adjustments.

Four fluorescence peaks were selected from different regions on fluorescence spectra previously defined by Chen et al. (2003). The fluorescence intensities of selected peaks were used as representative indices of dissolved organic matter in wastewater to study the effect of radical exposure on effluent organic matter (EfOM) during UV/H_2O_2 and UV/PDS (Sgroi et al., 2017). The excitation and emission wavelengths of selected peaks are presented in Table A-1-4.

Text A- 1-2. Second-order rate constants of TOrCs with $SO_4^{\bullet-}$

The second-order rate constants for the reaction of TOrCs with $SO_4^{\bullet-}$ were determined by competition kinetics based on the methods published before (Lutze et al., 2015; Lian et al., 2017). *para*-chlorobenzoic acid (*p*CBA) was used as a probe compound, K ($SO_4^{\bullet-}$ + *p*CBA) = 3.6×10^8 M^{-1} s^{-1} (Neta et al., 1977). Experiments were conducted in phosphate buffer (2.5 mM) at pH=7 with 20 µM of *p*CBA and target compound. $SO_4^{\bullet-}$ was generated by UV photolysis of PDS (1 mM). 10 mM of *tert*-Butanol was also added into the solution as the $^{\bullet}OH$ scavenger. Nitrobenzene can be used as $^{\bullet}OH$ probe compound ($k_{\bullet OH}$=3.9×10^9 M^{-1} s^{-1}) (Buxton et al., 1988) during sulfate radical-based experiments due to its low reaction rate constant with $SO_4^{\bullet-}$ ($k_{SO_4^{\bullet-}} < 10^6$ M^{-1} s^{-1}) (Neta et al., 1977). UV/PDS experiment on nitrobenzene was conducted before the competition kinetics to confirm that 10 mM of *tert*-BuOH was sufficient to scavenge $^{\bullet}OH$ in these experimental conditions. For benzotriazole, iopromide and phenytoin, the degradation by direct photolysis was considered when calculating their second-order rate constants with $SO_4^{\bullet-}$. The concentrations of *p*CBA and TOrCs were analyzed by a HPLC (Agilent 1100) coupled with a DAD detector. Compounds were separated on

a XDB-C18 column (5 µm, 4.6 × 150 mm, Agilent). Mobile phase composition followed various isocratic mixtures of methanol (or acetonitrile) and water (0.1% or 0.3% phosphoric acid). All compounds were analyzed on their maximum UV absorption. HPLC-UV parameters are listed in Table A-1-5.

Text A- 1-3. Estimation of the second-order rate constants of gabapentin and TCEP with $SO_4^{\bullet-}$

The $k_{SO_4^{\bullet-}}$-values of gabapentin and TCEP were estimated based on the steady-state concentration of $SO_4^{\bullet-}$ (i.e., $[SO_4^{\bullet-}]_{ss}$) during UV/PDS treatment of TOrCs in pure water (Fluence=7.5-57.5 mJ/cm^2 and PDS=0.15 mM). Primidone was used to calculated $[SO_4^{\bullet-}]_{ss}$. The pseudo-first order degradation of a TOrC can be expressed as follows:

$$-\frac{d[TOrC]}{dt} = K\,(TOrC + SO_4^{\bullet-})[TOrC][SO_4^{\bullet-}]_{ss} \qquad \text{(S1)}$$

$$ln\frac{[TOrC]_0}{[TOrC]} = K\,(TOrC + SO_4^{\bullet-})[SO_4^{\bullet-}]_{ss}t = k_{obs,TOrC}t \qquad \text{(S2)}$$

As shown in Figure A-1-14, the k_{obs} of primidone, gabapentin and TCEP was 0.142 (s^{-1}), 0.106 (s^{-1}), and 0.005 (s^{-1}), respectively. The second-order rate constant of primidone with $SO_4^{\bullet-}$ is 5.29 ×10^8 ($M^{-1}s^{-1}$) (Table 2-2). Thus, $[SO_4^{\bullet-}]_{ss}$ was calculated to be 2.6 ×10^{-10} M. According to equation S2, the second-order rate constant of gabapentin and TCEP with $SO_4^{\bullet-}$ was calculated to be 4.1 ×10^8 ($M^{-1}s^{-1}$) and 1.92×10^7 ($M^{-1}s^{-1}$), which were lower than 1 ×10^9 ($M^{-1}s^{-1}$).

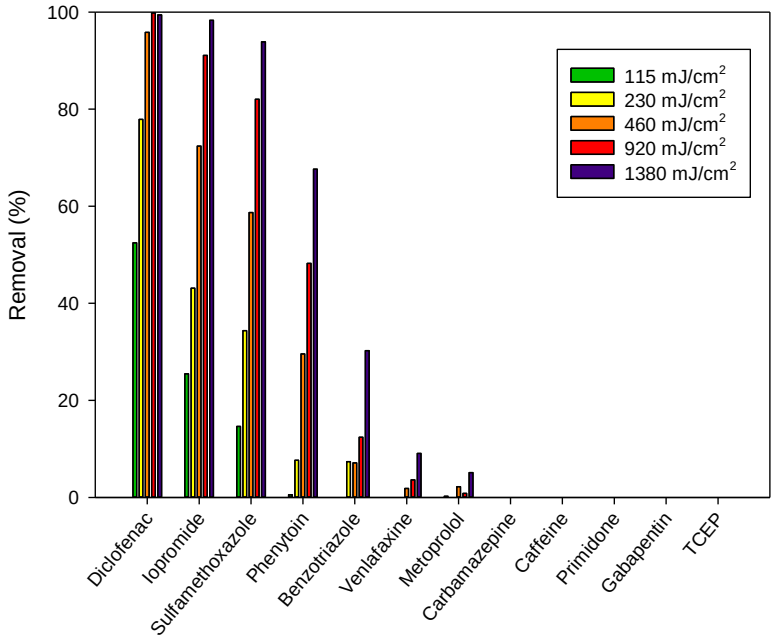

Figure A- 1-1. Percent removal of TOrCs in wastewater effluent by direct UV photolysis (Fluence=115−1,380 mJ/cm^2)

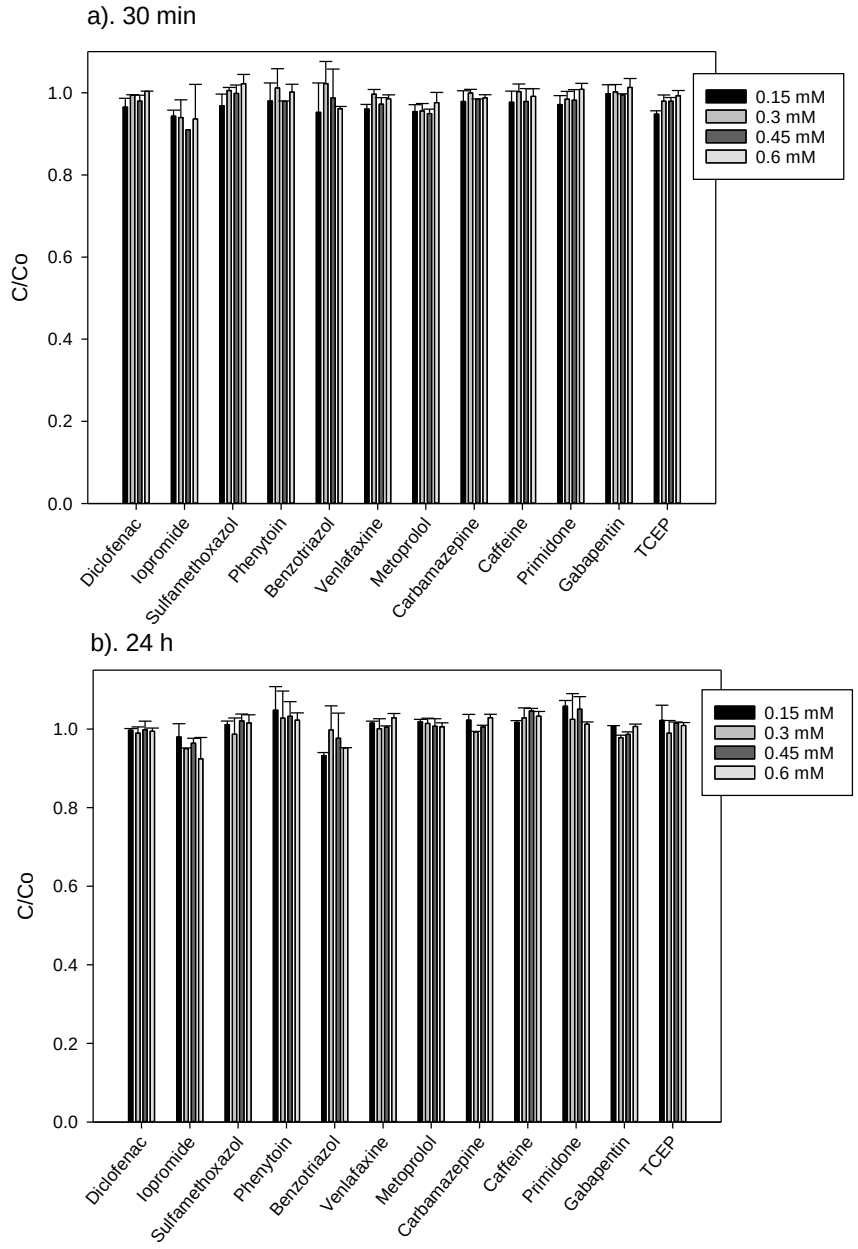

Figure A- 1-2. Effect of PDS on the removal of TOrCs in the dark within a) 30 min and b) 24 h of contact time (5 mM phosphate buffer, pH 7, PDS=0.15, 0.3, 0.45 and 0.6 mM)

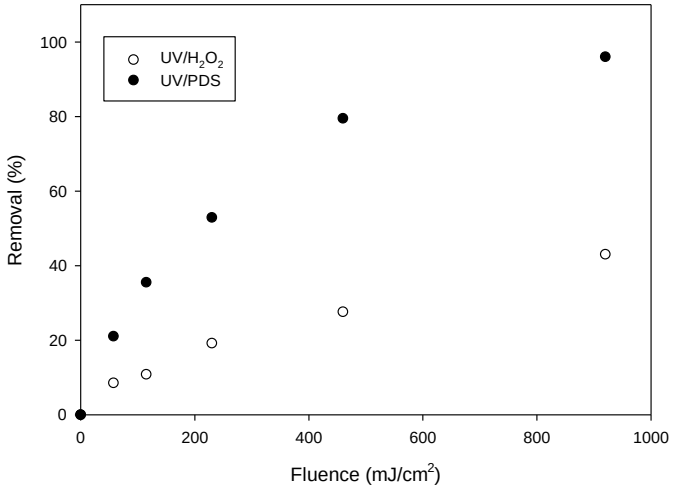

Figure A- 1-3. Relative removal of TCEP in pure water during UV/H_2O_2 and UV/PDS (pH=7, 5 mM phosphate buffer; oxidants=0.15 mM)

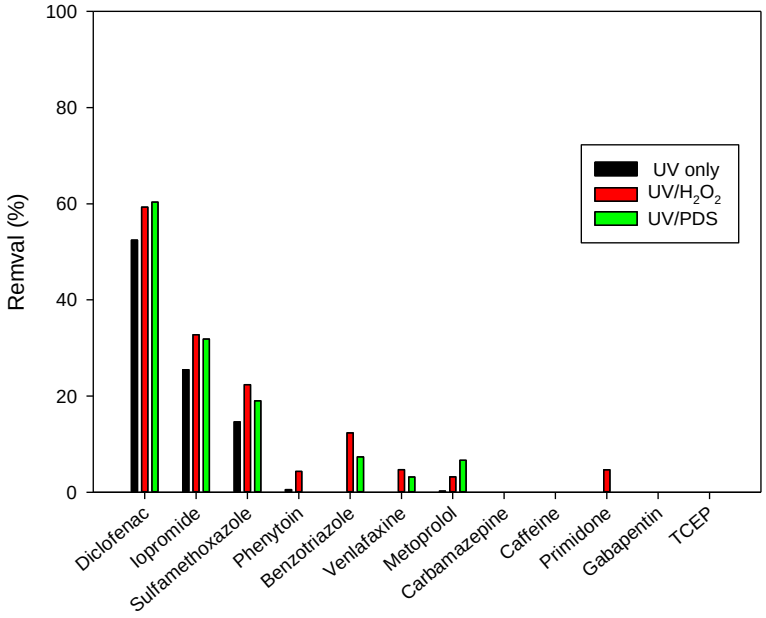

Figure A- 1-4. Relative removal of TOrCs in wastewater effluent during UV/H_2O_2 and UV/PDS (Fluence=115 mJ/cm^2; Oxidant=0.15 mM).

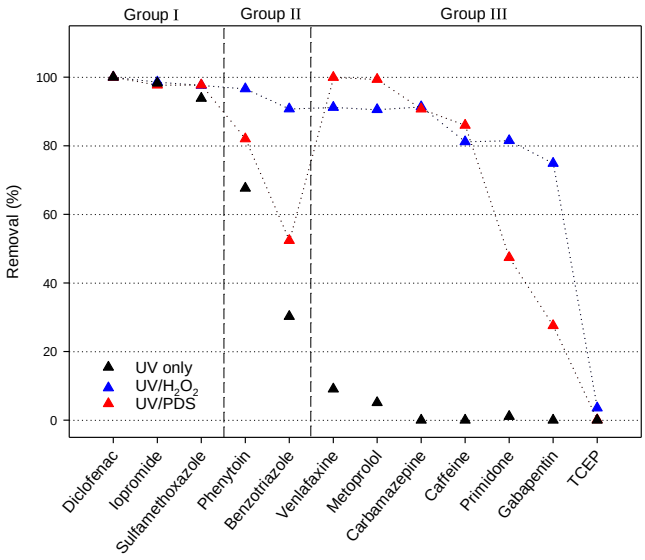

Figure A- 1-5. Percent removal of TOrCs in wastewater effluent during UV/H_2O_2 and UV/PDS (Fluence=1380 mJ/cm^2; Oxidant=0.6 mM).

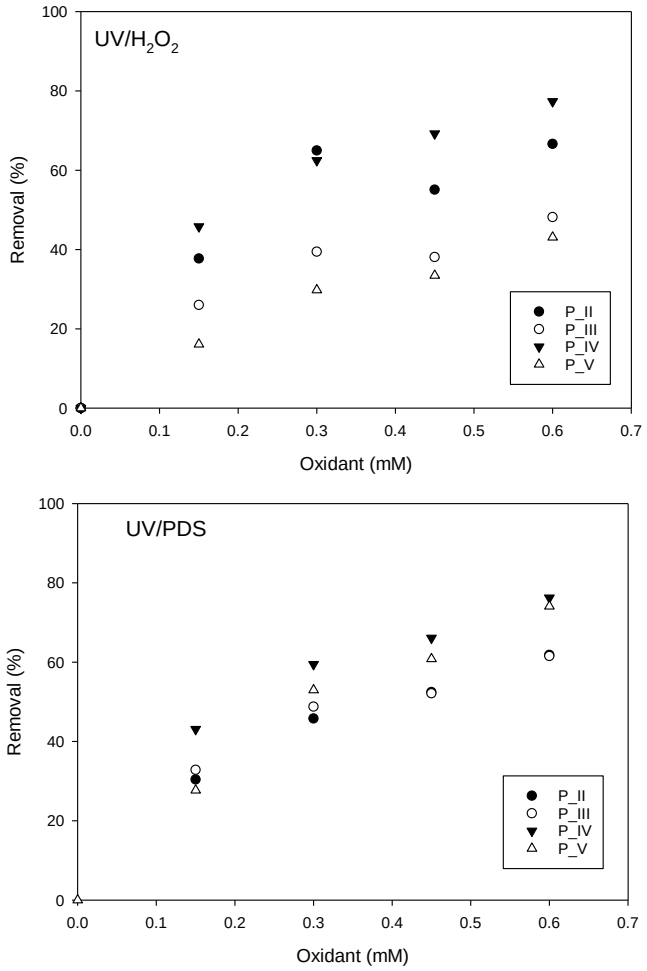

Figure A- 1-6. Relative removal of fluorescence intensities of selected peaks in wastewater effluent during UV/H2O2 and UV/PDS (Fluence =1,380 mJ/cm2; Oxidant= 0.15, 0.3, 0.45 and 0.6 mM)

a). UV/H_2O_2

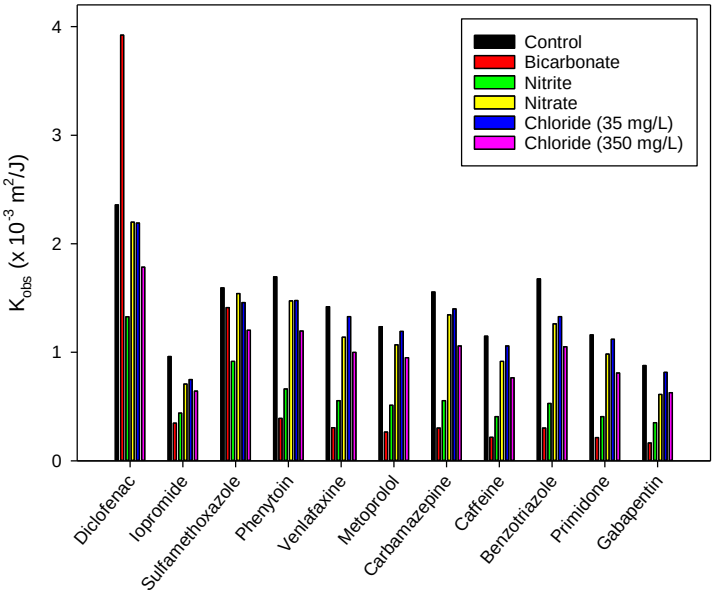

b). UV/PDS

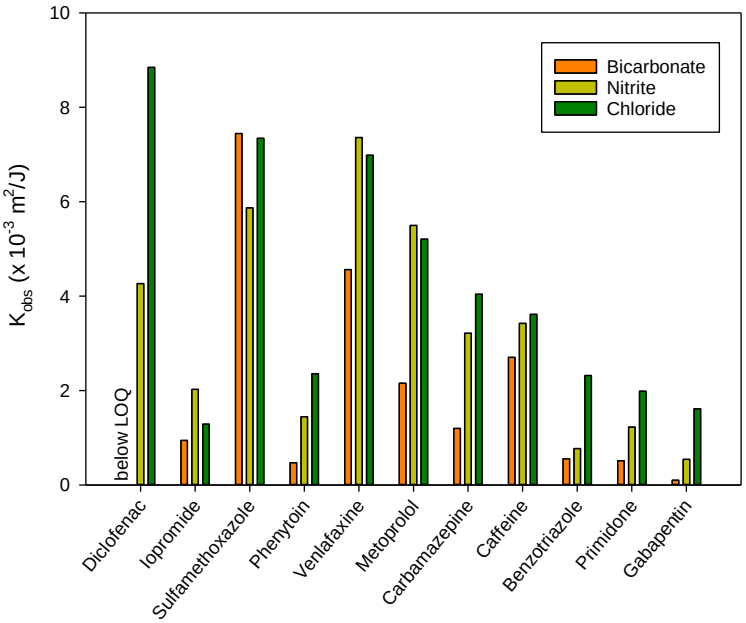

Figure A- 1-7. Effect of individual inorganic compounds on the efficiency of UV/H_2O_2 and UV/PDS processes in phosphate buffer at pH 7

Experimental conditions: Fluence= 57.5-920 mJ/cm^2; Oxidant=0.15 mM; Bicarbonate=300 mg/L; Nitrite=0.028 mg-N/L; Nitrate=10.6 mg-N/L; Chloride= 35

mg/L and 350 mg/L (The concentration of TOrCs were below LOQ during the control experiments as well as in the presence of nitrate and 35 mg/L of chloride during UV/PDS; the concentration of diclofenac was below LOQ during UV/PDS in the presence of bicarbonate).

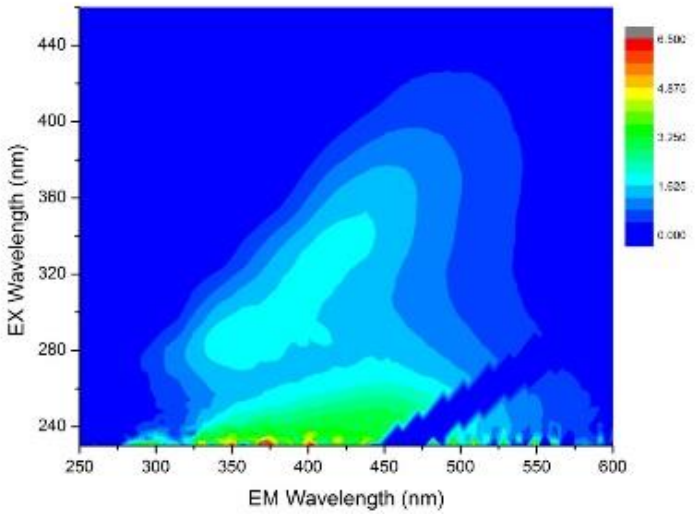

a)

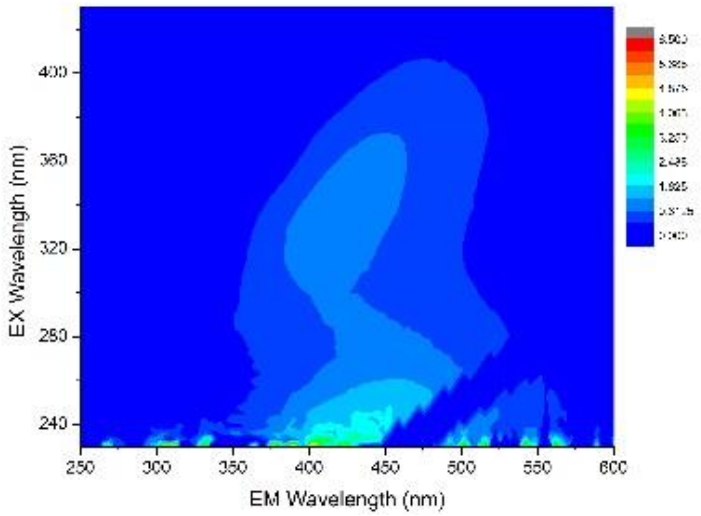

b)

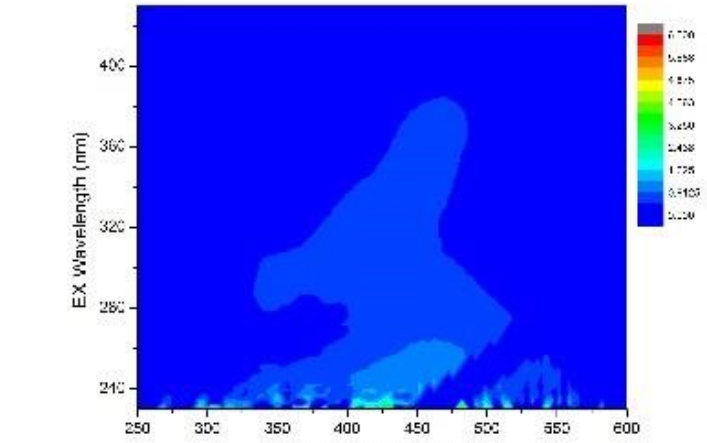

Figure A- 1-8. Fluorescence excitation–emission matrices (EEMs) of wastewater effluent before treatment (a), after UV/H_2O_2 (b) and UV/PDS (c) treatment. (Experimental conditions for UV/H_2O_2 and UV/PDS: oxidants=0.6 mM; fluence=1,380 mJ/cm^2)

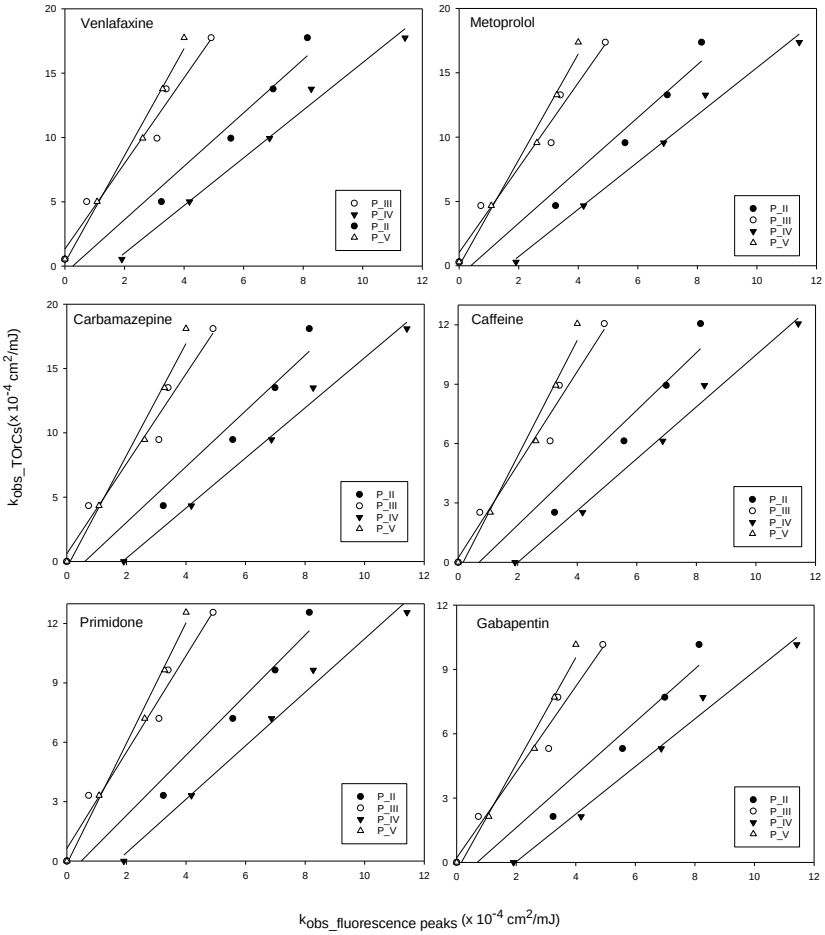

Figure A- 1-9. Correlations between the fluence-based rate constants of group III compounds (except TCEP) and selected fluorescence peaks during UV/H2O2 (Fluence=115−1,380 mJ/cm2; Oxidants = 0, 0.15, 0.3, 0.45 and 0.6 mM).

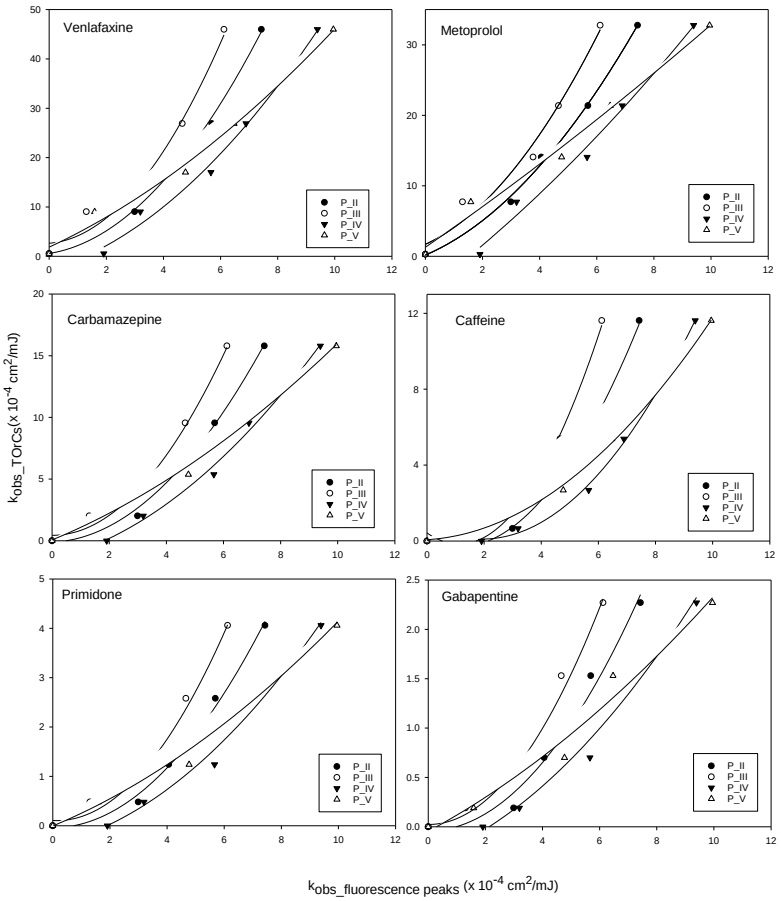

Figure A- 1-10. Correlations between the fluence-based rate constants of group III compounds (except TCEP) and selected fluorescence peaks during UV/PDS (Fluence=115−1,380 mJ/cm^2; Oxidants = 0, 0.15, 0.3, 0.45 and 0.6 mM).

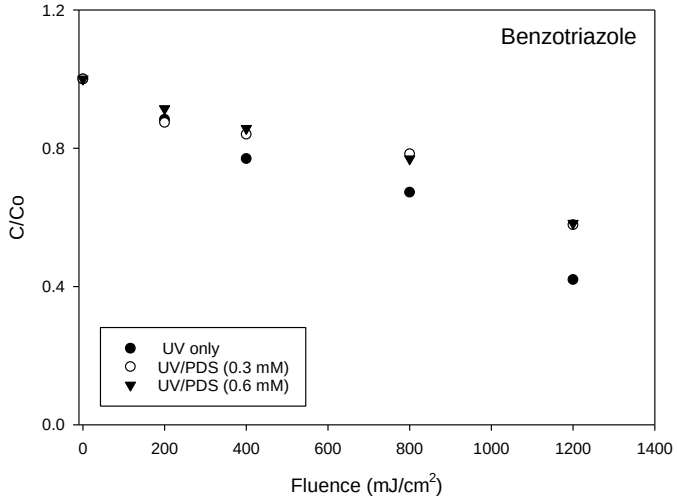

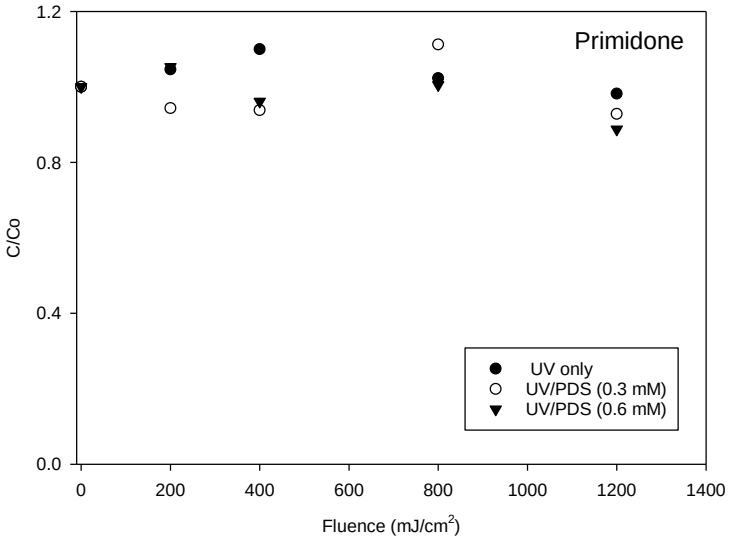

Figure A- 1-11. Relative removal of benzotriazole and primidone in pilot-scale experiments by direct photolysis and UV/PDS (PDS=0.3 and 0.6 mM)

a).

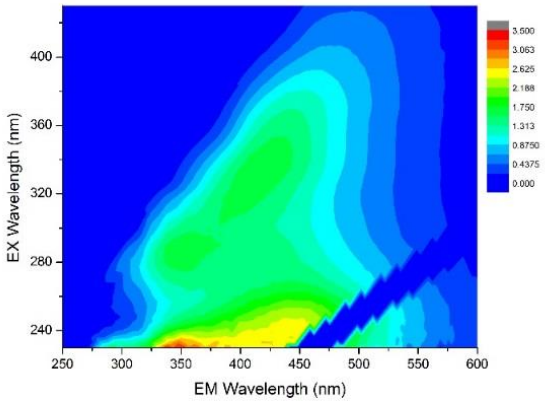

b).

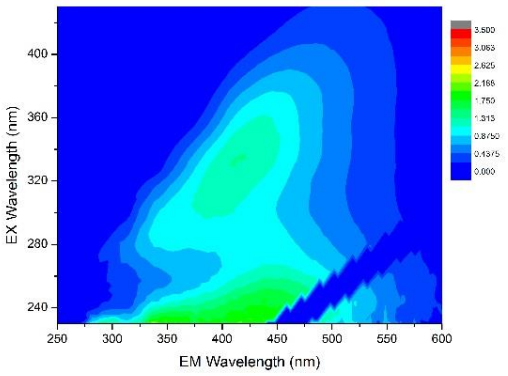

c).

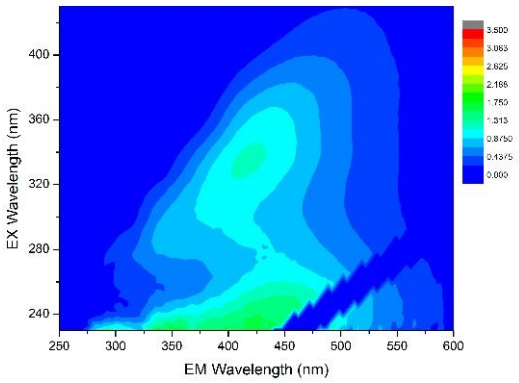

Figure A- 1-12. Fluorescence excitation–emission matrices (EEMs) of wastewater effluent before treatment (a) and after UV/PDS at 1,200 mJ/cm2 (b. PDS= 0.3 mM; c. PDS=0.6 mM) in pilot scale experiments

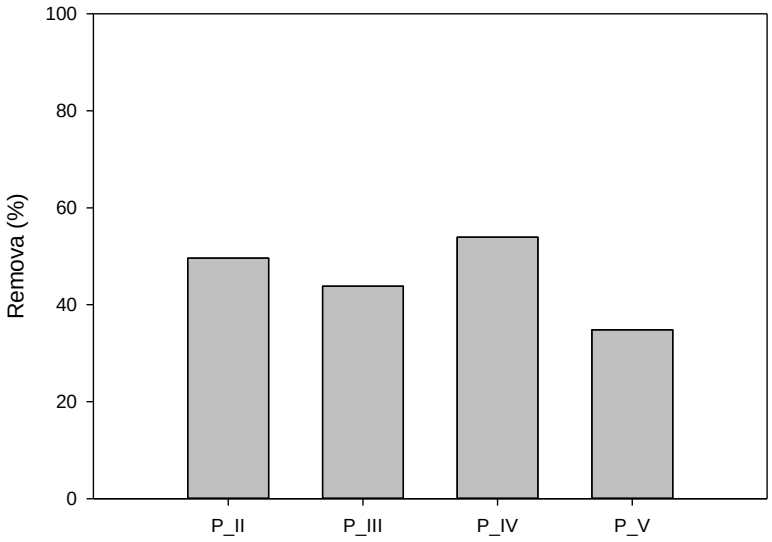

Figure A- 1-13. Relative removal of fluorescence intensities of selected peaks in wastewater effluent during UV/PDS pilot-tests (Fluence =1,200 mJ/cm^2; Oxidant= 0.6 mM)

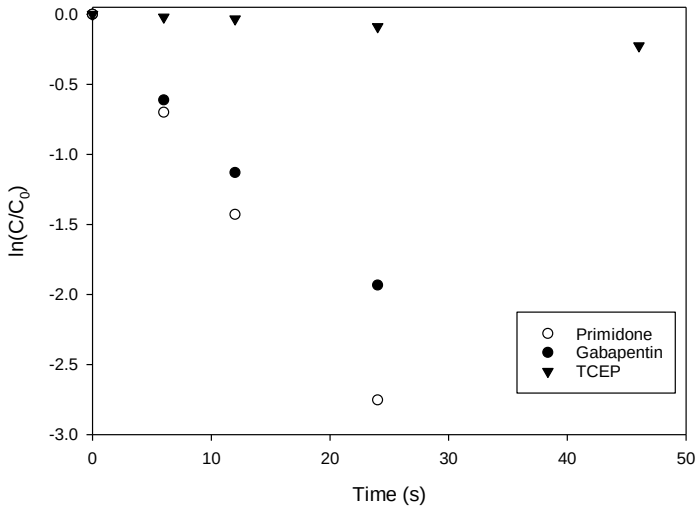

Figure A- 1-14. Pseudo-first order removal of primidone, gabapentin and TCEP during UV/PDS in ultrapure water at pH 6 (Fluence= 7.5-57.5 mJ/cm^2; PDS= 0.15 mM)

Reference

Buxton, G. V., Greenstock, C. L., Helman, W. P., and Ross, A. B. (1988). Critical Review of rate constants for reactions of hydrated electrons, hydrogen atoms and hydroxyl radicals (·OH/·O−) in Aqueous Solution. *Journal of Physical and Chemical Reference Data, 17*(2), 513-886.

Chen, W., Westerhoff, P., Leenheer, J. A., and Booksh, K. (2003). Fluorescence Excitation-Emission Matrix Regional Integration to Quantify Spectra for Dissolved Organic Matter. *Environmental Science and Technology, 37*(24), 5701-5710.

Coddington, J. W., Hurst, J. K., and Lymar, S. V. (1999). Hydroxyl Radical Formation during Peroxynitrous Acid Decomposition. *Journal of the American Chemical Society, 121*(11), 2438-2443.

Crittenden, J. C., Hu, S., Hand, D. W., and Green, S. A. (1999). A kinetic model for H2O2/UV process in a completely mixed batch reactor. *Water Research, 33*(10), 2315-2328.

Das, T. N. (2001). Reactivity and Role of SO5•- Radical in Aqueous Medium Chain Oxidation of Sulfite to Sulfate and Atmospheric Sulfuric Acid Generation. *The Journal of Physical Chemistry A, 105*(40), 9142-9155.

Huie, R. E., and Clifton, C. L. (1990). Temperature dependence of the rate constants for reactions of the sulfate radical, SO4-, with anions. *The Journal of Physical Chemistry, 94*(23), 8561-8567.

Jayson, G. G., Parsons, B. J., and Swallow, A. J. (1973). Some simple, highly reactive, inorganic chlorine derivatives in aqueous solution. Their formation using pulses of radiation and their role in the mechanism of the Fricke dosimeter. *Journal of the Chemical Society, Faraday Transactions 1: Physical Chemistry in Condensed Phases, 69*, 1597-1607.

Keen, O. S., Love, N. G., and Linden, K. G. (2012). The role of effluent nitrate in trace organic chemical oxidation during UV disinfection. *Water Research, 46*(16), 5224-5234.

Matthew, B. M., and Anastasio, C. (2006). A chemical probe technique for the determination of reactive halogen species in aqueous solution: Part 1 - Bromide solutions. *Atmospheric Chemistry and Physics, 6*(9), 2423-2437.

Neta, P., Huie, R. E., and Ross, A. B. (1988). Rate Constants for Reactions of Inorganic Radicals in Aqueous Solution. *Journal of Physical and Chemical Reference Data, 17*(3), 1027-1284.

Neta, P., Madhavan, V., Zemel, H., and Fessenden, R. W. (1977). Rate constants and mechanism of reaction of SO4·- with aromatic compounds. *Journal of the American Chemical Society, 99*(1), 163-164.

Sgroi, M., Roccaro, P., Korshin, G. V., Greco, V., Sciuto, S., Anumol, T., Snyder, S. A., and Vagliasindi, F. G. A. (2017). Use of fluorescence EEM to monitor the removal of emerging contaminants in full scale wastewater treatment plants. *Journal of Hazardous Materials, 323*(Part A), 367-376.

Yang, Y., Pignatello, J. J., Ma, J., and Mitch, W. A. (2016). Effect of matrix components on UV/H2O2 and UV/S2O82− advanced oxidation processes for trace organic degradation in reverse osmosis brines from municipal wastewater reuse facilities. *Water Research, 89*, 192-200.

Yu, X. Y., and Barker, J. R. (2003). Hydrogen Peroxide Photolysis in Acidic Aqueous Solutions Containing Chloride Ions. II. Quantum Yield of HO•(Aq) Radicals. *The Journal of Physical Chemistry A, 107*(9), 1325-1332.

Appendix 2

Table A- 2-1. HPLC-UV parameters [a] for quantification of compounds investigated in this study

Compounds	Mobile phase	Flow rate (mL/min)	Wavelength (nm)
Ciprofloxacin	25% Methanol+75% Phosphoric acid (0.1%)	1	278
Norfloxacin	25% Methanol+75% Phosphoric acid (0.1%)	1	278
Enrofloxacin	25% Methanol+75% Phosphoric acid (0.1%)	1	278
Flumequine	60% Methanol+40% Phosphoric acid (0.1%)	1	248
1-(2-fluorophenyl) piperazine	25% Methanol+75% Phosphoric acid (0.1%)	1	232
Metoprolol	30% Methanol+70% phosphoric acid (0.1%)	1	225
Venlafaxine	25% Acetonitrile+75% phosphoric acid (0.1%)	1	225
[a] Compounds were separated on a XDB-C18 column (5 µm, 4.6 × 150 mm, Agilent).			

Table A- 2-2. LC-HRMS parameters

Time (min)	Pump A (%)	Pump B (%)
0	95	5
20	30	70
22	5	95
28	5	95
28.1	95	5
40	95	5
Injection volume	25 µL	
Flow rate	200 µL/min	

Eluent A	pure water with 0.1% formic acid
Eluent B	methanol with 0.1% formic acid
Column	Kinetex C18 (2.6 µm, 100× 2.1 mm, Phenomenex)
capillary temperature	275 ℃
Analyzer	FTMS
Mass range (m/z)	70-500
Collision energy	MS^2: 45 V; MS^3: 35 V

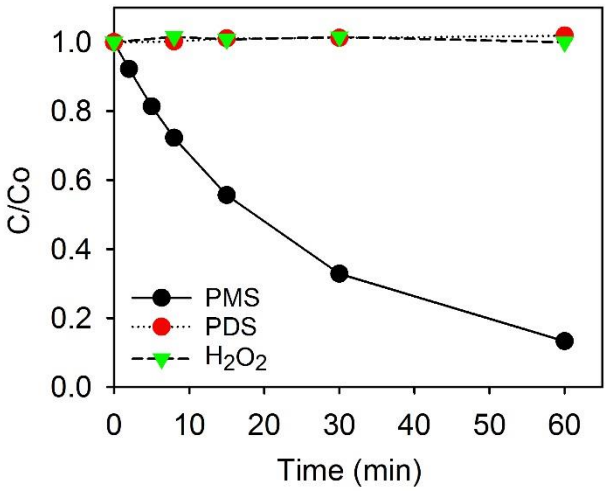

Figure A- 2-1. Relative removal of ciprofloxacin by PMS, PDS, and H_2O_2 (Ciprofloxacin=5 µM; Oxidants=100 µM; 10 mM phosphate buffer at pH 8)

Appendix 3

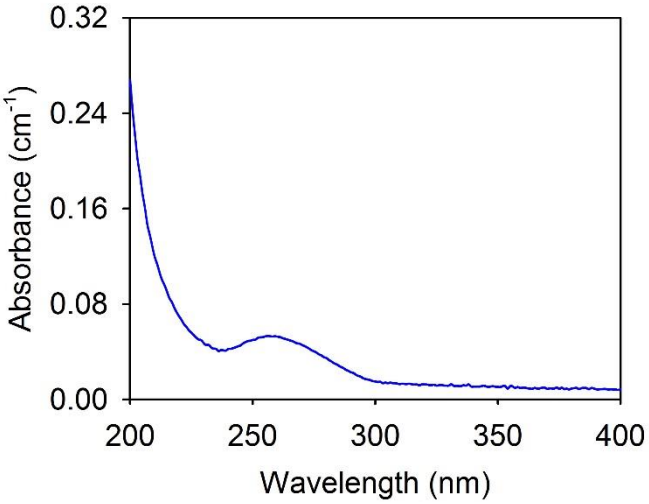

Figure A- 3-1. UV absorbance of 0.31 ng/µL of plasmid DNA (2 mM phosphate buffer at pH 7)

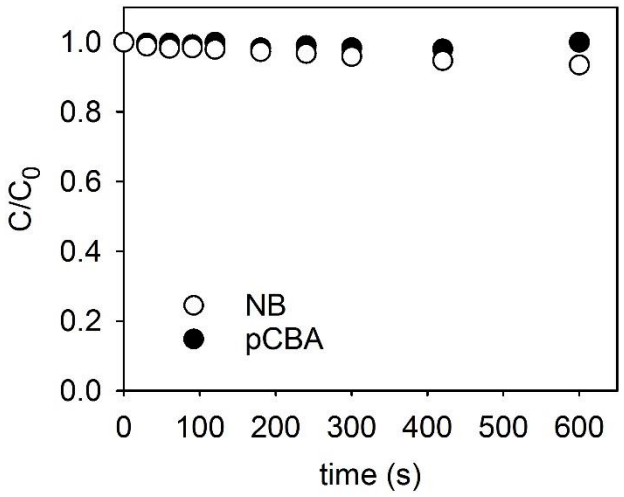

Figure A- 3-2. Effect of UV direct irritation at 254 nm on pCBA (1 µM) and nitrobenzene (NB, 1 µM)) (Fluence= 0−180 mJ/cm^2, 2 mM phosphate buffer at pH 7)

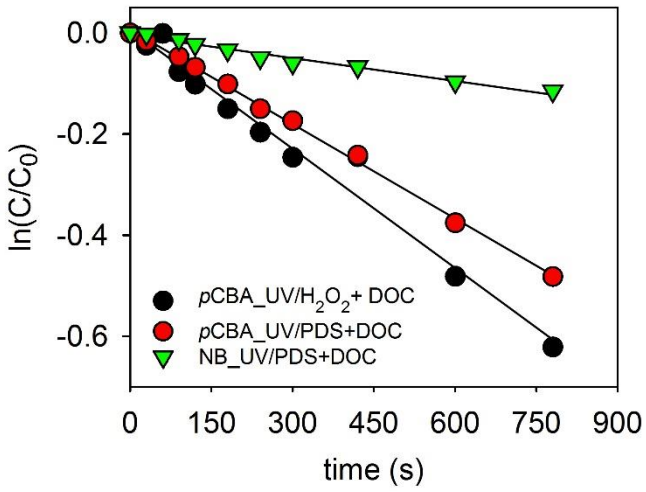

Figure A- 3-3. Degradation of pCBA (1 µM) and nitrobenzene (NB, 1 µM) during UV/H_2O_2 and UV/PDS in the presence of DOC (DOC=5.4 mg-C/L, Fluence= 0−180 mJ/cm^2, H_2O_2= PDS= 0.5 mM, 2 mM phosphate buffer at pH 7)

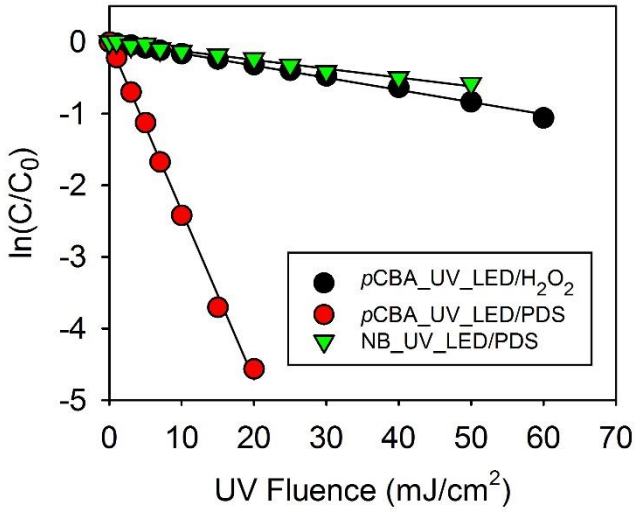

Figure A- 3-4. Degradation of pCBA (1 µM) and nitrobenzene (NB, 1 µM) during UV_{300}/H_2O_2 and UV_LED/PDS (Fluence= 0−2,160 mJ/cm^2, H_2O_2= PDS= 10 mM, 2 mM phosphate buffer at pH 7)

Appendix 4

Table A- 4-1. Model aromatic compounds investigated in this study

Non-nitrogenous compounds				
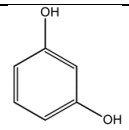	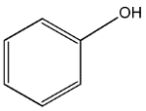	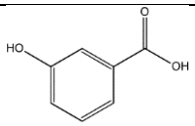	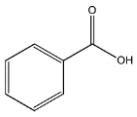	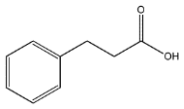
Resorcinol	Phenol	3-Hydroxybenzoic acid	Benzoic acid	3-Phenylpropionic acid
Nitrogenous compounds				
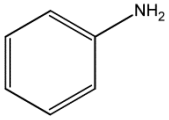	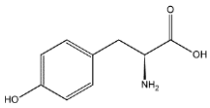	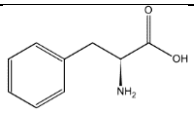		
Aniline	L-Tyrosine	L-Phenylalanine		

Table A- 4-2. EI and PCI fragments of P215

m/z	Possible formula	Error (ppm)
243.9681	$C_5H_4NO_2Cl_3$ ($C_2H_5^+$)	5.07
215.9379	$C_5H_4NO_2Cl_3(H^+)$	0.64
197.9269	$C_5H_3NOCl_3$	5.67
179.9607	$C_5H_4NO_2Cl_2$	6.72
163.9663	$C_5H_3NOCl_2(H^+)$	0.89
143.9849	$C_5H_3NO_2Cl$	2.30
131.9843	$C_4H_3NO_2Cl$	4.78
113.9741	C_4HNOCl	8.48
Fragmentation Pattern		

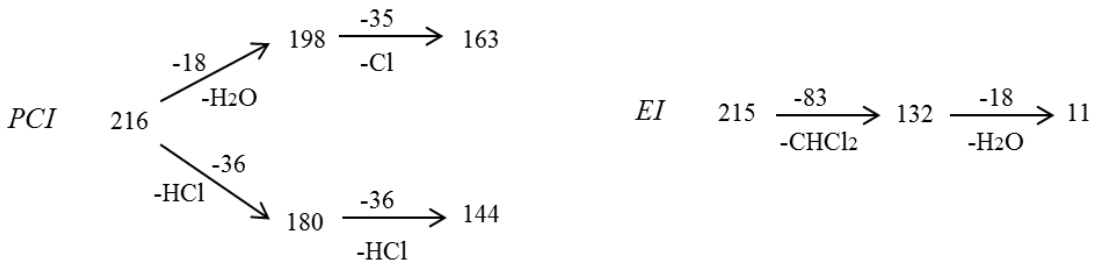

Table A- 4-3. Halogenated heterocyclic by-products reported in previous studies

Name	Structure	Previous study	References
MX	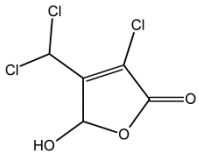	chlorinated drinking water and humic water	(Hemming et al., 1986; Kronberg and Vartiaine, 1988)
chloromethylmaleic anhydride and substituted furanones	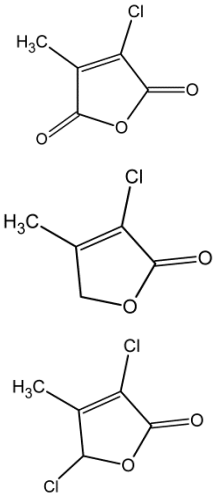	chlorination of orcinol	(Tretyakova et al., 1994)
3-chloro -2,5-furandione and 3,4-dichloro-2,5-furandione	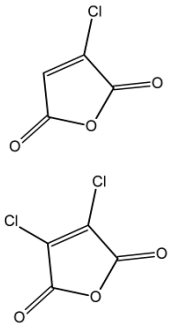	chlorination of resorcinol and swimming pool waters	(Rook, 1980; Richardson et al., 2010)

3-bromo-2,5-furandione	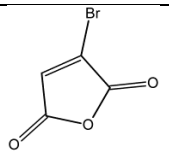	bromination of resorcinol	(Boyce and Hornig, 1983)
3,4-dichloro-2,5-pyrroledione and cyclic imides	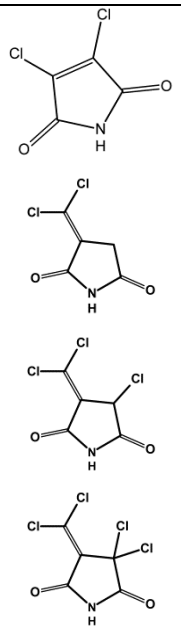	chlorination of poultry chiller water	(Haddon et al., 1996)
halogenated pyrroles	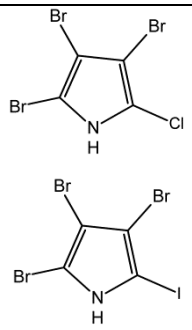	chlorinated saline wastewater effluents	(Yang and Zhang, 2014)
2,3,5-tribromopyrrole	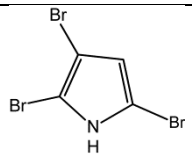	chlorination of bromide-containing waters	(Richardson et al., 2003)

Table A- 4-4. EI and PCI fragments of methyl ester form of P215

m/z	Possible formula	Error (ppm)
229.9515	$C_6H_6NO_2Cl_3(H^+)$	9.52
197.9252	$C_5H_3NOCl_3$	14.26
162.9568	$C_5H_3NOCl_2$	14.54
145.9993	$C_5H_5NO_2Cl$	10.83

113.9741	C_4HNOCl	4.97
82.9448	$CHCl_2$	8.81
Fragmentation Pattern		

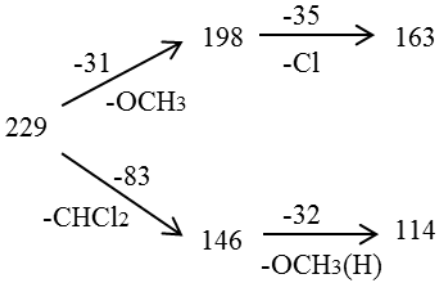

Table A- 4-5. EI and PCI fragments of P249

	m/z	Possible Formula	Error (ppm)
	277.9292	$C_5H_3NO_2Cl_4$ ($C_2H_5^+$)	4.20
	249.8988	$C_5H_3NO_2Cl_4(H^+)$	1.06
	231.8878	$C_5H_2NOCl_4$	5.39
	213.9222	$C_5H_3NO_2Cl_3$	3.44
	177.9458	$C_5H_2NO_2Cl_2$	2.58
	149.9506	$C_4H_2NOCl_2$	4.96
	131.9847	$C_4H_3NO_2Cl$	4.02
	113.9739	C_4HNOCl	6.72
MS/MS fragments of m/z 252	132.9914	$C_4H_3NO_2Cl(H^+)$	8.33
	97.0156	$C_4H_3NO_2$	8.02
	69.0210	C_3H_3NO	1.23
	54.0104	C_3H_2O	0.16
	42.0104	C_2H_2O	3.92
Fragmentation Pattern			

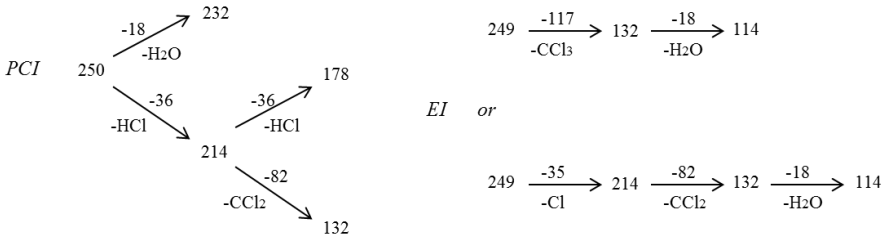

MS/MS analysis of m/z 252
$133\ (\text{CID@20,40,60}) \xrightarrow[-\text{HCl}]{-36} 97\ (\text{CID@40,60}) \xrightarrow[-\text{CO}]{-28} 69\ (\text{CID@40,60}) \xrightarrow[-\text{NH}]{-15} 54\ (\text{CID@40,60}) \xrightarrow[-\text{C}]{-12} 42\ (\text{CID@40,60})$
CID@20, 40, 60: collision energies (i.e., 20 eV, 40 eV and 60 eV)

Table A- 4-6. EI and PCI fragments of P131

m/z	Possible formula	Error (ppm)
131.9850	$C_4H_2NO_2Cl(H^+)$	-2.41
130.9991	$C_4H_2NO_2Cl$	165.63
103.0518	C_3H_2NOCl	673.01
87.9707	C_3HOCl	10.14
59.9756	C_2HCl	17.97
Fragmentation Pattern		
$131 \xrightarrow[-\text{CO}]{-28} 103 \xrightarrow[-\text{NH}]{-15} 88 \xrightarrow[-\text{CO}]{-28} 60$		

Text A- 4-1. Quantification of DBPs and full scan analysis of unknown by-products

THMs and HANs were quantified after liquid-liquid extraction following EPA method 551. 20 mL of sample was spiked with 100 µL of decafluorobiophenyl solution as the internal standard, and then transferred into a 40 mL glass vial containing 4 g of anhydrous sodium chloride. 3 mL of MTBE was used as the solvent. The extract was analyzed using an Agilent 7890A GC system coupled with a 5975C mass spectrometer (GC-MS). 1µL of solvent was injected (temperature: 200°C) in pulsed splitless mode. DBPs were separated on a DB-1701 (30 m x 250 µm x 0.25 µm) column. The oven program was held at 35ºC for 6 min, ramping to 125 °C at 10 °C/min, and then increased to 220 °C at 25 °C/min and held for 2 min. The total run time was 20.8 min.

HAcAms were analyzed following the same method, except that ethyl acetate was used as the extraction solvent instead of MTBE.

HAAs were quantified following the EPA method 552. 20 mL of sample was spiked with 50 µL of internal standard (2-bromopropionic acid), and then transferred into a 40 mL glass vial containing 4 g of anhydrous sodium chloride. The solution pH was adjusted to acidic condition with addition of 0.8 mL concentrated sulfuric acid. HAAs were extracted with 4 mL of MTBE. Then, MTBE layer was transferred into a 10 mL of glass vial containing 1 mL of H_2SO_4/CH_3OH (10% v/v). The glass vial was placed in a heating bath at 50 °C for 2 h. After neutralization with 4 mL of saturated $NaHCO_3$ and shaking for 2min, the MTBE layer was transferred into an autosampler vial. The extract was analyzed using an Agilent 7890A GC system coupled with a 5975C mass spectrometer (GC-MS). The oven program was held at 35ºC for 6 min, ramping to 220 °C at 10 °C/min. The total run time was 24.5 min. Other parameters of GC-MS (e.g., injection volume, column type) were the same as the HANs method.

Full scan analysis in electronic impact (EI) and positive chemical ionization (PCI, using methane as reagent gas) modes were performed on MTBE extracts at various reaction times. Preparation of MTBE extracts were mentioned above (i.e., extracts for HANs analysis and HAAs analysis). Two different GC-MS systems were used for full scan analysis: an Agilent 5975C GC-MSD and an Agilent 7200 Accurate-Mass Quadrupole Time-of-Flight (GC-QTOF). 1µL of solvent was injected (temperature: 200°C) in pulsed splitless mode. The column used for GC-MSD was a DB-1701 (30m × 250 µm × 0.25 µm) or a ZB-5MS (30m × 250 µm × 1 µm). GC separation on GC-QTOF was performed with a DB-5MS UI column (30m × 0.25mm × 0.25 µm). The oven program was held at 35ºC for 1 min, ramping to 75 °C at 10 °C/min, and then

increased to 250 °C at 25 °C/min. Scan range was between m/z 40 and 300. MS/MS analysis at three different collision energies (i.e., 20 eV, 40 eV and 60 eV) were performed on GC-QTOF for all main peaks detected. Agilent MassHunter Qualitative analysis B.07.00 was used for deconvolution of data from GC-QTOF. The mass spectral similarity search was performed by using NIST MS Search 2.0 (NIST/EPA/NIH Mass Spectral Library, NIST 08, National Institute of Standards and Technology, 2008, Gaithersburg, MD, USA).

Text A- 4-2. Formula and Structure Identification of methyl ester form of P215

Figure A-4-11 presents the EI mass spectrum at RT 10.5min, which shows main ion clusters m/z 146/148 and m/z 114/116, each comprising one chlorine and m/z 198/200/202/204 with 3 chlorine. The ion cluster m/z 114/116 was also detected from EI mass spectrum of P215 (Figure A-4-5). The corresponding PCI spectrum contained m/z 230 (i.e., $[M+H]^+$ adduct). The odd-numbered molecular mass (229) suggests odd-numbered nitrogen. Loss of 31 from m/z 229 to m/z 198 indicates the compound is probably with ($–OCH_3$) group. Loss of 83 from m/z 229 to m/z 146 suggests there is a ($–CHCl_2$) group. Accordingly, we proposed this compound as the methylated equivalent of compound P215. The molecular formula $C_6H_6NO_2Cl_3$ was confirmed by the accurate mass of $C_6H_6NO_2Cl_3(H^+)$ (i.e., 229.9515, 9.52 ppm) obtained from GC-QTOF. The fragmentation pattern and accurate mass of each fragment are compatible with the proposed structure and formula (Table A-4-4).

Text A- 4-3. Formula and Structure Identification of P249

As shown in Figure A-4-12 a, the EI mass spectrum of P249 is similar to that of P215 (Figure A-4-5 a), exhibiting two dominant ion clusters (m/z 132/134 and 114/116) each comprising one chlorine. The difference between m/z 132 and m/z 114 (i.e., 18) indicates the loss of one water. The corresponding PCI mas spectrum contained a major ion cluster m/z 250/252/254/256 (i.e., $[M+H]^+$ adduct), with four chlorine (Figure A-4-12 b). The odd-numbered m/z value (i.e., m/z 249) indicates it is a nitrogenous compound. The PCI mass spectrum obtained from GC-QTOF showed an accurate mass of 249.8988 for $[M+H]^+$. In order to get more fragments for structure identification, MS/MS analysis was performed on ion m/z 252 by application of 3

different collision energies (i.e., 20eV, 40eV and 60eV) (Figure A-4-13). Two molecular ion formula of this compound were proposed by molecular formula predictor software based on the accurate mass (relative mass accuracy within ±5ppm): $C_5H_3NO_2Cl_4(H^+)$ (1.06ppm) and $C_3HN_4OCl_4(H^+)$ (-4.31ppm). The latter was excluded due to its high nitrogen content. Accordingly, $C_5H_3NO_2Cl_4$ was confirmed to be the molecular formula of this compound. Based on the fragmentation pattern and accurate mass of fragments obtained in EI/PCI mode and MS/MS analysis, we proposed this compound as the four chlorinated analogue of P215 or 6-hydroxy-2-pyridone with four chlorine (Table A-4-5).

Text A- 4-4. Formula and Structure Identification of P131

The EI mass spectrum of P131 contained ion clusters m/z 131/133, 103/105 and 88/90 (Figure A-4-14 a), corresponding to which was very similar to the mass spectrum of 3-chloro-2,5-furandione as found by the NIST 08 database. The PCI spectra of this compound showed an ion cluster m/z 132/134 (i.e., $[M+H]^+$ adduct), which confirmed a molecular mass of 131 (Figure A-4-14 b). The odd-numbered molecular mass (131) indicates there may be odd-numbered nitrogen in this molecule. Accordingly, we proposed this compound as 3-chloro-2,5-pyrroledione (C_4H_2NOCl), which is structurally very similar to 3-chloro-2,5-furandione and compatible with fragmentation pattern in GC-MS. The calculated exact mass of C_4H_2NOCl (H^+) is 131.9845. The accurate mass of this ion obtained from GC-QTOF in PCI mode was 131.9847, with relative mass accuracy of -0.13 ppm (Table A-4-6).

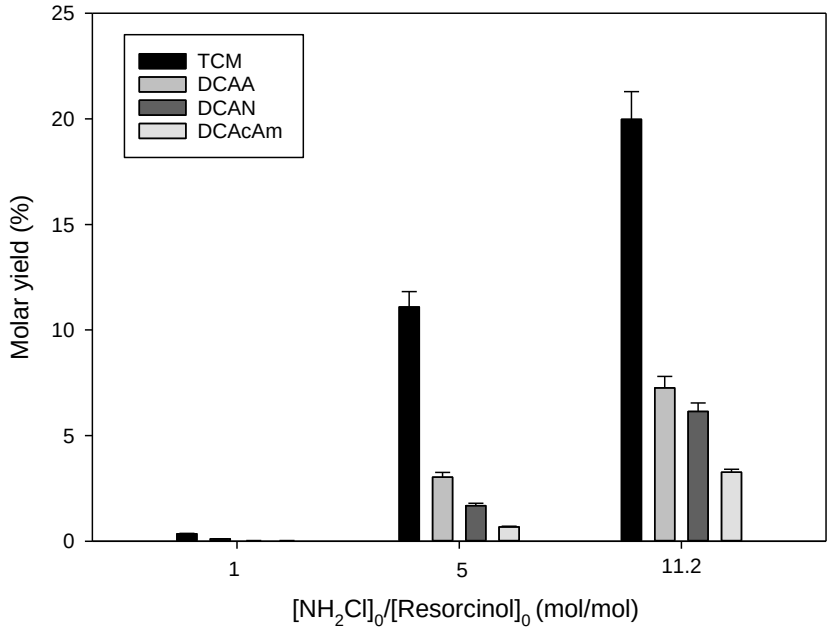

Figure A- 4-1. Effect of monochloramine dose on DBPs formation from chloramination of resorcinol (Resorcinol=500 µM; pH 7.0, 10 mM phosphate buffer; 72 h)

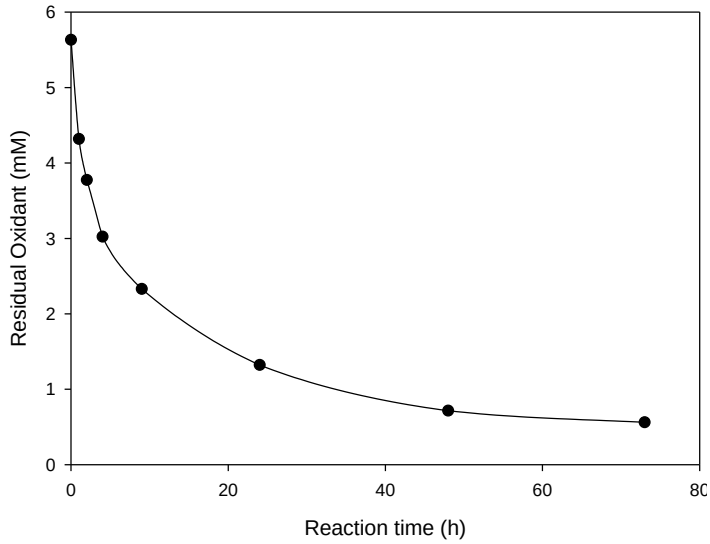

Figure A- 4-2. Residual oxidant measured during chloramination of resorcinol (Resorcinol= 500 µM; Initial NH2Cl = 5.6 mM; pH 7.0, 10 mM phosphate buffer)

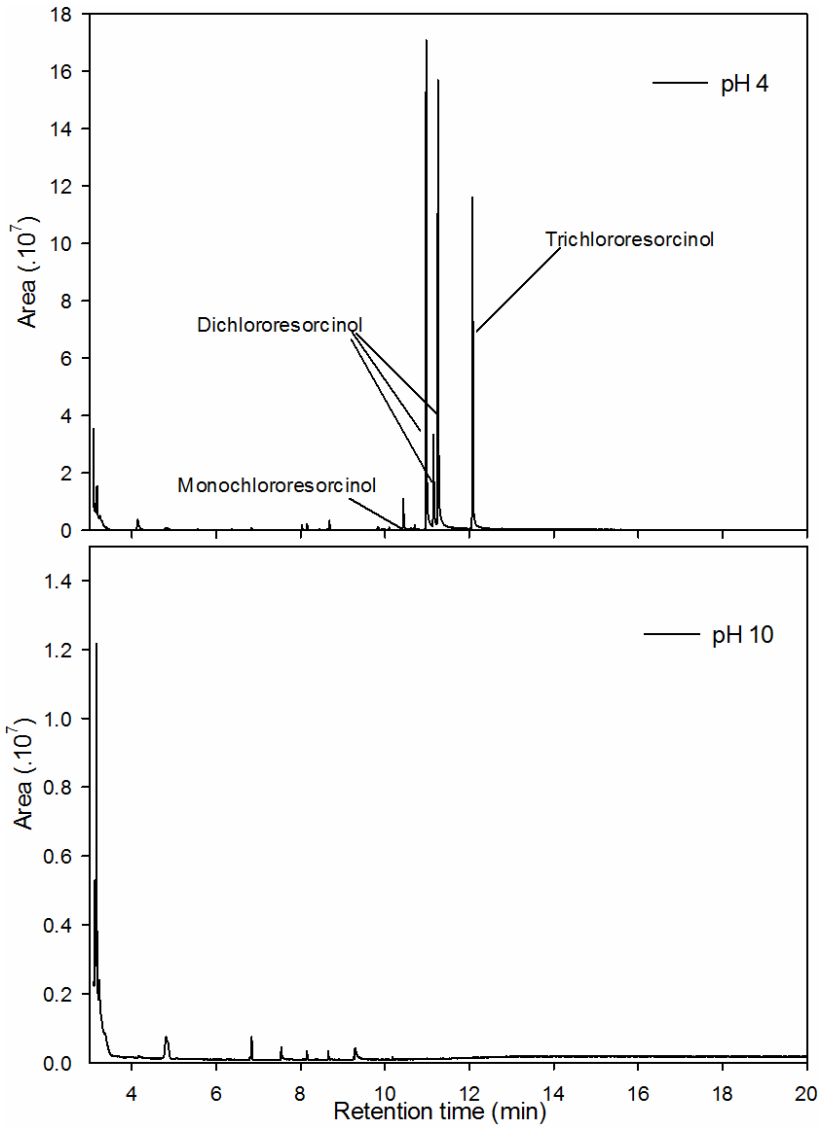

Figure A- 4-3. Total ion chromatogram of resorcinol after 72 h of chloramination at pH 4 and 10 (Resorcinol= 500 µM; NH_2Cl = 5.6 mM; Spectrum obtained in EI mode)

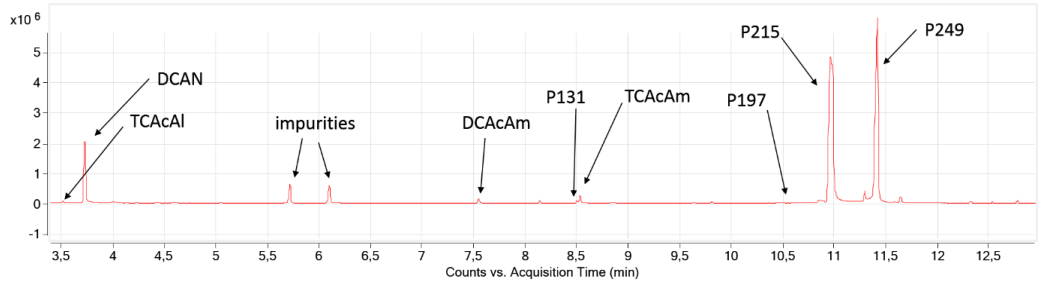

Figure A- 4-4. Total ion chromatogram of resorcinol after 72h of chloramination (Resorcinol= 500 µM; NH_2Cl = 5.6 mM; pH 7.0, 10 mM phosphate buffer; Spectrum obtained in EI mode)

a)

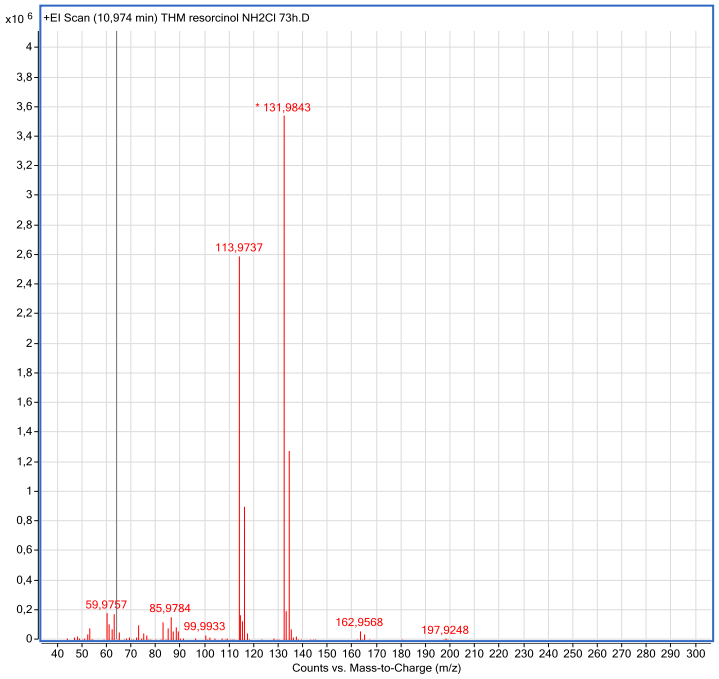

b)

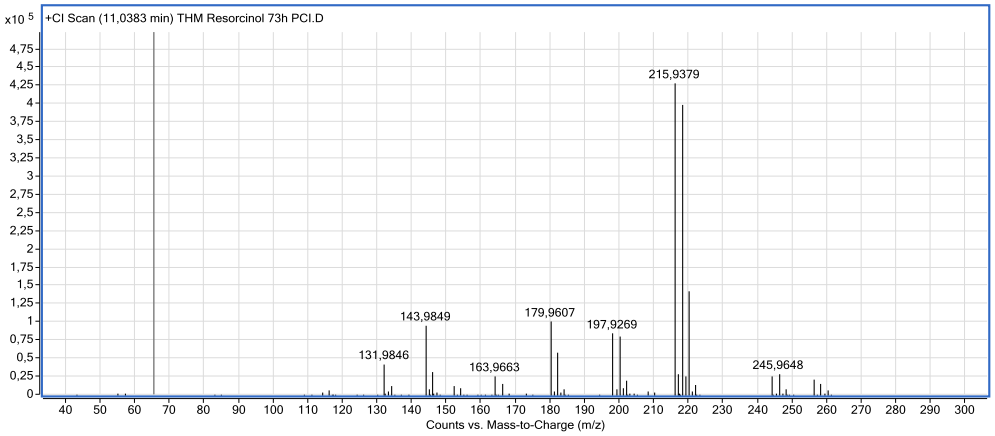

Figure A- 4-5. a) EI and b) PCI (CH_4 as reagent gas) mass spectrum of P215 obtained from GC-QTOF

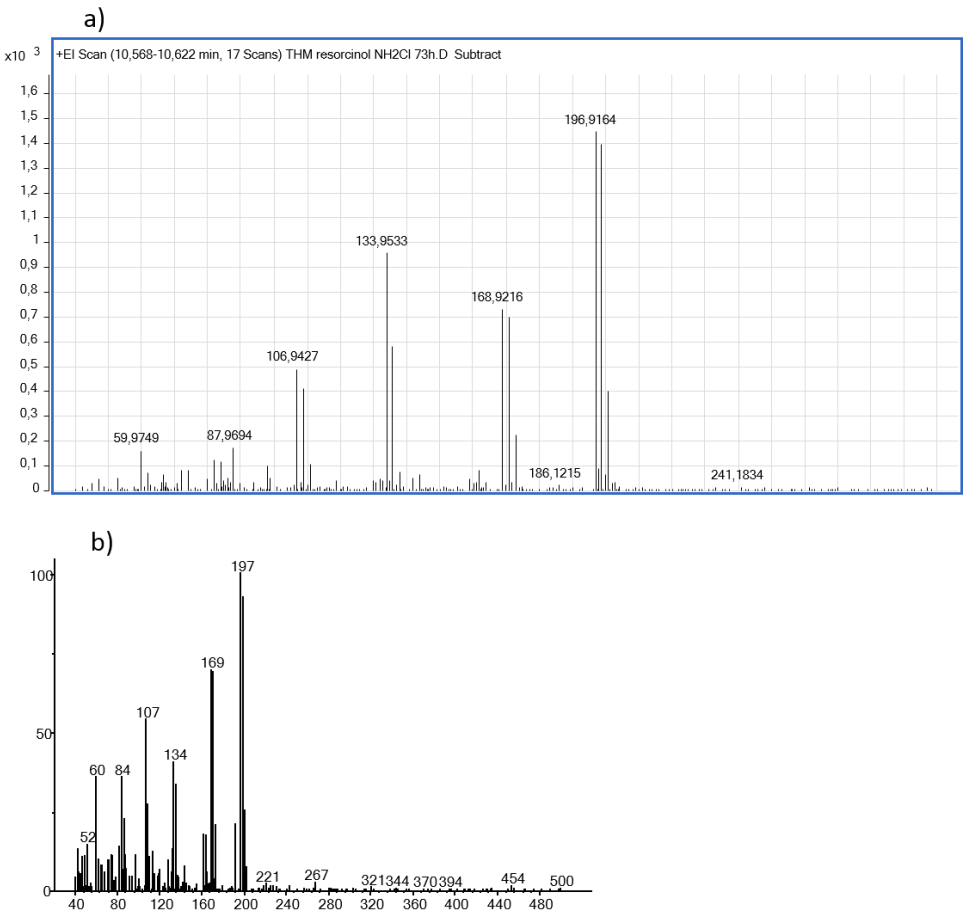

Figure A- 4-6. EI Mass Spectrum of P197 obtained from a) GC-QTOF and b) GC-MSD

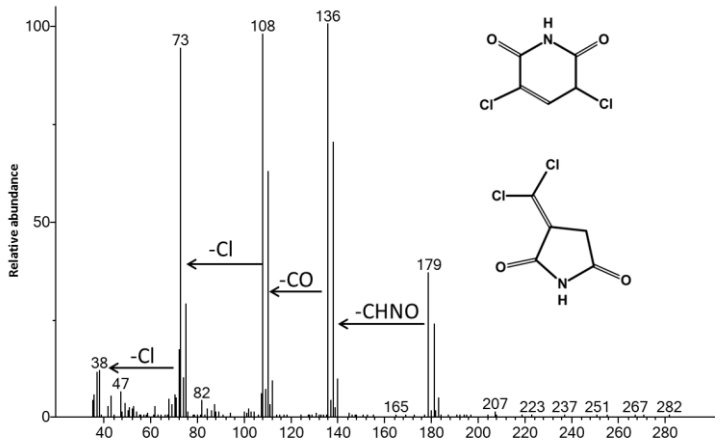

Figure A- 4-7. EI Mass Spectrum of P179 obtained from GC-MSD

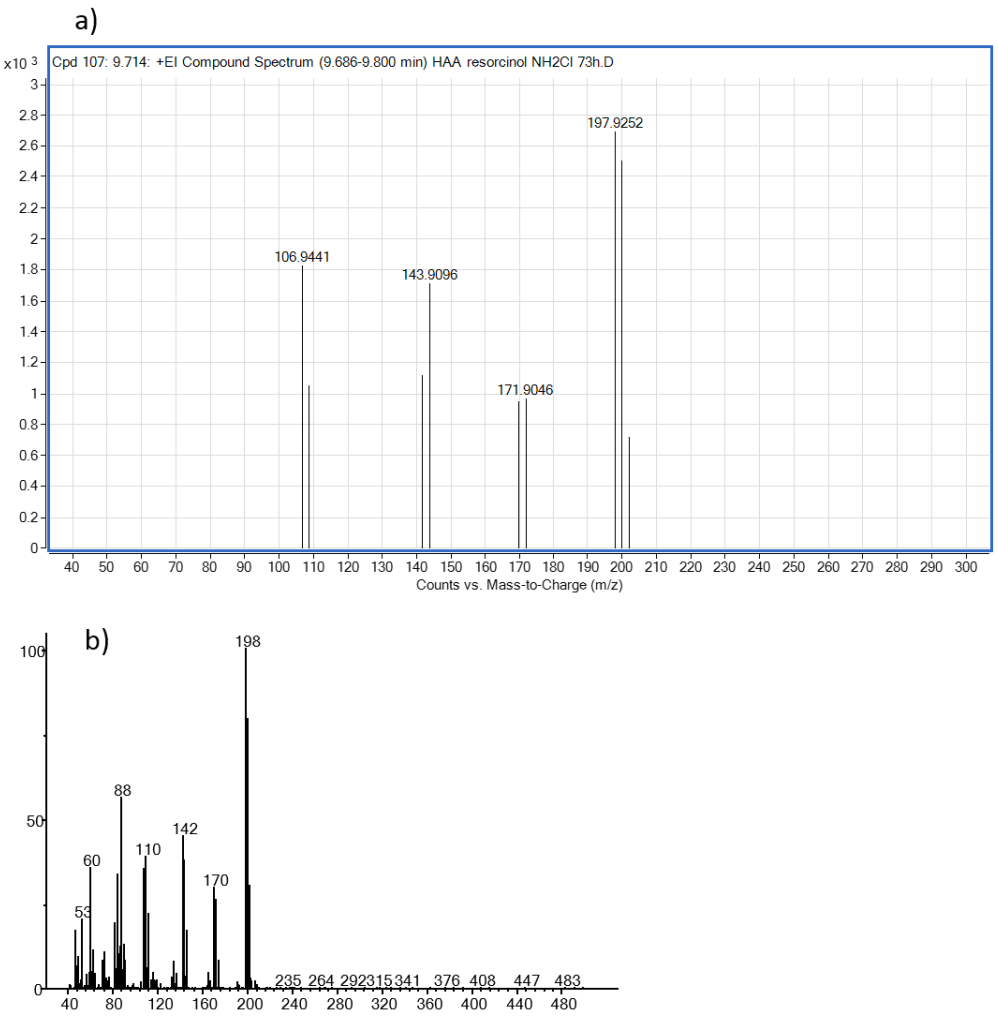

Figure A- 4-8. EI Mass Spectrum of P198 obtained from a) GC-QTOF and b) GC-MSD

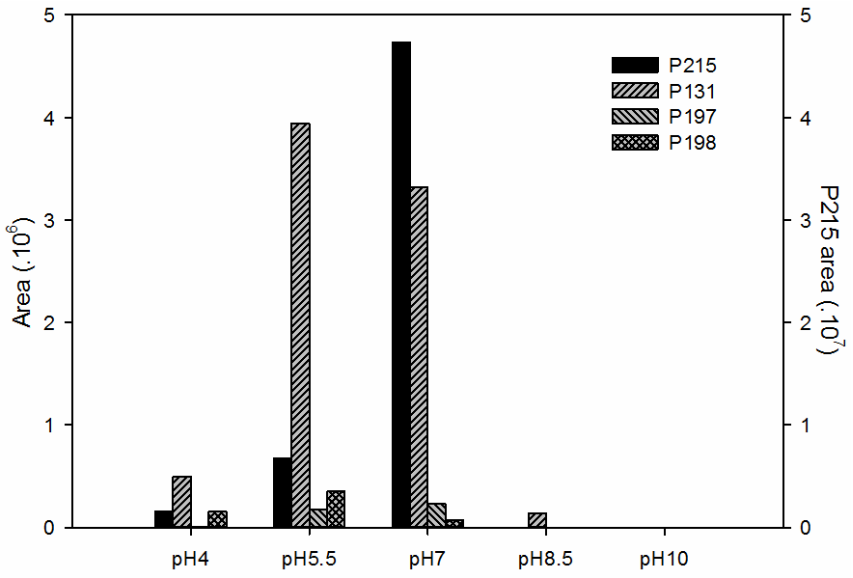

Figure A- 4-9. Effect of pH on the formation of heterocyclic compounds from chloramination of resorcinol (Resorcinol= 500 µM; NH2Cl = 5.6 mM; 72 h)

a)

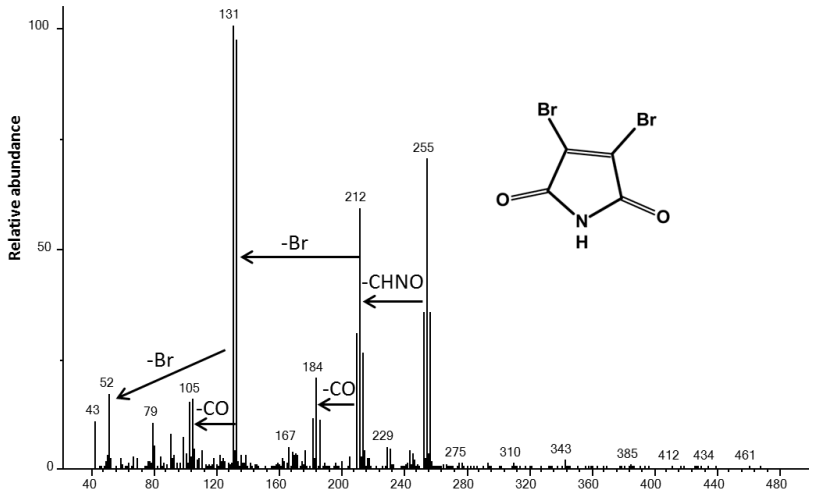

b)

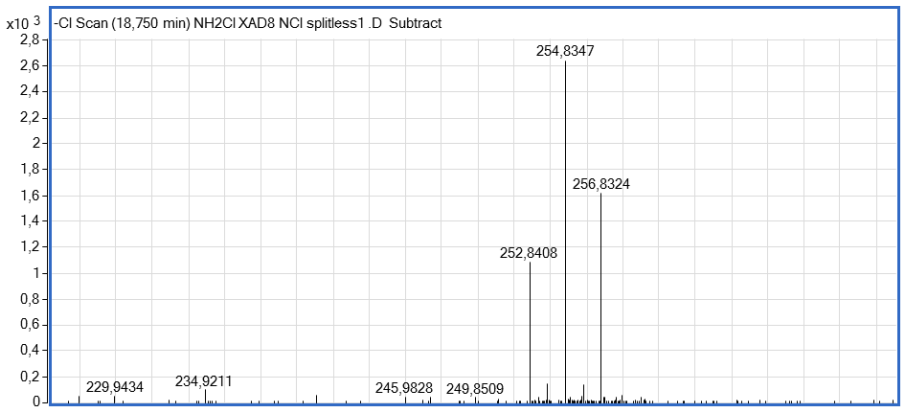

Figure A- 4-10. Mass Spectrum of dibromopyrroledione obtained from a) GC-MSD and b) GC-QTOF

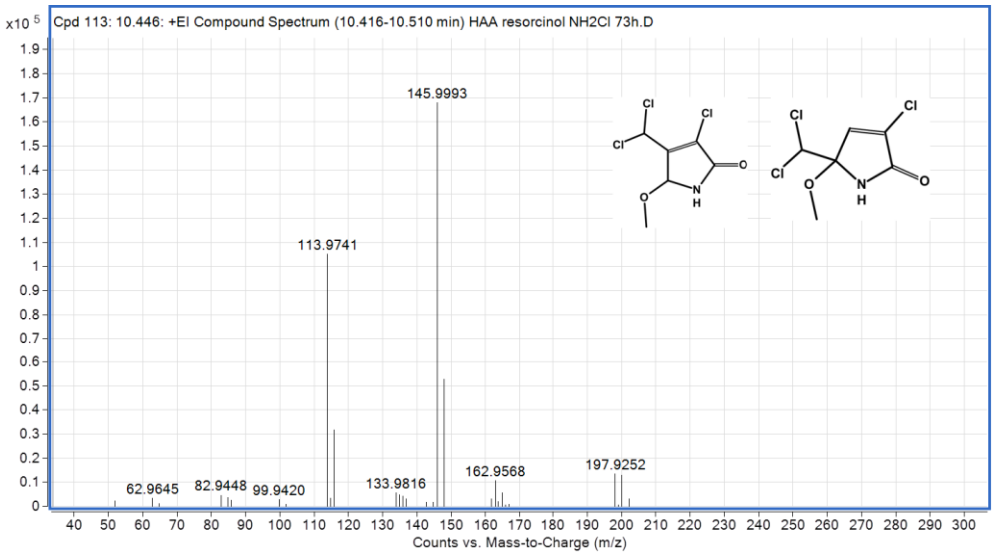

Figure A- 4-11. EI Mass Spectrum of methyl ester form of P215 obtained from GC-QTOF

a)

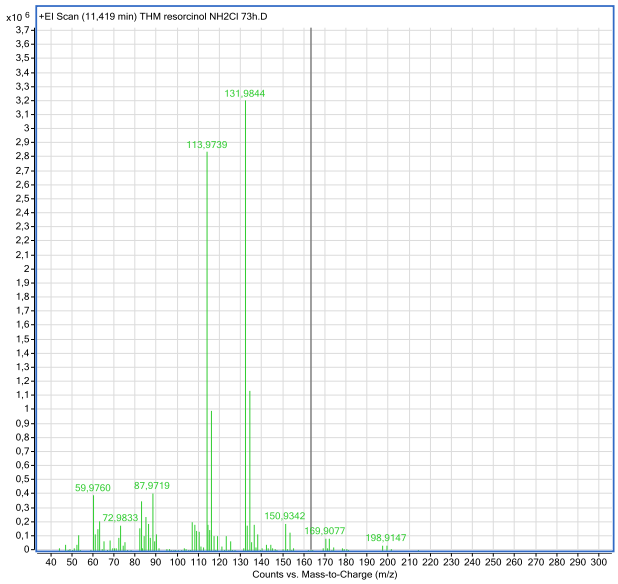

b)

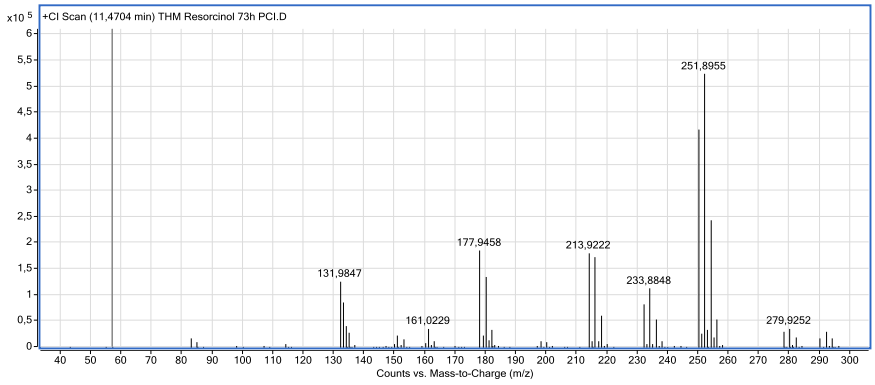

Figure A- 4-12. a) EI and b) PCI (CH4 as reagent gas) mass spectrum of P249 obtained from GC-QTOF

a)

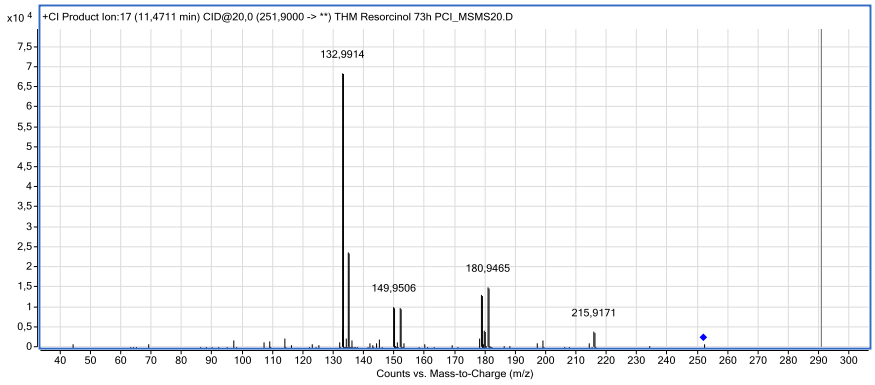

b)

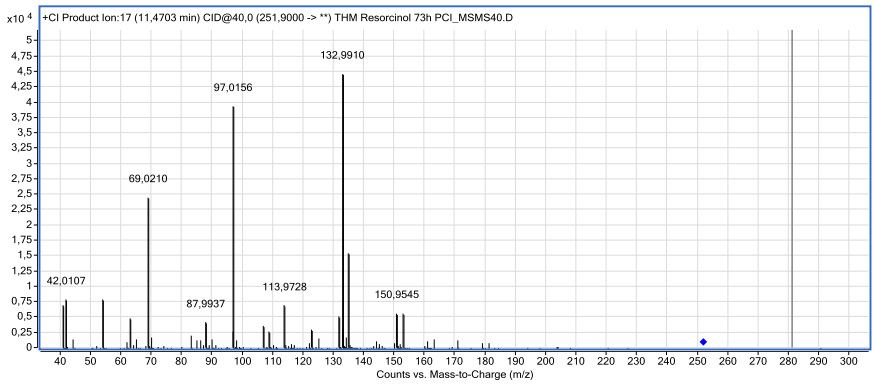

c)

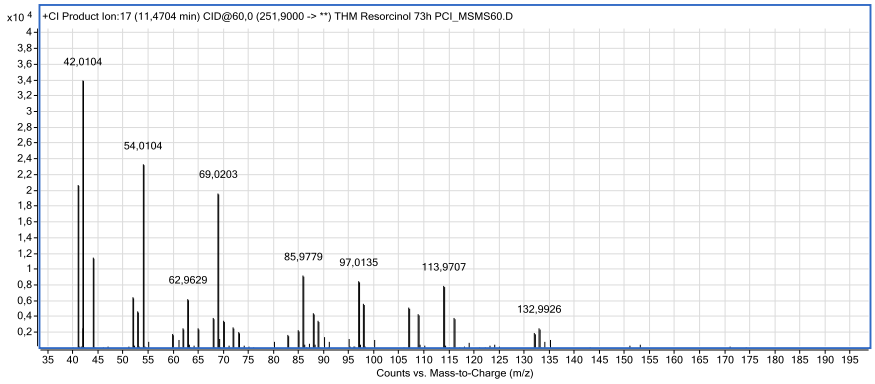

Figure A- 4-13. MS/MS mass spectrum of ion m/z 252 at different collision energies: a) 20eV, b) 40eV and c) 60 eV

a)

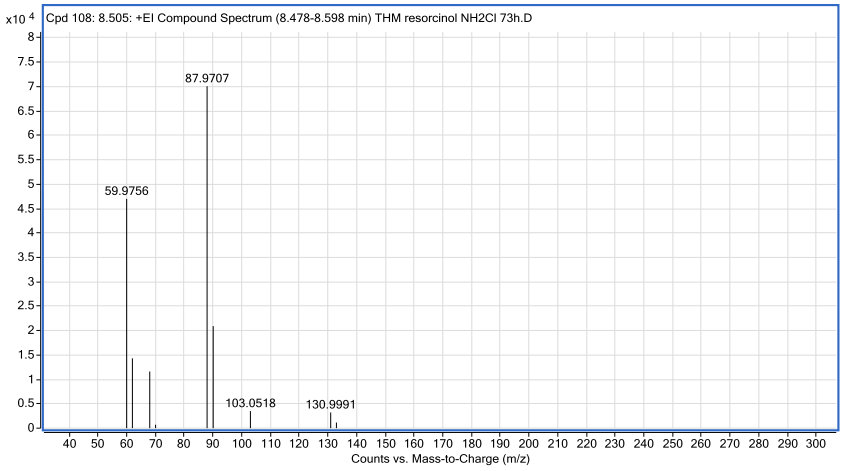

b)

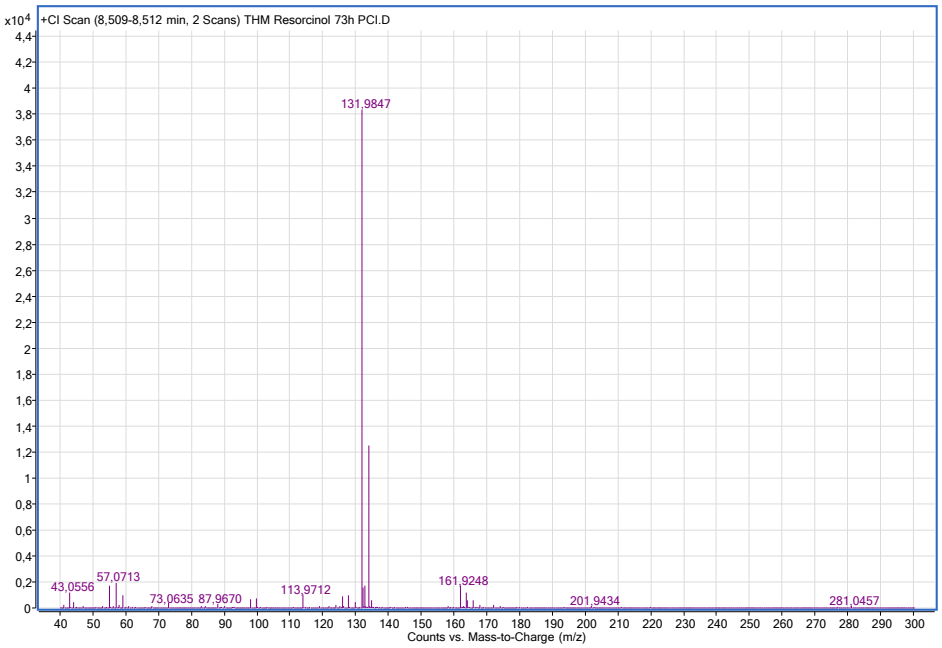

Figure A- 4-14. a) EI and b) PCI (CH4 as reagent gas) mass spectrum of P131 obtained from GC-QTOF

Reference

Boyce, S. D., and Hornig, J. F. (1983). Reaction pathways of trihalomethane formation from the halogenation of dihydroxyaromatic model compounds for humic acid. *Environmental Science & Technology, 17*(4), 202-211.

Haddon, W. F., Binder, R. G., Wong, R. Y., Harden, L. A., Wilson, R. E., Benson, M., and Stevens, K. L. (1996). Potent Bacterial Mutagens Produced by Chlorination of Simulated Poultry Chiller Water. *Journal of Agricultural and Food Chemistry, 44*(1), 256-263.

Hemming, J., Holmbom, B., Reunanen, M., and Kronberg, L. (1986). Determination of the strong mutagen 3-chloro-4-(dichloromethyl)-5-hydroxy-2(5H)-furanone in chlorinated drinking and humic waters. *Chemosphere, 15*(5), 549-556.

Kronberg, L., and Vartiaine, T. (1988). Ames mutagenicity and concentration of the strong mutagen 3-chloro-4-(dichloromethyl)-5-hydroxy-2(5H)-furanone and of its geometric isomer E-2-chloro-3-(dichloromethyl)-4-oxo-butenoic acid in chlorine-treated tap waters. *Mutation Research/Genetic Toxicology, 206*(2), 177-182.

Richardson, S. D., DeMarini, D. M., Kogevinas, M., Fernandez, P., Marco, E., Lourencetti, C., Ballesté, C., Heederik, D., Meliefste, K., McKague, A. B., Marcos, R., Font-Ribera, L., Grimalt, J. O., and Villanueva, C. M. (2010). What's in the pool? a comprehensive identification of disinfection by-products and assessment of mutagenicity of chlorinated and brominated swimming pool water. *Environmental Health Perspectives, 118*(11), 1523-1530.

Richardson, S. D., Thruston, A. D., Rav-Acha, C., Groisman, L., Popilevsky, I., Juraev, O., Glezer, V., McKague, A. B., Plewa, M. J., and Wagner, E. D. (2003). Tribromopyrrole, brominated acids, and other disinfection byproducts produced by disinfection of drinking water rich in bromide. *Environmental Science and Technology, 37*(17), 3782-3793.

Rook, J. J. (1980). Possible pathways for the formation of chlorinated degradation products during chlorination of humic acids and resorcinol. In R. L. Jolley, Brungs, W. A., Cumming, R. B. (Ed.), *Water Chlorination: Environmental Impact and Health Effects* (pp. 85-98). Michigan: Ann Arbor Science.

Tretyakova, N. Y., Lebedev, A. T., and Petrosyan, V. S. (1994). Degradative pathways for aqueous chlorination of orcinol. *Environmental Science and Technology, 28*(4), 606-613.

Yang, M., and Zhang, X. (2014). Halopyrroles: A new group of highly toxic disinfection byproducts formed in chlorinated saline wastewater. *Environmental Science and Technology, 48*(20), 11846-11852.

Appendix 5